Assaying the biological role of the PKD1L1-PKD2 interaction

A thesis presented for the degree of Doctor of Philosophy (DPhil)

Jesus College, University of Oxford

Dragoș-Vasile Leordean

Mammalian Genetics Unit, MRC Harwell

Department of Physiology, Anatomy and Genetics, University of Oxford

Supervisors: Dr. Dominic Norris (MGU, MRC Harwell)

Prof. Shankar Srinivas (DPAG, University of Oxford)

Hilary term 2018

Word count: 39611

Abstract

Polycystins are a family of transmembrane proteins found in metazoan species that play a plethora of roles, at multiple stages, throughout the lifespan of the animal organism. In human, two loci encoding polycystins, *PKD1* and *PKD2*, were found to be causative of autosomal dominant polycystic kidney disease. Later studies identified these two genes in other organisms, such as mouse and zebrafish, which served as models for investigating the function and regulation of the two proteins. PKD1 and PKD2 behave as interacting partners and form cation-permeable channels, which are thought to control cellular proliferation. The interaction of the two proteins was shown to involve the respective coiled-coil (CC) domains of each protein, a typical protein-protein interaction domain. Later studies then determined that PKD2 is also able to interact with other PKD2 molecules through the CC domain, as well as other domains distributed throughout the protein.

PKD2 has also been shown to play a role in left-right (L-R) asymmetry determination, in partnership with a PKD1 paralog, PKD1L1 (PKD1-like-1). The two have also been suggested to interact, presumably through their respective CC domains. The aim of the work described in this thesis is to test the differences and similarities between the interaction mechanisms of PKD1-PKD2 and PKD1L1-PKD2, in order to better understand how these molecules perform their function.

I first investigated the molecular mechanisms involved in the PKD1L1-PKD2 interaction, through the use of biochemical techniques, by comparing the interaction of PKD2 WT or mutant proteins fragments with destabilized or truncated CCs. The results obtained suggest that the molecular mechanisms of interaction are likely different between the PKD1-PKD2 and PKD1L1-PKD2 complexes, in that the PKD1L1-PKD2 interaction does not appear to require the CC domain for interaction. I performed phenotypic analysis on embryos carrying truncation or insertion mutations in the region of *Pkd2* encoding the CC region. The phenotypic data indicates, for the first time, a separation between the role played by PKD2 in L-R and kidney development. Furthermore, the results described in this thesis also indicate that the PKD2 CC performs distinct functions, at the molecular level, in different contexts.

Acknowledgements

I would like to start by thanking my supervisor, Dominic Norris, for the opportunity to work in his lab, as well as the guidance he has provided throughout the years that we have worked together. I also want to thank him for the faith he has placed in me, by letting me carry this project in uncharted directions. I would also like to thank members of the Norris lab, past and present: Jenny Keynton, Dan Grimes, Rebecca Walker, Hannah Farley, Rosie Little and Laura Dyer. A special mention goes to David Asante, for sharing his biochemical and cell biology expertise, as well as his friendship and moral support in times of need. I would also like to thank the Greenfield lab, whom we share lab meetings with and who have provided interesting discussions relating to this project.

Core services in Harwell have been invaluable in realising the work described herein, especially Protein Core, GEMS, the Transgenics/LacZ group and Histology. On the same note, Lucie Vizor (and Ward 4), Sara Wells, Anju Paudyal and Jackie Harrison (and Ward 5) have contributed a great deal to my work by managing the mouse colonies involved in this project. I want to also mention Chris Esapa and Helen Hilton (Protein core), who have helped me greatly with the biochemical work described; Zsombor-Szoke Kovács, without whom I could not have done the µCT analysis; and Jeremy Sanderson, who has also contributed to the microscopy work presented, has helped with reading this thesis, and provided guidance throughout my time at Harwell. Sam Laber, Tom Agnew and Pedro Romão have provided plenty of good company, laughs and friendship, especially during trying times – thank you.

In Oxford, I would like to thank my Oxford supervisor, Shankar Srinivas, and college supervisor, Paul Riley, for all their help and support. My Oxford-based friends have also been an invaluable resource for discussing my project and maintaining me in good spirits: Mariela and Daniel Bălănescu, Mihai Vidrighin, Cora Miron and Sándor Kruk. I would like to also mention and thank friends elsewhere: Fulvia Iancu, Diana and Ionuț Trifu, Flaviu Vișan, Tudor Morar, Freddy Ciocoiu, Silvia Bota, Andreea and Rolf de Graaf, Andrei Fărcaș and Vlad Petrovan. For help and support on other fronts, I would like to mention Horațiu Crișan, Dan Buzdugan, Viorica Cristea and Michael Palij. A number of people have also been involved formally in my education, and I would like to also thank them here: Kathryn Hentges, Ray O'Keefe, Aurora Mureșan, Alin Câmpean, Claudia Vlaica, Corina Sitaru and Reghina Liscan.

Finally, my family has been a constant source of support throughout this DPhil and beyond. Both my mother and father have inspired and encouraged me to always give my best. I should probably also add that whatever affinities I have towards the µCT work presented in this thesis I owe to my parents, who are both medics. I also wish to thank my grandparents, brother and extended family for all their support. Last but by no means least, I wish to thank my late grandfather, Vasile Leordean. I would not have trekked so far, nor climbed as high without his influence. In his absence, I can only hope that I can live up to the standards that his example has set.

Abbreviations and acronyms

Abbreviation/acronym	Definition
AA	**A**mino **A**cid
ADPKD	**A**utosomal **D**ominant **P**olycystic **K**idney **D**isease
AFM	**A**tomic **F**orce **M**icropscopy
BSA	**B**ovine **S**erum **A**lbumin
CC	**C**oiled-**c**oil
CIP buffer	**CoIP** buffer
CoIP	**Co**immuno**p**recipitation
COS-7	**C**V-1 in **O**rigin, and carrying **S**V40 genetic material
dpc	***d**ies **p**ost **c**oitum* (days after mating)
DORV	**D**ouble **O**utlet **R**ight **V**entricle
DRG	**D**orsal **R**oot **G**anglion
ECM	**E**xtra**c**ellular **m**atrix
ER	**E**ndoplasmic **r**eticulum
FRET	**F**örster **R**esonance **E**nergy **T**ransfer
GPS	**G**PCR **P**roteolytic **S**ite
HEK293T	**H**uman **E**mbryonic **K**idney **293**, SV40 Large **T**-antigen containing
IAA	**I**nterrupted **A**ortic **A**rch
IVS	**I**nter**v**entricular **s**eptum
KV	**K**upffer's **V**esicle
LPM	**L**ateral **P**late **M**esoderm
mIMCD3	**m**urine **I**nner **M**edulary **C**ollecting **D**uct
NMR	**N**uclear **M**agnetic **R**esonance
PFA	**P**ara**f**orm**a**ldehyde
PKD#	**P**olycystic **K**idney **D**isease **#**
PKD#L#	**P**olycystic **K**idney **D**isease #-**l**ike #
PLAT	**P**olycystin-1, **L**ipoxygenase and ***α*-t**oxin
REJ	**R**eceptor for **E**gg **J**elly
TM	**T**rans**m**embrane (domain)
TOP	**T**etragonal **O**pening for **P**olycystins
TRP	**T**ransient **R**eceptor **P**otential
VSLD	**V**oltage-**S**ensor **L**ike **D**omain
WISH	**w**hole mount ***in s**itu* **h**ybridization
WIF	**w**hole mount **i**mmuno**f**luorescence
Y2H	**y**east two-**h**ybrid
µCT	micro-**c**omputer **t**omography

Table of contents

Abstract	**i**
Acknowledgements	**ii**
Abbreviations and acronyms	**iii**
Chapter 1: Introduction	**1**
1.1. Overview	**1**
1.2. The polycystin family of proteins	**5**
1.2.1. The TRP superfamily	**8**
1.2.2. PKD1	**8**
1.2.3. PKD2	**10**
1.2.4. Paralogs of PKD1 and PKD2	**13**
1.2.5. Molecular aspects	**16**
1.2.5.a. Aspects of molecular function of polycystins	**16**
1.2.5.b. Sub-cellular localisation and trafficking	**18**
1.3. Laterality	**23**
1.3.1. Development of organ asymmetries in the mouse embryo	**23**
1.3.2. Abnormal *situs* development	**27**
1.3.3. The role of PKD1L1 and PKD2 in breaking embryonic L-R symmetry	**28**
1.4. ADPKD	**31**
1.4.1. The role of PKD2 in ADPKD	**32**
1.4.2. ADPKD and the PKD1-PKD2 interaction	**32**
1.5. PKD1 and PKD2 in other contexts	**33**
1.5.1. Skeletal development	**33**
1.5.2. Cardiovascular development	**34**
1.5.3. Lymphatic system development	**35**
1.6. Aim of thesis	**37**
Chapter 2: Investigating the molecular mechanism of the PKD1L1-PKD2 interaction	**38**
2.1. Introduction	**38**
2.1.1. Interacting with PKD2: from domains to function	**38**
2.1.2. Models of PKD2-based interaction	**43**
2.1.3. Hypothetical model for the interaction of PKD1L1 with PKD2	**44**
2.2. Results	**45**
2.2.1. Designing mutations that affect the PKD2 CC	**45**
2.2.2. Using protein fragments to study the PKD1L1-PKD2 interaction	**49**
2.2.3. The involvement of the PKD2 CC	**57**
2.2.4. The C630 residue of PKD2 is not required for the interaction with PKD1L1	**63**
2.2.5. Testing previous findings regarding the PKD1L1- and PKD1-PKD2 interaction	**65**
2.2.6. Testing the interaction of PKD2 with NPR3	**72**
2.3. Summary of results and discussion	**74**
2.3.1. Designing PKD2 CC mutations	**74**
2.3.2. Validation of PKD2 protein fragments	**75**
2.3.3. Testing PKD2 CC requirement for the PKD1L1-PKD2 interaction	**76**
2.3.4. Assessing PKD2 C630 residue involvement in PKD1L1-PKD2 interaction	**78**
2.3.5. Testing previous findings and validating interactions	**79**
2.3.6. Conclusion	**80**
Chapter 3: Phenotypic analysis of mouse *Pkd2* mutants lacking the PKD2 CC region	**81**
3.1. Introduction	**83**

Table of contents

3.1.1. Previous results and rationale	83
3.2. Results	85
3.2.1. Description of mutant lines and alleles used	85
3.2.2. Phenotypic analysis of *Pkd2*$^{del/del}$ embryos at 15.5 dpc	86
3.2.3. Phenotypic analysis of *Pkd2*$^{fsX7/del}$ and *Pkd2*$^{fsX7/fsX7}$ embryos at 15.5 dpc	97
3.2.3.a. Gross *situs* analysis	97
3.2.3.b. Histological sectioning of kidneys	101
3.2.3.c. Phenotypic analysis through µCT	103
3.2.4. Phenotypic analysis of *Pkd2*$^{S818X/del}$ and *Pkd2*$^{S818X/S818X}$ embryos at 15.5 dpc	117
3.2.4.a. Gross *situs* analysis	117
3.2.4.b. Histological sectioning of kidneys	122
3.2.4.c. Phenotypic analysis through µCT	124
3.2.5. Phenotypic analysis of *Pkd2*$^{R870X/R870X}$ embryos at 15.5 dpc	138
3.2.5.a. Gross *situs* analysis	138
3.2.5.b. Histological sectioning of kidneys	141
3.2.5.c. Phenotypic analysis through µCT	143
3.2.6. Phenotypic analysis of *Pkd2*$^{ins/ins}$ embryos at 15.5 dpc	152
3.2.6.a. Gross *situs* analysis	152
3.2.6.b. Histological sectioning of kidneys	153
3.3. Summary of results and discussion	156
3.3.1. Description and predicted impact of CRISPR/Cas9-derived alleles	156
3.3.2. Summary and interpretation of *Pkd2*$^{del/del}$ embryo µCT phenotypic analysis	158
3.3.3. Interpreting *Pkd2*$^{fsX7/del}$ and *Pkd2*$^{fsX7/fsX7}$ embryo phenotypes	160
3.3.4. Interpreting *Pkd2*$^{S818X/del}$ and *Pkd2*$^{S818X/S818X}$ embryo phenotypes	163
3.3.5. Characterising the *Pkd2*^{R870X} allele	164
3.3.6. Preliminary characterisation of the *Pkd2*^{ins} allele	165
3.3.7. Novel findings	167
3.3.8. Conclusion	168
Chapter 4: Final discussion and future work	172
4.1. Summary and interpretation of results	172
4.1.1. Molecular mechanisms of PKD1L1-PKD2 interaction	172
4.1.2. Phenotypic analysis of CC mutants	174
4.1.2.a. *Pkd2*^{fsX7}	174
4.1.2.b. *Pkd2*^{S818X}	175
4.1.2.c. *Pkd2*^{R870X}	176
4.1.2.d. *Pkd2*^{ins}	177
4.1.2.e. Inference of mechanism	178
4.1.3. Synthesis	180
4.1.4. The role of the PKD2 CC	180
4.2. Future work	181
4.2.1. Chapter 2	181
4.2.2. Chapter 3	182
4.3. Conclusion	186
Chapter 5: Materials and methods	188
5.1. Mouse work	188
5.1.1. Mouse handling	188

Table of contents

5.1.2. Background and lines	189
5.1.3. Histology and µCT	190
5.1.4. Genotyping	190
5.2. Tissue culture	191
5.2.1. Cell thawing	191
5.2.2. Freezing cell stocks	191
5.2.3. Counting cells	192
5.2.4. Passaging	192
5.2.5. HEK293T line maintenance and handling	193
5.2.6. COS-7 line maintenance and handling	193
5.2.7. mIMCD3 line maintenance and handling	194
5.3. Immunofluorescence	194
5.4. Biochemistry	195
5.4.1. Coimmunoprecipitation using sepharose beads	195
5.4.2. Coimmunoprecipitation using kit	198
5.4.3. Western blotting	198
5.5. Molecular biology	199
5.5.1. PCR amplification	199
5.5.2. PCR-based mutagenesis	199
5.5.3. Agarose gel electrophoresis	201
5.5.4. RNA extraction	201
5.5.5. cDNA generation	202
5.5.6. Bacterial transformation	202
5.5.7. DNA purification	202
5.5.8. Restriction digest	202
5.5.9. Ligation	203
5.5.10. Sequencing	203
5.5.11. Constructs used	203
5.6. Bioinformatics	203
Bibliography	207
Appendix 1: Figures	223
Appendix 2: Tables of µCT data	255

Chapter 1: Introduction

1.1. Overview

In 2010, pleiotropy celebrated a century since its first formal postulation in the scientific literature by the German geneticist Ludwig Plate (Stearns, 2010). Pleiotropy refers to a situation in which a single gene plays a role in two or more apparently unrelated phenotypic traits. Despite the century-long study behind pleiotropy, the numerous genome projects and extensive cataloguing, there are no systematic ways of determining whether genes qualify as pleiotropic, without phenotypic analysis.

Confusingly, the scientific literature employs the term pleiotropy in reference to multiple, distinct but overlapping, phenomena: molecular gene pleiotropy, referring to the number of functions of a gene; developmental pleiotropy, addressing how particular mutations impact phenotype; and selectional pleiotropy, in which the effects of a mutation on separate aspects of fitness are assessed (Paaby and Rockman, 2013). In contrast, Hodgkin approaches these phenomena differently in an attempt to assess how mutations impact molecular function, resulting in a list of seven types of pleiotropy (Hodgkin, 1998). For the purposes of this work, I take the liberty of defining two very broad categories of pleiotropy, encompassing some of Hodgkins' own categories and focusing on developmental and molecular pleiotropy: spatial pleiotropy, whereby a gene has various functions – similar or differing – in multiple tissues at the same time; and temporal pleiotropy, whereby a gene plays a role in multiple processes at different points in time. The gene encoding insulin is a good example of spatial pleiotropy; aside from its clearly defined endocrine role in regulating blood glucose concentration, it is also produced in brain cells where it is argued that it could play roles in memory, cognition and feeding behaviour (Blázquez et al., 2014). The absolute requirement of certain genes early on in development has hindered the study of their roles at later stages. The advent of inducible knockouts has allowed the study of the function of genes in cases where they might play multiple

important roles at different developmental timepoints. One striking example is that of the gene encoding sonic hedgehog, which participates in formation of midline structures, neural tube patterning and limb morphogenesis at different stages of the developmental process in the mouse embryo (Varjosalo and Taipale, 2008).

The focus of my thesis is the protein encoded by the mouse polycystic kidney disease 2 (*Pkd2*) gene and its roles in establishing left-right (L-R) asymmetry, as well as autosomal dominant polycystic kidney disease (ADPKD). In the early mouse embryo, the symmetry of the L-R axis is broken to yield a left- and right-side of the embryo that are different with regards to gene expression patterns and biochemical signalling events, and then later in the morphology and arrangement of the internal organs. Polycystic kidney disease, in its autosomal dominant form, causes fluid-filled sacs called cysts to develop in the kidneys, which leads to the impairment of renal function, as well as other organs, including the liver and pancreas. In humans, cysts typically develop throughout the lifetime of the affected individual, leading to renal failure on average by age 60 (Hateboer et al., 1999). The earliest stage at which the hallmark of ADPKD can be seen in the mouse embryo – appearance of cysts – is more than a full week later than the establishment of L-R asymmetry (Lu et al., 1997, Wu et al., 2000). Though the two areas of interest for my thesis are well-separated by time and tissue identity, both phenomena involve the cation-permeable channel polycystic kidney disease 2 (PKD2) and its interaction with different – but related – binding partners.

The roles played by PKD2 are numerous, participating in skeletal, cardiovascular and lymphatic system development (Wu et al., 2000, Garcia-Gonzalez et al., 2010, Xiao and Quarles, 2010, Outeda et al., 2014). The various roles played highlight its spatial and temporal pleiotropy. Historically, PKD2 was first identified in the context of ADPKD. Mutations in two loci in the human genome were found to be causative of ADPKD: *PKD1* and *PKD2* (Mochizuki et al., 1996, Ward et al., 1996). The proteins encoded by these loci were shown to interact (Tsiokas et al., 1997, Qian et

al., 1997) and the interaction of these two proteins is argued to be central to renal tubule development and homeostasis, as evidenced by genetic studies involving mouse mutants for *Pkd1* and *Pkd2*, which display polycystic kidneys (Lu et al., 1997, Wu et al., 1998a, Wu et al., 2000, Wu et al., 2002). The PKD1-PKD2 complex is thought to control intracellular signalling events regulating cell proliferation, potentially in response to renal tubule fluid flow (Hanaoka et al., 2000, Nauli et al., 2003, Li et al., 2005a). The physical interaction of the two is thought to be central to the biological role of the complex, as mutations in regions proposed to be central for the interaction of PKD1 and PKD2 – the C-terminal coiled-coil (CC) domains of either protein (**Fig. 1.1**) – lead to ADPKD (Torres et al., 2007, Harris and Torres, 2009). Subsequently, the role of PKD2 in L-R asymmetry was discovered in the mouse (Pennekamp et al., 2002, McGrath et al., 2003), then zebrafish (Bisgrove et al., 2005). Unlike for ADPKD, this action of PKD2 was shown to be independent of PKD1 (Karcher et al., 2005). Later studies showed that *Pkd1l1*, encoding a close paralog of PKD1, substitutes for PKD1 in L-R determination in mouse (Vogel et al., 2010, Field et al., 2011) and medaka fish (Kamura et al., 2011). Subsequent studies established that mutations in *PKD2* and *PKD1L1* underlie some cases of human *situs* defects (Bataille et al., 2011, Vetrini et al., 2016).

By comparison to the PKD1-PKD2 complex, the PKD1L1-PKD2 complex remains understudied at the molecular level, though genetic data has provided some indications regarding their roles in the early stages of L-R asymmetry establishment (Field et al., 2011, Grimes et al., 2016). Biochemical experiments have suggested that the interaction of the complex occurs through the CC domains of the two proteins (Field et al., 2011), whilst *in vitro* studies have indicated that PKD1L1 can facilitate flow-sensation (Grimes et al., 2016). The PKD1L1-PKD2 complex is thought to activate intracellular signalling in response to directional flow across the node, a transient midline embryonic structure important for L-R establishment. This indicates that

the PKD1L1-PKD2 and PKD1-PKD2 complexes may play similar roles in different contexts – initiating intracellular signalling events in response to extracellular fluid flow.

Given the homology of PKD1 and PKD1L1 (**Fig. 1.1**), their analogous function as putative regulators of PKD2, I set out to determine the differences and similarities at the molecular level between the two complexes: PKD1-PKD2 and PKD1L1-PKD2, by focusing on PKD2. Through this approach, the present study also addresses the pleiotropic nature of PKD2 and how it is able to serve different biological roles.

1.2. The polycystin family of proteins

Polycystins are a family of transmembrane proteins within the transient receptor potential (TRP) superfamily (see section **1.2.1**). This family was first identified when two distinct loci were found to be causative of ADPKD, a disease characterized by formation of fluid-filled cysts within the renal tubule, ultimately leading to renal failure. These loci encode polycystic kidney disease 1 (PKD1) and PKD2 (Mochizuki et al., 1996, Ward et al., 1996), the "flagship" members of this family. Aside from their role in ADPKD (see section **1.4**), PKD1 and PKD2 are also hypothesised to participate in skeletal, cardiovascular and lymphatic system development (see section **1.5**). In spite of their homology, the proteins differ principally in size and domain composition (**Fig. 1.1**). Later studies identified other members within the same family, in close homology to *PKD1* or *PKD2*: PKD1L1 (Yuasa et al., 2002), PKD1L2, PKD1L3 (Li et al., 2003) and PKDREJ (Hughes et al., 1999); PKD2L1 (Nomura et al., 1998, Wu et al., 1998b) and PKD2L2 (Veldhuisen et al., 1999), respectively. Thus, the family can be broadly split into two sub-groups, based on the size of the genes and size and structure of the proteins, respectively: PKD1- and PKD2-like.

The first group, the PKD1-like proteins, contains proteins that have a large, extracellular N-terminal region, 11 transmembrane domains (TM), and an intracellular C-terminal region. The PKD1-like proteins are more than double the size of their PKD2-like paralogs. However, they do share homology with the PKD2-like proteins in their six C-terminal TMs and contain the large polycystin/mucolipin-specific extracellular loop between the first and second homologous TMs (Pan et al., 2011, Shen et al., 2016, Grieben et al., 2017). The PKD2-like sub-group consists of proteins that have a typical TRP structure, consisting of six TM and two N- and C-terminal intracellular regions (**Fig. 1.1**).

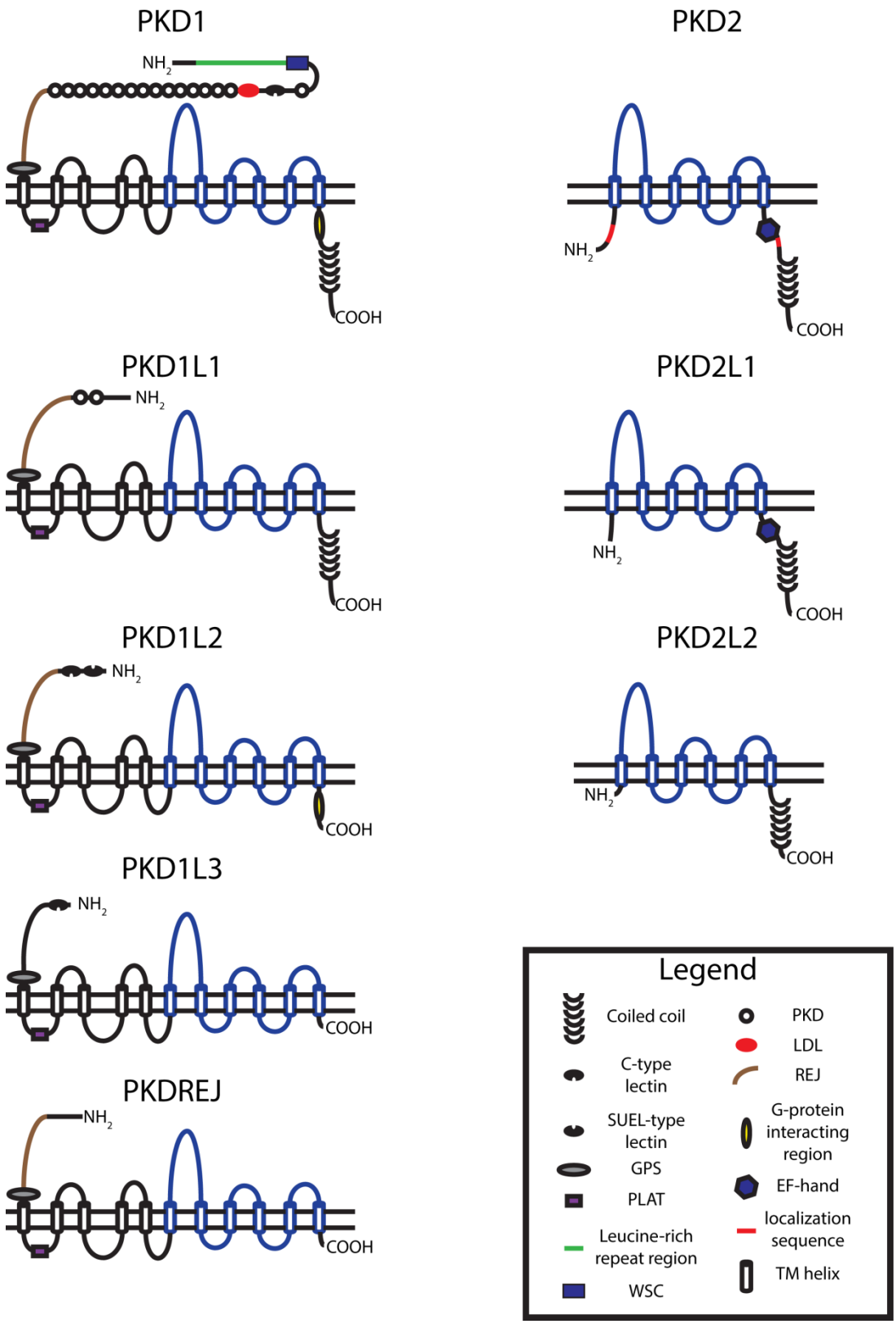


Figure 1.1: The polycystin family of proteins. The domain composition of each protein is based on data available on UniProtKB database. The segments highlighted in blue represent areas of homology specific to the polycystin family. The diagrams are inspired by figures found in (Torres and Harris, 2009).

With respect to nomenclature, PKD1 and PKD2 were initially also known as transient receptor potential polycystin 1 and 2 (TRPP1 and TRPP2), as well as polycystin-1 and polycystin-2 (PC1 and PC2), respectively. However, despite the homology between PKD2 and PKD1 (and their paralogs), and due to the differences in protein structure, gene size and an apparent lack of channel activity of PKD1 proteins, the International Union of Basic and Clinical Pharmacology/British Pharmacological Society (IUPHAR/BPS) Guide to Pharmacology nomenclature excludes PKD1 and PKD1-like proteins from the TRP superfamily (Wu et al., 2010, Hellmich and Gaudet, 2014). Thus, according to IUPHAR, PKD2 (previously TRPP2) has been renamed TRPP1, PKD2L1 (previously TRPP3) is now TRPP2 and PKD2L2 (previously TRPP5) is dubbed TRPP3 (Wu et al., 2010). The field is confused currently, with respect to which nomenclature to use. Whilst the decision to rename the channels does have logical arguments behind it, this will only add to the confusion until a consensus is reached in the field. In order to prevent any confusion, I will be adhering to the genetic nomenclature, referring to the proteins as PKDx (e.g. PKD1, PKD2L1 etc.). See **Table 1.1** for nomenclature details.

Table 1.1: Nomenclature of the polycystin family members

Genetic nomenclature	TRPP	IUPHAR/BPS	Other
PKD1	TRPP1	Excluded from TRPP family	Polycystin-1 (PC1)
PKD1L1	–	Excluded from TRPP family	Polycystin-1-like 1 (PC1L1)
PKD1L2	–	Excluded from TRPP family	Polycystin-1-like 2 (PC1L2)
PKD1L3	–	Excluded from TRPP family	Polycystin-1-like 3 (PC1L3)
PKDREJ	TRPP4	Excluded from TRPP family	–
PKD2	TRPP2	TRPP1	Polycystin-2 (PC2)
PKD2L1	TRPP3	TRPP2	Polycystin-2-like 1 (PC2L1); polycystin-2-like
PKD2L2	TRPP5	TRPP3	Polycystin-2-like 2 (PC2L2)

1.2.1. The TRP superfamily

The TRP superfamily of proteins consists of membrane proteins that function as subunits of non-selective mono- and divalent cation channels. These channels display variable mono- and divalent cation permeability ratios, depending on which subunits comprise the channel. Members of this superfamily are conserved in fungi, animals and, potentially, chlorophyte algae (Wheeler and Brownlee, 2008, Nilius and Owsianik, 2011). The TRP superfamily is divided into two groups, comprising seven families: group 1 – TRPC (canonical), TRPV (vanilloid), TRPM (melastatin), TRPA (Ankyrin) and TRPN ("no mechanoreceptor"); and group 2 – TRPP (polycystin) and TRPML (mucolipin) (Wu et al., 2010, Li et al., 2011, Pan et al., 2011).

TRP proteins typically contain six TMs, a cation-permeable pore between TM5 and TM6 and intracellular N- and C-termini of variable length. These intracellular domains, together with the intracellular and extracellular loops, are involved in TRP protein function, channel assembly, activation and regulation (Wu et al., 2010, Li et al., 2011, Hellmich and Gaudet, 2014). Throughout this thesis, the transmembrane domains will be referred to as TMs – in the cited literature, they are often referred to as 'S', followed by their respective numbers.

Evidence currently supports the hypothesis that TRP channels assemble as tetramers of TRP subunits (Hoenderop et al., 2003, Mio et al., 2007, Zhang et al., 2009, Shen et al., 2016, Grieben et al., 2017). These channels are either homotetrameric – e.g. the PKD2 channel, formed by four PKD2 molecules (Shen et al., 2016, Grieben et al., 2017), or heterotetrameric – e.g. TRPC1-PKD2 channels (Zhang et al., 2009, Du et al., 2014).

1.2.2. PKD1

The largest member of the polycystin family is PKD1, a 4303 amino acid (AA) protein in human, or 4293 AA in mouse. The structure of the protein can be described as consisting of three

main regions: a large, N-terminal extracellular region; a membrane-spanning region, consisting of 11 TMs; and a small, intracellular C-terminal region (**Fig. 1.1**).

The extracellular region contains a number of protein motifs and domains: leucine-rich repeats flanked by cysteine-rich domains, a C-type lectin WSC (cell-wall and stress-response component) domain, low-density lipoprotein domain (LDL), as well as immunoglobulin-like PKD repeats. The leucine-rich repeat domains have been shown to facilitate cell-matrix interaction (Malhas et al., 2002, Markoff et al., 2007), whilst PKD domains are thought to mediate cell-cell adhesion (Streets et al., 2003). Further towards the membrane-spanning region are the receptor for egg jelly (REJ) domain and GPCR proteolytic site (GPS) motif. The GPS motif facilitates proteolytic cleavage of the extracellular region (Qian et al., 2002). This cleavage is argued to be required for function and intracellular transportation (see section **1.2.5.b**). Deletions of the REJ domain, partially or completely, as well as mutations within this domain, disrupt the proteolytic cleavage at the GPS motif and PKD1 function (Qian et al., 2002). The REJ domain is required for GPS cleavage, but has also been suggested to function in ion transport homeostasis (Moy et al., 1996).

The membrane-spanning region contains 11 TMs and has been suggested to be important for interacting with PKD2 (Salehi-Najafabadi et al., 2017). Furthermore, the first intracellular loop, between TM1 and TM2, contains a PLAT (Polycystin-1, Lipoxygenase and α-toxin) domain, required for membrane localisation of PKD1 (Xu et al., 2016). The region between TM6-TM11 bears homology to PKD2-like proteins and, by extension, TRP channels. Moreover, the extracellular loop between TM6-TM7 is able to bind to the extracellular loop between TM1-TM2 of PKD2 (Salehi-Najafabadi et al., 2017), and has been proposed to form a tetragonal opening for polycystin (TOP) domain, similarly to PKD2 (Grieben et al., 2017) – *vide infra*. The cation transport properties of channels containing a PKD1 subunit remain under debate. In contrast to PKD2-like proteins and potentially PKD1L3 (Yu et al., 2012), the pore-forming region of PKD1 – between

TM10-TM11, is hypothesised to block cation passage due to the presence of two arginine residues on TM11. The side-chains of these are predicted to lie on the pore axis, blocking the cation from passing through the pore (Grieben et al., 2017). This is consistent with previous findings that PKD1 alone is unable to form cation-permeable channels (Hanaoka et al., 2000). However, there is evidence that PKD1 overexpression is able to confer non-selective cation currents in the absence of PKD2 (Babich et al., 2004).

The cytosolic part of PKD1 contains a CC domain that has previously been shown to be necessary and sufficient for PKD1-PKD2 fragment interaction (Qian et al., 1997, Tsiokas et al., 1997, Tsiokas et al., 1999, Casuscelli et al., 2009, Zhu et al., 2011). The same CC contributes to interacting with SIAH1 (Kim et al., 2004). A putative G-protein activation site is also found in this region (Parnell et al., 1998), which allows PKD1 to modulate JNK and AP-1 activity through heteromeric G-proteins (Delmas et al., 2002, Parnell et al., 2002). The intracellular C-terminus also participates in regulating the CHOP pathway, by binding to the transcription factors TCF and CHOP, disrupting their interaction with p300 (Chauvet et al., 2004, Merrick et al., 2012). The PKD1-mediated regulation of JNK and CHOP pathway has been linked to controlling cell proliferation and apoptosis (Nishio et al., 2005, Merrick et al., 2012). Furthermore, the cytosolic C-terminus has been shown to interact with calmodulin, enabling PKD1 to respond to Ca^{2+} concentration (Doerr et al., 2016).

1.2.3. PKD2

The canonical interaction partner of PKD1, PKD2, is a 968 or 966 AA protein – in human or mouse, respectively – and functions as a non-selective cation channel. The protein contains N- and C-terminal intracellular regions, which flank a transmembrane region consisting of six TMs (**Fig. 1.1**).

The N-terminal cytosolic region contains a domain argued to be sufficient for PKD2 homo-oligomerization (Feng et al., 2008), as well as an RVxP ciliary trafficking motif (Geng et al., 2006). By contrast, in *C. elegans*, the N-terminal domain has been argued to not be necessary for ciliary localisation (Knobel et al., 2008). This region also contains a GSK-3 phosphorylation site, which has been shown to regulate PKD2 trafficking to the plasma membrane (Streets et al., 2006), and a fibrocystin interaction region (Kim et al., 2008), as well as a region required for the interaction with RyR2 (Anyatonwu et al., 2007).

The transmembrane region is homologous to the TRP family, consisting of six TMs with a voltage-sensor-like domain (VSLD) between TM1-4 and a pore region formed by the extracellular loop between TM5-6. The first extracellular loop, between the first two TMs, is typical of group 2 TRPs and, together with the second extracellular loop, forms a TOP domain; this is hypothesised to regulate the activity of the channel in response to physical and chemical stimuli (Grieben et al., 2017). Furthermore, the first extracellular loop has been shown to interact with PKD1 and PKD2 (Salehi-Najafabadi et al., 2017). A larger segment of the transmembrane region, from TM4 to TM6, was previously shown to be required for interaction with TRPC1 (Tsiokas et al., 1999). Curiously, two protein-protein interactions have been described to occur via the pore-forming region: HAX-1 is able to bind via the final extracellular loop (Gallagher et al., 2000), whilst a cysteine residue within the same region may be responsible for PKD2 homo-oligomerization (Feng et al., 2011).

The C-terminal cytosolic region has been studied more extensively, as it contains domains which are believed to be central to the regulation of PKD2 as a channel subunit and its interaction with other proteins. This region, much like the N-terminal cytosolic region, has been shown to interact with open RyR2 and regulate its activity (Anyatonwu et al., 2007), as well as interact with TRPC1 (Tsiokas et al., 1999), TRPV4 (Köttgen et al., 2008), CD2AP (Lehtonen et al., 2000), and PIGEA-14 (Hidaka et al., 2004). This region contains two EF-hand domains, only one of which

contains an active Ca^{2+}-binding site (Celić et al., 2008, Schumann et al., 2009b, Kuo et al., 2014). This domain is believed to control the activity and conformation of the cation channel, in response to Ca^{2+} concentration (Schumann et al., 2009a, Petri et al., 2010, Celić et al., 2012, Kuo et al., 2014, Yang et al., 2016, Yang and Ehrlich, 2016). Recently, Cryo-EM structures have been determined for PKD2 in different Ca^{2+}-bound states. These results suggest a role for Ca^{2+} binding to the pore of the channel as a putative regulatory mechanism of channel activity (Wilkes et al., 2017). The two mechanisms, in spite of their differences, are not mutually exclusive. Immediately C-terminal to the EF-hand lies an ER retention signal (Cai et al., 1999); truncated PKD2 proteins lacking the ER retention signal were only found localised to the plasma membrane (Chen et al., 2001, Delmas et al., 2004). This motif also contains a phosphorylation site, which is believed to regulate the trafficking of PKD2 to the plasma membrane or ER (Fu et al., 2008), as well as the calcium dependence of the channel activity (Cai et al., 2004). The CC domain has been the focus of a number of studies, as it has been shown to be necessary for PKD1-PKD2 fragment interaction. Although initially described as overlapping with the EF-hand domain (Qian et al., 1997, Knobel et al., 2008, Schumann et al., 2009a), mainly due to bioinformatics predictions, further analysis revealed that the CC is situated C-terminal to the ER retention signal (Tsiokas et al., 1997, Tsiokas et al., 1999, Casuscelli et al., 2009). Tsiokas and colleagues also determined that the region encompassing the CC can be divided into two, based on their distinct functions: an N-terminal part of the coil responsible for homo-oligomerization, and a C-terminal part responsible for hetero-oligomerization, namely, interaction with PKD1 and TRPC1 (Tsiokas et al., 1997, Tsiokas et al., 1999). Some of these results were later confirmed in other studies, by defining a minimal homo-oligomerization region (Molland et al., 2010), as well as a minimal PKD1-PKD2 hetero-oligomerization region (Giamarchi et al., 2010). These studies also established that PKD2 CC homo-oligomerization is required prior to interaction with PKD1 (Tsiokas et al., 1999, Giamarchi et al., 2010). The CC domain has also been implicated in other protein-protein

interactions, including with: IP_3R (Li et al., 2005b), CD2AP (Lehtonen et al., 2000) and PIGEA-14 (Hidaka et al., 2004).

Both PKD1 and PKD2 contain sites for post-translational modification throughout their length. These include sites for glycosylation (Harris et al., 1995, Cai et al., 1999, Hofherr et al., 2014, Inoue et al., 2014), myristoylation (Knobel et al., 2008) and phosphorylation (Cai et al., 2004, Knobel et al., 2008, Miyakawa et al., 2013). These post-translational modifications are required for normal function and trafficking of the two proteins (Cai et al., 1999, Newby et al., 2002, Hofherr et al., 2014, Inoue et al., 2014, Kim et al., 2014) (see section **1.2.5.b**).

1.2.4. Paralogs of PKD1 and PKD2

The PKD1 subgroup of polycystins in mouse and man consists of PKD1, PKDREJ, PKD1L1, PKD1L2 and PKD1L3. These proteins are larger in size than their PKD2-like counterparts: in human, PKD1L3, the smallest of the PKD1 paralogs, is 2201 AA, whilst PKD2, the largest of the PKD2 paralogs, is 968 AA. The PKD1-like proteins show more variability than their PKD2-like counterparts in terms of structure and domain composition, especially in their N-terminal extracellular regions (**Fig. 1.1**).

The extracellular regions of PKD1-like proteins vary in their domain composition between paralogs. Analysis of databases, such as UniProtKB and Ensembl, reveals some discrepancies in annotation between entries for the same protein. Bioinformatic analysis predicts all PKD1 paralogs to share PLAT and GPS domains. Curiously, the defining PKD domains vary greatly in number, or are absent (or unannotated) between PKD1 paralogs (**Fig. 1.1**). An entry in the InterPro database, dubbed PKD/REJ-like domain, defines the REJ domain, which is also present in PKDREJ, PKD1, PKD1L1, PKD1L2, but not PKD1L3, as containing tandem PKD-like domains. Given the fact that the sequence of the PKD1 REJ domain was initially described to not contain any repeating sequences or motifs (Moy et al., 1996), and that databases such as Ensembl annotate

PKD domains onto separate tracks, but not overlapping with the PKD/REJ-like domain, it is unlikely that the REJ domain contains PKD domains. Later studies established, through biophysical, structural and *in silico* methods, that the region corresponding to the REJ domain contains four FNIII domains, which are homologous to the Ig-like PKD domains (Schröder et al., 2011, Xu et al., 2013).

Previous studies have established, through glycosylation reporter assays, that PKD1 has 11 TMs (Nims et al., 2003). The 11 TM structure is likely shared by PKD1L1, according to initial bioinformatics predictions (Yuasa et al., 2002). This can also be seen on the annotation in Ensembl and UniProtKB. However, for PKD1L2 and PKD1L3, UniProtKB predicts 12 TMs, which is in contrast to the initial bioinformatics predictions for these proteins (Li et al., 2003). Given that 12 TMs would mean that the proteins have two cytoplasmic N- and C-terminal domains, much like PKD2 paralogs, a 12 TM conformation would represent a major difference in protein structure. Similarly, PKDREJ is predicted by Ensembl to have 13 TMs – this is more realistic, given that the protein would retain the extracellular N-terminal domain. However, in absence of further structural studies and in light of the fact that the initial studies describing PKD1-like proteins predicted an 11 TM conformation (Hughes et al., 1999, Yuasa et al., 2002, Li et al., 2003), the most parsimonious assumption is that the PKD1 paralogs all share 11 TMs. All PKD1 paralogs have homology to TRP channels in the last 6 TMs. However, convincing evidence is lacking that these PKD1-like proteins can contribute as subunits to cation-permeable channels, with the potential exception of PKD1L3 (Yu et al., 2012). Indeed, PKD1 and PKD1L1 are hypothesised to be involved in regulating TRPP channel activity, as opposed to directly participating in cation transport (Nauli et al., 2003, Nauli and Zhou, 2004, Grimes et al., 2016).

While the CC of PKD1 has been shown to be important for its function and proper sub-cellular localisation (see section **1.2.2** and **1.2.5.b**), not all PKD1 paralogs are predicted to have a CC, according to bioinformatic predictions. The studies initially describing PKD1L2 and PKD1L3

predicted that PKD1L2 does not have a CC domain, whilst PKD1L3 only had a weak CC signature, argued to be non-functional (Li et al., 2003). A later study established that the interaction between PKD1L3 and PKD2L1 does not require the CC of PKD2L1 (Ishimaru et al., 2010). Similarly to PKD1L2 and PKD1L3, PKDREJ has not been described to have a CC domain (Hughes et al., 1999).

PKD1L1 overview

Although smaller than PKD1, containing 2615 AA in mouse and 2849 AA in human, PKD1L1 also contains two PKD domains, as well as REJ, GPS, PLAT, alongside 11 TM domains and a CC domain, at the C terminus (Yuasa et al., 2002). Similarly to what has been argued for PKD1 (Ma et al., 2009), the PKD domains have been argued to be required for flow sensation, according to evidence from a combination of structural, biophysical and genetic analyses (Grimes et al., 2016). Furthermore, the CC domain has been argued to be sufficient for the PKD1L1-PKD2 interaction (Field et al., 2011). Like PKD1 (Parnell et al., 1998, Delmas et al., 2002, Parnell et al., 2002), PKD1L1 is hypothesised to act as a GPCR, as the first intracellular loop and C-terminal cytoplasmic end of the protein have been shown to interact with G-proteins (Yuasa et al., 2004).

The PKD2 sub-group of polycystins contains PKD2, PKD2L1 and PKD2L2. All three proteins share structural homology with TRP channels, containing six TMs, and an N- and C-terminal cytoplasmic region. The TOP domain, specific to polycystins, located in the first extracellular loop, can be found in all three proteins, as well as PKD1-like proteins (Grieben et al., 2017). Furthermore, evidence suggests that all three PKD2 paralogs are able to function as non-selective cation-permeable channels (Hanaoka et al., 2000, Chen et al., 2008, Yu et al., 2012, DeCaen et al., 2013). Both PKD2 and PKD2L1 are predicted to have an EF-hand and CC domain in the C-terminal cytoplasmic region, whilst PKD2L2 has only a small probability of CC formation and no EF-hand (Veldhuisen et al., 1999).

The biological roles of PKD1- and PKD2-like proteins are wide-ranging and these molecules can form complexes in different combinations: PKD1 and PKD2 are known to participate in kidney development, potentially by forming a mechanosensitive Ca^{2+}-permeable channel (Wilson, 2004, Torres and Harris, 2009). PKD2 also interacts with PKD1L1 in the mouse

embryonic node crown cells, where it is required for the proper establishment of the left side of the body; in this context, PKD1L1-PKD2 is hypothesised to mediate flow-induced Ca^{2+}-release (McGrath et al., 2003, Field et al., 2011, Grimes et al., 2016)**.** The PKD1L3-PKD2L1 complex may play a role in sour taste perception, as a cation channel (Ishimaru et al., 2006). The other members of the polycystin family are less-well characterised, with PKD2L2 believed to play a role in spermatogenesis (Chen et al., 2008) and PKD1L2 playing a role in mediating neuronal activity in distinct populations of neurons of the mouse spinal cord, in complex with PKD2L1 (Petracca et al., 2016), as well as being implicated in neuromuscular disease (Mackenzie et al., 2009). Finally, PKDREJ has been shown to localise to the plasma membrane of sperm in mice (Butscheid et al., 2006) and, whilst not absolutely required for fertility, has been shown to play an important role in sperm post-copulatory behaviour (Sutton et al., 2008). One study has suggested that the polycystin family as a whole may be important for various aspects of reproduction in mammals (England et al., 2017).

1.2.5. Molecular aspects

1.2.5.a. Aspects of molecular function of polycystins

The main GO term associated with all polycystin proteins is “calcium channel activity”, according to UniProtKB, a database for functional information on proteins. Current data indicates that there is a difference in function between the PKD1- and PKD2-like proteins. The first studies investigating the molecular function of polycystins focused on PKD1 and PKD2: when co-transfected together, the two proteins form a non-selective Ca^{2+}-permeable cation channel; however, neither protein is capable of producing currents by themselves (Hanaoka et al., 2000). Later studies established that PKD2, independently of PKD1, is able to form non-selective Ca^{2+}-permeable cation channels in *C. elegans* (Barr et al., 2001), as well as in CHO cells (Koulen et al., 2002). Members of the PKD2 sub-group are also able to self-regulate in response to voltage

and/or pH changes, as well as cation concentration. Recent studies have described that the first four TMs of PKD2 form a voltage sensor-like domain (VSLD) (Grieben et al., 2017), which may contribute to the voltage/pH sensitivity of PKD2 (Gonzalez-Perrett et al., 2002). Interestingly, a cluster of ADPKD-causing mutations in humans can be found in the TOP domain, which is formed by the N-terminal-most two extracellular loops of the VSLD (Grieben et al., 2017). The EF-hand, present in PKD2 and PKD2L1, is a known Ca^{2+}-binding domain situated in the cytoplasmic C-terminus of the protein. In the case of PKD2, this has been shown to be able to control the channel activity in response to Ca^{2+} concentration (Cai et al., 2004, Kuo et al., 2014). In contrast, the role of the EF-hand in regulating PKD2L1 channel activity has been debated by other studies (DeCaen et al., 2016). A recent study has shown that PKD2, independently of PKD1, functions as a cation channel within the primary cilium; although this channel is regulated by intraciliary Ca^{2+}, it preferentially conducts K^+ and Na^+ (Liu et al., 2018).

PKD1 paralogs contain more domains than their PKD2-like counterparts (*vide supra*). These are believed to allow the protein to facilitate different molecular functions, such as G-protein signalling (Parnell et al., 1998, Delmas et al., 2002), regulation of cell-cell adhesion complexes (Boca et al., 2007, Markoff et al., 2007), and potentially mechanosensation, in the case of PKD1 and PKD1L1 (Nauli et al., 2003, Ma et al., 2009, Grimes et al., 2016). Whether PKD1 paralogs actively participate in transporting cations across the membrane or just regulate the activity of the PKD2-like counterparts of the channel requires further investigation. The exception, according to one study, is that of PKD1L3 – mutations within the pore region of the protein are able to alter the ion selectivity of the PKD1L3-PKD2L1 channel. The same study has indicated, using photobleaching experiments, that the channel is composed of three PKD2L1 molecules and one PKD1L3 subunit (Yu et al., 2012).

The stoichiometry and interaction of polycystin complexes has been the subject of debate in the field for some time. Initial structural studies employed nuclear magnetic resonance (NMR)

and focused on the CC region of PKD2: these had shown that the C-terminal end of PKD2 is able to form trimers (Yu et al., 2009) – later confirmed by a separate study (Yang et al., 2015). A separate study confirmed that the PKD1 CC is able to bind to the PKD2 trimer (Zhu et al., 2011). The results of these studies were problematic for two reasons: 1) they contradicted the widely-held hypothesis that TRP channels assemble in a tetrameric fashion; 2) the studies focused on the C-terminal CC, thereby excluding other putative interaction domains. For further discussion on this, see (Kobori et al., 2009, Yang and Ehrlich, 2016). Further studies challenged this trimeric assembly, either through directly investigating the volumes and shapes of the PKD2 complexes through atomic force microscopy (AFM) (Kobori et al., 2009, Zhang et al., 2009), or through biochemical methods employing the full-length molecule (Feng et al., 2008, Feng et al., 2011). Recently, two separate studies have described the structure of PKD2 and the tetrameric assembly of the PKD2 channel (Shen et al., 2016, Grieben et al., 2017). Given the availability of these structures and the data presented so far, one further question remains to be addressed regarding the interaction of PKD1- and PKD2-like proteins to form complexes: does the PKD1 subunit replace a PKD2 subunit in the tetrameric channel, as in the case of PKD1L3-PKD2L1 (Ishimaru et al., 2010), or does a PKD2 homotetramer interact separately with PKD1 molecules (Feng et al., 2011)? The molecular functions associated with each region or domain of PKD2 are summarised in **Table 1.2**.

1.2.5.b. Sub-cellular localisation and trafficking

The majority of data regarding the localisation of polycystin proteins comes from studies involving the PKD1-PKD2 complex in cells, where it is suggested to function as a flow-responsive Ca^{2+} channel during renal development (Nauli et al., 2003, Nauli and Zhou, 2004). This complex has been described to be localised to the plasma and ciliary membrane (Ward et al., 2011, Hoffmeister et al., 2011), as a mature complex, as well as in the ER (Kim et al., 2014, Gainullin et al., 2015) and Golgi network (Kim et al., 2014) (**Fig. 1.2**).

Table 1.2: Summary of functions associated with domains in PKD2

Region	Sub-region/domain	Function
N-terminal	• RVxP motif	Ciliary localisation
	• N-terminal interaction domain	Homo-oligomerization
	• GSK-3 phosphorylation site	Trafficking
	• Fibrocystin interaction region	Hetero-oligomerization
	• RyR2 interaction region	Hetero-oligomerization
Transmembrane	• TM1-4	VSLD
	• First extracellular loop	Homo- and hetero-oligomerization, channel activity regulation
	• Second extracellular loop	Channel activity regulation
	• TM4-TM6	Hetero-oligomerization
	• Third extracellular loop	Cation transport, channel activity regulation, homo- and hetero-oligomerization
C-terminal	• EF-hand	Channel activity regulation
	• ER retention signal	Trafficking
	• N-terminal CC sub-region	Homo-oligomerization
	• C-terminal CC sub-region	Hetero-oligomerization

The PKD1-PKD2 interaction results in post-translational modifications, which are required for further trafficking; these modifications include: cleavage of PKD1 extracellular N-terminus and glycosylation of PKD2 and PKD1 (Kim et al., 2014, Kurbegovic et al., 2014, Gainullin et al., 2015). The requirement of the PKD1-PKD2 interaction for proper sub-cellular localisation has been described to be important for both PKD1 (Kim et al., 2014, Su et al., 2015), as well as PKD2 (Nauli et al., 2003). However, PKD2 can traffic independently of PKD1 to a number of compartments (*vide infra*). Furthermore, the requirement of the PKD1-PKD2 interaction and specific PKD1 post-translational modifications for ciliary trafficking has been debated by some studies. Cai and colleagues have shown that PKD1 mutant proteins that are unable to interact with PKD2 or undergo GPS-cleavage can localise to the cilium (Cai et al., 2014). It is possible that PKD1 by itself may also have a separate trafficking pathway from the PKD1-PKD2 complex, which might account for the differences in requirements reported (Cai et al., 2014, Kim et al., 2014, Su et al., 2015). Moreover, PKD1 has been described to localise to adherens junctions (Xu et al., 2015), which potentially explains the role of PKD1 in cell-cell adhesion described by earlier studies (Streets et al., 2003).

Whilst the two proteins are often studied in the context of their interaction, PKD2 is also found, independently of PKD1, within the ER, or at the plasma membrane. The trafficking of PKD2 to these two locations is dependent on interaction with PACS-1 or PACS-2, respectively (Köttgen et al., 2005), and the subsequent phosphorylation of PKD2. Work in zebrafish embryos has shown that defects in sub-cellular trafficking of Pkd2 to specific compartments are linked to L-R defects and kidney cyst formation. Specifically, $Pkd2^{S812A}$, which lacks the phosphorylatable serine residue required for ER retention, is able to rescue body curvature and *situs* anomalies, as well as the cystic kidney phenotypes observed in Pkd2-depleted zebrafish embryos. Conversely, $Pkd2^{S812D}$, a protein which resembles the phosphorylated form of Pkd2, is retained in the ER and does not rescue the cystic phenotype observed in Pkd2-depleted embryos, but rescues body curvature and

L-R phenotypes (Fu et al., 2008). The trafficking of PKD2 to various subcellular compartments may also depend on the glycosylation of the protein, as PKD2 molecules that are differentially glycosylated localise to different compartments (Cai et al., 1999); similarly, PKD1 sub-cellular distribution also varies with glycosylation (Cai et al., 2014). Golgi localisation of PKD2 has been shown to occur via interaction with PIGEA-14, via the CC domain of PKD2 (Hidaka et al., 2004).

In the case of the PKD1L1-PKD2 complex, ciliary trafficking has been suggested to occur independently of the PKD1L1-PKD2 interaction. The $PKD2^{E442G}$ protein, which is unable to reach the cilium (Yoshiba et al., 2012), should still interact with PKD1L1, as it bears a mutation in a different region of the protein than the CC, a domain sufficient for the PKD1L1-PKD2 interaction (Field et al., 2011). However, further studies have shown that PKD2 localises less efficiently to nodal cilia, in the absence of PKD1L1 (Grimes et al., 2016). Furthermore, $PKD2^{L703X}$, a protein unable to interact with PKD1, can localise to the cilium without interacting with PKD1. These studies indicate that PKD2 is also able to traffic to the cilium independently of PKD1 or PKD1-like proteins (Geng et al., 2006). The ciliary transport of PKD2 from the Golgi complex likely occurs via proteins such as IFT20, GMAP210, BLOC-1 and TULP3 (Follit et al., 2006, Follit et al., 2008, Badgandi et al., 2017, Monis et al., 2017), whilst PKD1 is believed to be trafficked to the cilium independently of PKD2 (Cai et al., 2014, Kim et al., 2014, Gainullin et al., 2015).

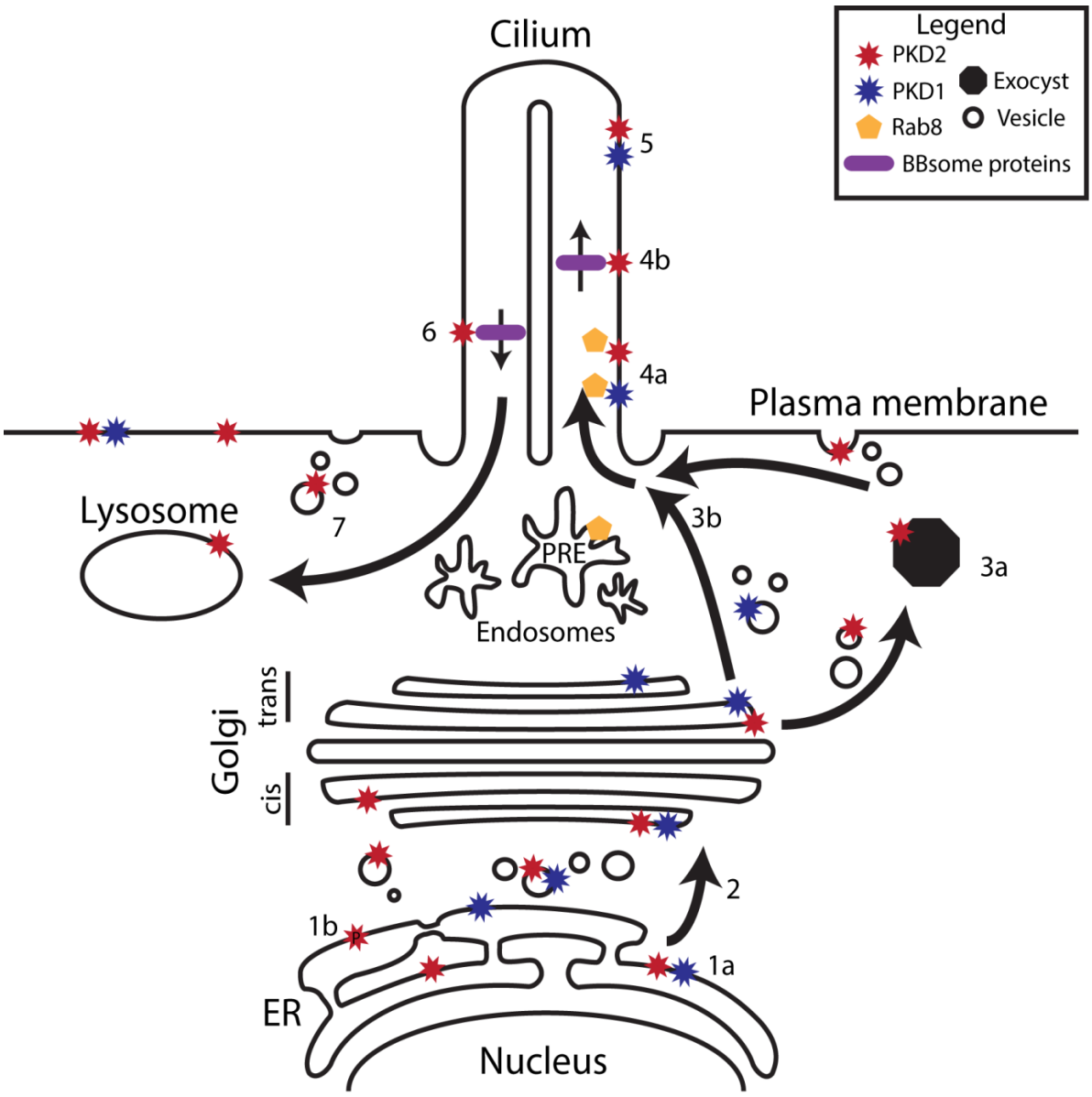


Figure 1.2: Trafficking of PKD1 and PKD2. PKD1 (blue) and PKD2 (red) are produced in the endoplasmic reticulum (ER), where they also interact (1a), leading to the cleavage of the N-terminal region of PKD1. At this stage, PKD2 can also be phosphorylated and retained in the ER (1b). The two proteins are then transported to the cis-Golgi (2) and through the Golgi network. From the trans-Golgi onwards, PKD2 can be transported to the exocyst (black) (3a), and from there to the plasma and ciliary membrane. Alternatively, PKD1 and PKD2 are transported to the plasma membrane (3b) and, through interacting with Rab8 (yellow), which is activated in the proximal recycling endosome (PRE), are trafficked to the ciliary membrane (4a). PKD2 can also traffic through the cilium with the help of BBsome proteins (purple) (4b). PKD1 and PKD2 interact once localised to the cilium (5). Retrograde transport of PKD2 is mediated by BBsome proteins (6) and, upon exiting the cilium, PKD2 is trafficked to the lysosome for degradation (7). Figure adapted from (Avasthi et al., 2017).

1.3. Laterality

Whilst we are superficially symmetric between the left and right sides of the body, there is an observable difference and asymmetry in the arrangement of internal organs. In vertebrates, examples of asymmetrically-patterned organs include the heart, with the apex positioned on the left side, the left and right lungs, which have different lobation patterns, and the positioning of the stomach and spleen on the left side of the body. This asymmetric pattern, dubbed *situs solitus*, is conserved within a species, but also across most vertebrate species, arguing for an ancient origin for L-R asymmetry. However, conditions exist in which L-R patterning is perturbed. Examples include *situs inversus totalis*, in which all of the organs are in a mirror image to their normal arrangement, or *situs ambiguus*, in which the arrangement of one or more organs is perturbed in relation to other organs. Such conditions are described in association with diseases that include Kartagener syndrome, Ivemark syndrome and the ciliopathies (Sutherland and Ware, 2009). Furthermore, L-R patterning defects are associated with congenital heart disease (Afzelius, 2004, Li et al., 2015). In extreme cases, abnormal L-R patterning results in embryonic lethality, presumably due to heart defects (Ramsdell, 2005, Peeters and Devriendt, 2006, Li et al., 2015).

1.3.1. Development of organ asymmetries in the mouse embryo

In mice, asymmetries in organ patterning are preceded by asymmetric gene expression. The identity of the left side of the body is established through the *Nodal* cascade (reviewed in Nakamura et al., 2006), whilst an antagonistic BMP pathway has been hypothesised to play a similar role for the right side of the body (Patel et al., 1999, Murray and Gridley, 2006, Ocaña et al., 2017). These pathways are activated in the left and right lateral plate mesoderm (LPM), respectively, at 8.5 *dies post coitum* (dpc). In the left LPM, activation of *Pitx2* acts to translate asymmetric gene expression into asymmetric organogenesis. PITX2 plays an important role in atrial patterning, as well as acting as a left determinant affecting multiple organs, but not gross

cardiac *situs* (Campione et al., 2001, Liu et al., 2001). Upstream of *Pitx2*, *Nodal* is activated in the left LPM. NODAL activates itself, *Pitx2* and *Lefty2*, an inhibitor of *Nodal* activation. Together with LEFTY1, LEFTY2 acts to restrict NODAL signalling to the left side of the embryo, in a reaction-diffusion system dubbed Self-Enhancement Lateral Inhibition (reviewed in Nakamura et al., 2006, Nakamura et al., 2012).

In mouse, the activation of the NODAL cascade in the left LPM depends on the *Nodal* expression around a transient embryonic structure, dubbed the node (Brennan et al., 2002). This is a pit of 200-300 cells, most of which have a motile cilium. This structure appears around 7-7.5 dpc on the ventral side of the embryo; it is located at the anterior end of the primitive streak and is contiguous with the notochord (Blum et al., 2009). Like the LPM, the node also shows patterns of asymmetric gene expression, the first being that of *Cerl2*, followed by expression of *Nodal*. Both *Cerl2* and *Nodal* are expressed on the left and right sides of the node, showing opposite expression patterns: *Cerl2* stronger on the right, *Nodal* stronger on the left. CERL2 acts to inhibit NODAL signalling (Marques et al., 2004), allowing greater signalling power for NODAL on the left side of the node.

The mechanism by which asymmetric events around the node activate NODAL expression in the LPM is still being debated. Two distinct, but not mutually exclusive, hypotheses have been proposed to explain this. One hypothesis posits that NODAL protein from the node is transported through the extracellular matrix of the paraxial mesoderm, to the left LPM, where it directly activates *Nodal* (Oki et al., 2007). The second hypothesis states that the Ca^{2+} response to flow at the node (*vide infra*) is propagated through the endoderm via gap junctions and leads to the activation of NODAL in the LPM (Viotti et al., 2012, Saund et al., 2012). For a more detailed discussion of the two hypotheses, see (Norris, 2012).

The asymmetric peri-nodal expression of *Cerl2* and *Nodal* lie downstream of a mechanical event: fluid flow. Due to the posterior tilt and clockwise rotation of the motile cilia, a leftward fluid flow is generated across the nodal cavity. Experiments subjecting *Dnah11*$^{iv/iv}$ mouse embryos, which lack flow and show randomisation of *situs*, to artificial flow provide evidence that the directionality of flow establishes the "left" identity. Embryos were also subjected to rightward fluid flow and developed *situs inversus* (Nonaka et al., 2002). Considering this data, it is accepted in the field that the initial event in mouse embryos leading to establishment of L-R asymmetry is the leftward fluid flow, generated by nodal cilia. Given that mutations in genes encoding proteins required for ciliary motility are associated with defects in L-R patterning in humans (Kartagener, 1935, Brueckner, 2007), it is likely that an equivalent mechanism is acting in humans.

Three competing hypotheses currently aim to describe how nodal flow is detected and interpreted. The 'morphogen hypothesis' proposes that a short-lived molecule becomes enriched, by flow, on the left side of the node (Nonaka et al., 1998). Experimental and *in silico* investigation argue that this hypothesis is plausible in the context of morphogens between 15 and 50 kDa in size (Cartwright et al., 2004, Okada et al., 2005); the morphogen and relevant receptors, however, remain to be identified. A second, related, hypothesis claims that FGF signalling induces the release of vesicles, dubbed 'nodal vesicular parcels' (NVPs), carrying morphogens, such as SHH and RA to the left side of the node. This similarly establishes a differential concentration of morphogens between the left and right sides, resulting in asymmetric gene expression. This hypothesis is based on the observations made in one paper (Tanaka et al., 2005), describing NVPs, and has been contested by the field, as the physical characteristics of NVPs and mechanism of delivery of morphogens remain unknown (Cartwright et al., 2008). The third hypothesis posits direct mechanosensation of nodal flow and was originally called the two-cilia hypothesis. This argues that flow created by motile cilia is detected by immotile cilia on the crown cells, which surround the node. In response to flow, PKD2 acts to induce an intracellular Ca^{2+} influx, which

results in an asymmetric Ca^{2+} signal at the left edge of the node; mouse embryos lacking PKD2 do not elicit this Ca^{2+} response (McGrath et al., 2003). A later study confirmed these findings, as well as showing that PKD2 localisation to crown cell cilia is required for proper L-R differentiation (Yoshiba et al., 2012). This asymmetric Ca^{2+} influx has been suggested to play a direct role in repressing CERL2 production through degradation of its mRNA (Nakamura et al., 2012) and is correlated with asymmetric *Nodal* expression around the node (Yoshiba et al., 2012). In summary, the two-cilia model hypothesises that fluid flow, detected by immotile cilia at the periphery of the node, leads to asymmetric peri-nodal Ca^{2+} signalling, as well as to downregulation of *Cerl2* and relief of inhibition of *Nodal* on the left side of the node. Despite this, the direct involvement of Ca^{2+} in peri-nodal asymmetric gene expression remains to be tested, as well as whether Ca^{2+} influx in nodal crown cell cilia occurs through PKD2. One study has shown that the initial Ca^{2+} influx occurs in the cilioplasm, in zebrafish embryos, which then leads to intracellular Ca^{2+} influx (Yuan et al., 2015). This has subsequently been contested by a study claiming that Ca^{2+} influx following flow occurs in the cytoplasm and only subsequently back-fills into cilia (DeCaen et al., 2013, Delling et al., 2016). This work also questions whether ciliary Ca^{2+} is the direct molecular response to mechanical flow (Delling et al., 2016).

It is important to mention that the mechanism of L-R development shows conservation throughout the vertebrate lineage and beyond. On one hand, the asymmetrically activated *Nodal-Pitx2* cascade plays a role in breaking L-R symmetry in vertebrates, as well as other animal lineages, including snails and lancelets (reviewed in Blum and Ott, 2018). In spite of the conservation of the asymmetrically expressed *Nodal-Pitx2* pathway in establishing *situs*, the upstream mechanisms appear to be more divergent. Whilst most vertebrates appear to employ cilia-driven flow to break symmetry, certain vertebrate lineages (avian and potentially reptiles) do not (Blum and Ott, 2018). In spite of the differences in L-R symmetry-breaking, it is likely that L-R organ asymmetries evolved from a single origin and diverged throughout evolution.

1.3.2. Abnormal *situs* development

Mutations in proteins which affect specific processes have been shown to cause *situs* defects. Firstly, mutations in genes required for ciliogenesis, such as *Kif3a* and *Kif3b* (Nonaka et al., 1998, Marszalek et al., 1999, Takeda et al., 1999), lead to loss of cilia and randomisation of *situs*. Secondly, mutations affecting ciliary motility, such as *Dnah5* or *Dnah11*, cause abnormal or absent nodal flow, resulting in randomised *situs* (Olbrich et al., 2002, Nonaka et al., 2002). Thirdly, mutations affecting the perception and response to flow impact *situs* development. Mutations in *Pkd2* lead to *situs* phenotypes in mouse and zebrafish (Pennekamp et al., 2002, Bisgrove et al., 2005, Obara et al., 2006, Ermakov et al., 2009), and in human (Bataille et al., 2011). Similarly, *Pkd1l1* mutations lead to abnormal L-R development in mouse and medaka fish (Vogel et al., 2010, Field et al., 2011, Kamura et al., 2011), as well as human (Vetrini et al., 2016) (see section **1.3.3**). Fourthly, the transmission of the asymmetrically-activated signal from the node to the LPM is also highly important. Xenopus embryos with decreased levels of *connexin26* in display L-R defects (Beyer et al., 2012). These genes encode gap junction proteins, which are required for relaying the asymmetric signals from the L-R organiser to the LPM (Viotti et al., 2012, Saund et al., 2012). Similarly, failure to correctly form definitive endoderm in *Sox17* mutants results in normal peri-nodal asymmetric gene expression, but absent asymmetric LPM gene expression (Kanai-Azuma et al., 2002), potentially due to loss of gap junctions (Viotti et al., 2012, Saund et al., 2012). The ECM of the paraxial mesoderm, which lies beneath the endoderm, has been argued to be required for the transmission of the asymmetric signal from the node to the LPM. Pharmacological inhibition of ECM biosynthesis in cultured embryos leads to loss of *Nodal* expression in the LPM (Oki et al., 2007).

1.3.3. The role of PKD1L1 and PKD2 in breaking embryonic L-R symmetry

Both PKD1L1 and PKD2 have been shown to traffic to cilia. For PKD2, this has been demonstrated in mouse nodal cilia (McGrath et al., 2003) and cilia of the zebrafish Kupffer's Vesicle (KV), the analogous structure in zebrafish (Roxo-Rosa et al., 2015). In contrast, PKD1L1 has only been shown to localise to cilia *in vitro* (Field et al., 2011), or to cilia of the medaka fish KV (Kamura et al., 2011). However, the mouse *Pkd1l1* gene is expressed in the node, consistent with PKD1L1 localisation to nodal cilia (Field et al., 2011). It has been shown that PKD2 localisation to mouse nodal cilia is required for proper L-R asymmetry establishment (Yoshiba et al., 2012). Despite this, in the zebrafish, a Pkd2 mutant protein unable to traffic to the cilium can rescue the *situs* phenotype of *pkd2*-deficient embryos (Fu et al., 2008).

Genetic studies have firmly established the involvement of both *Pkd1l1* and *Pkd2* in L-R development, in mouse and other model organisms (Pennekamp et al., 2002, Bisgrove et al., 2005, Vogel et al., 2010, Field et al., 2011, Kamura et al., 2011), as well as human (Bataille et al., 2011, Vetrini et al., 2016). A study in the mouse characterising a null allele of *Pkd1l1* showed that adult *Pkd1l1*$^{tm1Lex/tm1Lex}$ mice display L-R patterning defects (Vogel et al., 2010). A second study analysed an ENU-derived mutant allele, *Pkd1l1*^{rks}, demonstrating that *Pkd1l1* was required for embryonic *situs* development (Field et al., 2011). In tandem with the second study, another group characterised a *pkd1l1* point mutant in the medaka fish, again showing the involvement of *pkd1l1* in *situs* determination (Kamura et al., 2011). Interestingly, *Pkd1l1*$^{rks/rks}$ embryos recapitulated the defects seen in *Pkd2*$^{E442G/E442G}$ (Ermakov et al., 2009) and *Pkd2*$^{tm1Dwo/tm1Dwo}$ – *Pkd2* null – embryos (Pennekamp et al., 2002). Namely, the *Pkd1l1*$^{rks/rks}$ embryos displayed right lung isomerism and aberrant expression of L-R markers, despite having normal nodal cilia motility (Field et al., 2011). Together, these facts suggest that *Pkd1l1* and *Pkd2* act downstream of flow, but upstream of gene expression asymmetries. Considering: 1) previously published data on PKD1-PKD2 (Nauli et al., 2003) argues that this complex facilitates a flow-induced Ca^{2+} signal in renal cells; 2) the

homology between PKD1 and PKD1L1; and 3) data showing the correlation between asymmetric peri-nodal Ca^{2+} signalling and normal L-R determination (McGrath et al., 2003), it seemed reasonable to modify the two-cilia hypothesis (see section **1.3.1**) to include the PKD1L1-PKD2 complex as a potential flow sensor/interpretor. However, *Pkd1l1*$^{tm1Lex/tm1Lex}$ embryos, bearing a null allele of *Pkd1l1*, display a different phenotype from *Pkd1l1*$^{rks/rks}$ embryos: homozygous *Pkd1l1* null embryos have a tendency towards left isomerism (Grimes et al., 2016). The opposite phenotypes of the *Pkd1l1*$^{tm1Lex/tm1Lex}$ and *Pkd2*$^{tm1Dwo/tm1Dwo}$ embryos, together with the epistatic analysis to order the sequence of roles for these genes (Grimes et al., 2016), argue that *Pkd2* is repressed by *Pkd1l1*, which in turn is repressed by flow.

The elevation of intracellular Ca^{2+} levels on the left side of the node provides a readout for flow in the mouse embryonic node (McGrath et al., 2003). This Ca^{2+} spike then spreads out towards the LPM (McGrath et al., 2003, Viotti et al., 2012). The exact mechanism by which Ca^{2+} leads to the activation of the asymmetric gene expression cascade remains poorly characterised. A study provides evidence that flow regulates *Cerl2* expression at the node, in response to flow and Wnt signalling (Nakamura et al., 2012). In addition, complementation analysis demonstrates that *Pkd2* lies upstream of *Cerl2* (Yoshiba et al., 2012). The same study demonstrated that *Pkd2* expression is required for the asymmetry of Ca^{2+} signalling in response to flow. Furthermore, they demonstrate that *Pkd2* expression is required specifically in node crown cells for normal L-R determination. Abnormal L-R development can also be seen in *Pkd2*$^{E442G/E442G}$ embryos, which fail to localise PKD2 to the cilium (Yoshiba et al., 2012, Grimes et al., 2016). The evidence presented suggests that PKD1L1 and PKD2 are required for flow sensation. Therefore, it is tempting to speculate that these two molecules form part of the flow sensor complex. The ability of the two proteins to interact has been demonstrated through biochemical methods (Field et al., 2011). Furthermore, PKD1L1 mis-expression rescues the ability of *Pkd1*$^{-/-}$ vascular endothelial cells to elicit a flow-induced Ca^{2+} influx. A current hypothesis is that PKD1L1 blocks the Ca^{2+} influx

mediated by PKD2 (Grimes et al., 2016), which is, in turn, required to define the left side of the body. This model can account for the phenotypes described in *Pkd1l1*$^{rks/rks}$, *Pkd1l1*$^{tm1Lex/tm1Lex}$, *Pkd2*$^{tm1Dwo/tm1Dwo}$ and *Pkd2*$^{E442G/E442G}$. Namely, *Pkd1l1*$^{rks/rks}$, *Pkd2*$^{tm1Dwo/tm1Dwo}$ and *Pkd2*$^{E442G/E442G}$ are unable to sense or respond to flow (Grimes et al., 2016), and therefore display two right sides. By contrast, *Pkd1l1*$^{tm1Lex/tm1Lex}$ is unable to stop PKD2-mediated Ca^{2+} influx, due to lack of PKD2 inhibition by PKD1L1, thereby tending to develop two left sides. However, there is a random element that should also be considered: the asymmetric gene expression pathways are initially primed for activation on both sides of the midline, with flow influencing the activation; this is evidenced by the randomized *situs* phenotypes observed in mutants lacking flow (**Fig. 1.3**).

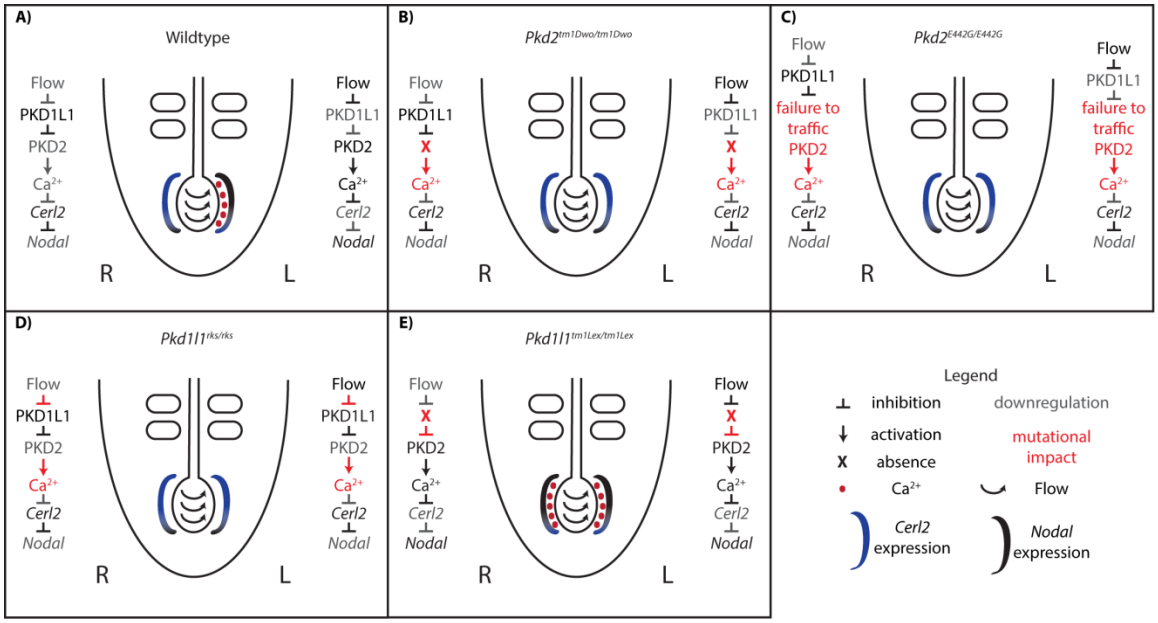


Figure 1.3: Hypothetical model for activation of asymmetric gene expression around the node. All diagrams depict the posterior end of the embryo, showing the node, notochord and two pairs of somites. **A)** normally, flow inhibits PKD1L1 on the left side of the node, which leads to the de-repression of PKD2, driving a Ca^{2+} response on the left side of the node; this then leads to the repression of *Cerl2* and activation of *Nodal* on the left side. The absence of flow on the right side of the node means that PKD1L1 inhibits PKD2 activity, which is unable to repress *Cerl2*. **B)** in the *Pkd2*$^{tm1Dwo/tm1Dwo}$ embryo, PKD2 and Ca^{2+} are missing from the system, meaning that *Cerl2* expression is maintained on both sides of the node. **C)** in *Pkd2*$^{E442G/E442G}$ embryos, PKD2 cannot localise to the cilium, thereby failing to activate Ca^{2+} influx in response to flow and failing to repress *Cerl2,* on the left side. **D)** in *Pkd1l1*$^{rks/rks}$, the inhibition of PKD2 by PKD1L1 is not relieved by flow; *Cerl2* expression thus remains active on both sides of the node. **E)** in *Pkd1l1*$^{tm1Lex/tm1Lex}$ embryos, PKD1L1 is absent from the system and PKD2 is active on both sides, potentially driving Ca^{2+} influx and repressing *Cerl2* expression. *Nodal* is therefore activated on both sides. Figure adapted from (Grimes, 2012).

1.4. ADPKD

ADPKD is a dominant inherited disorder, with a prevalence of 1:400-1:1000 in humans, in which cysts form primarily in the kidney. The cysts accumulate and grow throughout life. This leads to blockage of kidney tubules and, ultimately, end-stage renal disease in 45% of cases by the age of 60 (Gabow, 1993). ADPKD is caused by mutations in two genes: *PKD1* and *PKD2*, accounting for 85% and 15% of clinical cases, respectively (Mochizuki et al., 1996, Ward et al., 1996, Rossetti et al., 2007).

1.4.1. The role of PKD2 in ADPKD

Mutations in *PKD2* account for approximately 15% of ADPKD cases (Rossetti et al., 2007). The most common pathogenic mutations result in truncation of the protein, or cluster within specific areas of the gene, which encode domains important for the function of PKD2 (Rossetti et al., 2007), such as the CC or TOP domain (see section **1.2.3** and **1.2.5.a**).

In renal tubule cells, PKD2 interacts with PKD1 and forms a complex which localises to immotile cilia, as well as the plasma membrane, either at cell-matrix or cell-cell contact points. This complex is argued to control cellular proliferation, via intracellular Ca^{2+} signalling, in response to the flow of fluid within the lumen of the tubule (Nauli et al., 2003, Nauli and Zhou, 2004, Wilson, 2004). The exact mechanism by which Ca^{2+} signalling impacts cell proliferation, or whether Ca^{2+} is an important player in the development of the disease, remain under debate.

1.4.2. ADPKD and the PKD1-PKD2 interaction

Mutations in *PKD1* lead to earlier end-stage renal disease than those in *PKD2*, on average (Hateboer et al., 1999), and account for up to 85% of all ADPKD cases (Rossetti et al., 2007). As with *PKD2* mutations, the most common pathogenic mutations are truncations of the protein, or mutations that cluster within domains important for the functions of the protein (Rossetti et al., 2007); the CC domain, required for interaction with PKD2, is one such example (see section **1.2.2**). This is consistent with the CC domains of PKD1 and PKD2 being central to the function of the complex in renal cells.

1.5. PKD1 and PKD2 in other contexts

PKD2 is known to play roles beyond the kidney, independently of or complexed with PKD1. This section is not meant to be an exhaustive list of other roles played by the two polycystins, but an indication of functions performed in other contexts. Aside from the specific roles discussed below, PKD2 also plays a more generic role as a cation channel in the ER in several tissues, where it may facilitate Ca^{2+}-induced Ca^{2+} release, in complex with other, potentially tissue-specific, proteins (Koulen et al., 2002, Qian et al., 2003, Cai et al., 2004, Li et al., 2005b, Patel et al., 2007). The understanding of the role of PKD2 also stems from the fact that *Pkd2* null homozygote embryos show a range of defects and die *in utero* (Wu et al., 2000, Pennekamp et al., 2002, Walker, 2016). The evidence presented below serves to illustrate that *Pkd1* and *Pkd2*, despite being associated with ADPKD, display pleiotropy.

1.5.1. Skeletal development

The primary cilium plays an important role in skeletal development (Qiu et al., 2012). The study of models has shown PKD1 and PKD2 to play important roles in the development of the skeletal system (Boulter et al., 2001, Lu et al., 2001, Xiao et al., 2006, Xiao et al., 2010, Xiao et al., 2014). Moreover, both proteins localise to cilia in osteoblasts (Xiao et al., 2008), which has led to the hypothesis that the PKD1-PKD2 complex plays a mechanotransductory role in bone (Xiao and Quarles, 2010). The bone is a matrix-type structure filled with liquid (lacuno-canalicular network). Mechanostimulation aids in maintaining bone structure in long bones (Xiao and Quarles, 2010), and also plays a role in post-natal cranial development (Moss, 1960, Babler et al., 1982, Engström et al., 1986, Herring and Teng, 2000). Abolishing *Pkd1* expression in adult mice leads to decreased bone density (Xiao et al., 2010) and impaired post-natal bone formation (Qiu et al., 2012).

The most severe effects on embryonic skeletal development were seen in the *Pkd1* null allele, $Pkd1^{tm1Rsa}$: homozygous embryos displayed abnormal axial and long bone development, as

well as defective neural crest-derived cranial tissues (Boulter et al., 2001). This phenotype was recapitulated in mice homozygous for a point mutant allele, *Pkd1*^{m1Bei}, described by Xiao *et alia* (Boulter et al., 2001, Xiao et al., 2006). Other studies have similarly implicated *Pkd1* in bone development, both in the axial skeleton (Lu et al., 2001) and craniofacial development (Kolpakova-Hart et al., 2008, Hou et al., 2009). It is also of note that human ADPKD sufferers with *PKD1* mutations have a rare incidence of skeletal abnormalities (Turco et al., 1993, Shute et al., 2014).

Pkd2 has been shown to be important for post-natal skeletal development (Khonsari et al., 2013). Although ADPKD patients with mutations in *PKD2* were not reported to have any skeletal abnormalities, the same study demonstrated that there are characteristic craniofacial features in ADPKD patients bearing mutations in *PKD2*. Osteoblast-specific deletion of *Pkd2* in mouse embryos has also been shown to lead to low-turnover osteopenia and, contrary to *Pkd1* loss, reduced bone marrow adipocity (Xiao et al., 2014).

1.5.2. Cardiovascular development

Cardiovascular abnormalities have been associated with the ADPKD loci. Deletion of *Pkd1* in mouse embryos leads to abnormal cardiac development; the defects observed affected cardiac structure and the outflow tract of the heart (Boulter et al., 2001). However, a different null allele, *Pkd1*^{tm2Jzh}, did not affect cardiovascular development (Lu et al., 2001). Two *Pkd2* knockout alleles, *Pkd2*^{tm1Som} and *Pkd2*^{tm1Dwo}, also displayed cardiac defects, affecting cardiac structure (Wu et al., 2000, Pennekamp et al., 2002). Whilst *Pkd1* mutant alleles do not show *situs* defects (Karcher et al., 2005), *Pkd2* mutant alleles affect heart *situs*. It is worth noting that, independently of the position of the heart, these alleles also cause defects in heart structure (Pennekamp et al., 2002).

A role for both *Pkd1* and *Pkd2* has also been defined in placental vasculature development, and mouse embryos lacking *Pkd1* and *Pkd2* in endothelial cells display abnormal

placental vasculature (Garcia-Gonzalez et al., 2010). PKD2 has also been shown to play a role in Ca^{2+} homeostasis in adult vascular smooth muscle cells, although in this case its association with PKD1 was not assessed (Qian et al., 2003). Loss of PKD1, on the other hand, has been associated with vascular fragility in mouse *Pkd1* knockout embryos (Kim et al., 2000). The PKD1-PKD2 complex is believed to also play a mechanosensory role in endothelial cells (Nauli et al., 2008, AbouAlaiwi et al., 2009), regulating Ca^{2+} and nitric oxide signalling in response to fluid flow. Endothelial cells lacking or having reduced levels of *Pkd2* have altered responses to fluid flow in both mouse and human cells (AbouAlaiwi et al., 2009). As is the case of renal cells, both PKD1 and PKD2 localise to primary cilia in endothelial cells (Nauli et al., 2008, AbouAlaiwi et al., 2009).

1.5.3. Lymphatic system development

The consensus in the field is that *Pkd1*$^{-/-}$ and *Pkd2*$^{-/-}$ embryos display oedema due to cardiac, great vessel or vascular abnormalities (Arnaout, 2000, Wu et al., 2000, Boulter et al., 2001). However, a number of studies have suggested that the oedema may be due to the roles played by PKD2 and PKD1 in the development of the lymphatic system. This was first suggested by Garcia-Gonzalez and colleagues (Garcia-Gonzalez et al., 2010), and later argued by Outeda *et alia*. The group showed that *Pkd1*$^{-/-}$ mouse embryos display oedema phenotypes in the absence of cardiac structure defects. Importantly, however, these embryos display abnormally patterned cutaneous lymphatic vessels, showing a grossly disorganised and distended lymphatic capillary tree. The same lymphatic vessel phenotype was seen in *Pkd2*$^{-/-}$ embryos (Outeda et al., 2014). This study also showed that lymphatic endothelial cells lacking or with lower levels of PKD1 and/or PKD2 are unable to migrate properly (Outeda et al., 2014).

The abnormal subcutaneous lymphatic system phenotype is thought to be linked to Ca^{2+} signalling. Strikingly, both Ca^{2+} channel blockers and agonists recapitulated the phenotype observed in mutant *pkd1a* zebrafish embryos, which show abnormal lymphatic vasculature

(Coxam et al., 2014). The authors argue that the role played by *Pkd1* in lymphatic system development may be independent of the primary cilium, as evidenced by localisation studies (Coxam et al., 2014) and by normal lymphatic vasculature in a ciliogenesis mutant (Huang and Schier, 2009). Furthermore, Coxam *et alia* have shown that Pkd2 depletion recapitulates the phenotype seen in mutant *pkd1a*; *pkd1b* knockdown zebrafish embryos, suggesting a direct role for Pkd2 in providing the calcium signalling required for normal lymphatic vasculature development and normal body curvature. However, the same study has shown that mouse embryos with an endothelial cell-specific *Pkd1* knockout allele showed only altered subcutaneous lymphatic vessel structure and did not display the oedema characteristic of *Pkd1* null embryos (Coxam et al., 2014). Similarly, *Pkd1* and *Pkd2* blood vessel-specific knockout embryos also failed to show oedema (Garcia-Gonzalez et al., 2010). *N.B.*: Garcia-Gonzalez and colleagues initially argued that their study showed an endothelial-specific knockout of both *Pkd1* and *Pkd2*, however, the knockout was later shown to be specific only to blood vessels, but not subcutaneous lymphatic vessels (Coxam et al., 2014). Together, these data suggest that the oedema phenotype may be due to a combination of abnormal development in different tissues, potentially both lymphatic and blood vessels.

1.6. Aim of thesis

The pleiotropic nature of *Pkd2* has been revealed principally through genetic studies. Studies have shown that *Pkd2* plays an important role in the development and homeostasis of the kidney, as well as in establishment of L-R asymmetry. By comparison, the molecular mechanisms of interaction between the polycystin proteins PKD1, PKD1L1 and PKD2, as well as the molecular function of the resulting complexes, remain poorly studied. This thesis addresses the CC-based molecular mechanism of the interaction of PKD2 with PKD1 and PKD1L1, using biochemical methods. I further explore these interactions by creating and analysing L-R and renal development in mouse lines bearing mutations in the region encoding the CC of PKD2.

Chapter 2: Investigating the molecular mechanism of the PKD1L1-PKD2 interaction

2.1. Introduction

2.1.1. Interacting with PKD2: from domains to function

To date, PKD2 has been the subject of a number of biochemical studies and remains, at the molecular level, the best characterised polycystin family member. In spite of the fact that the molecule is smaller in size than its PKD1-like paralogs, working with the full-length molecule directly still presents difficulties, potentially due to a number of factors. Firstly, in overexpression systems, the molecule can induce ER remodelling, by formation of whorls – focal points for the accumulation of PKD2 – which are not seen in cells expressing PKD2 endogenously (Giamarchi et al., 2010). Secondly, difficulties in validating particular overexpression constructs; certain constructs would show abnormal localisation patterns (*vide supra*), or fail to localise to the expected compartments (personal communication from R. Walker and D. Asante). It is the author's opinion that these reasons prompted the use of PKD2 fragments in the majority of studies aiming to characterise PKD2 at a molecular level.

The first protein-protein interaction domain to be characterised using protein fragments was the CC domain of PKD2. Initial bioinformatic analysis of PKD2 and PKD1 sequence predicted CC domains in their intracellular C-termini. This study then employed yeast two-hybrid (Y2H) and *in vitro* pull down approaches to determine that larger segments of the C-termini of these proteins are able to interact (**Table 2.1**). Notably, this study also showed that a human ADPKD pathogenic mutation, located downstream of the predicted CC domain of PKD2, abrogated binding to the C-terminal fragment of PKD1 (Qian et al., 1997). A parallel study used similar approaches to determine that PKD2 contains two distinct CC domains necessary for interaction with PKD2 and PKD1 fragments (**Table 2.1**) – henceforth referred to as homo- and hetero-

oligomerization sub-regions, respectively (Tsiokas et al., 1997). In both these studies, the region predicted to contain the CC overlapped with the EF-hand domain of PKD2. Tsiokas *et alia* later showed that a region contained in between the necessary PKD2 homo- and hetero-oligomerization sub-regions is sufficient for interaction with PKD1 (**Table 2.1**) and TRPC1 fragments. Mutating specific residues, namely L882H and D886A, abolished PKD1 (**Table 2.1**) and TRPC1 fragment binding, respectively, as assessed through Y2H experiments. Furthermore, the same study showed that this sufficient region has an α-helical conformation (Tsiokas et al., 1999). This was the first suggestion that the CC of PKD2 is located further downstream than initially predicted, and that it is distinct from the EF-hand domain. A separate study characterised the intracellular C-terminal domain of PKD2 and determined, through biochemical techniques, that the EF-hand domain alone was unable to oligomerize (**Table 2.1**) (Celić et al., 2008); the same study showed that the CC domain is C-terminal to the EF-hand, in a region overlapping with that sufficient for PKD2 hetero-oligomerization (Tsiokas et al., 1999, Celić et al., 2008). A later study established that the CC domain of PKD2, but not the EF-hand, is able to interact with PKD1 (**Table 2.1**); this interaction can be broken by a PKD1 pathogenic mutation in the CC (Casuscelli et al., 2009). A later study employed Y2H and pull down assays to show that the C-terminus of PKD2 interacts with other PKD2 C-terminal fragments, as well as PKD1 C-terminal fragments, through an α-helical region C-terminal to the EF-hand (**Table 2.1**) (Giamarchi et al., 2010). The sub-regions required for homo- and hetero-oligomerization are adjacent to each other, but distinct, and overlap with those previously described (Tsiokas et al., 1999). In addition, this study also showed that the homo-oligomerization sub-region is required for interaction with the PKD1 C-terminal fragment (Giamarchi et al., 2010). However, this study also showed that the CC region is only required for homo-oligomerization of C-terminal PKD2 fragments, but not full-length PKD2 (**Table 2.1**). Finally, mutations in the PKD2 N-terminal part of the α-helical region, required for homo-oligomerization, abolished pharmacologically-driven Ca^{2+} responses and currents observed in cells overexpressing PKD1 and PKD2, attributed to the PKD1-PKD2 complex (Giamarchi et al., 2010).

Table 2.1: Summary of published data regarding the interaction of the PKD1-PKD2 complex



Fragment	AA/mut	Interaction		Method
		PKD2	PKD1	
Giamarchi et al, 2010				
A	680-968	**FL, A**	**aa4107-4303**	Y2H, Co-IP
B	4M*	**X**	**aa4107-4303**	Y2H, Co-IP
C	680-871	**A**	-	Y2H
D	833-871	**A**	**X**	Y2H
E	680-798	**X**	-	Y2H
F	799-871	**A**	-	Co-IP
G	679-824	**X**	-	Co-IP
H	833-895	-	**aa4107-4303**	Y2H
I	FL/4M*	**FL, X (A), I**	**X**	Co-IP, non-reducing WB
J	FL/M849P	**X**	-	Co-IP
K	FL/R872X	**K**	-	non-reducing WB
L	FL/R742X	**L**	-	non-reducing WB
Feng et al, 2008				
A	FL/D511V	**FL, A**	-	non-reducing WB, Co-IP
B	FL/L703X	**B**	-	non-reducing WB
C	FL/R742X	**FL, C**	-	non-reducing WB, Co-IP
D	1-223	**D**	-	Y2H, Co-IP
E	1-207	**D**	-	Y2H
F	1-198	**X**	-	Y2H
G	1-117	**X**	-	Y2H
H	1-61	**X**	-	Y2H
Feng et al, 2011				
A	224-968	**A**	-	non-reducing WB
B	4M*	**B**	-	non-reducing WB
C	224-679	**C**	-	non-reducing WB
D	C632A	**X**	-	non-reducing WB
E	496-968	**E**	-	non-reducing WB
F	4M*	**F**	-	non-reducing WB
G	FL/C632A	**G**	**FL**	non-reducing WB
H	C632R	**H**	**FL**	non-reducing WB
I	C632A+4M*	**I**	-	non-reducing WB
Qian et al, 1997				
A	687-968	-	**aa4085-4303**	Y2H, Co-IP
B	687-872	-	**X**	Y2H
C	687-742	-	**X**	Y2H
Tsiokas et al, 1997				
A	679-968	**A**	**aa4077-4303**	Y2H, Co-IP
B	679-742	**X**	**X**	Y2H
C	742-968	**A**	**aa4077-4303**	Y2H
D	742-872	**A**	**aa4077-4303**	Y2H
Tsiokas et al, 1999				
A	679-968	-	**aa4124-4303**	Y2H
B	679-702	-	**X**	Y2H
C	679-742	-	**X**	Y2H
D	742-968	-	**aa4124-4303**	Y2H
E	798-968	-	**aa4124-4303**	Y2H
F	822-968	-	**aa4124-4303**	Y2H
G	798-871	-	**X**	Y2H
H	822-871	-	**X**	Y2H
I	822-928	-	**aa4124-4303**	Y2H
J	822-895	-	**aa4124-4303**	Y2H
K	D886A	-	**aa4124-4303**	Y2H
L	L884H	-	**X**	Y2H
Hanaoka et al, 2000				
A	FL	-	**FL**	Co-IP
B	R742X	-	**X**	Co-IP

* - mutation **X** - no interaction - - not assessed decreased interaction

Acronyms, in alphabetical order: **Co-IP** – co-immunoprecipitation; **FL** – full-length; **WB** – western blot; **Y2H** – yeast two-hybrid.

Table 2.1 (continued)



Fragment	AA/mut	Interaction PKD2	Interaction PKD1	Method
Celic et al, 2008				
A	704-968	**A**	-	AU, SEC
B	719-800	**X**	-	AU, SEC
C	827-927	**C**	-	AU, SEC
D	L842P	**X**	-	SEC
E	V846E	**X**	-	SEC
F	M849K	**X**	-	SEC
G	I853P	**X**	-	SEC
H	I856K	**X**	-	SEC
I	V846E/I856K	**X**	-	SEC
J	M849K/V863E	**X**	-	SEC
Casuscelli et al, 2009				
A	704-968	-	**aa4183-4270, aa4202-4243**	Co-IP
B	720-797	-	**X**	Co-IP
C	720-817	-	**X**	Co-IP
D	720-829	-	**X**	Co-IP
E	798-927	-	**aa4183-4270**	Co-IP, SPR
F	821-927	-	**aa4183-4270**	Co-IP
G	FL	-	**aa4183-4270**	Co-IP
Celic et al, 2012				
A	704-968	**A**	-	AU, SAXS
B	720-797	-	-	
C	FL/ T771A+E774A	-	-	
Yu et al, 2009				
A	821-926	**A**	**aa4191-4279**	static light scattering
B	mut6*	**X**	-	static light scattering
C	723-928	**C**	-	static light scattering
D	833-895	**D**	**aa4213-4248**	X-ray diffraction, Co-IP
E	833-872	**E**	**X**	X-ray diffraction, Co-IP
F	871-895	-	**X**	Co-IP
G	857-895	-	**X**	Co-IP
H	833-918	**H**	**aa4191-4279**	static light scattering
I	mut6*	-	**X**	Co-IP
J	FL/mut6*	**X**	**X**	Co-IP, BN-PAGE, crosslinking
K	FL	**K**	-	BN-PAGE, crosslinking
Zhu et al, 2011				
A	833-895	**A**	**aa4214-4248**	*in silico* docking
B	695-968	**X**	**X**	disulfide bond analysis
C	I860C	**C**	**aa4214-4248/ V4217C**	disulfide bond analysis
D	R877G+R878G	-	**aa4214-4248**	Co-IP
E	L881A+L885A	-	**X**	Co-IP
F	L881D+L885D	-	**X**	Co-IP
Yang et al, 2015				
A	704-968	**A**	-	SEC-MALS, dynamic light scattering
B	720-797	-	-	
Yang et al, 2016				
A	704-968	**A**	-	HDX-MS
B	704-797	-	-	
Shen et al, 2016				
A	53-792	**A**	-	Cryo-EM
B	198-792	**B**	-	Cryo-EM
C	198-703	**C**	-	Cryo-EM
Grieben et al, 2017				
A	185-723	**A**	-	Cryo-EM
Salehi-Najafabadi et al, 2017				
A	242-467	**FL, A**	**FL, aa3685-3895**	Co-IP
B	T448K	**A**	**aa3685-3895**	Co-IP

* - mutation **X** - no interaction **-** - not assessed decreased interaction

Acronyms, in alphabetical order: **AU** – analytical ultracentrifugation; **BN-PAGE** – blue native PAGE; **Co-IP** – co-immunoprecipitation; **Cryo-EM** – cryo-electron microscopy; **FL** – full-length; **HDX-MS** – hydrogen-deuterium exchange mass spectrometry; **SAXS** – small angle X-ray scattering; **SEC** – size-exclusion chromatography; **SEC-MALS** – size-exclusion chromatography-multiangle light scattering; **SPR** – surface plasmon resonance.

A number of studies have identified PKD2 domains required for protein-protein interaction. Through a combination of Co-IP, Y2H and non-reducing western blot analysis, one study has shown that the intracellular N-terminus of PKD2 contains a domain required for PKD2-PKD2 interaction (**Table 2.1**) (Feng et al., 2008). Furthermore, the study also showed that expression of a Pkd2 N-terminal fragment, containing the oligomerization domain, was able to phenocopy the effects seen in *pkd2* knockdown zebrafish embryos. In cells, this fragment was also able to inhibit endogenous PKD2 channel activity (Feng et al., 2008). A later study employed non-reducing western blot analysis to show that deletion of this N-terminal oligomerization domain still allowed PKD2 to assemble as tetramers and dimers; further deletion or mutation of the α-helical region (*vide supra*) still allowed N- and C-terminal PKD2 molecules to assemble as dimers, under non-reducing conditions (Feng et al., 2011). These findings argued that PKD2 contains a third interaction domain, potentially in the form of a cysteine residue. Mutation of the C632 residue in human PKD2 was able to abolish dimer formation, in the absence of both N- and C-terminal PKD2 interaction domains. However, mutating the C632 residue alone did not affect binding to PKD1, but affected ATP-sensitive Ca^{2+}-release from ER-localized PKD2 channels (Feng et al., 2011). Given the recently published structure of the tetrameric PKD2 channel, the C632 residue may not facilitate PKD2 oligomerization. This is due to the fact that the residue is not located on an interaction surface and is exposed to the cytoplasmic environment, being in an environment that is unlikely to lead to the formation of a disulphide bridge (Shen et al., 2016, Grieben et al., 2017). Feng *et alia* also suggested that the first extracellular loop of PKD2 is not involved in homo-oligomerization (Feng et al., 2011). This finding has been challenged by a recent study, which showed that the first extracellular loop of PKD2 alone is able to bind to the homologous region in PKD1. Furthermore, expression of this extracellular loop of PKD2 abolished Ca^{2+} currents in *Xenopus* oocytes, arguing that the extracellular loop can interfere with the assembly of PKD2 channels (Salehi-Najafabadi et al., 2017). Aside for domains required for PKD2 and PKD1-PKD2 interactions, PKD2 contains domains required for interaction with proteins such

as: TRPC1 (Tsiokas et al., 1999), fibrocystin (Kim et al., 2008), RyR2 (Anyatonwu et al., 2007) and HAX-1 (Gallagher et al., 2000) (see section **1.2.3**).

2.1.2. Models of PKD2-based interaction

The stoichiometry of polycystin complexes has been and remains debated in the field. Two separate models attempt to explain the formation of the PKD1-PKD2 complex. The first argues that PKD2 forms trimeric channels through CC-based interaction (Yu et al., 2009, Yang et al., 2015); the PKD2 CC trimer then interacts with the CC of PKD1 (Zhu et al., 2011). This model challenged the widely-held hypothesis that TRP channels assemble as tetramers and was problematic due to the fact that the studies supporting this model focused on C-terminal fragments of the proteins containing the CC domain (Kobori et al., 2009, Yang and Ehrlich, 2016). The second model posits that PKD2 assembles as a homotetrameric channel, through multiple protein-protein interaction domains. The studies that support this model made use both of protein fragments, as well as the full-length protein (Feng et al., 2008, Kobori et al., 2009, Feng et al., 2011). Two recent studies have established the structure of the PKD2 channel, demonstrating that PKD2 can assemble as a homotetramer (Shen et al., 2016, Grieben et al., 2017); these structures excluded the N- and C-terminal interaction domains of PKD2. The ability of these truncated constructs to form tetramers argues that neither the CC, nor the N-terminal domain, is required for assembly of PKD2 homotetrameric channels. However, given the data described in section **2.1.1**, it is likely that these domains are required for the interaction of the PKD2 channel with PKD1 molecules. Whether PKD1 displaces a PKD2 molecule from the tetrameric channel, similarly to what has been suggested for the PKD1L3-PKD2L1 interaction (Ishimaru et al., 2010), or whether PKD1 interacts with the PKD2 tetramer (Feng et al., 2011), remains to be addressed. The data described in section **2.1.1**, and in this section, is summarised in **Table 2.1**.

2.1.3. Hypothetical model for the interaction of PKD1L1 with PKD2

Few studies have endeavoured to characterise the PKD1L1-PKD2 complex directly and address the molecular mechanisms involved in their interaction. One study has used Co-IP and mutational analysis to show that the CC domain of PKD1L1 is sufficient for the interaction of a PKD1L1 fragment with PKD2, presumably by binding to the CC domain of PKD2 (Field et al., 2011). Given the homology between PKD1L1 and PKD1, a molecule that has been better characterised in terms of its interaction with PKD2 (see section **2.1.2**), I hypothesised that the PKD1L1-PKD2 interaction bears strong similarity to the interaction of PKD1 with PKD2, namely through binding mediated by the two proteins' respective CC domains. More specifically, this interaction occurs through the hetero-oligomerization domain of PKD2, which is either part of or an extension of the CC domain (see section **2.1.1**). This chapter describes the experiments employed to test that hypothesis, by focusing on PKD2 and its CC.

2.2. Results

2.2.1. Designing mutation that affect the PKD2 CC

Previous studies have established that the intracellular C-terminus of PKD2 facilitates protein-protein interactions, through a region that contains a CC domain (see section **2.1.1**). This region can be divided into two sub-regions, one involved in homo-oligomerization (interaction with other PKD2 molecules) and one involved in hetero-oligomerization (interaction with PKD1 and TRPC1 – **Fig. 2.1**). Given the involvement of the PKD1L1 CC in the interaction with PKD2, it seemed reasonable to hypothesise that the PKD1L1-PKD2 interaction also occurs through the binding of the PKD1L1 CC to the hetero-oligomerization sub-region of the PKD2 CC region.

In order to test this hypothesis, I searched for mutations that would impact the formation of the CC domain of PKD2. The likelihood of a CC forming within a given protein sequence can be predicted bioinformatically. The impact of candidate mutations can then be assessed by comparing the likelihood of CC formation in the presence or absence of a mutation. Two programmes were used for the work described in this section, Marcoil (Delorenzi and Speed, 2002) and Coiled-coils (Lupas et al., 1991); these were chosen as they employ different algorithms to predict the likelihood of CC formation. Similar bioinformatic approaches were used in previous publications that studied the CCs of polycystins (Qian et al., 1997, Giamarchi et al., 2010, Field et al., 2011). Marcoil predicts the presence of a large region of PKD2 (80 AA) with a high probability of CC formation: >90% for human and >80% for mouse PKD2, respectively (**Fig. 2.1** and **2.2**). Coiled-coils predicts two distinct regions with moderate CC formation probability: 40% and 50% for either region, for both human and mouse PKD2 (**Fig. 2.1** and **2.2**).

I initially examined mutations from previous studies (see section **2.2.3**) which had been shown to disrupt the interaction with PKD1 and TRPC1: L882H and D884A (mouse AA numbering), respectively (Tsiokas et al., 1999). Marcoil predicts that L882H decreases the CC formation

probability to 40% within the hetero-oligomerization sub-region of the mouse protein, and that of the homo-oligomerization sub-region to 59%; Coiled-coils predicts no effect on either sub-region by either mutation (**Fig. 2.2**). Given the predicted impact of these mutations, I designed novel mutations in an attempt to decrease the CC formation probability in the hetero-oligomerization sub-region of the PKD2 CC region. The mutational design process targeted random residues within the hetero-oligomerization sub-region and predicted the impact of the mutations using Marcoils and Coiled-coils. I selected two mutations on the basis of their predicted impact: L906P and V907D (mouse AA numbering). Marcoil predicts that the CC formation probability in the presence of the two mutations is lowered to >40% in the hetero-oligomerization sub-region of mouse PKD2. Coiled-coils predicted that both mutations reduced the probability to <10% (**Fig. 2.2**). Considering these bioinformatic predictions of the effects of the PKD2 mutations, L906P and V907D, on CC probability formation, it seemed likely that they would have an effect on CC structure. Therefore, these two mutations can be used in studying the involvement of the CC in the PKD1L1-PKD2 interaction. However, Marcoil also predicted a decrease in the homo-oligomerization sub-region of mouse PKD2, in the presence of the L906P and V907D mutations, to 62% and 60%, respectively. The CC formation probability in the mouse PKD2 hetero-oligomerization sub-region, in the presence of candidate mutations, is summarised in **Table 2.2.**

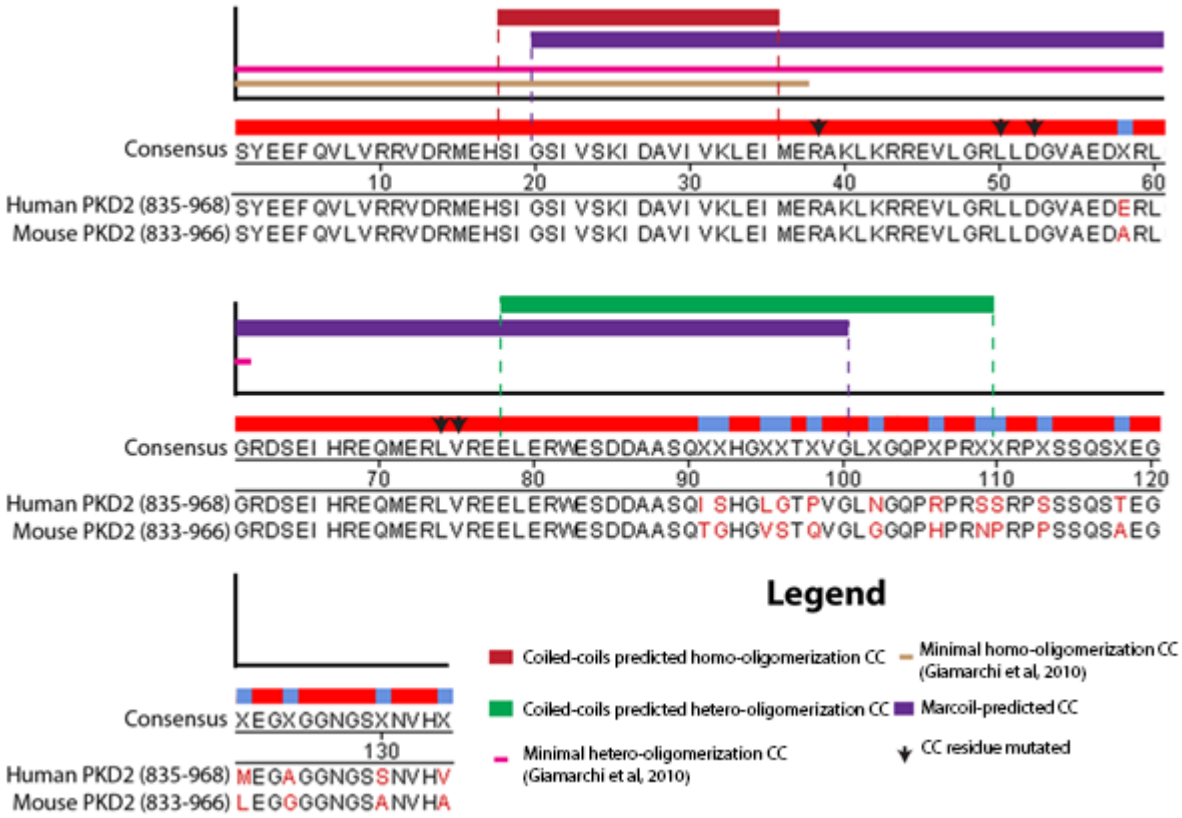


Figure 2.1: Alignment of human and mouse PKD2 protein sequences, showing positions of regions with probability of CC formation. Coiled-coils regions are shown as red and green blocks, Marcoils region is shown as a purple block. The pink and brown lines depict the minimal region of homo- and hetero-oligomerization described in (Giamarchi et al., 2010). The positions of mutations used in this study are also indicated with arrowheads, in order: R870X, L882H, D884A, L906P and V907D (mouse AA numbering).

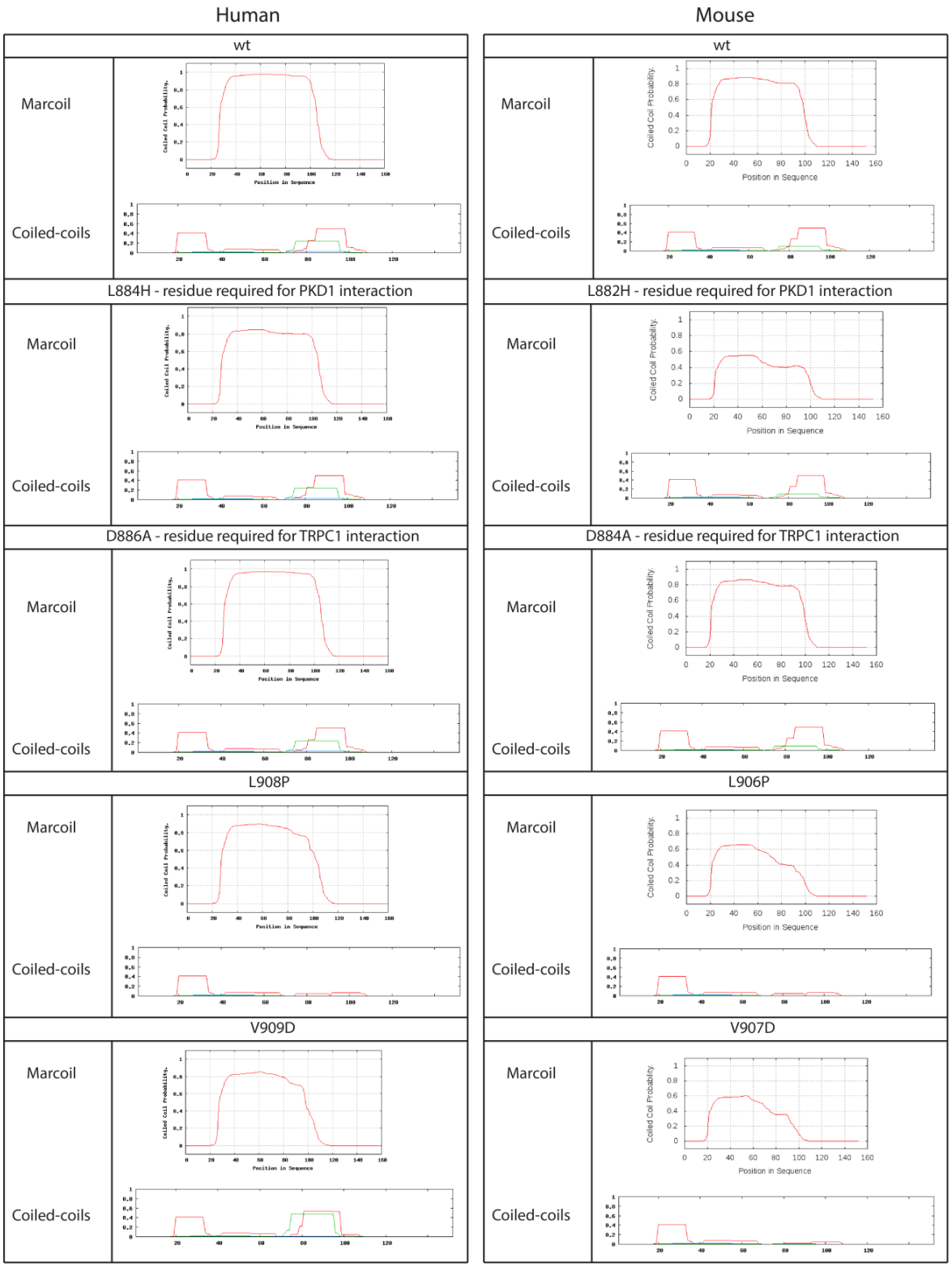


Figure 2.2: Effect of mutations on the CC formation probability at the C-terminus of human and mouse PKD2, as predicted by Marcoil or Coiled-coils. Marcoil detects a single, large (80 AA) region with a high probability of CC formation, whilst Coiled-coils detects the probability of CC formation for windows of 14 (green), 21 (blue) and 28 (red) residues.

Table 2.2: Effect of mutations on CC formation probability in mouse PKD2 hetero-oligomerization sub-region

Mutation	CC formation probability (Marcoil)	CC formation probability (Coiled-coils)
L882H	40%	50%
D884A	>80%	50%
L906P	>40%	<10%
V907D	>40%	<10%
WT	>80%	50%

2.2.2. Using protein fragments to study the PKD1L1-PKD2 interaction

In order to focus on the involvement of only the PKD2 CC in the PKD1L1-PKD2 interaction, I designed three different-length protein fragments: 1) TM5-COOH, containing the region from TM5 up to the C-terminus; 2) TM6-COOH containing the region from the final TM up to the C-terminus; 3) EFh-COOH, containing the region downstream of the final TM up to the C-terminus (**Fig. 2.3**). All the fragments include the EF-hand and CC. These fragments were designed based on the fact that the CC of PKD2 was shown to be sufficient for interaction with PKD1 fragments (Giamarchi et al., 2010), but also to avoid any issues with regards to orientation of the fragments within the membrane systems (**Fig. 2.3**). All three protein fragments contained an N-terminal Myc tag, to facilitate protein purification in Co-IP experiments (*vide infra*).

Firstly, the cellular localisation of the PKD2 protein fragments was analysed. Each of the fragments, as well as the full-length protein (PKD2-V5), was overexpressed in ciliated IMCD3 cells. This cell line was used due to its ability to ciliate robustly. The full-length protein localised to the membrane systems, as well as the cilium (**Fig. 2.4**, row **E**). This localisation pattern is in agreement with previous publications (Giamarchi et al., 2010, Grimes et al., 2016). By comparison, the fragments showed a similar pattern of localisation, trafficking to the membrane systems (**Fig. 2.4**, rows **A**, **B** and **C**). However, the fragments appeared to localise less efficiently to the cilium, if at all: the full-length protein marked the entirety of the cilium (**Fig. 2.4**, row **E**), whilst the fragments only showed puncta, which may be on the plasma membrane and not the ciliary membrane (**Fig.**

2.4, rows **A**, **B** and **C**). Given the published data on PKD1-PKD2 sub-cellular trafficking (see section **1.2.5.b**), the lack of localisation to cilia should still allow the proteins to interact.

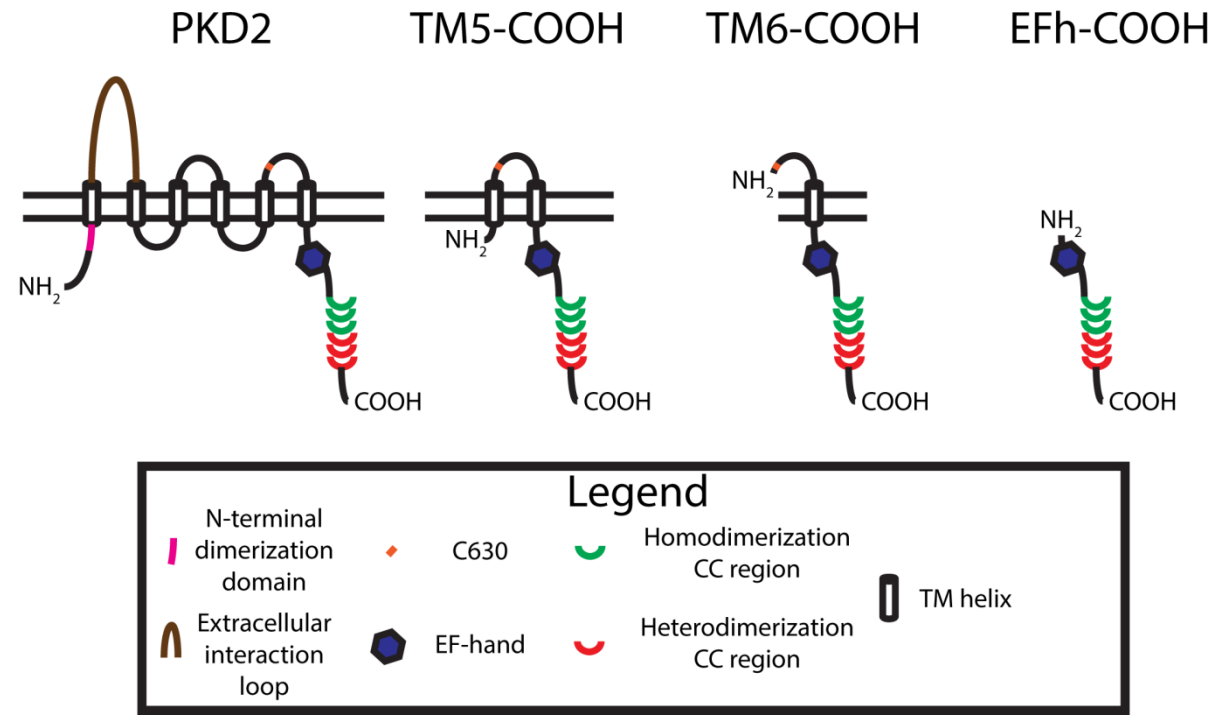


Figure 2.3: Diagrammatic representation of PKD2 and PKD2 fragments used in this study. Only the EF-hand and protein-protein interaction domains are represented.

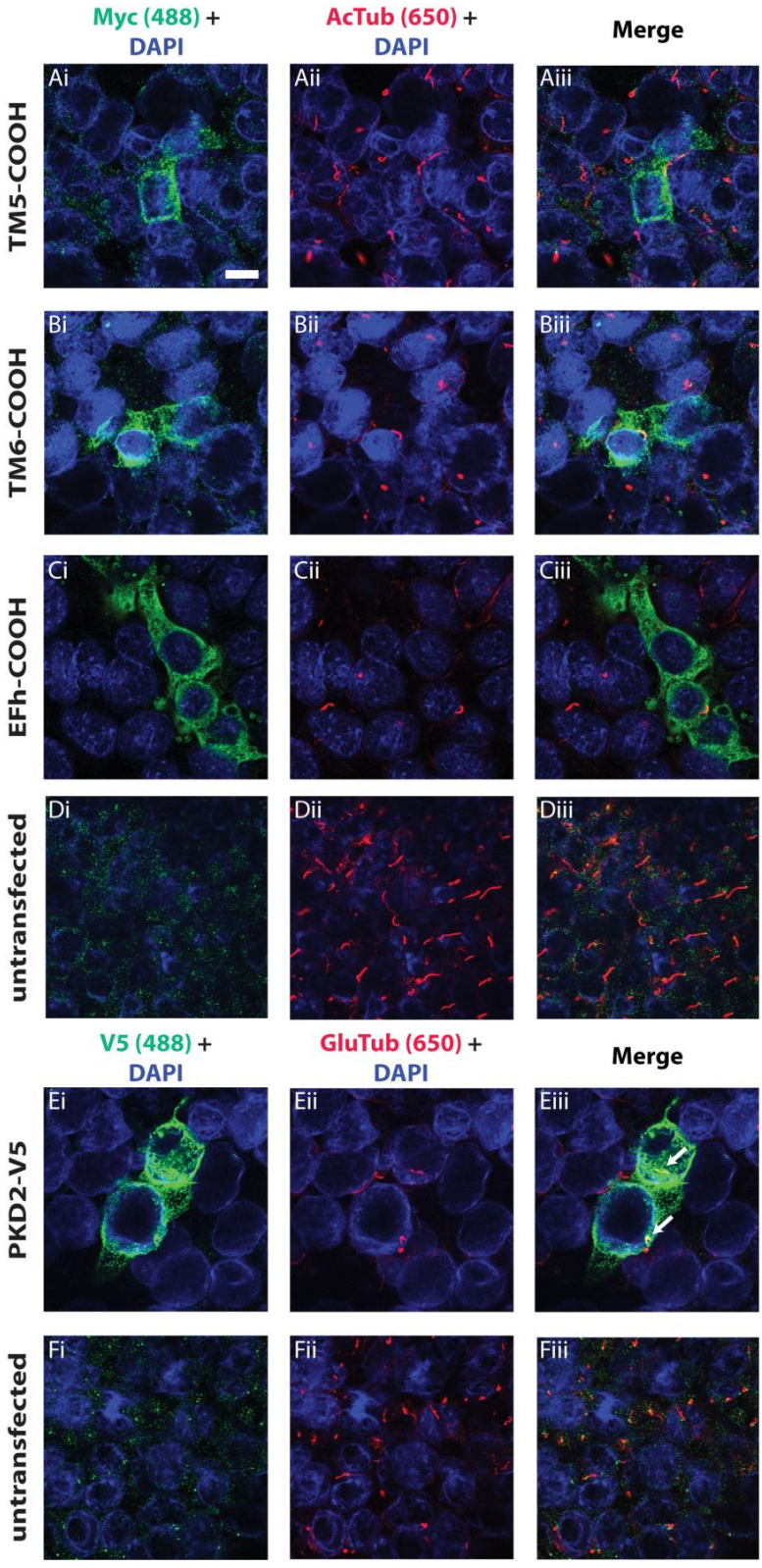


Figure 2.4: Localisation of PKD2 fragments or full-length protein in ciliated IMCD3 cells. Colours represent: green – PKD2 (Myc or V5 tag); red – cilia (acetylated or glutamylated tubulin); blue (DAPI) – nucleus. Rows **A**, **B** and **C** show localisation of the three PKD2 fragments, whilst row **E** shows localisation of the full-length protein, PKD2-V5. Rows **D** and **F** are untransfected controls. The two arrows in **Eiii** show localisation of PKD2-V5 to the cilium. Scale bar in **Ai**: 10 µm.

Secondly, the interaction of the three PKD2 fragments with a GFP-tagged PKD1L1 fragment (PKD1L1-CC-GFP) was tested. The PKD1L1 fragment contains the CC and the most C-terminal TM (Field et al., 2011). Each of the PKD2 fragments was transfected and co-expressed with PKD1L1-CC-GFP in HEK293T cells. This cell line was used due to ease of transfection and robust protein production capacity. The cell lysates were then used in Co-IP experiments to test for the interaction of the two proteins, by using antibodies raised against the protein tags, GFP or Myc, for purifying the PKD1L1 and PKD2 fragments, respectively. The largest PKD2 fragment, TM5-COOH, was co-purified with and co-purified PKD1L1-CC-GFP (**Fig. 2.5**, **A**, lane 4 and 7, respectively). Similarly, TM6-COOH was able to co-purify with and co-purify PKD1L1-CC-GFP (**Fig. 2.6**, **A**, lanes 4 and 7, respectively). In contrast, EFh-COOH, the shortest fragment, was unable to enrich PKD1L1-CC-GFP and *vice versa* (**Fig. 2.7**, **A**, lanes 9 and 10, respectively). These results indicate that the fragments containing TMs, TM5-COOH and TM6-COOH, are able to interact with PKD1L1-CC-GFP, whilst EFh-COOH is unable to do so. These findings suggest two possibilities: 1) the CC of PKD2 alone is not sufficient for the interaction with PKD1L1; 2) a potential requirement for plasma membrane anchorage of PKD2. In cell lysates expressing one interaction partner and only the protein tag of the other partner, Myc or GFP, the interaction partner is not found in the final fraction when purifying the tag (**Fig. 2.5** and **2.6**, **A**, lanes 6 and 9; **Fig. 2.7**, **A**, lanes 8 and 10). This demonstrates that the interaction is specific to the proteins or fragments being used, and not facilitated by the protein tags.

In addition to testing hetero-oligomerization, the interaction of the PKD2 fragments with a V5-tagged, full-length PKD2 was also tested, using the same approach described (*vide supra*). PKD2-PKD2 interaction was also tested given the fact that some of the mutations were predicted to have an effect on the homo-oligomerization sub-region. The longest PKD2 fragment, TM5-COOH, was pulled down with and pulled down PKD2-V5 (**Fig. 2.5**, **B**, lanes 4 and 7, respectively). The other two PKD2 fragments, TM6-COOH (**Fig. 2.6**, **B**, lanes 4 and 7) and EFh-COOH (**Fig. 2.7**, **B**,

lanes 9 and 10), were similarly co-purified with and co-purified PKD2-V5. This suggests that the fragments are capable of homo-oligomerization. The controls used are similar to those described above (**Fig. 2.5** and **Fig. 2.6**, **B**, lane 9**; Fig. 2.7**, **B**, lane 8). However, instead of attempting to co-purify the PKD2 fragments with an antibody raised against the V5 tag, from cell lysates co-expressing the V5 tag and the interaction partner, lysates expressing only the PKD2 fragments were used (**Fig. 2.5** and **Fig. 2.6**, **B**, lane 6**; Fig. 2.7**, **B**, lane 11). This was due to the empty vector expressing V5 not being available. This control showed that the V5 antibody does not have non-specific affinities to the PKD2 fragments.

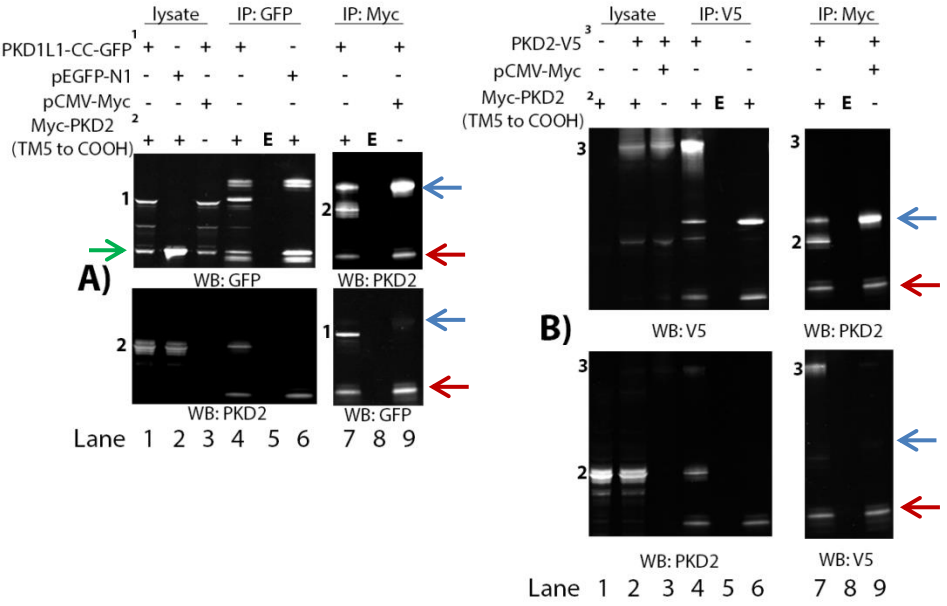


Figure 2.5: Interaction of TM5-COOH with PKD1l1-CC-GFP (**A**) or PKD2-V5 (**B**). PKD1L1-CC-GFP (**1**) and TM5-COOH (**2**) can be purified as interacting partners (**A**, lanes 4 and 7). Similarly, TM5-COOH (**2**) and PKD2-V5 (**3**) can be purified as interacting partners (**B**, lanes 4 and 7). Purifying the tag of one interaction partner alone (**A**, lanes 6 and 9; **B**, lane 9) fails to co-precipitate the other, co-expressed, interaction partner. Similarly, attempting to purify TM5-COOH with a V5 antibody fails to purify the co-expressed interaction partner (**B**, lane 6). Lanes 1-3 in **A** and **B** show the expression of the relevant proteins in the untreated lysates. **E**: empty lane (**A** and **B**, lanes 5 and 8). Green arrow: GFP; blue arrow: heavy-chain IgG; red arrow: light-chain IgG. Heavy- and light-chain IgG are only present in IP fraction (lanes 4, 6, 7 and 9).

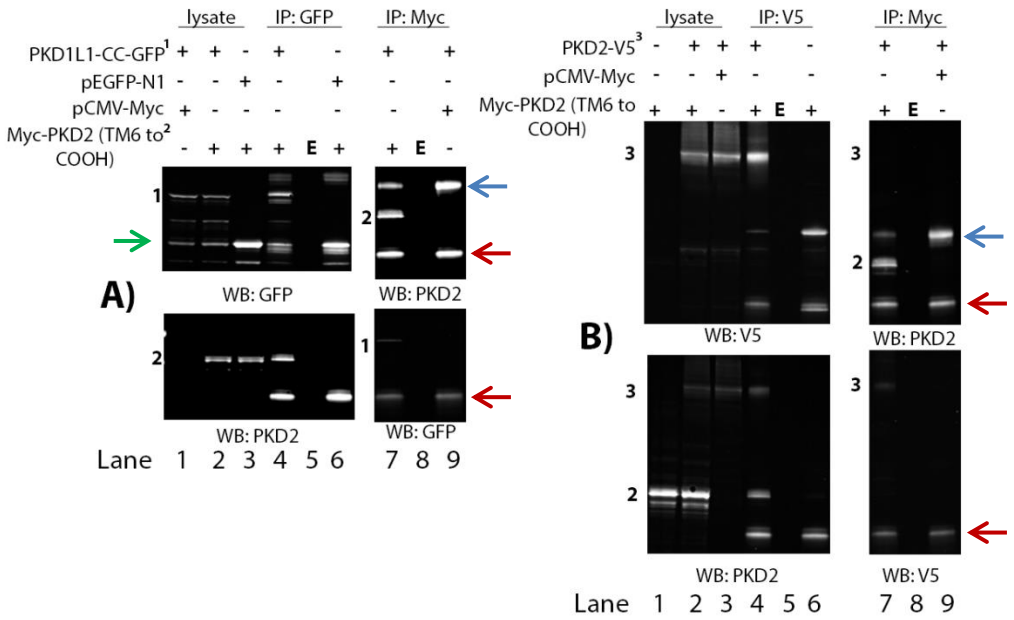


Figure 2.6: Interaction of TM6-COOH (**2**) with PKD1l1-CC-GFP (**1**) (**A**) or PKD2-V5 (**3**) (**B**). TM6-COOH can be purified together with PKD1L1-CC-GFP and PKD2-V5 (lanes 4 and 7 in **A** and **B**, respectively). For explanation on controls and layout, see **Fig. 2.5**.

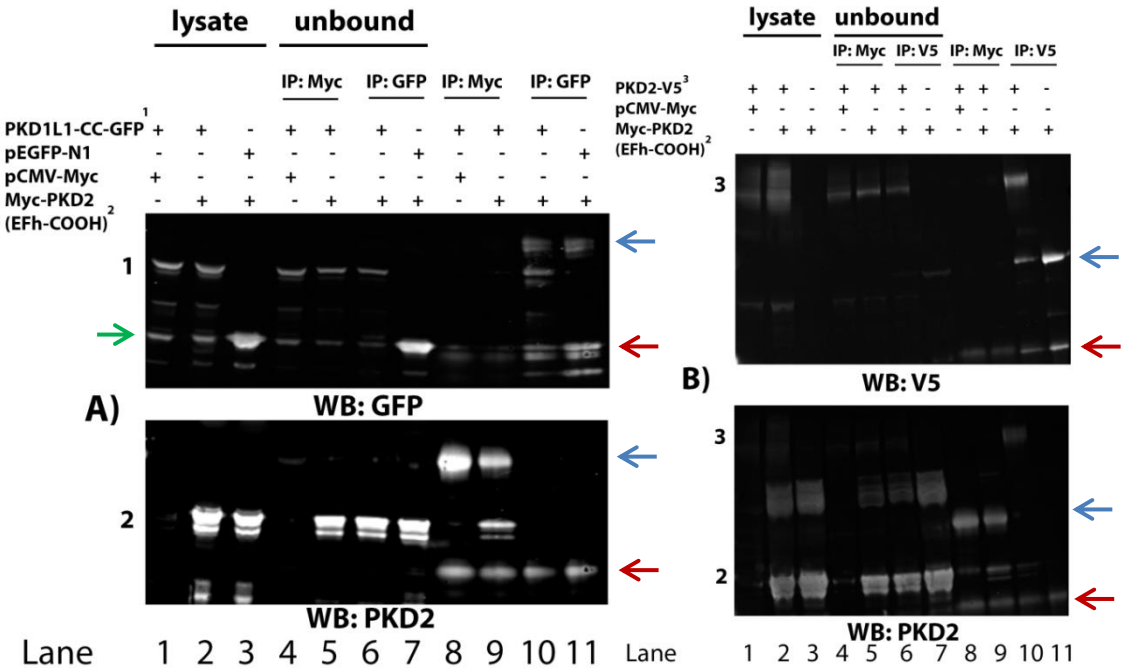


Figure 2.7: Interaction of EFh-COOH (**2**) with PKD1l1-CC-GFP (**1**) (**A**) or PKD2-V5 (**3**) (**B**). EFh-COOH can be purified together with PKD1L1-CC-GFP and PKD2-V5 (lanes 9 and 10 in **A** and **B**, respectively). For explanation on controls, see **Fig. 2.5** (shown **A** and **B**, lanes 8 and 11)**.** Lanes 1-3 in both **A** and **B** show the expression of the relevant proteins in the untreated lysates; lanes 4-7 in both **A** and **B** show the content of relevant proteins in the unbound fraction (protein not bound by antibody). Heavy- (blue arrow) and light-chain (red arrow) IgGs present only in unbound and IP fraction (lanes 4-11). Green arrow: GFP.

Given that the EFh-COOH fragment is unable to co-precipitate with PKD1L1-CC-GFP, it seemed reasonable to hypothesise that this lack of interaction occurs due to a difference in localisation between EFh-COOH and the membrane-tethered fragments. I therefore transfected COS-7 cells with TM6-COOH and EFh-COOH, with or without PKD1L1-CC-GFP, and assessed their localisation. These cells were used as they are larger, in terms of surface area, than HEK293T cells, and easier to transfect than IMCD3 cells. As a control, I also assessed the localisation of the full-length V5-tagged PKD2 in the presence or absence of PKD1L1-CC-GFP. PKD2-V5 localised to the ER and ER whorls (**Fig. 2.8**, row **F**), together with PKD1L1-CC-GFP (**Fig. 2.8**, row **G**). The PKD2 fragment containing one TM, TM6-COOH, showed localisation to the membrane systems, but did not induce ER whorls (**Fig. 2.8**, row **A**). The fragment lacking TMs, EFh-COOH, similarly localised to the membrane systems, but did not induce ER whorls (**Fig. 2.8**, row **B**). Both fragments showed similar localisation patterns. Moreover, when co-expressed with PKD1L1-CC-GFP, the localisation of both TM6-COOH (**Fig. 2.8**, row **C**) and EFh-COOH (**Fig. 2.8**, row **D**) overlapped with PKD1L1-CC-GFP. This indicates that the difference in interaction with PKD1L1-CC-GFP seen between EFh-COOH and the PKD2 fragments containing TM helices is not due to differences in localisation. However, this experiment does not rule out a potential requirement for plasma membrane anchorage of the PKD2 fragments, in order for the interaction with PKD1L1 to occur (*vide supra*).

N.B.: All Co-IP reactions described in this chapter were only performed once, aside for the interaction between EFh-COOH (**Fig. 2.7**) and the interactions summarised in **Fig. 2.17**. For these interactions, two and three technical replicates, respectively, were performed. Each transfection for the Co-IPs was performed in duplicates and pooled during the Co-IP procedure.

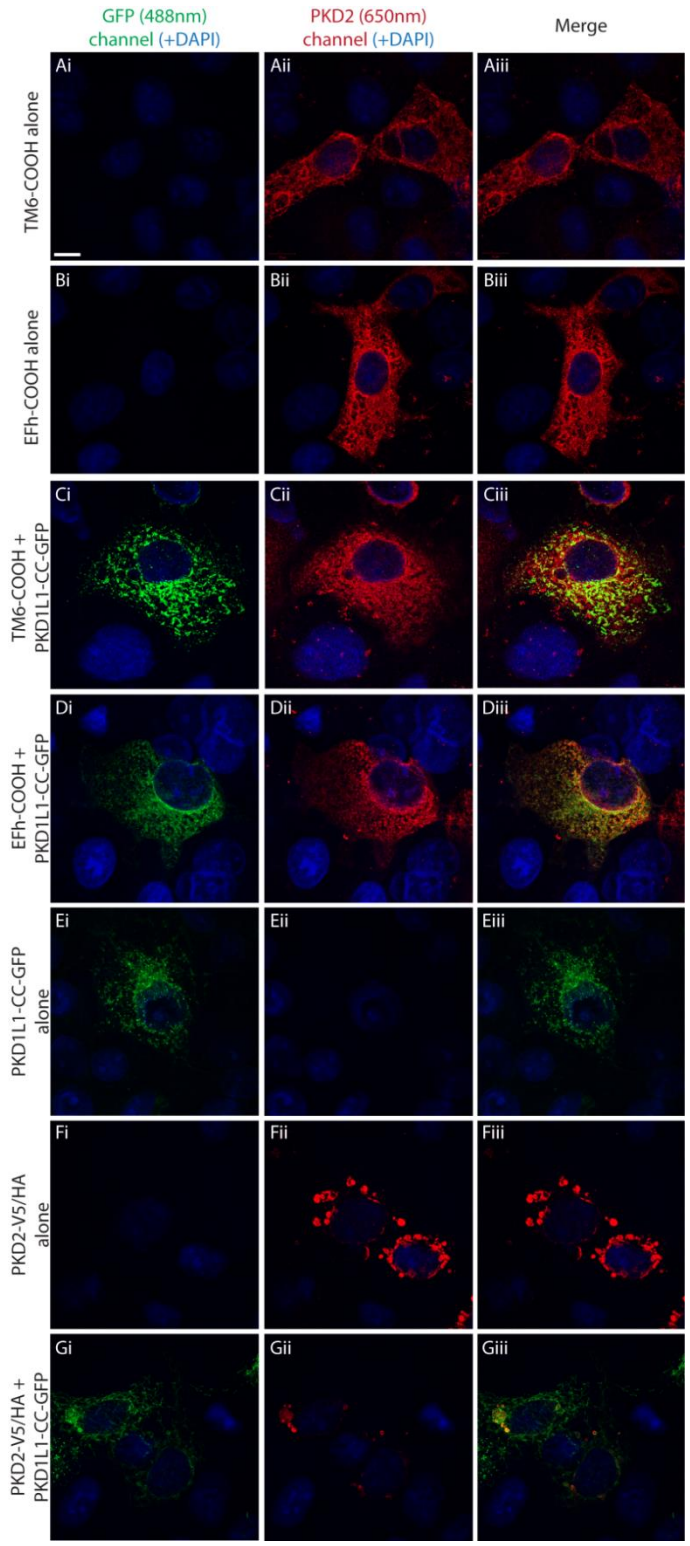


Figure 2.8: Localisation of PKD2 fragments or full-length protein in COS-7 cells, in the presence or absence of PKD1L1-CC-GFP. Colours represent: green – GFP; red – PKD2; blue (DAPI) – nucleus. Rows **A**, **B** and **C, D** show localisation of TM6-COOH and EFh-COOH, alone or in the presence of PKD1L1-CC-GFP, respectively. Row **E** shows localisation of PKD1L1-CC-GFP. Rows **F** and **G** show localisation of PKD2-V5, alone or in the presence of PKD1L1-CC-GFP, respectively. Scale bar in **Ai**: 10 µm.

2.2.3. The involvement of the PKD2 CC in the PKD1L1-PKD2 interaction

In order to test whether the PKD2 hetero-oligomerization sub-region of the CC is involved in the PKD1L1-PKD2 interaction, the mouse PKD2 fragment, TM5-COOH, was used to determine the effect of a number of PKD2 mutations on this interaction, *via* Co-IPs. Considering that some of the mutations were predicted to also affect the homo-oligomerization sub-region of the CC (**Fig. 2.2**), the interaction of the mutant TM5-COOH fragments with PKD2-V5 was also tested.

Using the same approach as described in section **2.2.2**, I used Co-IPs to test whether the PKD2 mutations of interest (see section **2.2.1**) influence the interaction between the longest PKD2 fragment, TM5-COOH, and PKD1L1-CC-GFP. In the presence of the L906P mutation, the TM5-COOH fragment was able to be enriched with and enrich PKD1L1-CC-GFP (**Fig. 2.9**, **A**, lanes 4 and 7, respectively), as well as PKD2-V5 (**Fig. 2.9**, **B**, lanes 4 and 7, respectively). Similarly, the presence of the V907D mutation allowed TM5-COOH to be pulled down with and pull down PKD1L1-CC-GFP (**Fig. 2.10**, **A**, lanes 4 and 7, respectively) and PKD2-V5 (**Fig. 2.10**, **B**, lanes 4 and 7, respectively). The mutation which affects the PKD1-PKD2 interaction, L882H (Tsiokas et al., 1999), did not affect TM5-COOH co-purification with and co-purification of PKD1L1-CC-GFP (**Fig. 2.11**, **A**, lanes 4 and 7, respectively) or PKD2-V5 (**Fig. 2.11**, **B**, lanes 4 and 7, respectively). D884A, a mutation previously shown to affect the interaction of PKD2 with TRPC1, but not PKD1 (Tsiokas et al., 1999), was similarly tested. In the presence of this mutation, TM5-COOH is able to co-purify with and co-purify PKD1L1-CC-GFP (**Fig. 2.12**, **A**, lanes 4 and 7, respectively) or PKD2-V5 (**Fig. 2.12**, **B**, lanes 4 and 7, respectively). Controls equivalent to those described in section **2.2.2** were used, and indicate that the interactions are specific to the protein fragments used. These results indicate that these mutations do not hinder the formation of the PKD2 CC, in spite of their predicted effect (see section **2.2.1**), and therefore do not impact the interaction between PKD1L1 and PKD2 fragments. Alternatively, it is possible that the PKD1L1-PKD2 interaction does not require the CC.

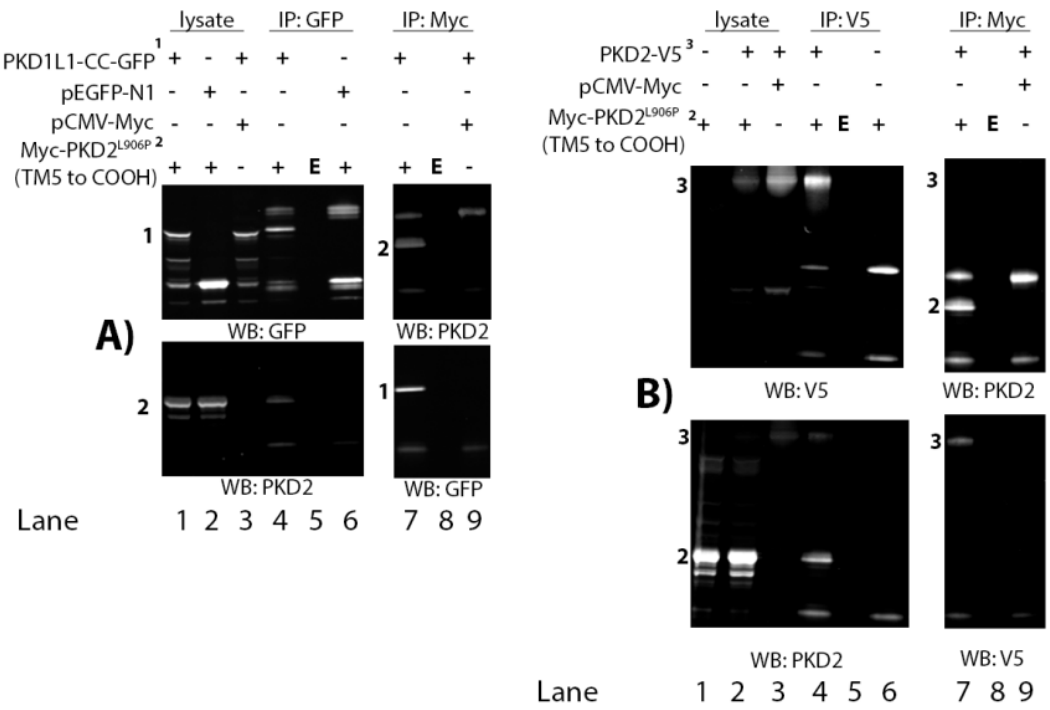


Figure 2.9: Interaction of TM5-COOH^{L906P} (**2**) with PKD1l1-CC-GFP (**1**) (**A**) or PKD2-V5 (**3**) (**B**). TM5-COOH^{L906P} can be purified together with PKD1L1-CC-GFP and PKD2-V5 (lanes 4 and 7 in **A** and **B**, respectively). For explanation on controls and layout, see **Fig. 2.5**.

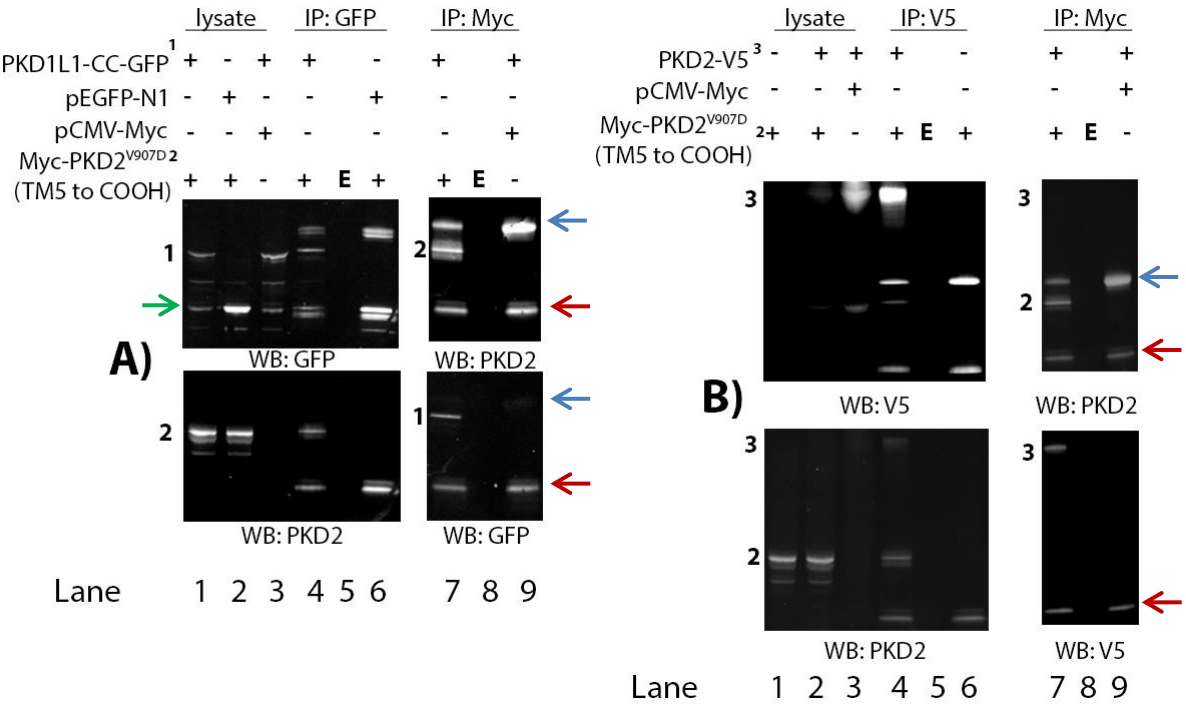


Figure 2.10: Interaction of TM5-COOH^{V907D} (**2**) with PKD1l1-CC-GFP (**1**) (**A**) or PKD2-V5 (**3**) (**B**). TM5-COOH^{V907D} can be purified together with PKD1L1-CC-GFP and PKD2-V5 (lanes 4 and 7 in **A** and **B**, respectively). For explanation on controls and layout, see **Fig. 2.5**.

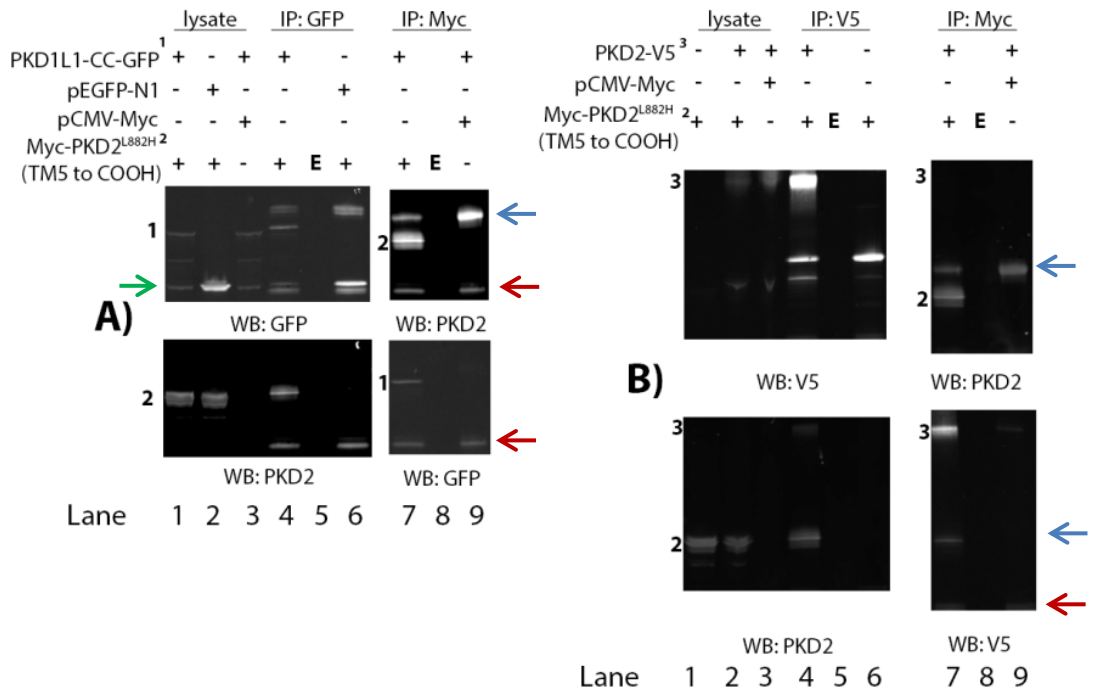


Figure 2.11: Interaction of TM5-COOH^{L882H} (**2**) with PKD1l1-CC-GFP (**1**) (**A**) or PKD2-V5 (**3**) (**B**). TM5-COOH^{L882H} can be purified together with PKD1L1-CC-GFP and PKD2-V5 (lanes 4 and 7 in **A** and **B**, respectively). For explanation on controls and layout, see **Fig. 2.5**.

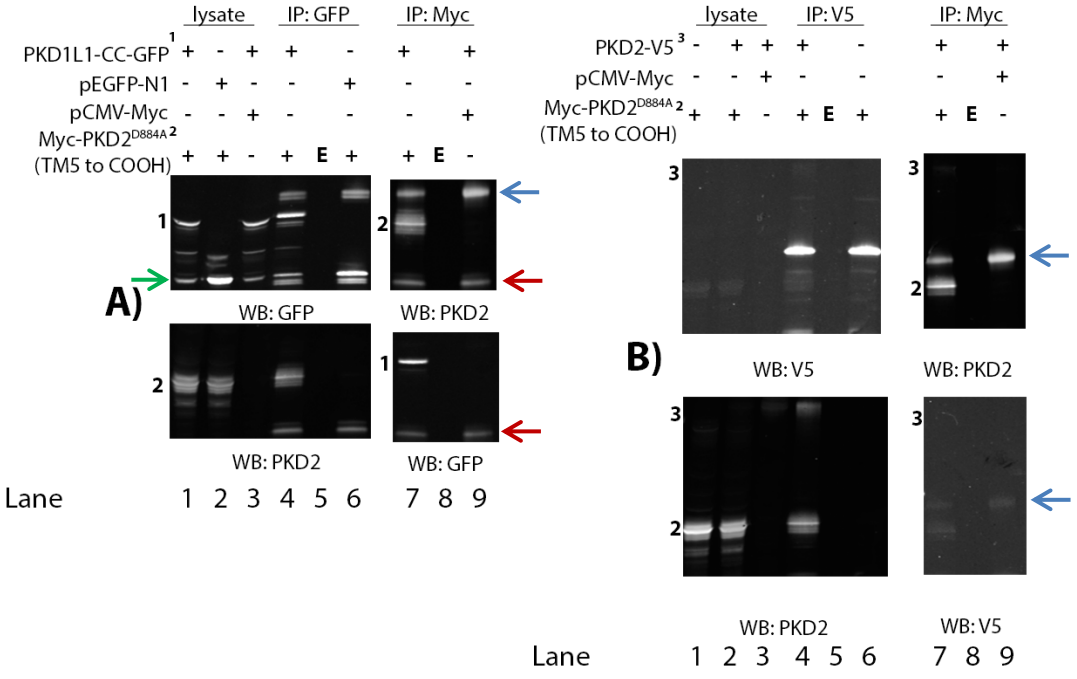


Figure 2.12: Interaction of TM5-COOH^{D884A} (**2**) with PKD1l1-CC-GFP (**1**) (**A**) or PKD2-V5 (**3**) (**B**). TM5-COOH^{D884A} can be purified together with PKD1L1-CC-GFP and PKD2-V5 (lanes 4 and 7 in **A** and **B**, respectively). For explanation on controls and layout, see **Fig. 2.5**.

In order to test whether the PKD2 CC is required for PKD1L1-PKD2 interaction, I next tested whether truncation of the two CC sub-regions, required for homo- or hetero-oligomerization, respectively, had any effect on the interaction of the two proteins. The same Co-IP approach as described in section **2.2.2** was used. Two PKD2 mutations were specifically chosen to truncate the protein: S818X, which truncates the protein just upstream of the CC region, and R870X, which truncates the hetero-oligomerization sub-region. The R870X mutation is of particular interest, given that the equivalent mutation in human, R872X, is one of the most common ADPKD-causing mutations in PKD2 (Rossetti et al., 2007, Harris and Rossetti, 2010). The presence of the R870X mutation did not affect the ability of TM5-COOH to co-purify with and co-purify PKD1L1-CC-GFP (**Fig. 2.13**, **A**, lanes 4 and 7, respectively) or PKD2-V5 (**Fig. 2.13**, **B**, lanes 4 and 7, respectively). In the presence of the mutation which removes the entire CC, S818X, TM5-COOH enriched or was enriched with PKD1L1-CC-GFP (**Fig. 2.14**, **A**, lanes 9 and 10, respectively) or PKD2-V5 (**Fig. 2.14**, **B**, lanes 9 and 10, respectively). These results indicate that neither of the two mutations abolished the PKD1L1-PKD2 fragment interaction, nor PKD2 homo-oligomerization. The controls are equivalent to those used in section **2.2.2**, and indicate that the interactions are specific to the protein fragments used.

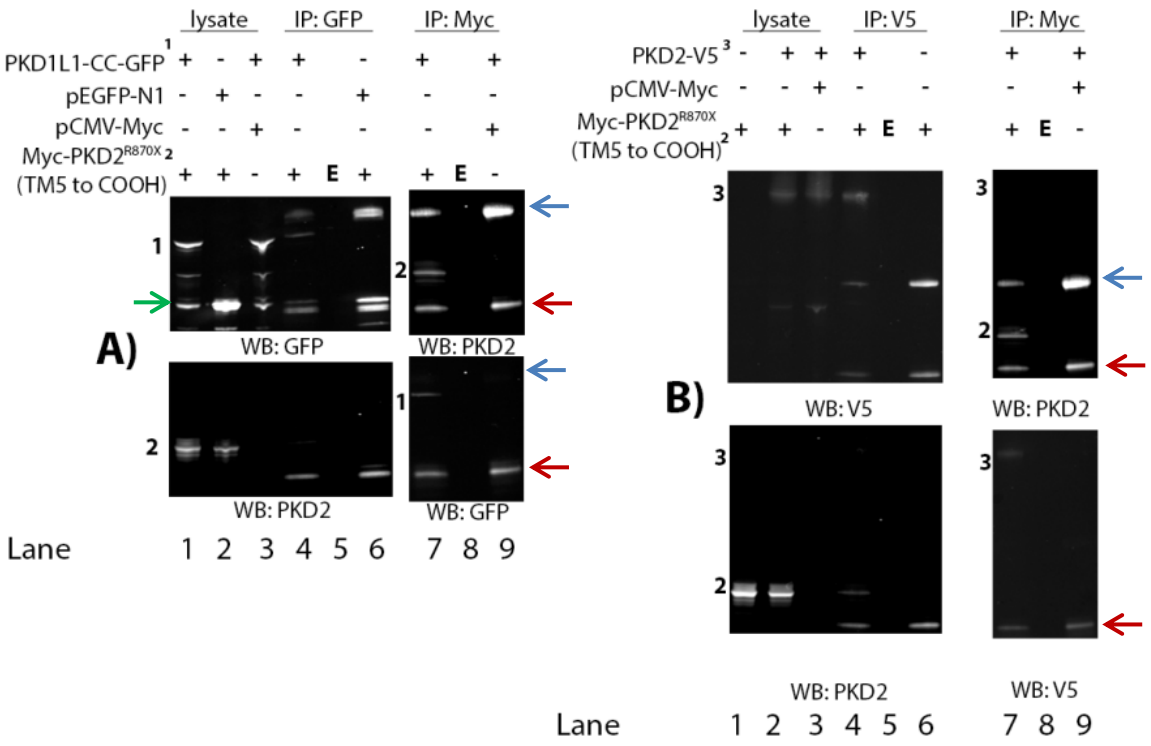


Figure 2.13: Interaction of TM5-COOH^{R870X} (**2**) with PKD1l1-CC-GFP (**1**) (**A**) or PKD2-V5 (**3**) (**B**). TM5-COOH^{R870X} can be purified together with PKD1L1-CC-GFP and PKD2-V5 (lanes 4 and 7 in **A** and **B**, respectively). For explanation on controls and layout, see **Fig. 2.5**.

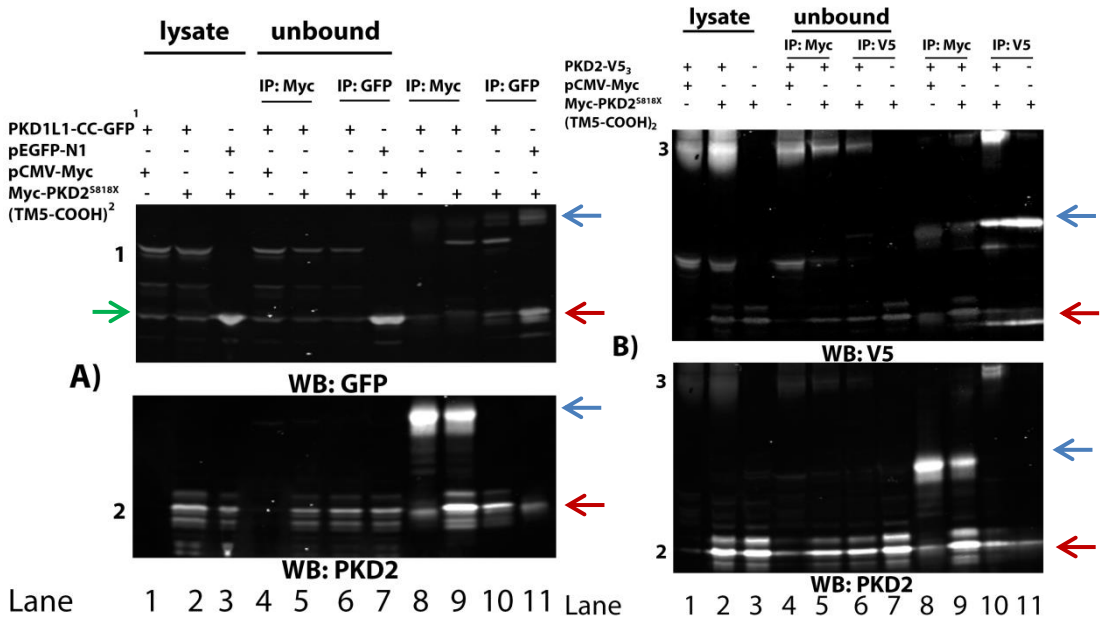


Figure 2.14: Interaction of TM5-COOH^{S818X} (**2**) with PKD1l1-CC-GFP (**1**) (**A**) or PKD2-V5 (**3**) (**B**). TM5-COOH^{S818X} can be purified together with PKD1L1-CC-GFP and PKD2-V5 (lanes 9 and 10 in **A** and **B**, respectively). For explanation on controls and layout, see **Fig. 2.5** and **Fig. 2.7**, respectively.

Given that the S818X mutation truncates the PKD2 protein N-terminally to the CC, but is still able to interact with PKD1L1-CC-GFP, I tested whether the TM5-COOH^{S818X} fragment interacts with PKD1L1-CC-GFP or PKD2-V5 less efficiently than the WT fragment. I performed a side-by-side Co-IP between the WT and S818X mutant TM5-COOH and PKD1L1-CC-GFP, using the same approach described in section **2.2.2**. Both forms of TM5-COOH were able to co-precipitate PKD1L1-CC-GFP (**Fig. 2.15**, **A**, lanes 7 and 8) and the two TM5-COOH fragments were co-precipitated by PKD1L1-CC-GFP (**Fig. 2.15**, **B**, lanes 7 and 8). However, the enrichment of PKD1L1-CC-GFP by the truncated form of TM5-COOH appears to be weaker than that of the WT fragment (**Fig. 2.15**, **A** and **B**, lanes 7 and 8, red highlight). The controls are equivalent to those described for the Co-IPs in section **2.2.2**, and indicate that the interactions are specific to the fragments used. This result argues that the PKD1L1-PKD2 fragment interaction is weakened in the presence of the S818X mutation.

Contrary to my initial hypothesis, the results presented in this section argue that neither sub-region of the CC of PKD2 appears to be required for the interaction with PKD1L1, given that the PKD1L1-CC-GFP fragment can interact with both TM5-COOH^{R870X} and TM5-COOH^{S818X}. These two fragments lack the hetero-oligomerization sub-region of the CC, or entire CC region, respectively.

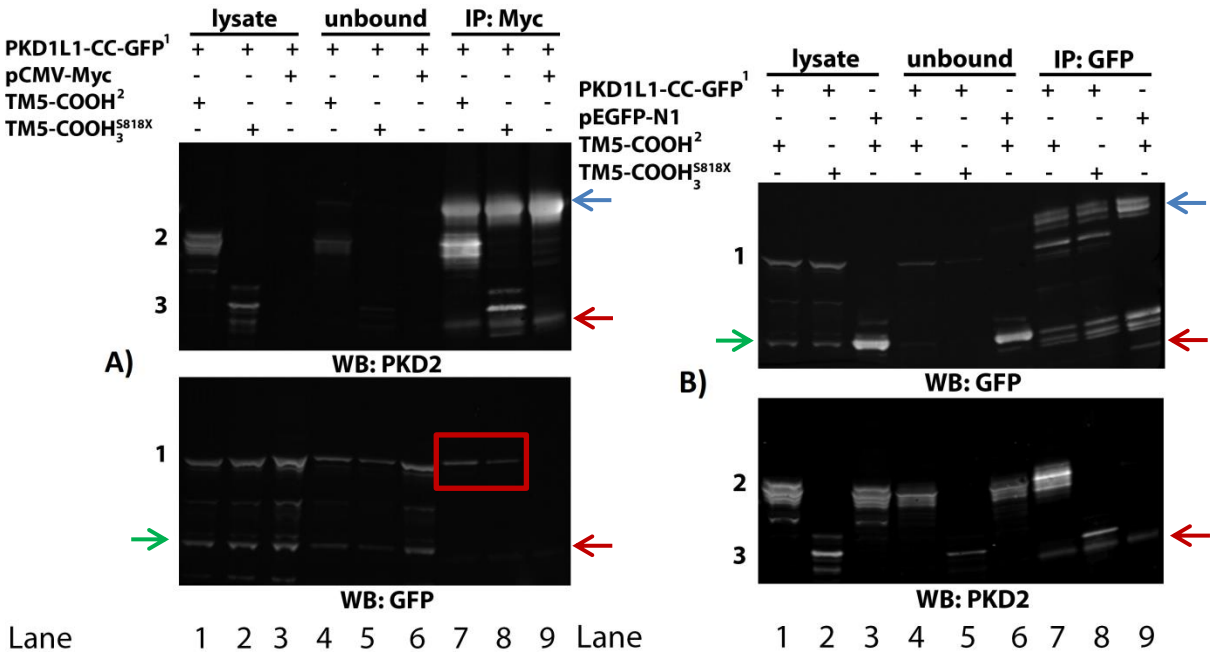


Figure 2.15: Interaction of WT TM5-COOH (**2**) or TM5-COOH^{S818X} (**3**) with PKD1l1-CC-GFP (**1**). Myc IP shown in **A**, GFP IP shown in **B**. Both TM5-COOH fragments can be purified together with PKD1L1-CC-GFP (**A** and **B**, lanes 7 and 8). Controls are identical to those of **Fig. 2.5**, and are shown in **A** and **B**, lane 9. Lanes 1-3 show untreated lysates, lanes 4-6 show the unbound fraction. WT (**A**, lane 7) and mutant (**A**, lane 8) PKD1L1-CC-GFP bands are highlighted in red.

2.2.4. The C630 residue of PKD2 is not required for the interaction with PKD1L1

Initially, I had hypothesised that the PKD1L1-PKD2 interaction is mechanistically similar to that of PKD1-PKD2, involving the hetero-oligomerization sub-region of the PKD2 CC. Considering the results presented in section **2.2.3**, which suggest that the CC of PKD2 is not required for the interaction of PKD1L1 and PKD2 fragments, I tested whether their interaction occurs through domains other than the CC contained within the fragments. The C632 residue of PKD2 (human AA numbering) was previously shown to be involved in PKD2 homo-oligomerization (Feng et al., 2011), and PKD1L1 contains a number of cysteine residues in the C-terminal region overlapping the PKD1L1-CC-GFP fragment. In theory, a cysteine bridge would be able to facilitate the interaction between PKD1L1 and PKD2, even in the absence of the CC domain, as the two molecules would remain covalently bound up to the final elution stage of a Co-IP. Using the equivalent mouse PKD2 mutation employed by Feng and colleagues (Feng et al., 2011), C630A, I

tested the interaction of TM5-COOH with PKD1L1-CC-GFP, using the Co-IP approach described previously (see section **2.2.2**). TM5-COOH^{C630A} was able to pull down and be pulled down with PKD1L1-CC-GFP (**Fig. 2.16**, **A**, lanes 9 and 10, respectively), as well as PKD2-V5 (**Fig. 2.16**, **B**, lanes 9 and 10, respectively). The controls were equivalent to those described for experiments in section **2.2.2**, and indicate that the interactions are specific. This result indicates that TM5-COOH^{C630A} is able to interact with PKD1L1-CC-GFP and PKD2-V5, and argues that the C630 residue is not necessary for the PKD1L1-PKD2 interaction. However, this experiment does not address whether this residue is sufficient for the PKD1L1-PKD2 interaction to occur.

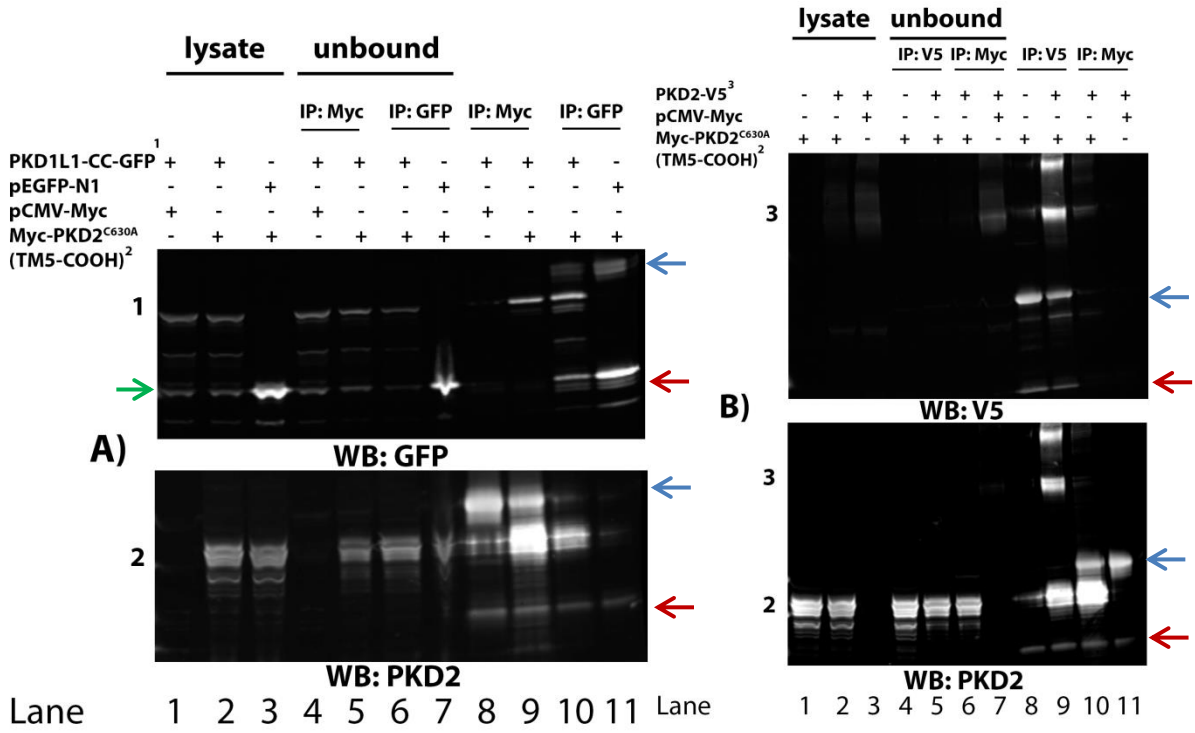


Figure 2.16: Interaction of TM5-COOH^{C630A} (**2**) with PKD1L1-CC-GFP (**1**) (**A**) or PKD2-V5 (**3**) (**B**). TM5-COOH^{C630A} can be purified together with PKD1L1-CC-GFP or PKD2-V5 (lanes 9 and 10 in **A** and **B**, respectively). For explanation on controls and layout, see **Fig. 2.5** and **Fig. 2.7**, respectively.

2.2.5. Testing previous findings regarding the PKD1L1- and PKD1-PKD2 interaction

The results presented thus far indicate that the PKD1L1-PKD2 interaction is mechanistically different from that of PKD1-PKD2, which requires the CC of both PKD1 and PKD2 for the interaction to occur. The hypothesis proposed at the beginning of this chapter (see section **2.1.3**) was based on previous findings, which suggested that the CC of PKD1L1 is required for the PKD1L1-PKD2 interaction (Field et al., 2011). However, removing the entirety of the CC domain from a PKD2 fragment, TM5-COOH, did not abolish the PKD1L1-PKD2 fragment interaction (**Fig. 2.14**). These findings are in contradiction to the interaction model proposed by previous studies (see section **2.1.1**), which argues for the importance of the PKD2 CC for the PKD1L1-PKD2 interaction.

I therefore tested the requirement of the PKD1L1 CC for the interaction of PKD1L1-CC-GFP with PKD2, using the same experimental protocol used to obtain the results described in section **2.2.2**. In order to test this, I employed a PKD1L1 CC mutation (L2564D) that was previously described to abolish the PKD1L1-PKD2 interaction (Field et al., 2011). Full-length 6xMyc-PKD2 was able to co-precipitate both WT and PKD1L1-CC-GFP^{L2564D} (**Fig. 2.17**, **A**, lanes 7 and 8, respectively); similarly, either WT or mutant PKD1L1-CC-GFP was able to co-precipitate 6xMyc-PKD2 (**Fig. 2.17**, **B**, lanes 7 and 8, respectively). The controls are equivalent to those described for previous experiments (see section **2.2.2**), and indicate that the interactions are specific. This result argues that the PKD1L1 CC mutation does not abolish PKD1L1-PKD2 interaction, as suggested by Field and colleagues (Field et al., 2011). Given that the lysis buffer used was different to those used in the experiments described in the aforementioned study, I next tested whether the difference in results is due to the differences in lysis buffer. Using the lysis buffer described in the initial study (Field et al., 2011), full-length PKD2 is able to co-precipitate or be co-precipitated by WT and mutant PKD1L1-CC-GFP (**Fig. 2.18**, **A** and **B**, lanes 7 and 8). In order to further validate my results, I employed a different Co-IP protocol, using a different buffer to those previously used. Under

these conditions, full-length PKD2 is also able to enrich or be enriched by WT and mutant PKD1L1-CC-GFP (**Fig. 2.19**, **A** and **B**, lanes 7 and 8). As with previous experiments, the controls indicate that the interactions are specific. All three conditions indicate that the presence of the PKD1L1 CC mutation, L2564D, does not abolish the interaction between PKD1L1-PKD2, as previously suggested (Field et al., 2011). However, under all three conditions, there is a difference between the interaction of PKD1L1-CC-GFP or PKD1L1-CC-GFP^{L2564D} with 6xMyc-PKD2. It appears that in the presence of the L2564D mutation, PKD2 enriches or is enriched with PKD1L1-CC-GFP less than with the WT PKD1L1-CC-GFP. This finding suggests that the PKD1L1 mutation impacts the efficiency of the PKD1L1-PKD2 interaction, even if it does not abrogate it, as previously described. For details regarding the protocols employed, see section **5.4.1**.

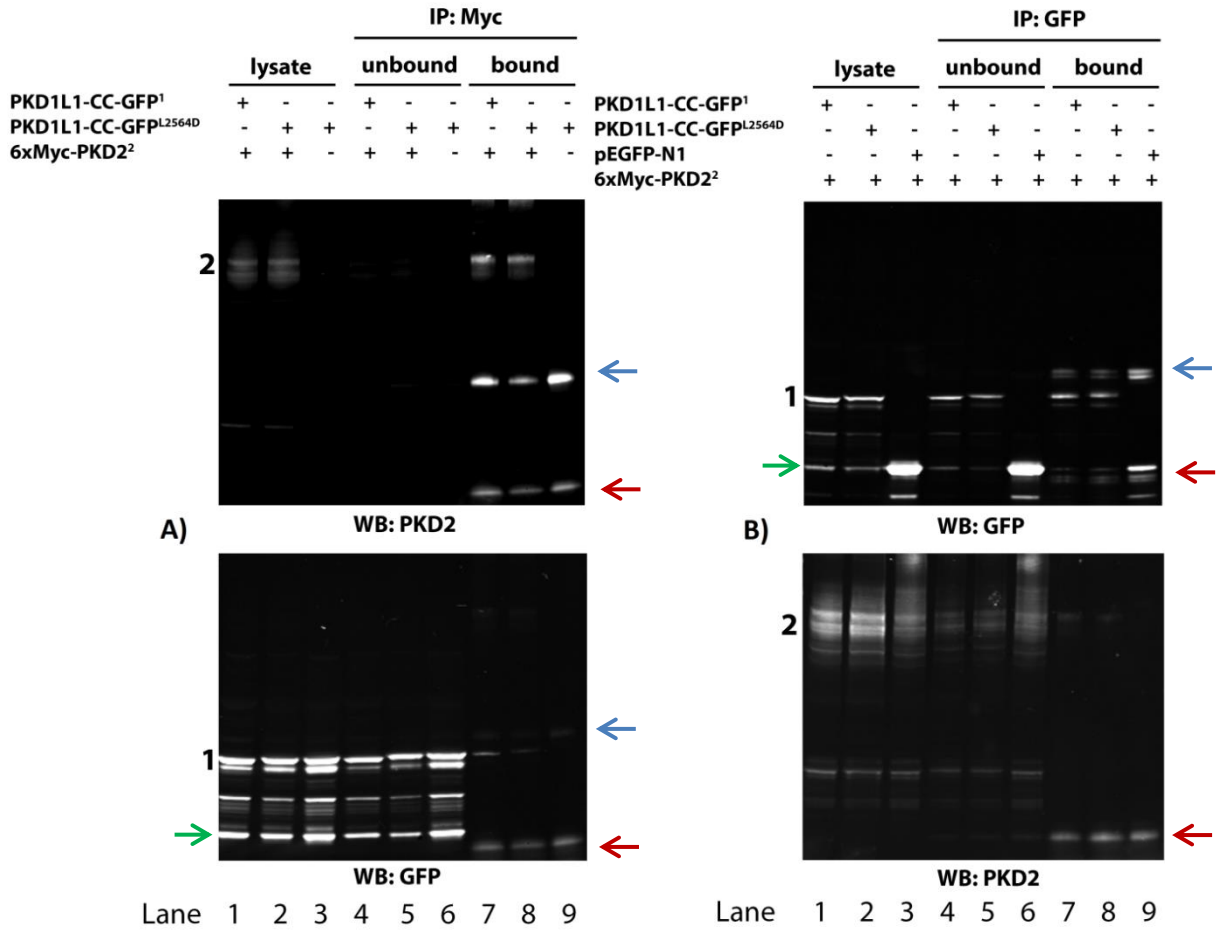


Figure 2.17: Interaction of 6xMyc-PKD2 (**2**) with WT or L2564D PKD1L1-CC-GFP (**1**). Myc IP shown in **A**, GFP IP shown in **B**. 6xMyc-PKD2 can be purified together with PKD1L1-CC-GFP, WT or L2564D (lanes 7 and 8 in **A** and **B**, respectively). Lanes 1-3 show untreated lysates, lanes 4-6 show unbound fraction. Controls are identical to those of **Fig. 2.5**. Experimental conditions were identical to experiments described in section **2.2.2**.

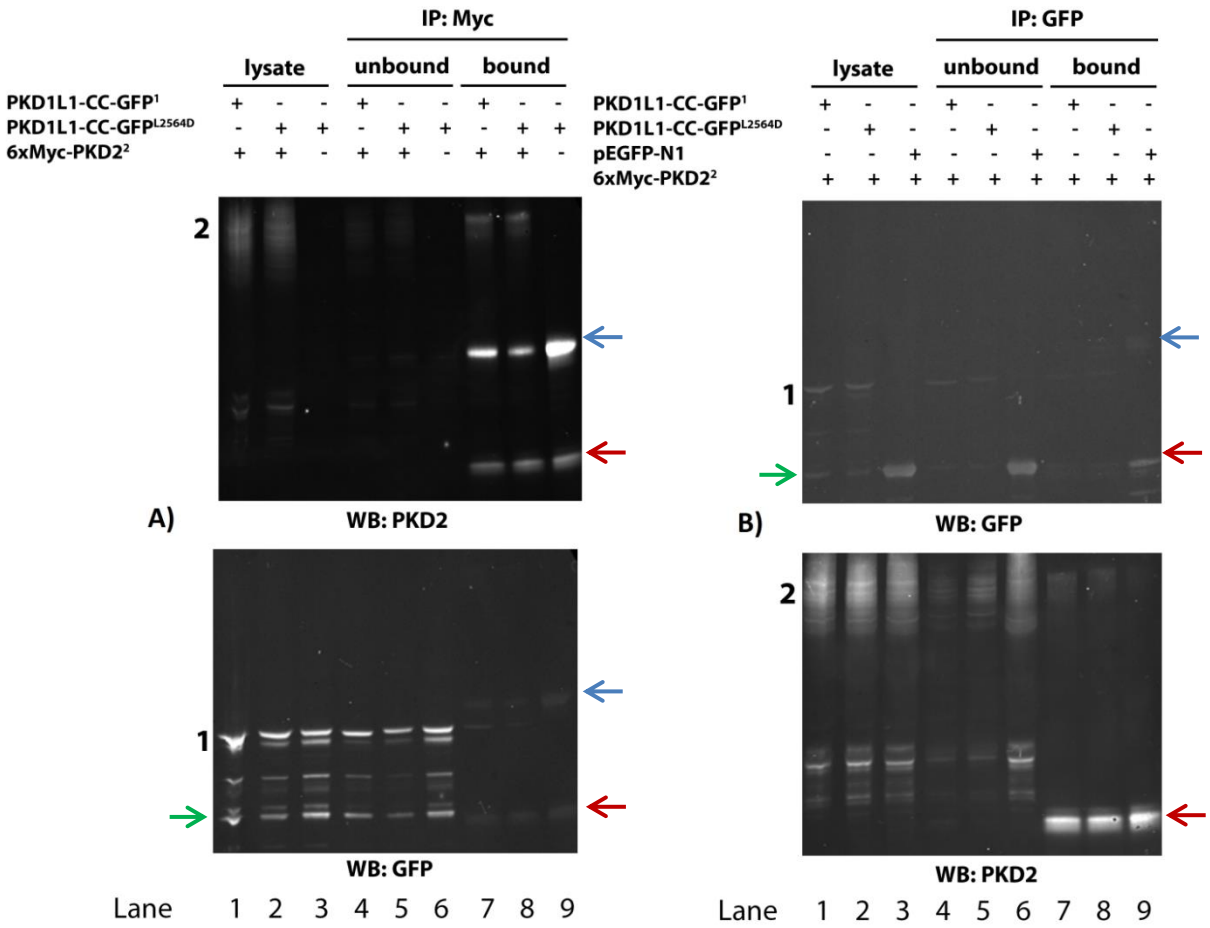


Figure 2.18: Interaction of 6xMyc-PKD2 (**2**) with WT or L2564D PKD1L1-CC-GFP (**1**). Myc IP shown in **A**, GFP IP shown in **B**. 6xMyc-PKD2 can be purified together with PKD1L1-CC-GFP, WT or L2564D (lanes 7 and 8 in **A** and **B**, respectively). Lanes 1-3 show untreated lysates, lanes 4-6 show unbound fraction. Controls are identical to those of **Fig. 2.5**. This experiment employed the same lysis buffer as used for the experiment described in (Field et al., 2011).

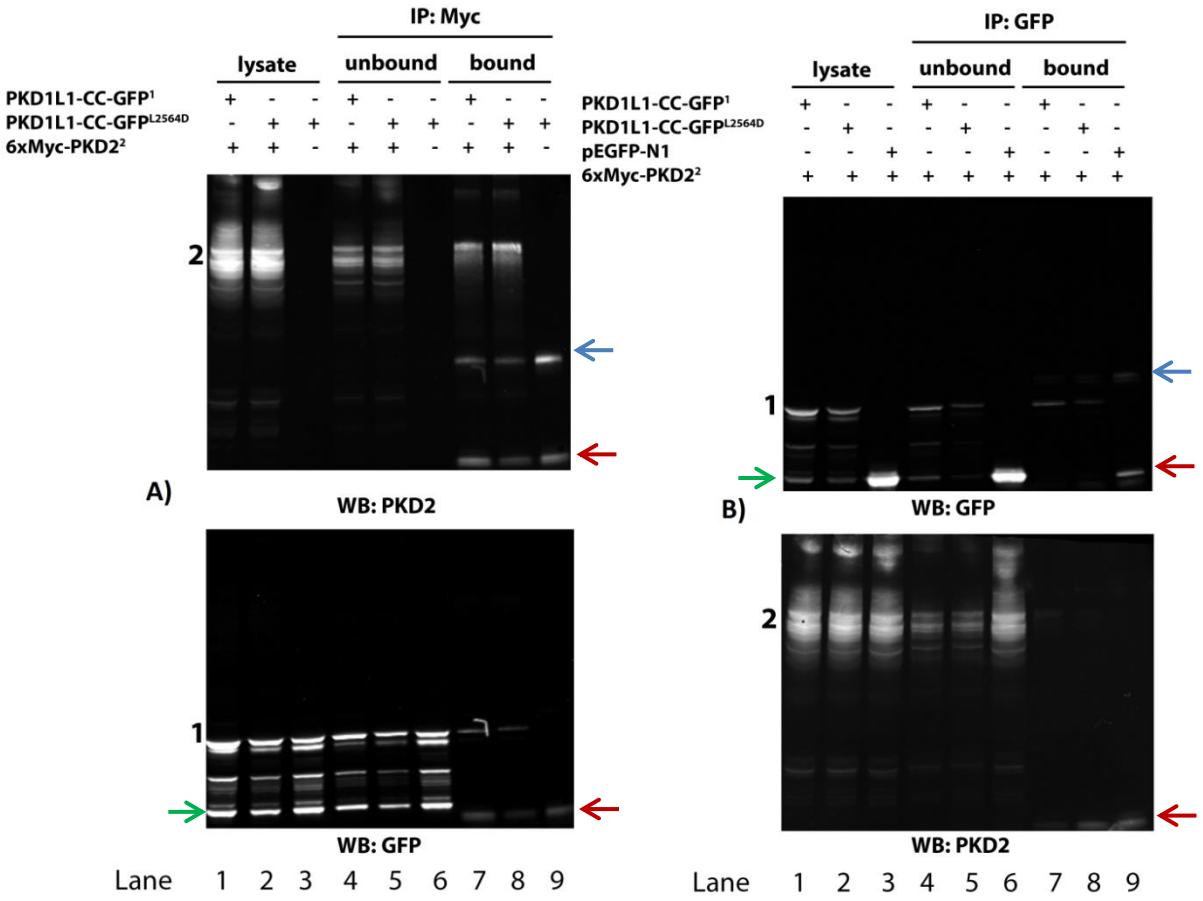


Figure 2.19: Interaction of 6xMyc-PKD2 (**2**) with WT or L2564D PKD1L1-CC-GFP (**1**). Myc IP shown in **A**, GFP IP shown in **B**. 6xMyc-PKD2 can be purified together with PKD1L1-CC-GFP, WT or L2564D (lanes 7 and 8 in **A** and **B**, respectively). Lanes 1-3 show untreated lysates, lanes 4-6 show unbound fraction. Controls are identical to those of **Fig. 2.5**. This experiment employed a different Co-IP protocol and lysis buffer.

In order to validate whether the mutations that affect PKD1-PKD2 interaction behave as expected, I designed a PKD1 fragment similar to PKD1L1-CC-GFP. PKD1-CC-GFP contains the last TM of PKD1 and the entire intracellular C-terminus, as well as a C-terminal GFP tag. I tested the ability of PKD1-CC-GFP to interact with WT or mutant TM5-COOH, using the same approach as for the experiments described in section **2.2.2**. Alongside TM5-COOH^{L882H}, I also tested the TM5-COOH^{V907D}, TM5-COOH^{R870X} and TM5-COOH^{S818X} fragments, as well as EFh-COOH. The TM5-COOH^{L906P} was transfected alongside PKD1-CC-GFP, but could not be expressed. TM5-COOH was pulled down with or pulled down PKD1-CC-GFP (**Fig. 2.20**, **A** and **C**, lane 9, respectively). The fragments containing point mutations, TM5-COOH^{V907D} (**Fig. 2.20**, **B** and **D**, lane 11), TM5-

COOH^{L882H} (**Fig. 2.20**, **A** and **C**, lane 10) were enriched with or enriched PKD1-CC-GFP, respectively. The fragments bearing truncation mutations, TM5-COOH^{S818X} (**Fig. 2.20**, **B** and **D**, lane 12) and TM5-COOH^{R870X} (**Fig. 2.20**, **A** and **C**, lane 11) were also co-purified with or co-purified the PKD1 fragment, respectively. The EFh-COOH fragment was not enriched by PKD1-CC-GFP (**Fig. 2.20**, **B**, lane 10), but was able to enrich PKD1-CC-GFP (**Fig. 2.20**, **D**, lane 10). However, the interaction is only specific for the GFP IPs, as evidenced by the controls: the Myc IPs non-specifically pulled down the GFP-tagged interaction partner, even in the absence of TM5-COOH (**Fig. 2.20**, **C,** lane 12), whilst the GFP IP did not enrich the TM5-COOH in the absence of its interaction partner (**Fig. 2.20**, **A,** lane 12). Apart from EFh-COOH, the results suggest that all of the other PKD2 fragments tested were able to interact with PKD1-CC-GFP. These results indicate that the mutations previously described or predicted to abolish PKD1-PKD2 fragment interaction behave differently in my hands. Furthermore, EFh-COOH is also unable to interact with PKD1-CC-GFP; the smallest of the PKD2 fragments contains the CC domain, which was previously described to be sufficient for PKD1-PKD2 fragment interaction (**Table 2.1**).

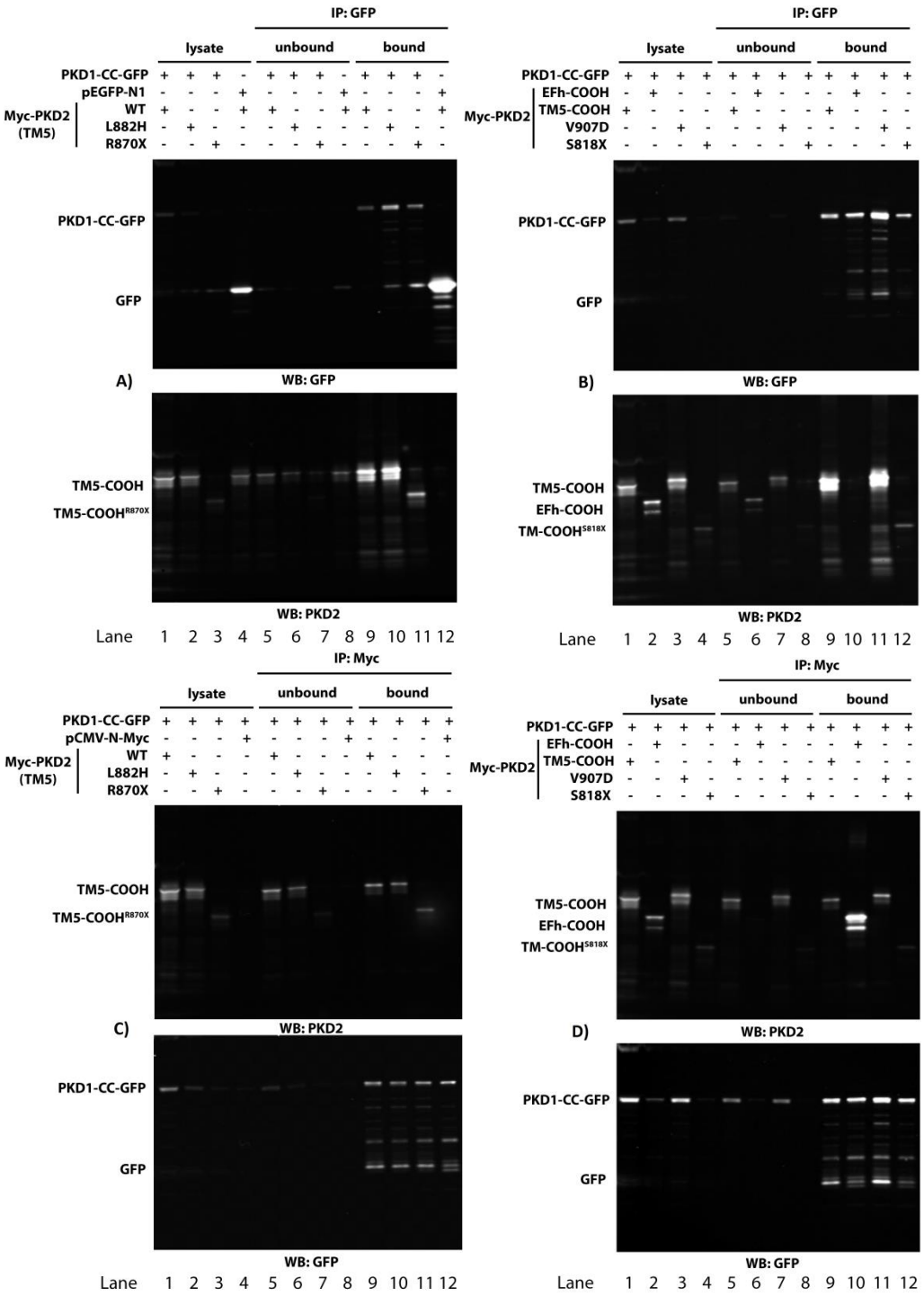


Figure 2.20: Interaction of PKD1-CC-GFP with various PKD2 fragments. GFP IP shown in **A** and **B**, Myc IP shown in **C** and **D**. All TM5-COOH fragments, mutant or WT, can be purified together with PKD1-CC-GFP (lanes 9-11, **A** and **C**, lanes 9, 11, 12, **B** and **D**, respectively). EFh-COOH only pulls down PKD1-CC-GFP when purifying Myc. Lanes 1-4 show untreated lysates, lanes 5-8 show unbound fraction. Controls are identical to those of **Fig. 2.5** and are shown in lane 12 of **A** and **C**.

2.2.6. Testing the interaction of PKD2 with NPR3

The PKD1L1-PKD2 and PKD1-PKD2 fragment interactions reported in this chapter are in disagreement with the results of previous studies. Given the discrepancy between the results described in this chapter and those of previous studies, one possibility is that the interactions are artefactual, occurring even in the absence of a CC due to hydrophobic clustering of protein fragments in the lipid membrane. In order to test this possibility, I used the same approach as described for the experiments in section **2.2.2** to compare the interaction of full-length PKD2 or TM5-COOH with a protein that does not interact with PKD2. One such protein is Natriuretic Peptide Receptor 3 (NPR3); it is also expressed in renal cells, has a single TM helix, but is not known to interact with PKD2. A comparison of the interaction of PKD2, full-length or TM5-COOH, with NPR3 will not only address whether this interaction normally occurs, but also suggest whether the PKD2 fragments with TM helices are prone to artefactual interactions due to hydrophobic clustering. NPR3 was GFP-tagged and expressed from the same vector used to express PKD1L1-CC-GFP. The results show that TM5-COOH co-purifies or is co-purified with NPR3-GFP (**Fig. 2.21**, **A**, lanes 9 and 10, respectively). Full-length PKD2 weakly pulls down NPR3 (**Fig. 2.21**, **B**, lane 9), but is not pulled down by NPR3 (**Fig. 2.21**, **B**, lanes 10). As with the other Co-IPs described in section **2.2.2**, the controls suggest that the Co-IPs are specific to the proteins being purified. These results argue that the TM5-COOH fragment is able to interact better with NPR3 than full-length PKD2; this may be due to the higher proportion of hydrophobic regions in the protein fragment, or due to mis-folding. This finding suggest that the PKD1L1-PKD2 interaction results reported in this chapter, using protein fragments, may be artefactual. Further study is required in order to validate the results described in this chapter.

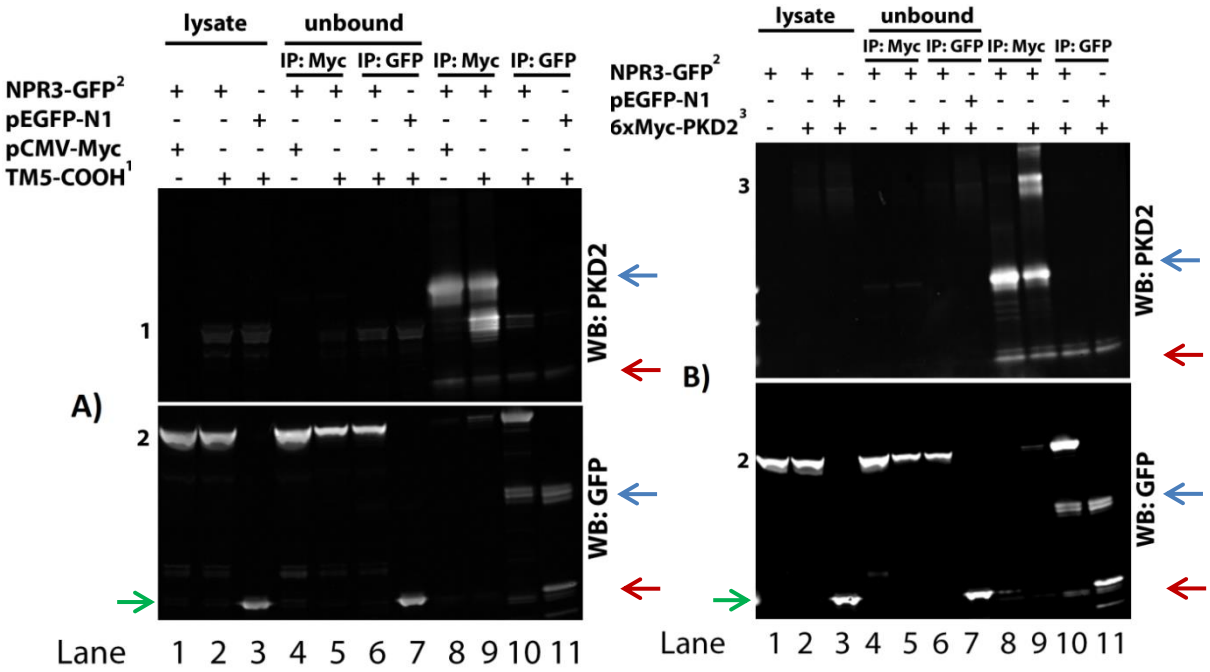


Figure 2.21: Interaction of TM5-COOH (**1**) (**A**) or full-length PKD2 (**3**) (**B**) with NPR3-GFP (**2**). TM5-COOH was able to co-precipitate with NPR3-GFP, and *vice versa* (lanes 9 and 10 in **A**), whilst 6xMyc-PKD2 weakly co-precipitated with NPR3-GFP, but not the other way around (lanes 9 and 10 in **B**). For explanation on controls and layout, see **Fig. 2.5** and **Fig. 2.7**, respectively.

2.3. Summary of results and discussion

In this chapter, I aimed to address whether the molecular mechanism of interaction of PKD1L1-PKD2 is similar to that of PKD1-PKD2. The C-terminal part of the PKD2 CC has previously been shown to be sufficient for the interaction with PKD1, and was thought to be necessary (see section **2.1.1**). I therefore hypothesised that the PKD1L1-PKD2 interaction would employ the same mechanisms, given: 1) the homology between PKD1L1 and PKD1; 2) previous studies argued for a CC-centric molecular mechanism of interaction between PKD1-PKD2 (see section **2.1.1**); 3) previous findings argued that the CC of PKD1L1 is necessary for the interaction of a PKD1L1 fragment with PKD2 (Field et al., 2011). However, a recent study, published after the work described in this chapter was completed, demonstrated that the PKD1-PKD2 interaction also involves an extracellular loop of either protein (Salehi-Najafabadi et al., 2017).

2.3.1. Designing PKD2 CC mutations

I used a bioinformatic approach, similar to that described by Field *et alia* (Field et al., 2011), to test which PKD2 mutations would affect the probability of CC formation (**Fig. 2.2**). The CC region showed a high degree of conservation between human and mouse PKD2 protein sequences (**Fig. 2.1**). However, the bioinformatic tools used predicted different outcomes between species (**Fig. 2.2**). It is worth keeping in mind that the results obtained *in silico* are predictive at best and require validation. At worst, the mutations may not have the predicted effect on the formation of the CC. Moreover, mutations described in previous studies, L884H, D886A and R872X (human AA numbering), have been validated in the context of human PKD2, using various protein fragments and different biochemical techniques from those employed in this chapter (**Table 2.1**). This could explain how some of the interaction results described in this chapter are in contrast to those described by the original studies (see section **2.1.1**), which could

be attributed to the presence or absence of domains not yet known to contribute to PKD2 interaction.

2.3.2. Validation of PKD2 protein fragments

Following bioinformatic prediction, I designed and validated fragments of PKD2 to investigate the PKD1L1-PKD2 interaction and asses the effect of mutations of interest. Three fragments of different lengths were designed (**Fig. 2.3**), all containing the EF-hand and CC region. The design of these fragments took into account the finding that the CC of PKD2 was thought to be both sufficient and necessary for the interaction with PKD1 (see section **2.1.1**) at the time, and necessary for the interaction of a PKD1L1-CC-GFP fragment with PKD2 (Field et al., 2011). The use of fragments should have also allowed me, given the extent of knowledge at the time, to focus only on one interaction domain: the CC. Furthermore, in order to avoid any issues regarding orientation of the protein in the plasma membrane, fragments with variable number of TM helices were designed. The localisation of these fragments was comparable to that of full-length PKD2, showing distribution to the membrane systems, but unlike full-length PKD2, the fragments showed differences in ciliary localisation (see section **2.2.2**) or ER whorls (**Fig. 2.4**). However, the reduction in or lack of ciliary localisation should not impede interaction with PKD1L1, given the data describing PKD1-PKD2 interaction in other sub-cellular compartments (see section **1.2.5.b**). Curiously, only the fragments containing TM helices, TM5-COOH (**Fig. 2.5**) and TM6-COOH (**Fig. 2.6**), were able to interact with a PKD1L1 fragment containing the CC (Field et al., 2011). The fact that the EFh-COOH fragment did not interact with PKD1L1-CC-GFP (**Fig. 2.7**) indicates one of two possibilities: 1) the PKD1L1-PKD2 interaction requires plasma membrane anchorage, unlike PKD1-PKD2; 2) the CC is not sufficient for the PKD1L1-PKD2 interaction, unlike that of PKD1-PKD2. However, all three fragments were able to homodimerize with PKD2-V5 (**Fig. 2.5**, **2.6** and **2.7**), a V5-tagged full-length PKD2 molecule. Given these results, I tested whether the difference in interaction between EFh-COOH and TM6-COOH can be accounted for by differences in

localisation in the presence or absence of PKD1L1-CC-GFP (**Fig. 2.8**). The similar behaviour, in terms of interaction with PKD1L1-CC-GFP (**Fig. 2.5** and **2.6**), and localisation (**Fig. 2.4**) of TM5-COOH and TM6-COOH argue that a comparison between EFh-COOH and TM6-COOH in the presence of PKD1L1-CC-GFP is sufficient. Both EFh-COOH and TM6-COOH are able to co-localise with PKD1L1-CC-GFP, showing distribution throughout the membrane systems. This finding suggests that a difference in localisation is not responsible for the lack of interaction of EFh-COOH with PKD1L1-CC-GFP. This also indicates that the interaction of PKD1L1-PKD2 either requires membrane-tethering, or specifically requires a domain not yet identified, contained in the interval between the N-terminus of TM6-COOH and that of EFh-COOH. The inability of EFh-COOH to interact with PKD1L1-CC-GFP is in contrast to previously-published results, which indicate that PKD2 fragments without TM helices should be able to interact with PKD1 fragments, whether membrane-tethered or not (see **Table 2.1**). The difference in results could be due to usage of different PKD2 fragments between different studies, or alternatively different molecular mechanisms for the PKD1L1-PKD2 interaction, as compared to that of PKD1-PKD2. Given that most studies have used different fragments of PKD2 in the study of the PKD1-PKD2 interaction, it seems more likely that there are differences between the mechanisms of interaction of PKD2 with PKD1 or PKD1L1. Furthermore, EFh-COOH is able to interact with PKD2-V5, which is membrane-tethered. This leads me to hypothesise that a yet-unidentified domain is required for the interaction of PKD1L1 with PKD2, and that the PKD2 CC alone is not sufficient for this interaction.

2.3.3. Testing PKD2 CC requirement for the PKD1L1-PKD2 interaction

Having indicated that the CC of PKD2 is not sufficient for the interaction of PKD1L1-PKD2 fragments, I next tested whether it is necessary, by using TM5-COOH. Neither of the mis-sense mutations with a predicted effect on CC formation (**Fig. 2.2**) were able to disrupt the PKD1L1-PKD2 fragment interaction (**Fig. 2.9**, **2.10** and **2.11**). Furthermore, truncation of the hetero- and

homo-oligomerization sub-regions, through the use of R870X and S818X mutations, respectively, does not abolish the PKD1L1-PKD2 fragment interaction (**Fig. 2.13** and **2.14**). The only mutation that behaves as predicted is D884A (**Fig. 2.12**), allowing PKD1L1-PKD2 fragment interaction – this mutation was not predicted to impact CC formation (**Fig. 2.2**) and was previously shown to not affect PKD1-PKD2 interaction (Tsiokas et al., 1999). These findings suggest that the CC of PKD2 is not necessary for the PKD1L1-PKD2 interaction and invalidate my initial hypothesis. This suggests that the molecular mechanisms of interaction are different between PKD1L1-PKD2 and PKD1-PKD2, in that the PKD1L1-PKD2 interaction involved other domains, not just the CC. However, one further possibility is that the results described in this chapter are artefactual in nature: either due to misfolding of protein fragments, or lack of predicted effect of the point mutations. The results obtained using truncation mutations further support the possibility that the CC of PKD2 is not necessary for the PKD1L1-PKD2 fragment interaction.

In spite of the suggestion that the mutations may not have the predicted effect, a direct comparison between the ability of the WT and S818X mutant TM5-COOH fragments to pull down PKD1L1-CC-GFP shows that the presence of the S818X may weaken the interaction with PKD1L1-CC-GFP (**Fig. 2.15**). Although at first glance this could be addressed using densitometry analysis, there are several obstacles that prevented me from doing so: 1) experimental set-up and innate variability of the Co-IP protocols used (see section **5.4.1**); 2) differences in banding patterns – WT TM5-COOH and TM5-COOH^{S818X} bands differ in size and shape (**Fig. 2.15**). Therefore, I would be unable to separate the effect of variability of the experimental protocol, as well as the differences in expression of WT and mutant fragments, from the differences in the interaction caused by the presence of the S818X mutation. Due to time constraints, I was unable to test whether the mutations lead to similar results in the context of the full-length PKD2 protein. It is possible that the results are artefactual due to usage of protein fragments; employing the full-length mutant PKD2 protein will also help address this.

Alongside the involvement of the PKD2 CC in hetero-oligomerization, I also tested the ability of the CC mutations to affect homo-oligomerization, given that the bioinformatic tools predict an effect of some of the mutations on the homo-oligomerization sub-region (**Fig. 2.2**). All three PKD2 fragments are capable of interacting with PKD2-V5 (**Fig. 2.5** to **Fig. 2.7**). However, when compared with TM5-COOH and TM6-COOH, EFh-COOH appears to enrich or be enriched by PKD2-V5 less than the other PKD2 fragments (**Fig. 2.7**). This could potentially be due to the absence of the C630 residue in the EFh-COOH fragment, which is known to facilitate PKD2 homo-oligomerization (Feng et al., 2011). All of the mutant TM5-COOH fragments tested were capable of interacting with PKD2-V5 (**Fig. 2.9** to **2.15**), even in the absence of the CC region (**Fig. 2.14**). Given the fact that the C630 residue, previously shown to be required for homo-oligomerization (Feng et al., 2011), is present in both fragments containing TMs, this could facilitate PKD2 homo-oligomerization between the fragment and full-length protein, even in the absence of the PKD2 CC. However, given the environment to which this residue is exposed, according to the published structure of PKD2 (Shen et al., 2016, Grieben et al., 2017), this mechanism of PKD2 oligomerization is unlikely.

2.3.4. Assessing PKD2 C630 residue involvement in PKD1L1-PKD2 interaction

The results discussed so far indicate that the CC of PKD2 is not necessary, nor sufficient, for PKD1L1-PKD2 fragment interaction. This interaction may require a different domain contained within the region between the N-termini of TM6-COOH and EFh-COOH. Given the presence of C630 – required for PKD2 homo-oligomerization (Feng et al., 2011) – within this region, as well as the presence of multiple cysteine residues within the PKD1L1-CC-GFP fragment, I tested whether this residue is required for PKD1L1-PKD2 interaction. The two fragments, PKD1L1-CC-GFP and TM5-COOH, are still able to interact in the presence of the C630A mutation (**Fig. 2.16**). This indicates that the C630 residue is not necessary for the PKD1L1-PKD2 fragment interaction.

Testing whether PKD1L1-CC-GFP and TM5-COOH can interact in the presence of both C630A and S818X mutations will address whether the C630 residue is sufficient for the interaction.

2.3.5. Testing previous findings and validating interactions

I also tested previous findings regarding the requirement of the PKD1L1 CC for the interaction of PKD1L1-CC-GFP with full-length PKD2. Contrary to previous findings, a PKD1L1 mutation that is predicted to disrupt CC formation, L2564D (Field et al., 2011), does not abolish the PKD1L1-PKD2 interaction in my hands (**Fig. 2.17**). Given the fact that the same results were obtained under different experimental conditions (**Fig. 2.17** and **2.19**), as well as the original conditions described by Field and colleagues (**Fig. 2.18**), the results described in the original study may be false positive in nature. This would align with the hypothesis that neither of the CCs of PKD1L1 or PKD2 are necessary for the interaction of the two proteins, as suggested by the results discussed in this section (*vide supra*). However, the PKD2 fragments described in this chapter do not behave as expected with regards to interacting with a PKD1 fragment, PKD1-CC-GFP (**Fig. 2.20**). EFh-COOH, the shortest fragment, is unable to interact with PKD1-CC-GFP, in spite of expectations from previous findings (Tsiokas et al., 1999). Moreover, PKD2 mutations previously described to stop the interaction with PKD1, L882H and R870X (Qian et al., 1997, Tsiokas et al., 1999), as well as S818X, permit the interaction of TM5-COOH with PKD1-CC-GFP. This finding raises questions with regards to the nature of the interaction between the PKD2 fragments used. In order to test whether these interactions are artefactual, I tested the interaction of TM5-COOH with a protein not known to interact with PKD2, NPR3, as well as the interaction of NPR3 with full-length PKD2. Surprisingly, the results of the Co-IPs showed that NPR3 is able to enrich with TM5-COOH and *vice versa*. In contrast, full-length PKD2 was only able to weakly co-precipitate NPR3 when purified directly, but not the other way around (**Fig. 2.21**). This finding strongly suggests that the Co-IP results involving TM5-COOH may be artefactual in nature. Given that TM5-COOH contains a higher proportion of hydrophobic residues, this protein fragment may be

able to interact non-specifically with NPR3 due to hydrophobic clustering of the proteins in the plasma membrane. However, this does not necessarily address the issue of why the full-length PKD2 is able to co-purify NPR3, but not the other way around. One potential explanation for this would be that the non-specific hydrophobic interactions are capable of keeping NPR3 bound to full-length PKD2, but the size of PKD2 may not allow it to remain bound to NPR3 during the CoIP procedure. Re-testing the effect of the PKD2 CC mutations in the context of the full-length PKD2 protein will further help address the validity of the results described in this chapter.

2.3.6. Conclusion

The results obtained so far indicate that the CC of PKD2 is neither sufficient nor necessary for the interaction with PKD1L1, and also suggest that a different domain may be involved. This contradicts my initial hypothesis, that the PKD1L1-PKD2 and PKD1-PKD2 interaction is similar, in terms of molecular mechanisms. However, the results of the experiments described in section **2.2.6** suggest that the interactions between the mutated TM5-COOH and PKD1L1-CC-GFP fragments may be artefactual. In order to further test this, I decided to analyse the phenotypes of mice carrying each of two of the PKD2 mutations described in this chapter, R870X and S818X. Should the molecular mechanisms of the interaction between PKD1L1-PKD2 be different from PKD1-PKD2, and the CC of PKD2 is not required for the interaction with PKD1L1, the only phenotypes displayed by mutants will be polycystic kidneys, but not L-R defects. Conversely, should the interaction of PKD1L1-PKD2 be identical to that of PKD1-PKD2, in terms of the involvement of the CC, both kidney and L-R phenotypes will be observed.

Chapter 3: Phenotypic analysis of mouse *Pkd2* mutant embryos lacking the PKD2 CC region

Notes on reading this chapter

The work described in this chapter is aimed at characterising *Pkd2* alleles. The analysis investigated the phenotypes of embryos that were either homozygous for a mutant allele, or were compound heterozygotes for two mutant alleles of *Pkd2.* Each sample (or embryo) was assigned a unique ID, consisting of the genetic cross that produced that particular embryo, as well as a number preceded by an 'X'. For example, an embryo that was harvested from a litter produced by a cross of heterozygous animals, $Pkd2^{Z/+}$, would be dubbed 'PKD2-ZxZ X#', where the # would be replaced by a number starting from 1, to identify each embryo produced by that cross. Similarly, embryos harvested from a litter produced by crossing $Pkd2^{Z/+}$ and $Pkd2^{X/+}$ animals would be identified by 'PKD2-ZxY X#'. The details of the alleles are outlined in **Table 3.1**. To give a specific example, 'PKD2-DELxS818X X12' would identify the 12th embryo produced by a cross between an animal with the $Pkd2^{del/+}$ genotype and an animal with the $Pkd2^{S818X/+}$ genotype.

The structure of this chapter is, in most part, repetitive in nature. The typical formula of 'Introduction', followed by 'Results' and concluding with 'Summary and discussion' is encountered in this chapter, much like in **Chapter 2**. However, the 'Results' section is divided into sub-sections, which, aside for the very first sub-section, are centred on a *Pkd2* allele described in the context of one or two genotypes. Each of the genotypes within a sub-section is then analysed in tandem through one of three methods, which are sequentially described in the following order: dissection to determine gross *situs* phenotype, histological sectioning to investigate the cystic phenotypes of embryonic kidneys and ending with µCT-based analysis. The exceptions are section **3.2.2**, which uses only µCT to describe the phenotype produced by an allele in homozygous embryos, as well as section **3.2.6**, which only employs dissection and histological sectioning. Each

sub-section, aside from the last one, ends with a table summarising the μCT data described within.

Finally, where fractions are specified for a particular phenotype, this indicates how many times this was seen within embryos of a particular genotype, across all methods of analysis. For example, for the *Pkd2*$^{S818X/del}$ genotype, dextrocardia (5/18), mesocardia (4/18) and normal heart *situs* (9/18) – or levocardia – are observed. This means that across all methods of analysis, 5 out of 18 embryos showed dextrocardia, 4 out of 18 embryos had mesocardia and 9 out of 18 embryos displayed levocardia (normal heart *situs*). Similarly, for lethality, both incidence and percentages are given. The numbers are given, together with the percentages, in the final table shown in this chapter, **Table 3.8**. The total numbers in this table vary in between rows, as not all organ systems could be assessed in all embryos.

3.1. Introduction

3.1.1. Previous results and rationale

The work described in **Chapter 2** aimed to address the molecular mechanism of interaction between PKD1L1 and PKD2, as well as to test the similarity of this mechanism to that of the PKD1-PKD2 complex. At first sight, the results presented argue that the mechanism of interaction of PKD1L1 with PKD2 is different to that of PKD1. Namely, the PKD1L1-PKD2 interaction does not involve the PKD2 CC, as PKD2 fragments bearing mutations predicted to affect its CC are still able to interact with a PKD1L1 fragment (see section **2.2.3**). Later experiments (see section **2.2.5**) also raised questions regarding the validity of results from previous studies, which served as a foundation to my initial hypothesis: that the PKD1L1-PKD2 interaction is similar, in terms of molecular mechanisms, to that of PKD1-PKD2 (see section **2.1.3**). Confusingly, experiments described in section **2.2.6** also raised the possibility that using protein fragments to test the PKD1L1-PKD2 interaction was a confounding factor, potentially leading to artefactual results. To better determine the validity of these results, further work is required.

I investigated the requirement of the PKD2 CC in the PKD1L1-PKD2 interaction by analysing the phenotypes of mouse embryos bearing mutations in the region encoding the PKD2 CC. If the results described in section **2.2.3** are valid, then there likely is a difference in the molecular mechanisms of PKD1L1-PKD2 and PKD1-PKD2 interactions. This would mean that mutations affecting the CC of PKD2 would only affect the interaction with PKD1, which is involved in renal development, but not the interaction with PKD1L1, involved in L-R determination. Therefore, the mouse lines analysed would display polycystic kidneys, but not L-R patterning defects. In contrast, should the mutants analysed display both *situs* defects and polycystic kidneys, this would indicate that the PKD1L1-PKD2 interaction is similar, in terms of molecular

mechanism and the involvement of CCs, to PKD1-PKD2. I therefore decided to analyse the phenotypes of mice bearing the two PKD2 CC truncation mutations described in section **2.2.3**: R870X, which truncates the CC prior to the hetero-oligomerization sub-region, and S818X, which truncates the protein prior to the start of the CC (**Fig. 3.1**).

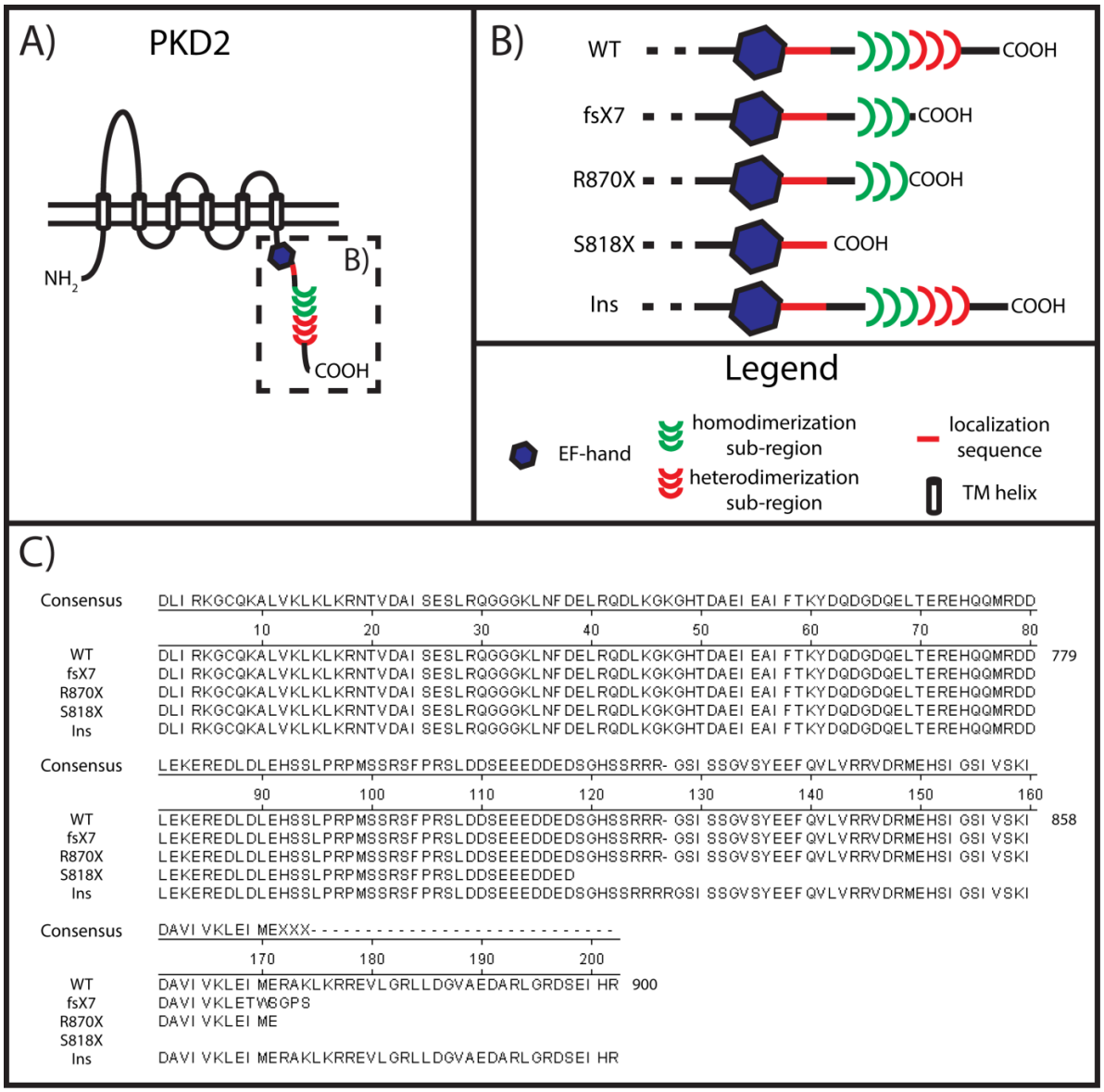


Figure 3.1: Impact of CRISPR/Cas9-generated mutations on mouse PKD2. **A)** diagram of PKD2, showing C-terminal intracellular domains. **B)** side-by-side comparison of the WT and CC mutant proteins, showing only the intracellular C-terminus of PKD2 (highlighted in **A**). **C)** sequence alignment of WT and CC mutant PKD2; the sequence shown spans from AA 700-900 and includes the domains shown in **B)**.

3.2. Results

3.2.1. Description of mutant lines and alleles used

Pkd2$^{tm1.2Tjwt}$, a conditional allele having exons 11-13 floxed, was initially studied in the context of placental and vascular development in mouse embryos (Garcia-Gonzalez et al., 2010), and was later adapted by R. Walker to give a null allele to study L-R and kidney phenotypes (Walker, 2016). Aside from this null allele, henceforth referred to as *Pkd2*^{del}, all of the mutant lines used in this chapter were generated by core services (Transgenics team) at MRC Harwell, using CRISPR/Cas9 technology. The initial aim was to generate lines carrying the R870X and S818X mutations. However, four alleles bearing different mutations were obtained, two from each of the initial projects aimed at generating the R870X and S818X mutations: 1) *Pkd2*^{fsX7}, bearing a 1 nucleotide deletion which results in a frameshift upstream of the targeted R870 residue, and truncation after 6 AA; 2) *Pkd2*^{R870X}, the planned truncation mutation; 3) *Pkd2*^{S818X}, an allele resulting in the desired S818X mutation, but also containing a 3 nucleotide insertion downstream of the stop codon; and 4) *Pkd2*^{ins}, an allele containing a 3 nucleotide insertion, shared with *Pkd2*^{S818X}. Details of the effects of the mutations at the protein level, as well as the names of the lines carrying the alleles maintained at MRC Harwell, are given in **Table 3.1**. A diagrammatic representation of the effect of the CRISPR/CAS9 mutations, henceforth referred to as CC mutations, on protein structure, as well as protein sequence information, is given in **Fig. 3.1**. Information regarding changes at the nucleotide level, as well as the proposed formal names of the alleles, is given in section **5.1.2**.

Table 3.1: information on *Pkd2* alleles used in this chapter

Allele name	Protein mutation	Line/Stock name	Comments
Pkd2^{del}	No protein	PKD2-DEL-B6	Lacks exons 11-13, allele is a null
Pkd2^{fsX7}	I867TfsX7	PKD2-DEL1-EM1-B6	Lacks hetero-oligomerization sub-region, frameshift
Pkd2^{R870X}	R870X	PKD2-R870X-EM2-B6	Lacks hetero-oligomerization sub-region
Pkd2^{S818X}	S818X	PKD2-S818X-INS3-EM1-B6	Lacks CC, 3 nucleotides inserted downstream of stop codon
Pkd2^{ins}	R823_R824insR	PKD2-INS3-EM1-B6	Extra AA, same 3 nucleotides as S818X

N.B.: although not strictly correct with regards to allele nomenclature, the allele names used in this chapter reference the effect that the mutations have on the proteins, for clarity and ease of understanding. The uppercase first letter of the superscript of alleles *Pkd2*^{R870X} and *Pkd2*^{S818X} does not indicate the dominance of the allele, but strictly refers to the amino acid.

3.2.2. Phenotypic analysis of *Pkd2*$^{del/del}$ embryos at 15.5 dpc

In order to determine whether the CC mutant alleles produce phenotypes that are different from those observed in *Pkd2*$^{del/del}$ mice (Walker, 2016), a detailed analysis of the phenotypes of *Pkd2*$^{del/del}$ embryos is required. To date, studies addressing the phenotype of *Pkd2*$^{del/del}$ mouse embryos have performed broad phenotypic analysis using light microscopy (Walker, 2016), or focused on particular organ systems (Garcia-Gonzalez et al., 2010, Outeda et al., 2014), though other null alleles of *Pkd2* have been characterised through light microscopy and other methods (Wu et al., 2000, Pennekamp et al., 2002). I therefore decided to perform micro-computer tomography (µCT) analysis on 15.5 dpc embryos. This stage was chosen as this is the earliest stage at which kidney cysts can be observed in mouse embryos (Walker, 2016), but also because it allows the study of the development of internal organs at the latest stages that *Pkd2*$^{del/del}$ embryos can reach (Walker, 2016). This analysis will provide the baseline to perform an in-depth comparison between the null allele and the mutant CC alleles.

Phenotypic analysis performed by R. Walker revealed that *Pkd2*$^{del/del}$ embryos display oedema, right lung isomerism and randomised stomach and heart *situs*; kidney cysts were observed in all *Pkd2*$^{del/del}$ embryos (Walker, 2016). However, this study did not assess cardiac great vessel (aorta and pulmonary artery) development and patterning. This is thought to result, in part, from the establishment of the L-R axis. Using μCT, I performed a broad spectrum analysis that included the same phenotypes studied previously, but also looked at great vessel development and patterning, as well as other phenotypes.

Four *Pkd2*$^{del/del}$ embryos were dissected, exsanguinated and fixed in 4% PFA (paraformaldehyde). Subsequently, the samples were further processed and scanned, using μCT, by core services (Transgenics team), as described in section **5.1.3**. Oedema was observed in all *Pkd2*$^{del/del}$ embryos before (**Fig. 3.2**, **C** and **D**) and after sample processing (**Fig. 3.3**, **Ci**, **Di** and **Ei**). In comparison, only small, localised regions of oedema were evident in WT and *Pkd2*$^{del/+}$ samples (**Table A2.2** and **A2.3**; **Fig. 3.3**, **Ai** and **Bi**). Kidney cysts were observed in all *Pkd2*$^{del/del}$ embryos (**Fig. 3.3**, **Ci**, **Di** and **Ei**), but not in WT or *Pkd2*$^{del/+}$ embryos (**Fig. 3.3**, **Ai** and **Bi**). As reported previously in both mouse models and human patients (Wu et al., 2000, Pennekamp et al., 2002, Boucher and Sandford, 2004, Nie and Arend, 2014), *Pkd2*$^{del/del}$ embryos also display pancreatic cysts (**Fig. 3.3**, **Ci**, **Di** and **Ei**), as well as testicular cysts (**Table 3.2**).

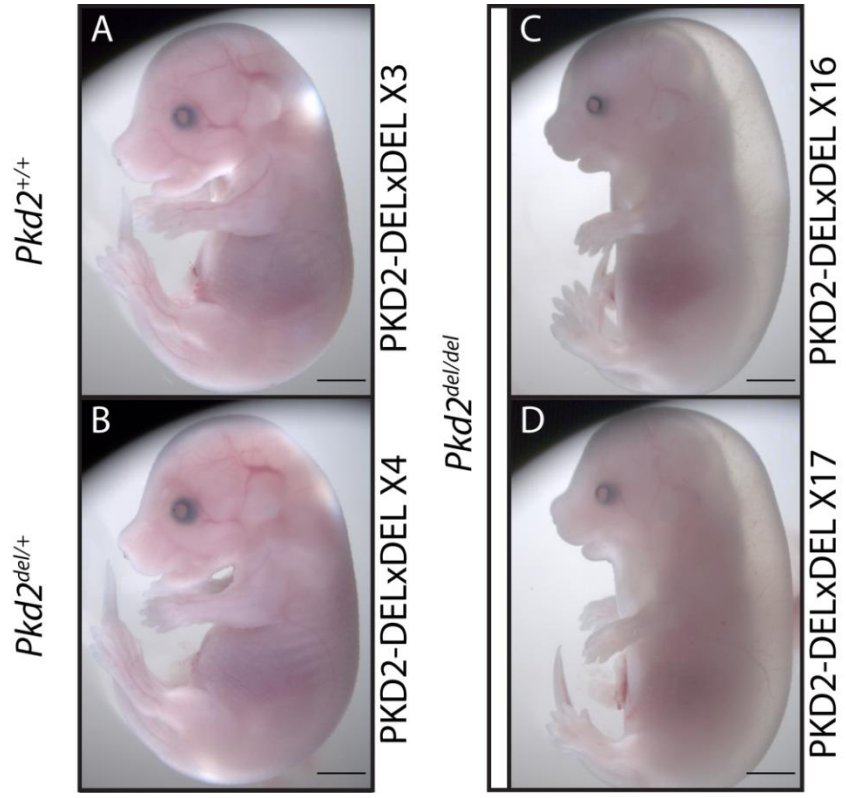


Figure 3.2: Wholemount embryos from PKD2-DELxDEL cross. **A**: WT embryo; **B:** *Pkd2*$^{del/+}$ embryo; **C** and **D**: *Pkd2*$^{del/del}$ embryos. Samples in **C** and **D** display generalised subcutaneous oedema. Genotypes are indicated to the left of each image, sample IDs are given to the right. Scale bar: 2 mm.

When analysing cardiac great vessel patterning, a range of abnormal phenotypes are observed: *situs inversus* of the great vessels (2/4, **Fig. 3.3**, **Cii** and **Dii**), fusion of the great vessels (1/4, **Fig. 3.3**, **Cii**), or other phenotypes (2/4). This category includes transposition of the great arteries (**Fig. 3.3**, **Dii** and **Eii**) and double outlet right ventricle (DORV – **Table A2.1**). *Pkd2*$^{del/del}$ embryos also displayed abnormal development of the thymus, showing smaller and displaced thymi (**Fig. 3.3**, **Ciii**, **Diii** and **Eiii**); notably, the developing epithelial structures of the thymus are reported as being a site of high *PKD2* expression in human embryos (Ong et al., 1999). All homozygous embryos also displayed cleft palate or abnormal soft palates (**Fig. 3.3**, **Civ** and **Eiv**, and **Fig. 3.3**, **Div**, respectively). A number of nervous system phenotypes were also observed in all *Pkd2*$^{del/del}$ embryos, including: enlargement of lateral extremities of the fourth ventricle and reduction in size of choroid plexi in the medial fourth ventricle (**Fig. 3.3**, **Cv**, **Dv** and **Ev**); abnormal

trigeminal ganglia (**Fig. 3.4**, **Ci**, **Di** and **Ei**); displaced dorsal root ganglia (**Table 3.2**); abnormal olfactory lobe spacing (**Table 3.2**); and distended subarachnoid space in the thoracic region (**Table 3.2**). In addition to these phenotypes, the shape of the brown fat pads was abnormal in *Pkd2*$^{del/del}$ embryos (**Fig. 3.3**, **Cii**, **Dii** and **Eii**), in comparison to WT or *Pkd2*$^{del/+}$ (**Fig. 3.3**, **Aii** and **Bii**). This phenotype may not be directly linked to *Pkd2*, but may be indirectly caused by the oedema, as homozygous embryos have a greatly distended subcutaneous space.

The position of the heart was also affected in homozygous mutants, with one mutant showing dextrocardia (**Fig. 3.4**, **Dii**), whilst three others displayed mesocardia (**Fig. 3.4**, **Cii** and **Eii**). Two of the mutants displaying mesocardia also displayed transposed great arteries. Three of the *Pkd2*$^{del/del}$ embryos also displayed interventricular septum (IVS) defects (**Fig. 3.4**, **Ciii** and **Diii**), whilst one mutant did not display this abnormality (**Fig. 3.4**, **Eiii**). Lung lobation was also abnormal in all four *Pkd2*$^{del/del}$ embryos: three embryos showed right isomerism (4:4 right to left – R:L – lung lobation, **Fig. 3.4**, **Civ** and **Eiv**) whilst one embryo showed isomeric 2:2 R:L lung lobation (randomised category; **Fig. 3.4**, **Div**). The patterning of the venous system was also assessed, particularly looking at the position of the azygos vein, a derivative of the left superior vena cava (normal in WT and *Pkd2*$^{del/+}$, **Fig. 3.4**, **Aiii** and **Biii**), and the inferior vena cava, which is positioned on the right side of the body (normal in WT and *Pkd2*$^{del/+}$, **Fig. 3.4**, **Aiii** and **Biii**). One mutant displayed *situs inversus* of the azygos vein (**Fig. 3.4**, **Eiv**), one mutant displayed bilateral azygos veins (**Fig. 3.4**, **Civ**), whilst two embryos had normally patterned azygos veins (**Fig. 3.4**, **Div**). A single embryo displayed bilateral inferior vena cava (**Fig. 3.4**, **Div**). Aside from the position of the heart apex, lung lobation and circulatory system L-R patterning, other *situs* abnormalities were also observed: two homozygous embryos displayed *situs inversus* of the stomach, spleen, pancreas and liver (**Fig. 3.4**, **Dv**), one of which is associated with right lung isomerism, whilst the other displays 2:2 lobation for the lungs. The abnormal phenotypes observed for *Pkd2*$^{del/del}$

embryos are summarised in **Table 3.2**; full phenotypic analysis data is given in **Appendix 2**, **Table A2.1**.

Of particular interest is the assessment of kidney cysts (**Fig. 3.3**, **Ai**-**Ei**), typically performed by sub-dissecting the kidneys and performing histological sectioning. The results suggest that μCT analysis can provide a time-efficient way of analysing this particular phenotype, alongside those of other organs. However, the resolution of the μCT scans was not optimal for the analysis of kidney cysts in some of the younger samples (**Fig. 3.3**, **Ci**), primarily due to the size of the cysts and developmental stage of the organ. Kidney cysts are evident in all samples older than 15.5 dpc (**Fig. 3.3**, **Di** and **Ei**) and can be inferred for younger samples by analysing tissue density (**Fig. 3.3**, **Ci**). *N.B.***:** the samples described throughout this chapter vary in stage, between 15.5-16 dpc; this was controlled by comparing the embryos to the WT sample of the same stage.

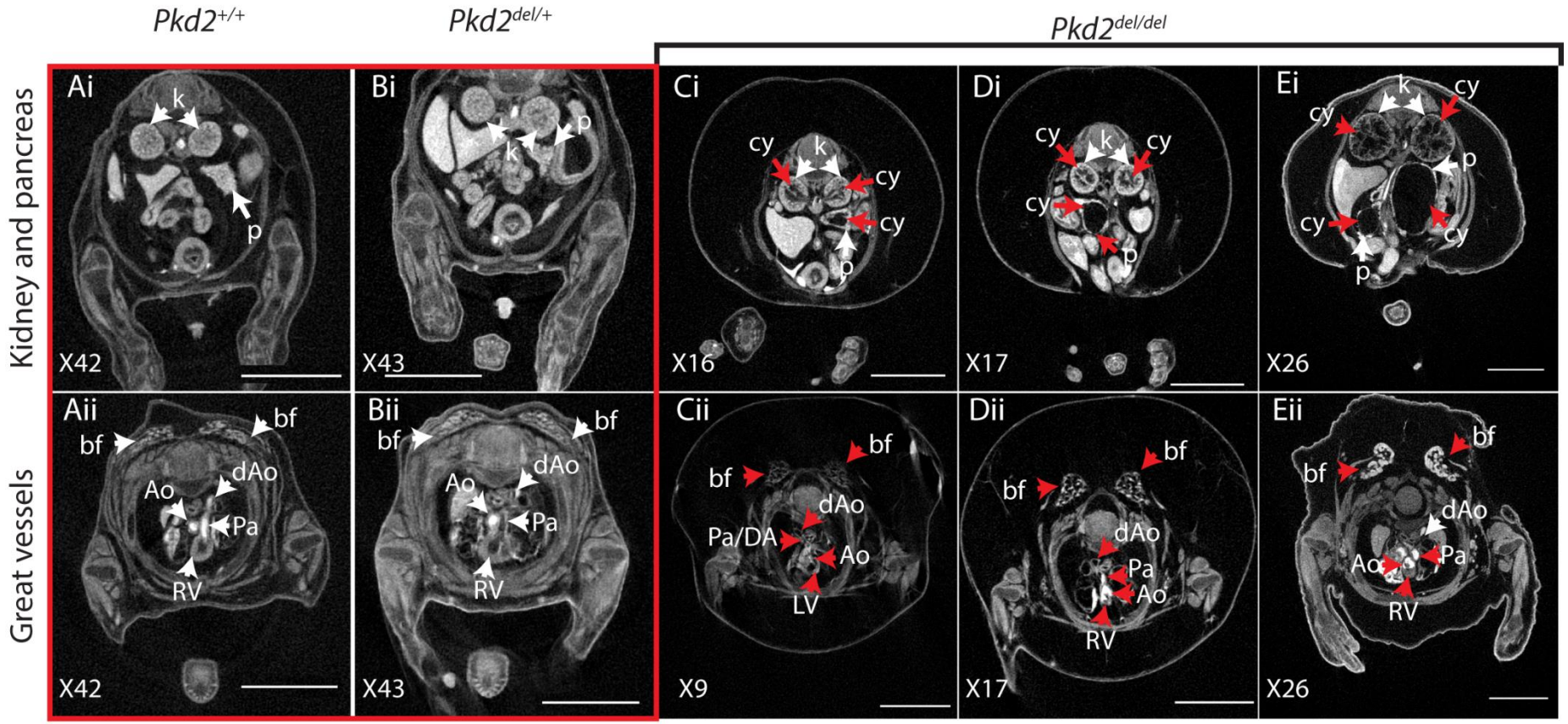


Figure 3.3: µCT sections of WT (**A**), *Pkd2*$^{del/+}$ (**B**) and *Pkd2*$^{del/del}$ (**C-E**) 15.5 dpc embryos, showing most-commonly observed phenotypes. White arrows: normal phenotypes; red arrows: abnormal phenotypes. Abbreviations (in alphabetical order): Ao – aorta; bf – brown fat; chp – choroid plexus; cp – cleft palate; cy – cyst; dAo – descending aorta; k – kidney; lefv – left extremity of the fourth ventricle; LV – left ventricle; nc – nasal cavity; p – pancreas; Pa – pulmonary artery; Pa/DA – pulmonary artery/ductus arteriosus; sp – soft palate; RV – right ventricle; thy – thymus; to – tongue. Samples highlighted in red are from a PKD2-DELxDEL1 cross (**A** and **B**), whilst samples in **C**, **D** and **E** are from PKD2-DELxDEL cross. Sample IDs are shown bottom left of each section. Scale bar: 2 mm. Unannotated figure is shown in **Appendix 1**, **Fig. A1.1**, pages 224-225.

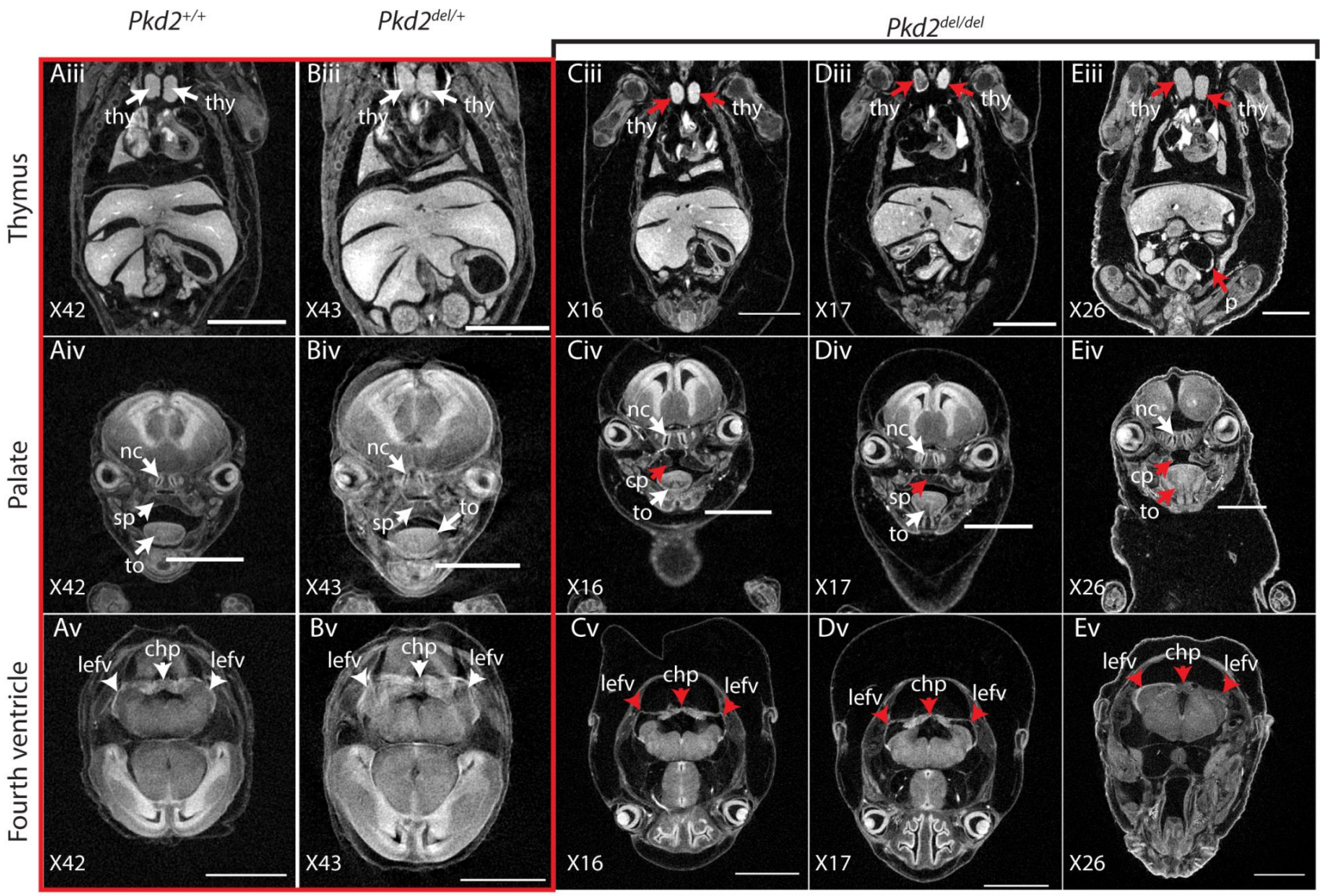


Figure 3.3 (continued)

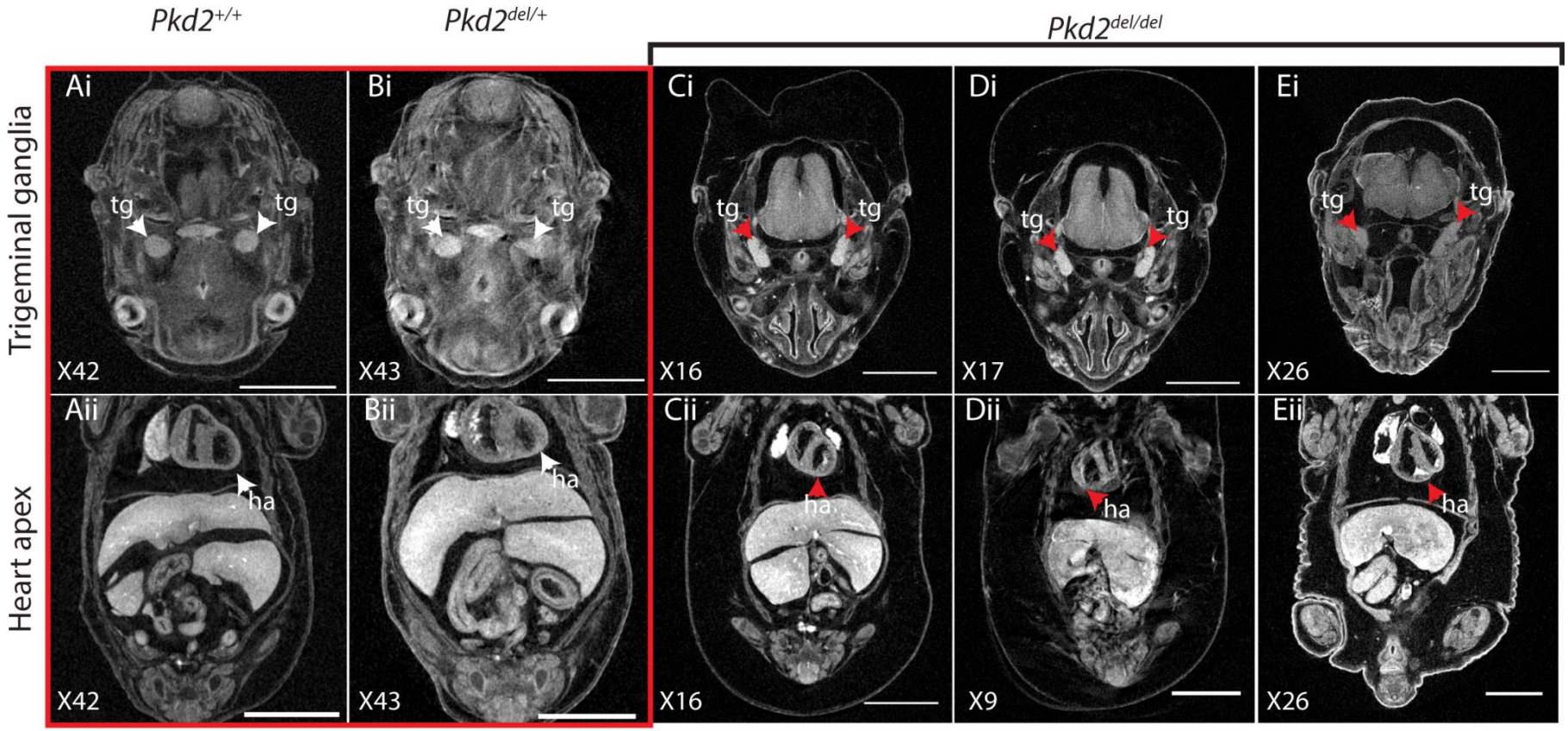


Figure 3.4: µCT sections of WT (**A**), *Pkd2*$^{del/+}$ (**B**) and *Pkd2*$^{del/del}$ (**C-E**) 15.5 dpc embryos, showing novel phenotypes or phenotypes with variable presentation or penetrance. White arrows: normal phenotypes; red arrows: abnormal phenotypes. Abbreviations (in alphabetical order): al – accessory lobe; av – azygos vein; cal – caudal lobe; cl – cranial lobe; ha – heart apex; ivc – inferior vena cava; ivs – interventricular septum; lat – left atrium; lll – left lateral lobe; lml – left medial lobe; LV – left ventricle; ml – medial lobe; p – pancreas; pp – papillary process; rat – right atrium; rll – right lateral lobe; rml – right medial lobe; RV – right ventricle; sl – single lobe; spl – spleen; st – stomach; tg – trigeminal ganglion. Samples highlighted in red are from a PKD2-DELxDEL1 cross (**A** and **B**), whilst samples in **C**, **D** and **E** are from PKD2-DELxDEL cross. Sample IDs are shown bottom left of each section. Scale bar: 2 mm. Unannotated figure is shown in **Appendix 1**, **Fig. A1.2**, pages 226-227.

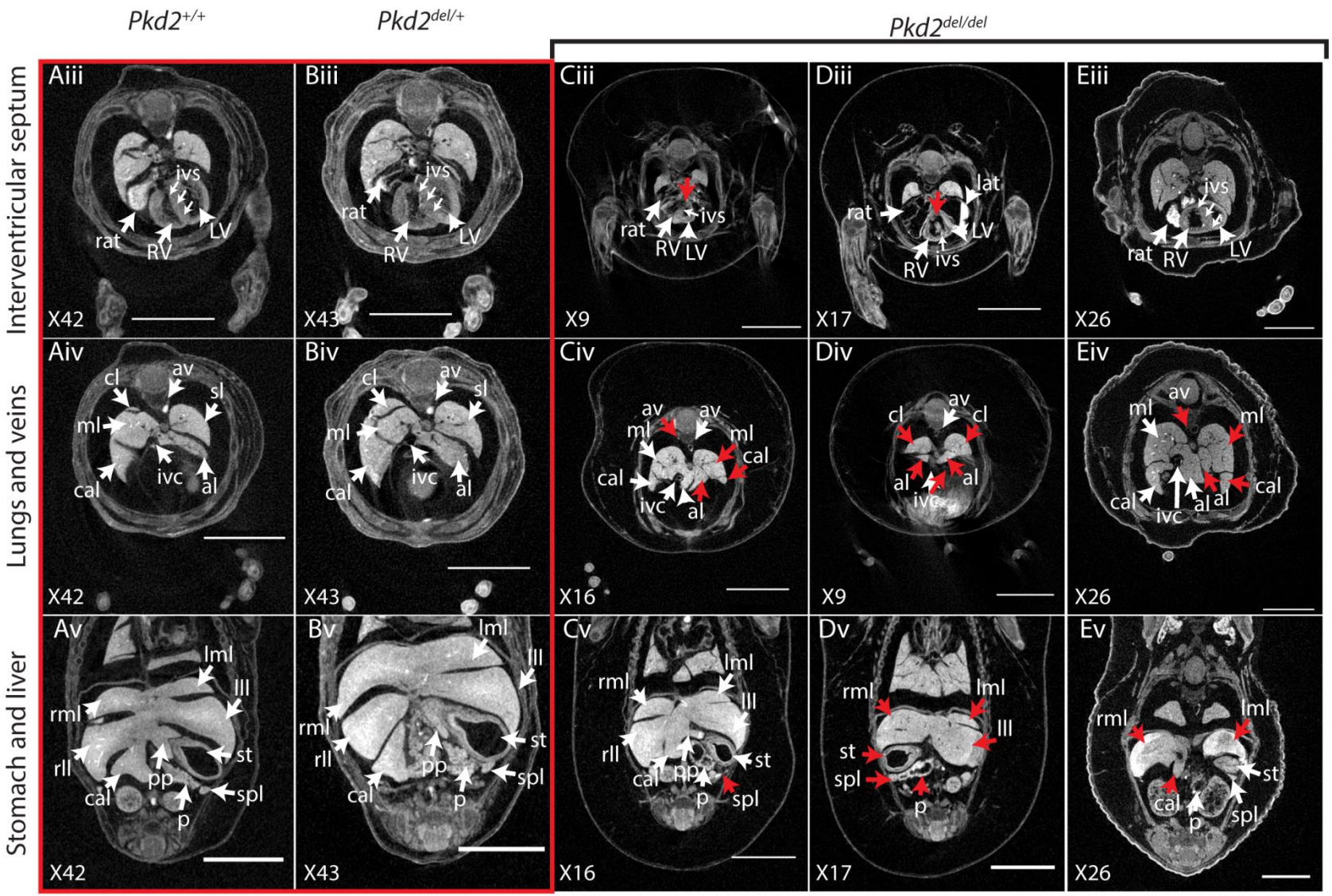


Figure 3.4 (continued)

Table 3.2: Heatmap summary of phenotypes observed in µCT-analysed *Pkd2*$^{del/del}$ embryos

Phenotype	PKD2-DELxDEL sample			
	X9	X16	X17	X26
Nervous System				
• Midbrain				
• Mesencephalic vesicle				
• 3rd Ventricle				
• Lateral vesicles				
• Cerebellum				
• CP (in medial 4th ventricle)				
• Lateral extremity of 4th ventricle				
• TG				
• Olfactory lobe				
• Emerging cervical spinal chord				
Cranial				
• Soft palate				
• Submandibular gland				
• C6 vertebra and DRG				
Thoracic				
• Thymus				
• Venous system				
• Ductus arteriosus	SI		SI	
• Lungs	2:2	4:4	4:4	4:4
• Heart apex	D	M	M	M
• Aorta	SI		SI	
• Atria				
• Ventricles				
• IVS				
Abdominal				
• Peritoneal cavity				
• Adrenal glands				
• Kidneys	C	C	C	C
• Liver lobes	SI		SI	
• Stomach position	SI		SI	
• Spleen	SI			
• Pancreas	C SI	C	C SI	C
• Ovaries	-			-
• Testes	C	-	-	C
Oedema				
Brown fat				
Spinal shape				

Gray cells represent normal phenotypes, red cells represent abnormal phenotypes. Abbreviations: C – cystic; CP – choroid plexus; D – dextrocardia; DRG – dorsal root ganglia; IVS – interventricular septum; M – mesocardia; SI – *situs inversus*; TG – trigeminal ganglia. Lung lobations are given R:L and are shown only where the lobation is abnormal.

3.2.3. Phenotypic analysis of *Pkd2*$^{fsX7/del}$ and *Pkd2*$^{fsX7/fsX7}$ embryos at 15.5 dpc

The *Pkd2*^{fsX7} mutant allele contains a 1 nucleotide deletion, resulting in a frameshift and termination of the protein after 6 AA (**Fig. 3.1**, **C**). The PKD2^{fsX7} protein contains the homo-oligomerization sub-region of the PKD2 CC, but not the hetero-oligomerization sub-region (**Fig. 3.1**, **B**), which is thought to be involved in the PKD1-PKD2 interaction. Given the results described in **Chapter 2**, which suggest that the domains affected by this mutation – the hetero-oligomerization sub-region of the CC – may not be involved in the PKD1L1-PKD2 interaction (see section **2.2.3**), it seems reasonable to hypothesise that this mutation will only lead to kidney but not *situs* phenotypes. However, further work described within the same chapter also raises questions about the validity of the results regarding the PKD1L1-PKD2 interaction (see section **2.2.6** and **2.3**). The fragments used in testing this interaction appear to be more prone to non-specific interactions, as compared to full-length PKD2. In order to test the differences in phenotypes produced by the two alleles, *Pkd2*^{del} and *Pkd2*^{fsX7}, I analysed both *Pkd2*$^{fsX7/del}$ and *Pkd2*$^{fsX7/fsX7}$ embryos. Direct comparison between the three genotypes will allow me to describe a hierarchy, in terms of phenotype, of the assessed genotypes. In order to provide a similar analysis to what has already been described for *Pkd2*$^{del/del}$ embryos, the first step was to perform gross *situs* analysis, followed by histological sectioning, for both *Pkd2*$^{fsX7/del}$ and *Pkd2*$^{fsX7/fsX7}$ embryos. µCT analysis was then performed on a different set of embryos.

3.2.3.a. Gross *situs* analysis

Embryos were collected at 15.5-16 dpc; WT, *Pkd2*$^{del/+}$ and *Pkd2*$^{fsX7/+}$ embryos displayed no oedema (**Fig. 3.5**, **Ai** and **Bi**), or very mild, localised oedema (**Fig. 3.5**, **Ci**). On sub-dissection, WT or heterozygous embryos showed normal L-R asymmetry. Lung lobation was normal (4:1 R:L) and the heart apex was positioned on the left side of the body (**Fig. 3.5**, **Aii**, **Bii** and **Cii**, respectively); the stomach and spleen were also normal, being positioned on the left side of the body. Great

vessel positioning and patterning was assessed and found to be normal in WT and heterozygous embryos (**Fig. 3.5**, **Aiii**, **Biii** and **Ciii**). All *Pkd2*$^{fsX7/del}$ compound heterozygote embryos showed variable levels of generalized oedema. In some instances, the skin was distended from the body visibly in multiple regions by 1 mm or more; this is henceforth referred to as severe oedema. Cases of severe oedema were seen in 12/18 samples and are shown in **Fig. 3.5**, **Di** and **Ei** (compare to **Fig. 3.5**, **Fi**). Sub-dissection for gross *situs* analysis was performed on 11 *Pkd2*$^{fsX7/del}$ embryos. The *situs* phenotype observed in these embryos varied in presentation, ranging from normal – levocardia (16/16) with 4:1 R:L lung lobation (13/16, **Fig. 3.5**, **Eii**) – to heterotaxic: levocardia with 2:1 R:L lung lobation (1/16, **Fig. 3.5**, **Dii**). Great vessel patterning and positioning was normal in most samples (13/16); abnormal phenotypes consisted of fused great vessels (1/16, **Fig. 3.5**, **Eiii**), and interrupted aortic arch (IAA – 2/16). Abdominal viscera were normally positioned in all sub-dissected *Pkd2*$^{fsX7/del}$ samples. Lethality at the point of dissection was only encountered in one sample (5.55%, 1/18 embryos), which is in contrast to the lethality encountered in *Pkd2*$^{del/del}$ (55.56%, 20/36 embryos). Gross *situs* analysis reveals that *Pkd2*$^{fsX7/del}$ embryos display oedema in all cases, with normal *situs* for thoracic and abdominal viscera, in most samples observed. Abnormal phenotypes were observed for lung lobation, with one sample showing 2:1 R:L lobation, and great vessel patterning, with two samples showing either IAA or fused great vessels.

In comparison to either *Pkd2*$^{del/del}$ or *Pkd2*$^{fsX7/del}$ samples, all 22 *Pkd2*$^{fsX7/fsX7}$ embryos also displayed oedema (**Fig. 3.5**, **Fi**), but had a lower incidence of severe oedema: 3/22. All four of the sub-dissected *Pkd2*$^{fsX7/fsX7}$ embryos displayed normal *situs*, showing 4:1 R:L lung lobation, levocardia (**Fig. 3.5**, **Fii**) and left-sided stomach and spleen positioning (**Table 3.8**). Great vessel patterning was also normal in all sub-dissected embryos of this genotype (**Fig. 3.5**, **Fiii**). Gross *situs* analysis revealed that all *Pkd2*$^{fsX7/fsX7}$ assessed displayed *situs solitus*.

The results of this analysis indicate that the *Pkd2*^{del} and *Pkd2*^{fsX7} alleles are different, in terms of phenotypes produced; *Pkd2*$^{del/del}$, *Pkd2*$^{fsX7/del}$ and *Pkd2*$^{fsX7/fsX7}$ embryos vary not just in the incidence of L-R phenotypes, but also in terms of which particular phenotypes they present. Specifically, none of the *Pkd2*$^{fsX7/del}$ or *Pkd2*$^{fsX7/fsX7}$ embryos display the right lung isomerism characteristic for the majority of *Pkd2*$^{del/del}$ samples. Similarly, abdominal viscera displayed normal *situs* in both *Pkd2*$^{fsX7/del}$ and *Pkd2*$^{fsX7/fsX7}$, whereas over half of *Pkd2*$^{del/del}$ embryos display abdominal *situs inversus*.

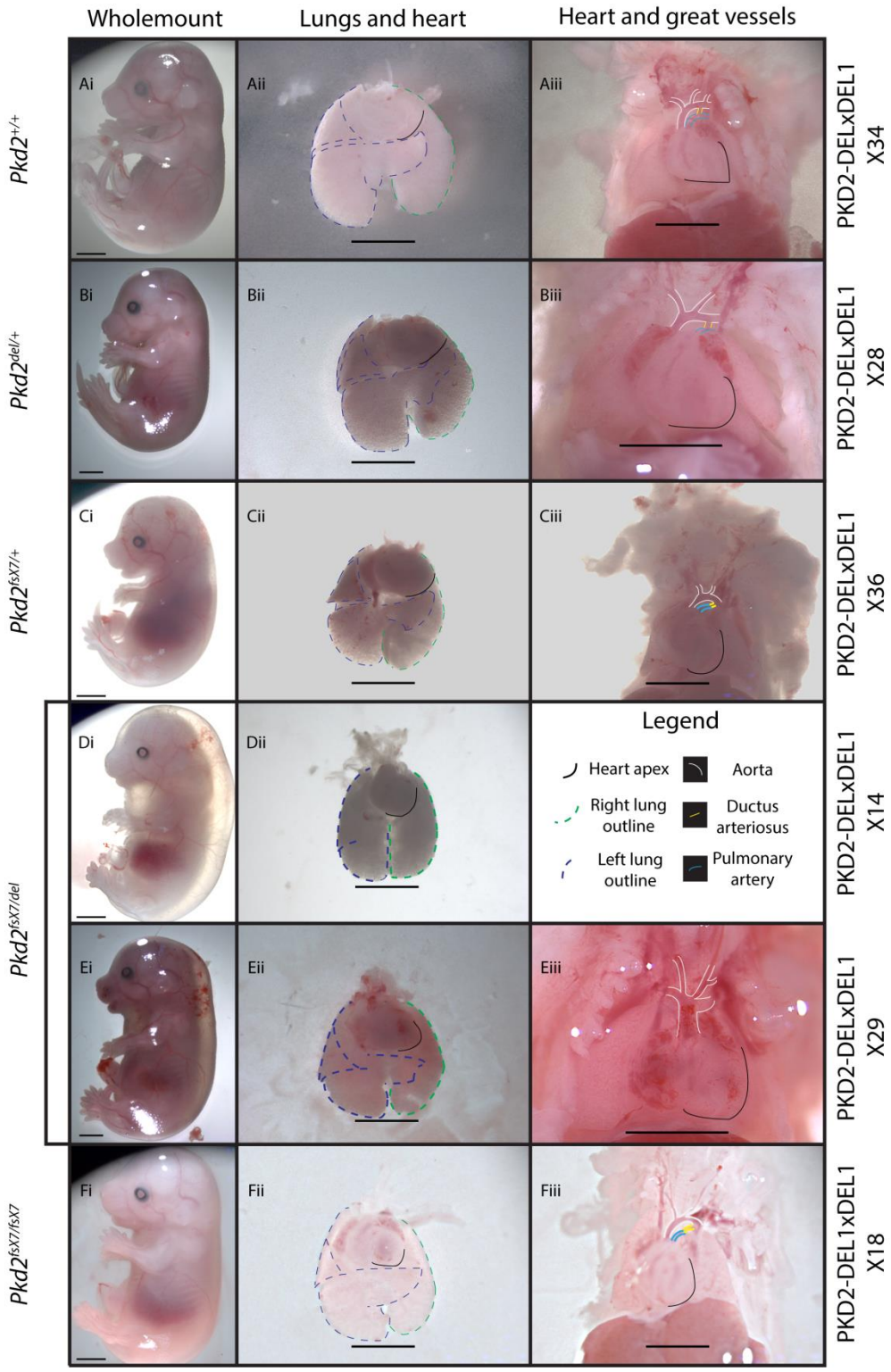


Figure 3.5: Analysis of great vessel and L-R patterning in WT (**A**), *Pkd2*$^{del/+}$ (**B**), *Pkd2*$^{fsX7/+}$ (**C**), *Pkd2*$^{fsX7/del}$ (**D** and **E**) and *Pkd2*$^{fsX7/fsX7}$ (**F**) embryos. Wholemounts are shown in the first column, lung and heart *situs* are shown in the second column, whilst great vessel patterning and positioning is shown in the final column. Sample IDs are given on the right hand side. Scale bar: 2 mm. Unannotated figure is shown in **Appendix 1**, **Fig. A1.3**, page 228**.**

3.2.3.b. Histological sectioning of kidneys

In order to assess the kidney phenotypes of *Pkd2*$^{fsX7/del}$ and *Pkd2*$^{fsX7/fsX7}$ embryos, kidneys were sub-dissected from embryos of the relevant genotypes, fixed in 4% PFA and processed by Histology core services by sectioning and staining with haematoxylin and eosin. WT, *Pkd2*$^{del/+}$ and *Pkd2*$^{fsX7/+}$ samples were similarly processed. Heterozygote (*Pkd2*$^{del/+}$ and *Pkd2*$^{fsX7/+}$) and WT kidneys displayed no cysts (**Fig. 3.6**, **A**-**F**). All three genotypes displayed apparently-normal glomeruli or proximal tubules. In contrast, cysts were observed in both *Pkd2*$^{fsX7/del}$ (**Fig. 3.6**, **G** and **H**) and *Pkd2*$^{fsX7/fsX7}$ (**Fig. 3.6**, **I** and **J**) samples, as previously reported in *Pkd1*- and *Pkd2*-null embryos (Lu et al., 1997, Wu et al., 2000). The cysts are largely glomerular, thereby increasing the size of the glomeruli. Both *Pkd2*$^{fsX7/del}$ and *Pkd2*$^{fsX7/fsX7}$ animals display cystic kidneys and are comparable to *Pkd2*$^{del/del}$ animals. In order to distinguish these genotypes from each other, further analysis is required (see section **4.2.2**).

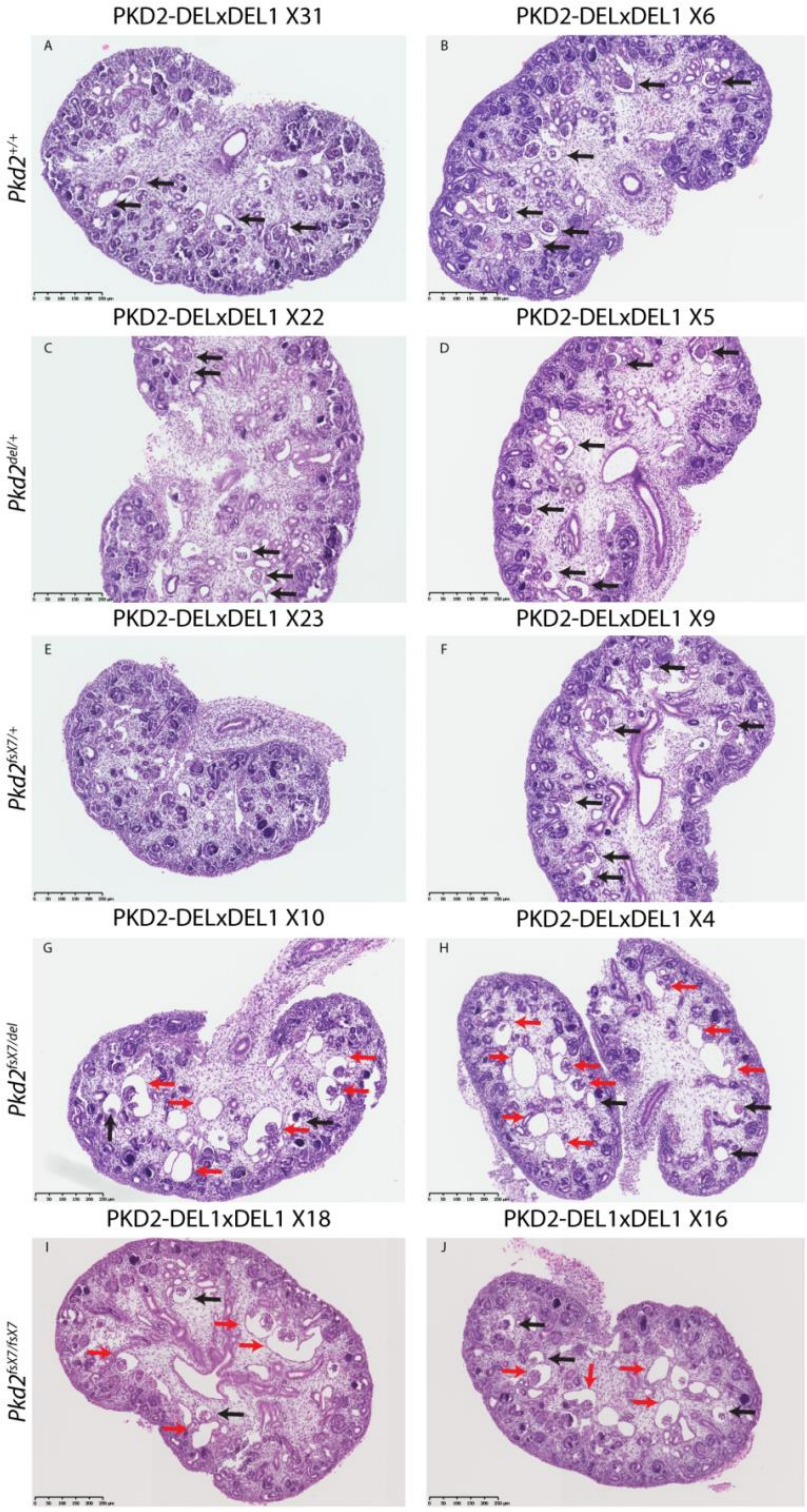


Figure 3.6: Histological sectioning of kidneys from offspring of PKD2-DEL1xDEL or PKD2-DEL1xDEL1 crosses. WT kidneys are shown in **A-B**, *Pkd2*$^{del/+}$ kidneys are shown in **C**-**D**, *Pkd2*$^{fsX7/+}$ kidneys are shown in **E**-**F**, *Pkd2*$^{fsX7/del}$ kidneys are shown in **G-H** and *Pkd2*$^{fsX7/fsX7}$ kidneys are shown in **I-J**. Normal glomeruli are indicated by black arrows, cysts are indicated by red arrows. Sample IDs are given, alongside the matings that produced them, at the top of each image. Scale bar: 250 µm.

3.2.3.c. Phenotypic analysis through µCT

In order to further assess the phenotypes of *Pkd2*$^{fsX7/del}$ and *Pkd2*$^{fsX7/fsX7}$ embryos, µCT analysis was performed on 15.5-16 dpc embryos, as described in section **5.1.3**. Alongside embryos of this genotype, WT, *Pkd2*$^{del/+}$ and *Pkd2*$^{fsX7/+}$ embryos were also analysed as controls. As described in section **3.2.2**, µCT analysis provides a time-efficient method of assessing multiple phenotypes in a non-invasive, minimally destructive method. Confirming the histological sectioning analysis (**Fig. 3.6**, **G**-**J**), kidney cysts were observed in all five *Pkd2*$^{fsX7/del}$ (**Fig. 3.7**, **Di** and **Ei**) and all nine *Pkd2*$^{fsX7/fsX7}$ (**Fig. 3.9**, **Ci**, **Di** and **Ei**) embryos. Cysts were not observed in WT (**Fig. 3.7**, **Ai** and **Fig. 3.9**, **Ai**), *Pkd2*$^{del/+}$ (**Fig. 3.7**, **Bi**) or *Pkd2*$^{fsX7/+}$ (**Fig. 3.7**, **Ci** and **Fig. 3.9**, **Bi**) embryos. As previously discussed (see section **3.2.2**), kidney cyst size and frequency increased in both *Pkd2*$^{fsX7/del}$ and *Pkd2*$^{fsX7/fsX7}$ embryos with age. In samples closer to 15.5 dpc, these are less evident (**Fig. 3.7**, **Di** and **Fig. 3.9**, **Di**). Pancreatic cysts were observed in all *Pkd2*$^{fsX7/del}$ embryos (**Fig. 3.7**, **Di** and **Ei**), but were observed only in 3/9 of *Pkd2*$^{fsX7/fsX7}$ samples analysed (**Fig. 3.10**, **Ci** and **Ei,** compare to **Fig. 3.10**, **Di**). None of the WT or heterozygous embryos displayed pancreatic cysts (**Fig. 3.7**, **Ai**, **Bi** and **Ci** and **Fig. 3.10**, **Ai** and **Bi**). Similarly to what was observed in male *Pkd2*$^{del/del}$ embryos (**Table 3.2**), all male *Pkd2*$^{fsX7/del}$ (**Fig. 3.7**, **Dii** and **Eii**) and all male *Pkd2*$^{fsX7/fsX7}$ samples (**Fig. 3.9**, **Eii**) displayed testicular cyst-like formations, which were not observed in WT or heterozygous samples (**Fig. 3.7**, **Aii**, **Bii** and **Cii**, and **Fig. 3.9**, **Aii**). In female samples, ovaries were normal for both genotypes (**Fig. 3.9**, **Cii** and **Dii**, **Table 3.3** and **Table 3.4**), as well as control genotypes (**Fig. 3.9**, **Bii**). The heart IVS was compromised in all *Pkd2*$^{fsX7/del}$ embryos (**Fig. 3.7**, **Diii** and **Eiii**), but none of the *Pkd2*$^{fsX7/fsX7}$ (**Fig. 3.9**, **Ciii**, **Diii** and **Eiii**), heterozygote (**Fig. 3.7**, **Biii**, **Ciii** and **Fig. 3.9**, **Biii**) or WT embryos (**Fig. 3.7**, **Aiii** and **Fig. 3.9**, **Aiii**). Similarly to what was observed in *Pkd2*$^{del/del}$ embryos (**Table 3.2**), brown fat pads were abnormal in shape in both *Pkd2*$^{fsX7/del}$ (**Fig. 3.7**, **Dv** and **Ev**) and *Pkd2*$^{fsX7/fsX7}$ samples (**Table 3.4**), potentially due to the presence of oedema. In contrast to *Pkd2*$^{del/del}$ embryos, two *Pkd2*$^{fsX7/del}$ embryos displayed cleft palate (**Fig. 3.8**, **Diii**); all WT (**Fig. 3.8**,

Aiii), heterozygous (**Fig. 3.8**, **Biii** and **Ciii**) and *Pkd2*$^{fsX7/fsX7}$ embryos (**Table 3.4**) had normally-formed palates.

Both *Pkd2*$^{fsX7/del}$ and *Pkd2*$^{fsX7/fsX7}$ embryos displayed nervous system abnormalities. In *Pkd2*$^{fsX7/del}$ embryos, dorsal root ganglia (DRG) were either displaced or abnormally shaped (**Fig. 3.7**, **Div** and **Eiv**). In *Pkd2*$^{fsX7/fsX7}$, DRG were displaced only in 6/9 samples analysed (**Fig. 3.10**, **Cii**, **Dii** and **Eii**). None of the WT (**Fig. 3.7**, **Aiv** and **Fig. 3.10**, **Aii**) or heterozygote samples (**Fig. 3.7**, **Biv**, **Civ** and **Fig. 3.10**, **Bii**) had displaced DRG. The subarachnoid space was distended in the thoracic region in both *Pkd2*$^{fsX7/del}$ (**Fig. 3.7**, **Div** and **Eiv**) and *Pkd2*$^{fsX7/fsX7}$ embryos (**Fig. 3.9**, **Cv**, **Dv** and **Ev**), but not WT (**Fig. 3.7**, **Aiv** and **Fig. 3.9**, **Av**) or heterozygous embryos (**Fig. 3.7**, **Biv, Civ** and **Fig. 3.9**, **Bv**). The olfactory lobes were also abnormally spaced in both *Pkd2*$^{fsX7/del}$ (**Table 3.3**) and *Pkd2*$^{fsX7/fsX7}$ embryos (**Fig. 3.9**, **Civ**, **Div** and **Eiv**), but not in control genotypes (**Fig. 3.9**, **Aiv** and **Biv**). The lateral extremity of the fourth ventricle was also abnormal in all *Pkd2*$^{fsX7/del}$ embryos (**Table 3.3**), but only in 8/9 *Pkd2*$^{fsX7/fsX7}$ samples (**Fig. 3.10, Ciii**, **Diii** and **Eiii**).

In terms of L-R development, none of the nine *Pkd2*$^{fsX7/fsX7}$ embryos showed any *situs* abnormalities (**Table 3.4**). However, two *Pkd2*$^{fsX7/del}$ embryos (out of five) displayed *situs* anomalies: one embryo displayed left isomerism of the lungs (**Fig. 3.11**, **B**) and azygos vein, right isomerism of the inferior vena cava (**Fig. 3.8**, **Di**) and *situs inversus* of the stomach, spleen, pancreas and liver (**Fig. 3.8**, **Dii**); the second embryo displayed 5:4 R:L lung lobation (4+:4 category; **Fig. 3.11**, **C**). The 5:4 lobation phenotype is highly unusual, primarily because the most severe situations reported in literature are either R- (4:4) or L-lung isomerisms (1:1). As such, this is either the first report of R-isomeric and R-supernumerary lobation, or is an artefact of this type of analysis. The abnormal phenotypes observed for *Pkd2*$^{fsX7/del}$ and *Pkd2*$^{fsX7/fsX7}$ embryos are summarised in **Table 3.3** and **Table 3.4**, respectively. Full phenotypic analysis data is given in **Appendix 2**, **Table A2.2** and **Table A2.3**, respectively. A 3D reconstruction of WT, *Pkd2*$^{fsX7/del}$ 5:4 and 1:1 lungs is shown in **Fig. 3.11**.

The data presented thus far indicates that there are differences between the *Pkd2*^{del} and *Pkd2*^{fsX7} alleles, as revealed by the phenotypes of *Pkd2*$^{del/del}$, *Pkd2*$^{fsX7/del}$ and *Pkd2*$^{fsX7/fsX7}$ embryos, which differ in phenotype presentation and severity. Confirming the findings of the gross *situs* analysis, the R-lung isomerism characteristic of the majority of *Pkd2*$^{del/del}$ embryos is not observed in either *Pkd2*$^{fsX7/del}$, or *Pkd2*$^{fsX7/fsX7}$ embryos. Instead, the *Pkd2*$^{fsX7/fsX7}$ embryos display *situs solitus*, whilst *Pkd2*$^{fsX7/del}$ display normal lung *situs* and great vessel patterning in the majority of cases, low incidences of *situs inversus* for abdominal viscera and normal heart *situs* in all cases. The lack of L-R phenotypes in *Pkd2*$^{fsX7/fsX7}$ embryos, but presence of kidney cysts, supports the hypothesis that PKD1-PKD2 and PKD1L1-PKD2 have different molecular mechanisms for interaction.

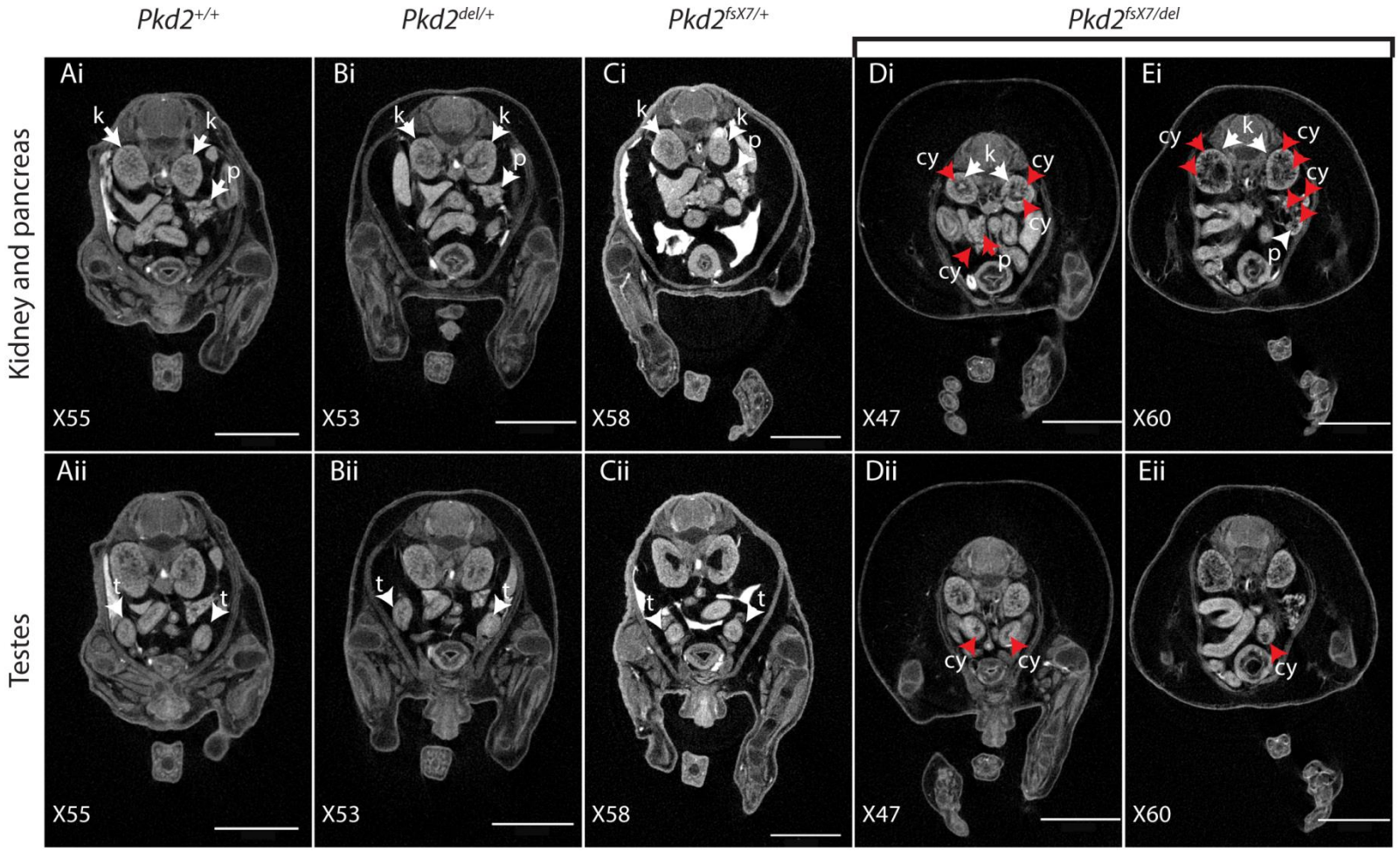


Figure 3.7: µCT sections of WT (**A**), *Pkd2*$^{del/+}$ (**B**), *Pkd2*$^{fsX7/+}$ (**C**) and *Pkd2*$^{fsX7/del}$ (**D**-**E**) 15.5 dpc embryos, showing most-commonly observed phenotypes. White arrows: normal phenotypes; red arrows: abnormal phenotypes. Abbreviations (in alphabetical order): bf – brown fat; cy – cyst; drg – dorsal root ganglion; ivs – interventricular septum; k – kidney; p – pancreas; sas – subarachnoid space; t - testis. Sample IDs are shown bottom left of each section. Scale bar: 2 mm. Unannotated figure is shown in **Appendix 1**, **Fig. A1.4**, pages 230-231.

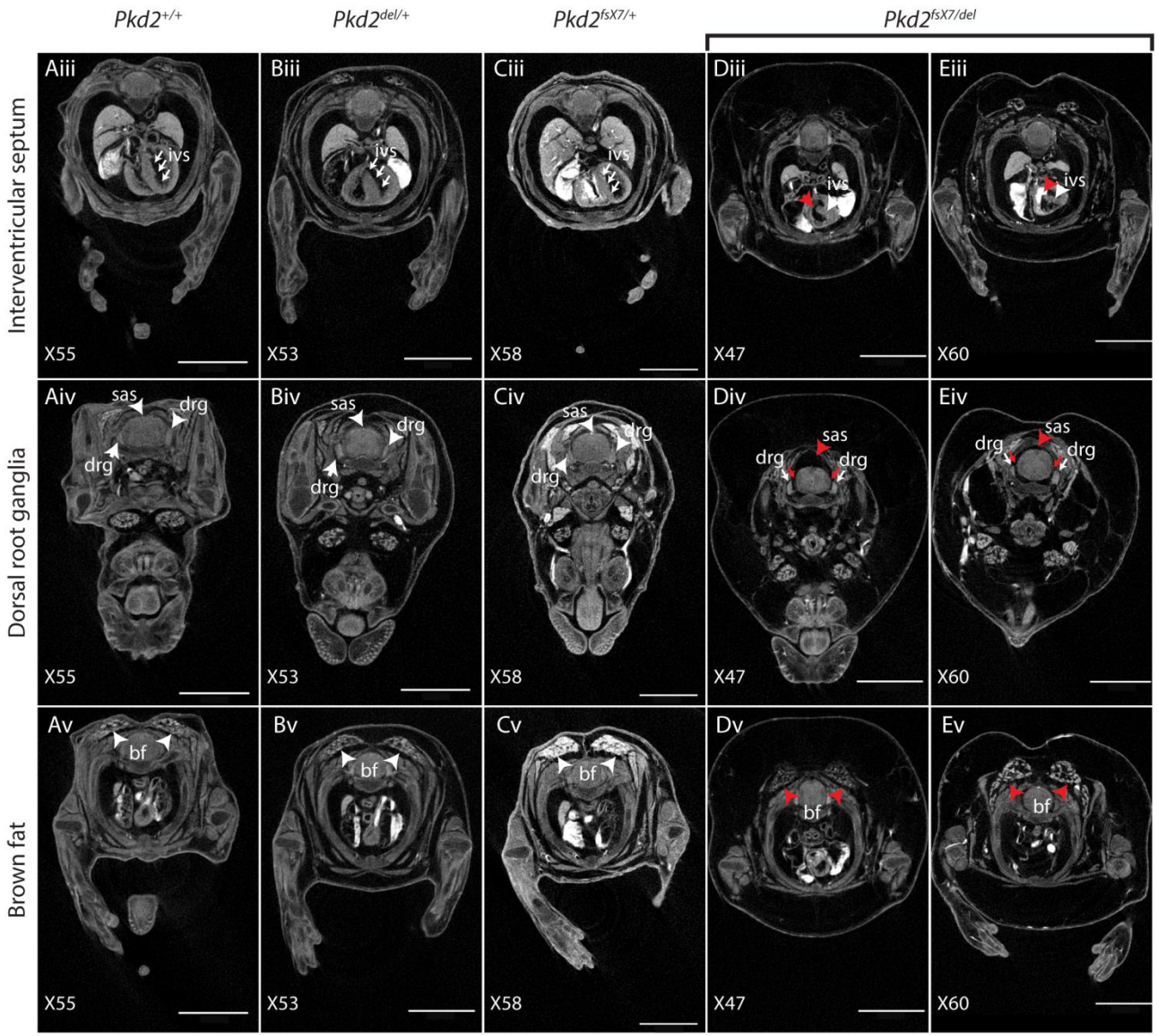


Figure 3.7 (continued)

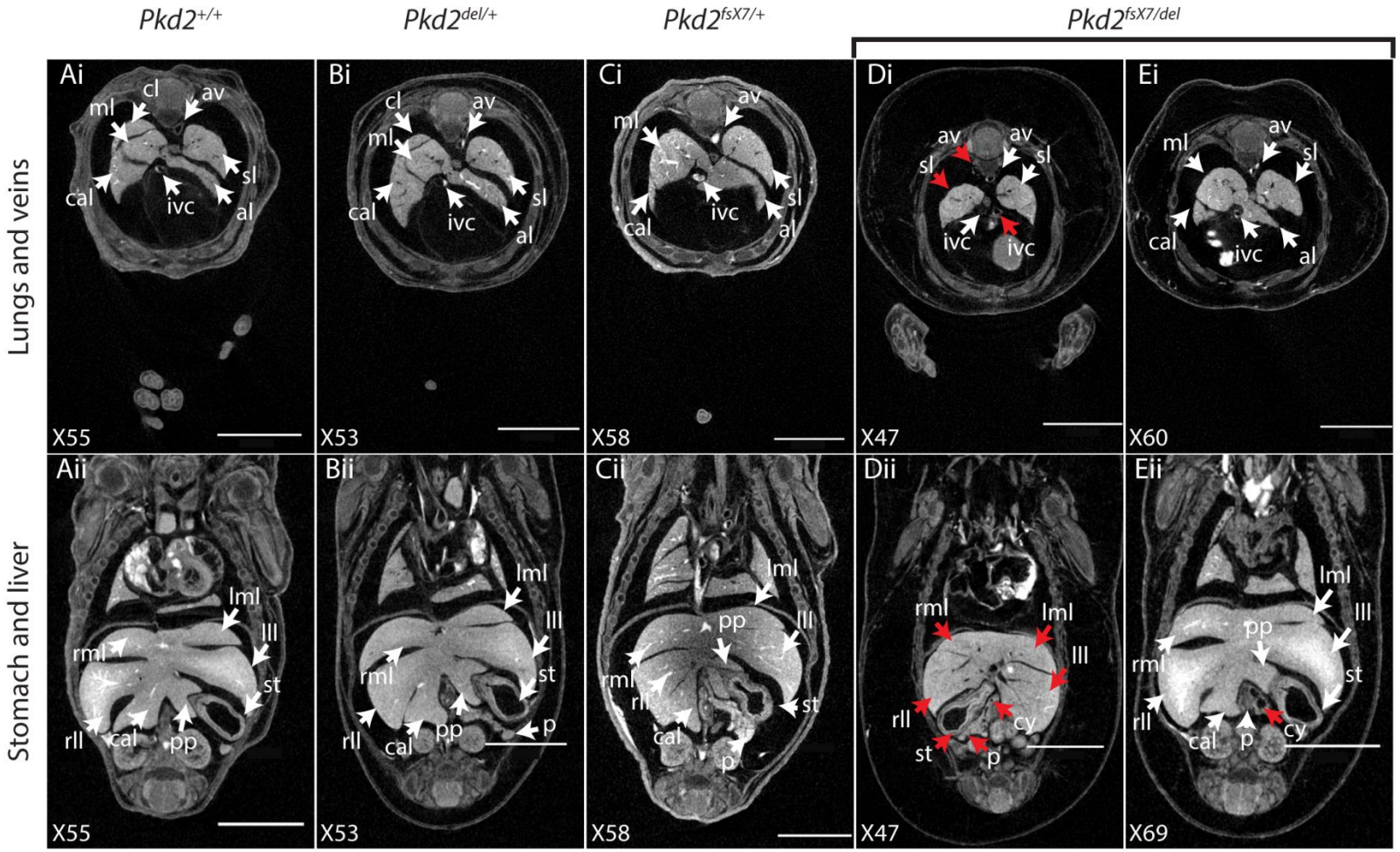


Figure 3.8: µCT sections of WT (**A**), *Pkd2*$^{del/+}$ (**B**), *Pkd2*$^{fsX7/+}$ (**C**) and *Pkd2*$^{fsX7/del}$ (**D**-**E**) 15.5 dpc embryos, showing phenotypes with variable presentation or penetrance. White arrows: normal phenotypes; red arrows: abnormal phenotypes. Abbreviations (in alphabetical order): al – accessory lobe; av – azygos vein; cal – caudal lobe; cl – cranial lobe; cp – cleft palate; cy – cyst; ivc – inferior vena cava; lll – left lateral lobe; lml – left medial lobe; ml – medial lobe; nc – nasal cavity; p – pancreas; pp – papillary process; rll – right lateral lobe; rml – right medial lobe; sl – single lobe; sp – soft palate; st – stomach; to - tongue. Sample IDs are shown bottom left of each section. Scale bar: 2 mm. Unannotated figure is shown in **Appendix 1**, **Fig. A1.5**, pages 232-233.

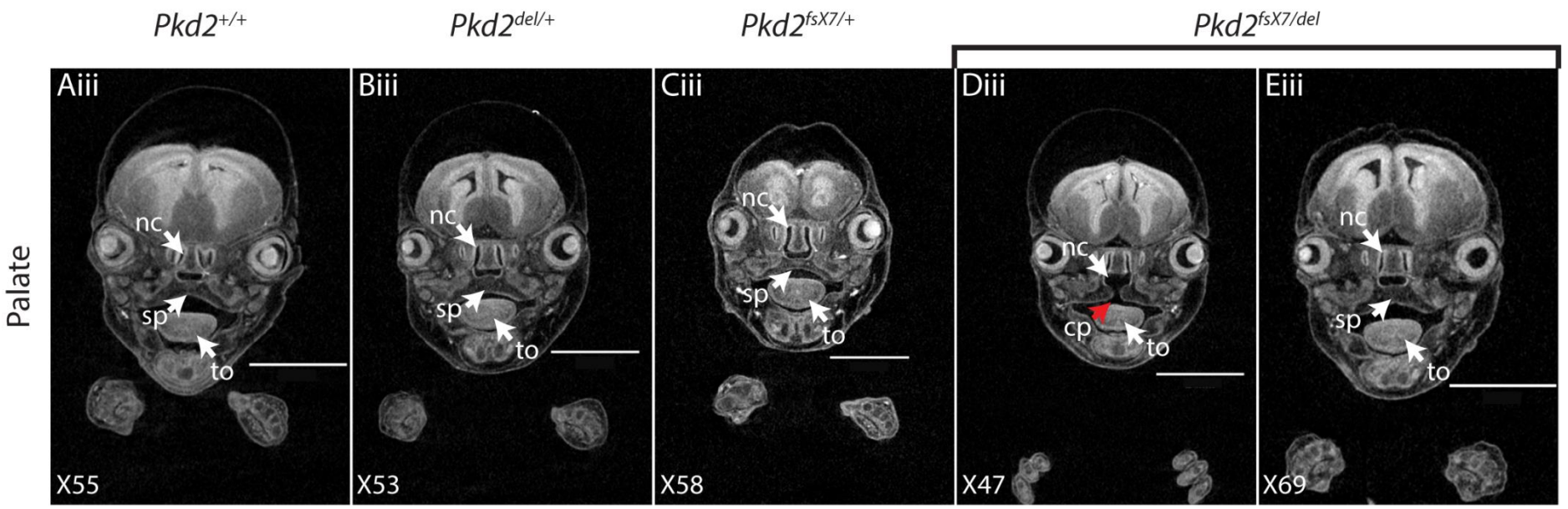


Figure 3.8 (continued)

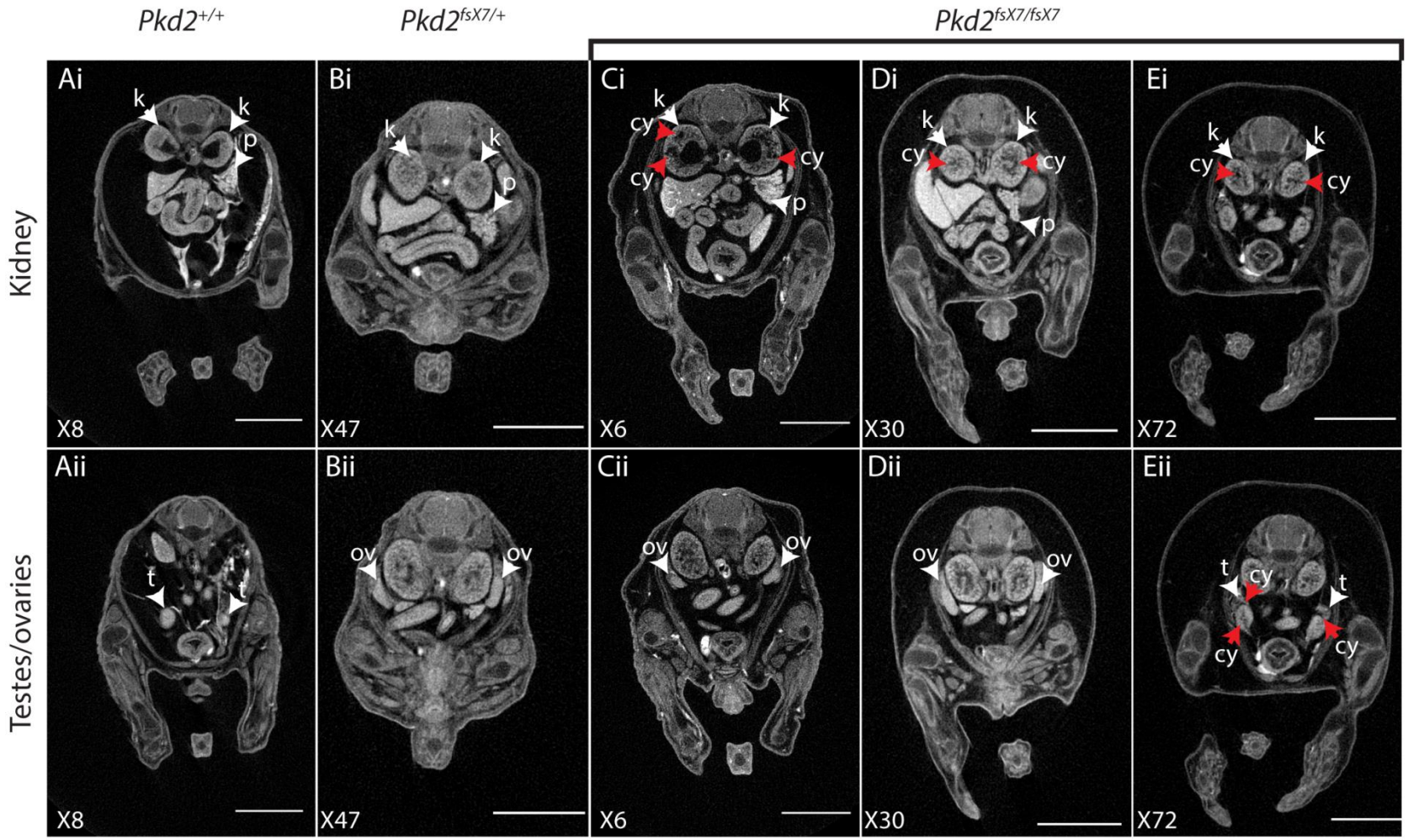


Figure 3.9: µCT sections of WT (**A**), *Pkd2*$^{fsX7/+}$ (**B**) and *Pkd2*$^{fsX7/fsX7}$ (**C**-**E**) 15.5 dpc embryos, showing most-commonly observed phenotypes. White arrows: normal phenotypes; red arrows: abnormal phenotypes. Abbreviations (in alphabetical order): cy – cyst; ils – interlobular space; ivs – interventricular septum; k – kidney; ov – ovary; p – pancreas; sas – subarachnoid space; t - testis. Sample IDs are shown bottom left of each section. Scale bar: 2 mm. Unannotated figure is shown in **Appendix 1**, **Fig. A1.6**, pages 234-235.

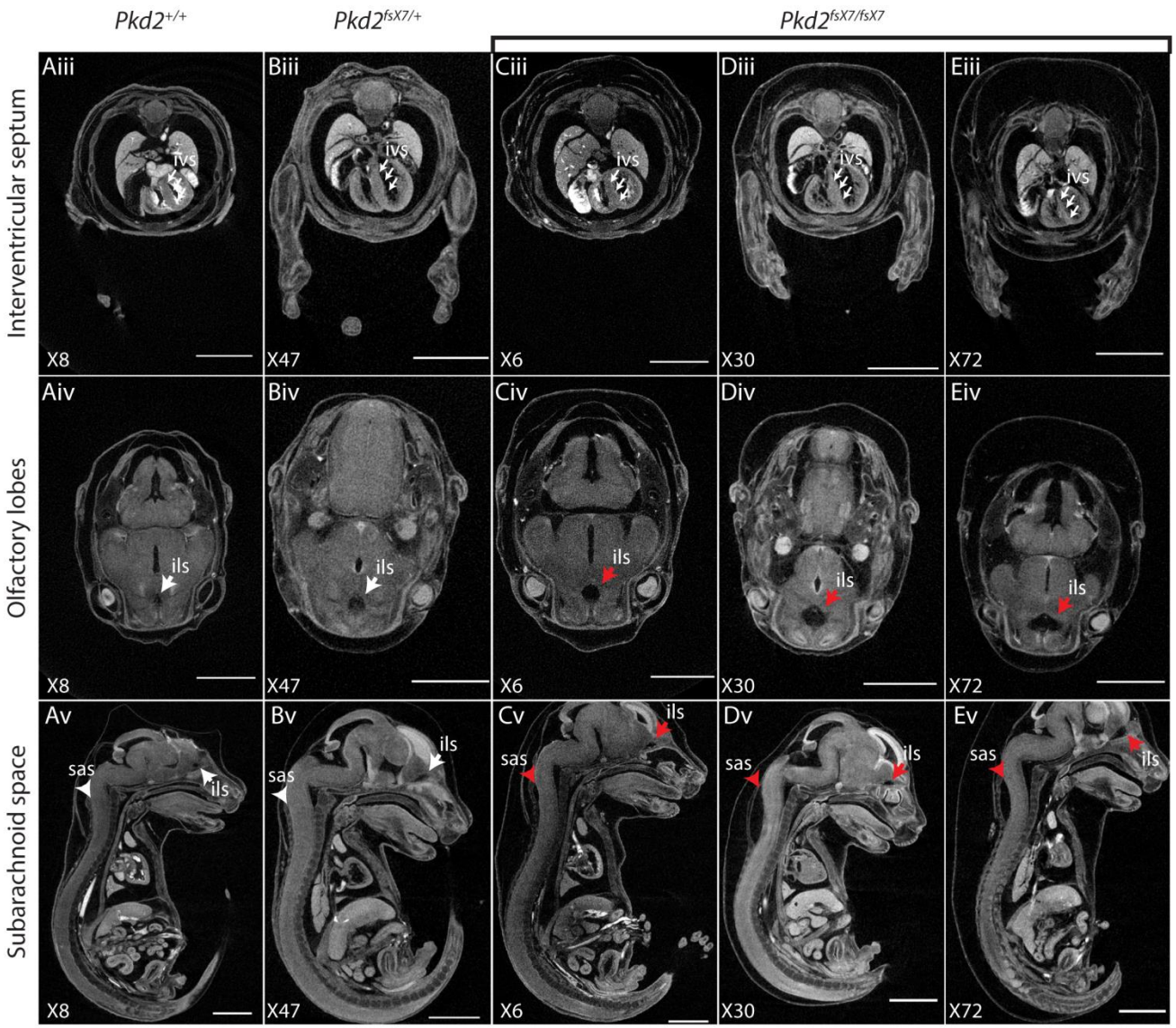


Figure 3.9 (continued)

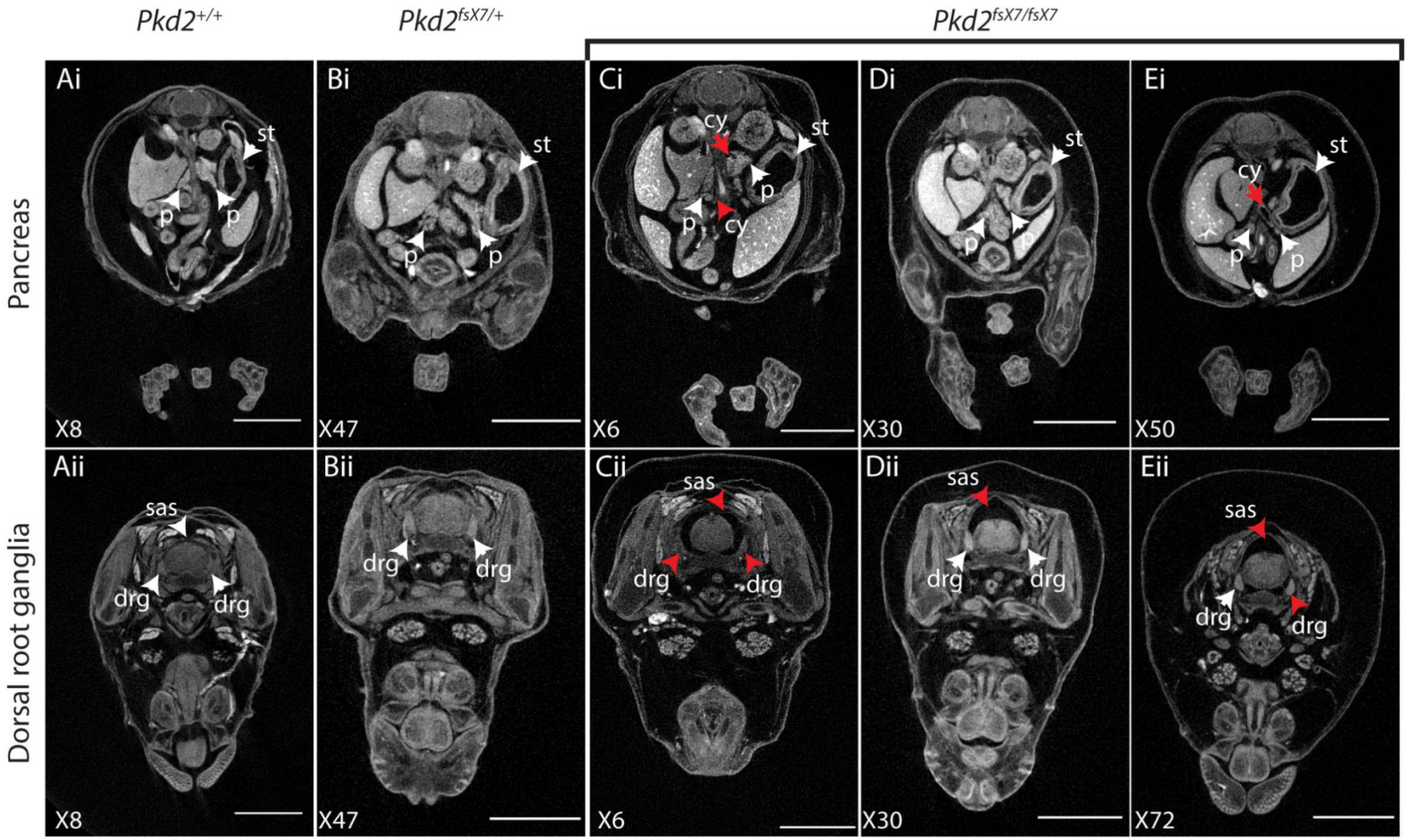


Figure 3.10: µCT sections of WT (**A**), *Pkd2*$^{fsX7/+}$ (**B**) and *Pkd2*$^{fsX7/fsX7}$ (**C**-**E**) 15.5 dpc embryos, showing phenotypes with variable presentation or penetrance. White arrows: normal phenotypes; red arrows: abnormal phenotypes. Abbreviations (in alphabetical order): cy – cyst; drg – dorsal root ganglion; lefv – lateral extremity of fourth ventricle; p – pancreas; sas – subarachnoid space; st – stomach. Sample IDs are shown bottom left of each section. Scale bar: 2 mm. Unannotated figure is shown in **Appendix 1**, **Fig. A1.7**, pages 236-237.

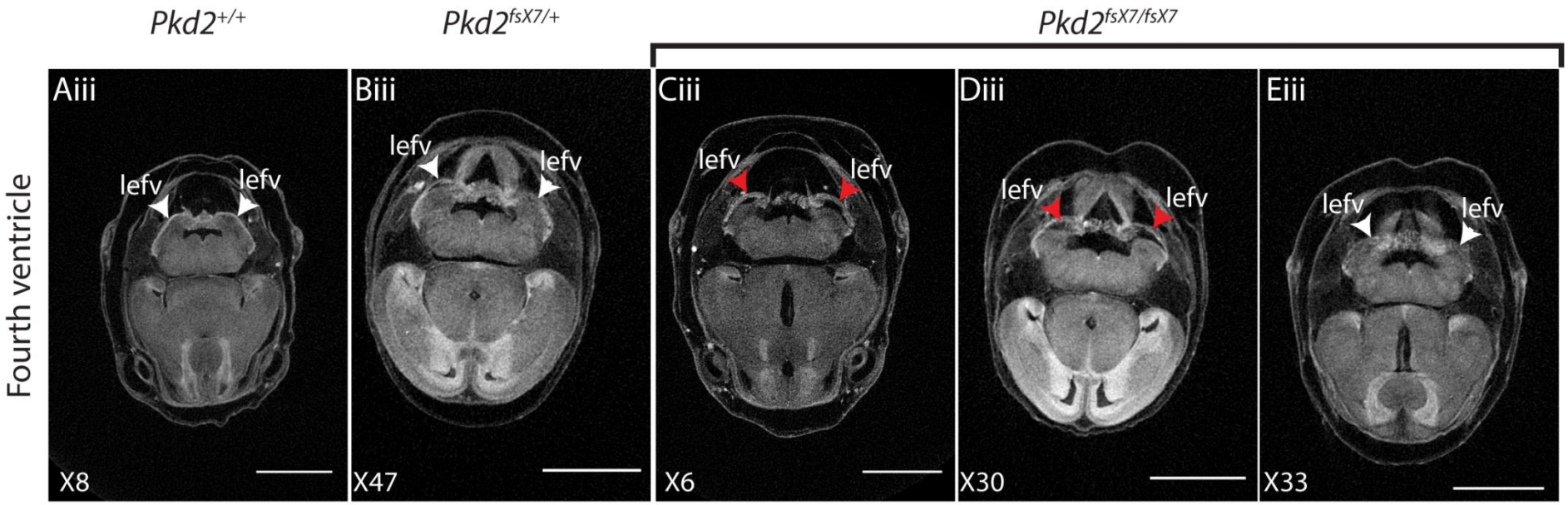


Figure 3.10 (continued)

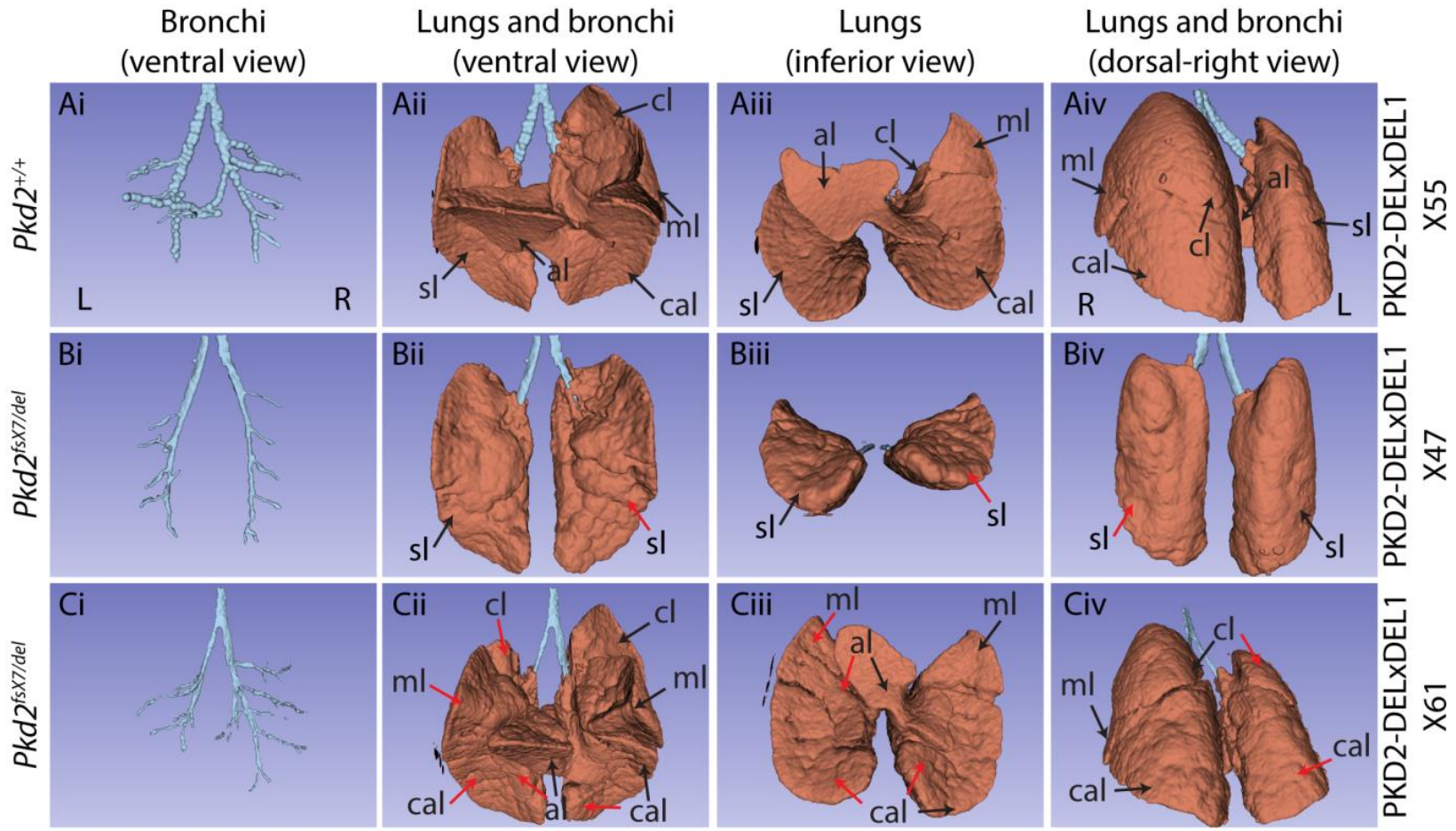


Figure 3.11: 3D reconstruction of lungs from embryos derived from PKD2-DELxDEL1 crosses, based on µCT sections. WT lungs, showing 4:1 R:L lobation are shown in **A**. Lungs from two *Pkd2*$^{fsX7/del}$, showing 1:1 and 5:4 R:L lobation are shown in **B** and **C**. Sample IDs are given on the right, genotypes are indicated on the left. L-R orientation indicated in **Ai** applicable to **Ai-iii**, **Bi-iii** and **Ci-iii**; L-R sides indicated in **Aiv** also applicable to **Biv** and **Civ**. Black arrows indicate normal structures, red arrows indicate abnormal structures. Abbreviations (in alphabetic order): al – accessory lobe; cal – caudal lobe; cl – cranial lobe; ml – medial lobe; sl – single (left) lobe.

Table 3.3: Heatmap summary of phenotypes observed in µCT-analysed *Pkd2*$^{fsX7/del}$ embryos

Phenotype	PKD2-DELxDEL1 sample				
	X40	X47	X60	X61	X69
Nervous System					
• Midbrain					
• Mesencephalic vesicle					
• 3rd Ventricle					
• Lateral vesicles					
• Cerebellum					
• CP (in medial 4th ventricle)					
• Lateral extremity of 4th ventricle					
• TG					
• Olfactory lobe					
• Emerging cervical spinal chord					
Cranial					
• Soft palate					
• Submandibular gland					
• C6 vertebra and DRG					
Thoracic					
• Thymus					
• Venous system					
• Ductus arteriosus					
• Lungs		1:1		4+:4	
• Heart apex					
• Aorta					
• Atria					
• Ventricles					
• IVS					
Abdominal					
• Peritoneal cavity					
• Adrenal glands					
• Kidneys	C	C	C	C	C
• Liver lobes		SI			
• Stomach position		SI			
• Spleen		SI			
• Pancreas	C	C SI	C	C	C
• Ovaries	-	-	-		-
• Testes	C	C	C	-	C
Oedema					
Brown fat					
Spinal shape					

Gray cells represent normal phenotypes, red cells represent abnormal phenotypes. Abbreviations: C – cystic; CP – choroid plexus; DRG – dorsal root ganglia; IVS – interventricular septum; SI – *situs inversus*; TG – trigeminal ganglia. Lung lobations are given R:L and are shown only where the lobation is abnormal.

Table 3.4: Heatmap summary of phenotypes observed in µCT-analysed *Pkd2*$^{fsX7/fsX7}$ embryos

Phenotype	PKD2-DEL1xDEL1 sample								
	X6	X29	X30	X33	X35	X49	X50	X67	X72
Nervous System									
• Midbrain									
• Mesencephalic vesicle									
• 3rd Ventricle									
• Lateral vesicles									
• Cerebellum									
• CP (in medial 4th ventricle)									
• Lateral extremity of 4th ventricle									
• TG									
• Olfactory lobe									
• Emerging cervical spinal chord									
Cranial									
• Soft palate									
• Submandibular gland									
• C6 vertebra and DRG									
Thoracic									
• Thymus									
• Venous system									
• Ductus arteriosus									
• Lungs									
• Aorta									
• Atria									
• Ventricles									
• IVS									
Abdominal									
• Peritoneal cavity									
• Adrenal glands									
• Kidneys	C	C	C	C	C	C	C	C	C
• Liver lobes									
• Stomach position									
• Spleen									
• Pancreas	C				C		C		
• Ovaries		-		-		-			-
• Testes	-	C	-	C	-	C	-	-	C
Oedema									
Brown fat									
Spinal shape									

Gray cells represent normal phenotypes, red cells represent abnormal phenotypes. Abbreviations: C – cystic; CP – choroid plexus; DRG – dorsal root ganglia; IVS – interventricular septum; SI – *situs inversus*; TG – trigeminal ganglia. Lung lobations are given R:L and are shown only where the lobation is abnormal.

3.2.4. Phenotypic analysis of *Pkd2*$^{S818X/del}$ and *Pkd2*$^{S818X/S818X}$ embryos at 15.5 dpc

The *Pkd2*^{S818X} allele contains a nonsense mutation, leading to early truncation of the protein downstream of the ER retention signal (**Fig. 3.1**, **C**). The mutated residues lie upstream of the region which codes for the CC region, thereby truncating both homo-oligomerization and hetero-oligomerization sub-regions of the PKD2 CC. This line also contains another mutation, which is shared with the *Pkd2*^{ins} allele, but lies downstream of the protein C-terminus. Given the data presented in **Chapter 2**, which argues that the CC of PKD2 is not required for PKD1L1-PKD2 interaction, I hypothesised that this mutation will not produce L-R phenotypes. However, previous studies have shown that the CC of PKD2 is involved in homo-oligomerization (see section **1.2.3**), but PKD2 is able to form tetrameric structures even in the absence of the CC (Giamarchi et al., 2010, Shen et al., 2016, Grieben et al., 2017) (see section **2.1.2**). Presently, there is little data regarding the impact of the truncation of the CC region on PKD2 function, but it is important to outline the possibility that the phenotypes produced by the presence of the *Pkd2*^{S818X} allele may be more severe than expected.

In order to compare this allele to *Pkd2*^{del}, phenotypic analysis was performed on both *Pkd2*$^{S818X/del}$ and *Pkd2*$^{S818X/S818X}$, similarly to what was described in section **3.2.3**. This analysis will also provide a means to validate the results described in **Chapter 2**, by determining whether this allele leads to both L-R and kidney phenotypes.

3.2.4.a. Gross *situs* analysis

Embryos were collected at 15.5-16 dpc, oedema was assessed, followed by sub-dissection to assess gross *situs*. None of the *Pkd2*$^{S818X/+}$ embryos analysed showed oedema. Lung (**Fig. 3.12**, **Bii**), heart, great vessel (**Fig. 3.12**, **Biii**), stomach and spleen *situs* (data not shown) was normal in all *Pkd2*$^{S818X/+}$ embryos analysed. In order to determine gross *situs* phenotypes, 11 *Pkd2*$^{S818X/del}$ and nine *Pkd2*$^{S818X/S818X}$ embryos were sub-dissected. Considering that some of these were dead at the

point of dissection, not all organs could be assessed. Both *Pkd2*$^{S818X/del}$ and *Pkd2*$^{S818X/S818X}$ embryos displayed a range of phenotypes, of different severities between genotype. Oedema was observed in all samples of both genotypes, and severe oedema was observed in the majority of *Pkd2*$^{S818X/del}$ (19/20, **Fig. 3.12**, **Ei** and **Ci**) and *Pkd2*$^{S818X/S818X}$ samples (16/17, **Fig. 3.13**, **Ci**, **Di** and **Ei**). Lethality at the point of dissection was recorded in 48.57% (17/35) of *Pkd2*$^{S818X/del}$ embryos (**Fig. 3.12**, **Di** and **Fi**) and 36% (9/25) of *Pkd2*$^{S818X/S818X}$ embryos. In *Pkd2*$^{S818X/del}$, levocardia was observed (9/18, **Fig. 3.12**, **Cii**, **Dii** and **Eii**), as well as dextrocardia (5/18, **Fig. 3.12**, **Fii**). In *Pkd2*$^{S818X/S818X}$ embryos, both levocardia (4/16, **Fig. 3.13**, **Cii** and **Dii**) and dextrocardia (10/16, **Fig. 3.13**, **Eii**) were observed. Mesocardia was only observed in samples analysed through μCT and accounts for the rest of the incidences in both genotypes.

Lung *situs* phenotypes also varied in both *Pkd2*$^{S818X/del}$ and *Pkd2*$^{S818X/S818X}$ embryos. *Pkd2*$^{S818X/del}$ samples showed 4:1 R:L (2/17 – **Table 3.8**), or randomised lung lobation. Examples of randomisation in *Pkd2*$^{S818X/del}$ embryos include: 4:3 (5/17, **Fig. 3.12**, **Cii**), 4:2 (3/17, **Fig. 3.12**, **Eii**) and 3:5 (1/17, **Fig. 3.12**, **Fii**) R:L. As with the 5:4 lung lobation presented in section **3.2.3.c**, the 3:5 R:L lobation is highly unusual. For the purposes of this analysis, this is classified under the randomisation category, as are the 4:3 and 4:2 lobation patterns. *Pkd2*$^{S818X/S818X}$ embryos had no normal embryos in terms of lung lobation. However, 4:3 (randomised, 3/16, **Fig. 3.13**, **Eii**), 4:4 (R-isomeric, 7/16, **Fig. 3.12**, **Dii**) and 4:6 – R-isomeric and L-supernumerary (4:4+ category; 1/16, **Fig. 3.12**, **Cii**) R:L patterns were observed in *Pkd2*$^{S818X/S818X}$ sub-dissected samples. As with the 5:4 R:L pattern presented in section **3.2.3.c**, the 4:6 R:L lobation pattern has not been previously reported; given that it appears to be a mirror-image equivalent, I assign it to the 4:4+ category.

Gross *situs* analysis reveals that sub-dissected *Pkd2*$^{S818X/del}$ embryos displayed normally-patterned cardiac great vessels (2/13, **Table 3.8**), IAA (4/13, **Fig. 3.12**, **Fii**), fused great vessels (2/13, **Fig. 3.12**, **Dii**) and reversed aortic arch (3/13, **Fig. 3.12**, **Eii**). Sub-dissected *Pkd2*$^{S818X/S818X}$ embryos displayed normal great vessels (1/11, **Table 3.8**), reversed aortic arch (7/11, **Fig. 3.13**,

Eiii), fused great vessels (1/11, **Fig. 3.13**, **Ciii**) and other phenotypes (8/11). This category includes transposition of the great vessels shown in **Fig. 3.13**, **Diii**, but also phenotypes such as DORV.

The analysis presented thus far indicates that there are differences between the *Pkd2*^{S818X} and *Pkd2*^{del} alleles. This conclusion is based on *situs* phenotypes observed in determining gross *situs*, as well as incidence of severe oedema and lethality between the *Pkd2*$^{del/del}$, *Pkd2*$^{S818X/del}$ and *Pkd2*$^{S818X/S818X}$ embryos. Whilst the 4:4 phenotype characteristic of *Pkd2*$^{del/del}$ embryos is encountered in *Pkd2*$^{S818X/S818X}$ embryos, both *Pkd2*$^{S818X/del}$ and *Pkd2*$^{S818X/S818X}$ samples display lung lobation patterns not encountered in *Pkd2*$^{del/del}$ samples. Unlike *Pdk2*$^{del/del}$ samples, both *Pkd2*$^{S818X/del}$ and *Pkd2*$^{S818X/S818X}$ embryos display normally-patterned cardiac great vessels. Analysis through µCT of both genotypes will aid in differentiating the *Pkd2*^{S818X} and *Pkd2*^{del} alleles further.

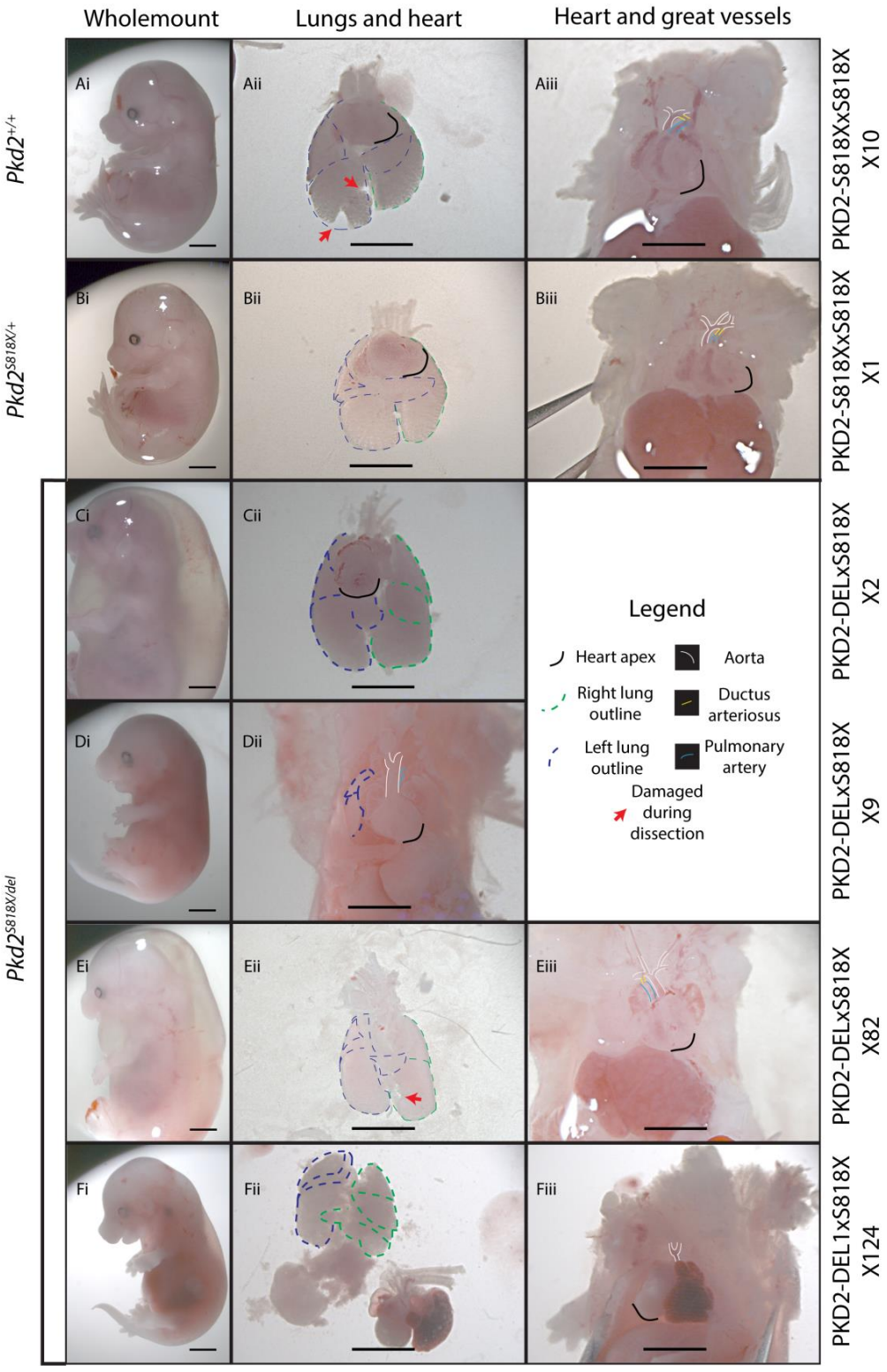


Figure 3.12: Analysis of great vessel and L-R patterning in WT (**A**), *Pkd2*$^{S818X/+}$ (**B**), *Pkd2*$^{S818X/del}$ (**C-F**) embryos. Wholemounts are shown in the first column, lung and heart *situs* are shown in the second column (except for row **D**), whilst great vessel patterning and positioning is shown in the final column (second column for row **D**). Sample IDs are given on the right hand side. Embryos shown in **A** and **B** are derived from a different (PKD2-S818XxS818X) mating. Scale bar: 2 mm. Unannotated figure is shown in **Appendix 1**, **Fig. A1.8**, page 238**.**

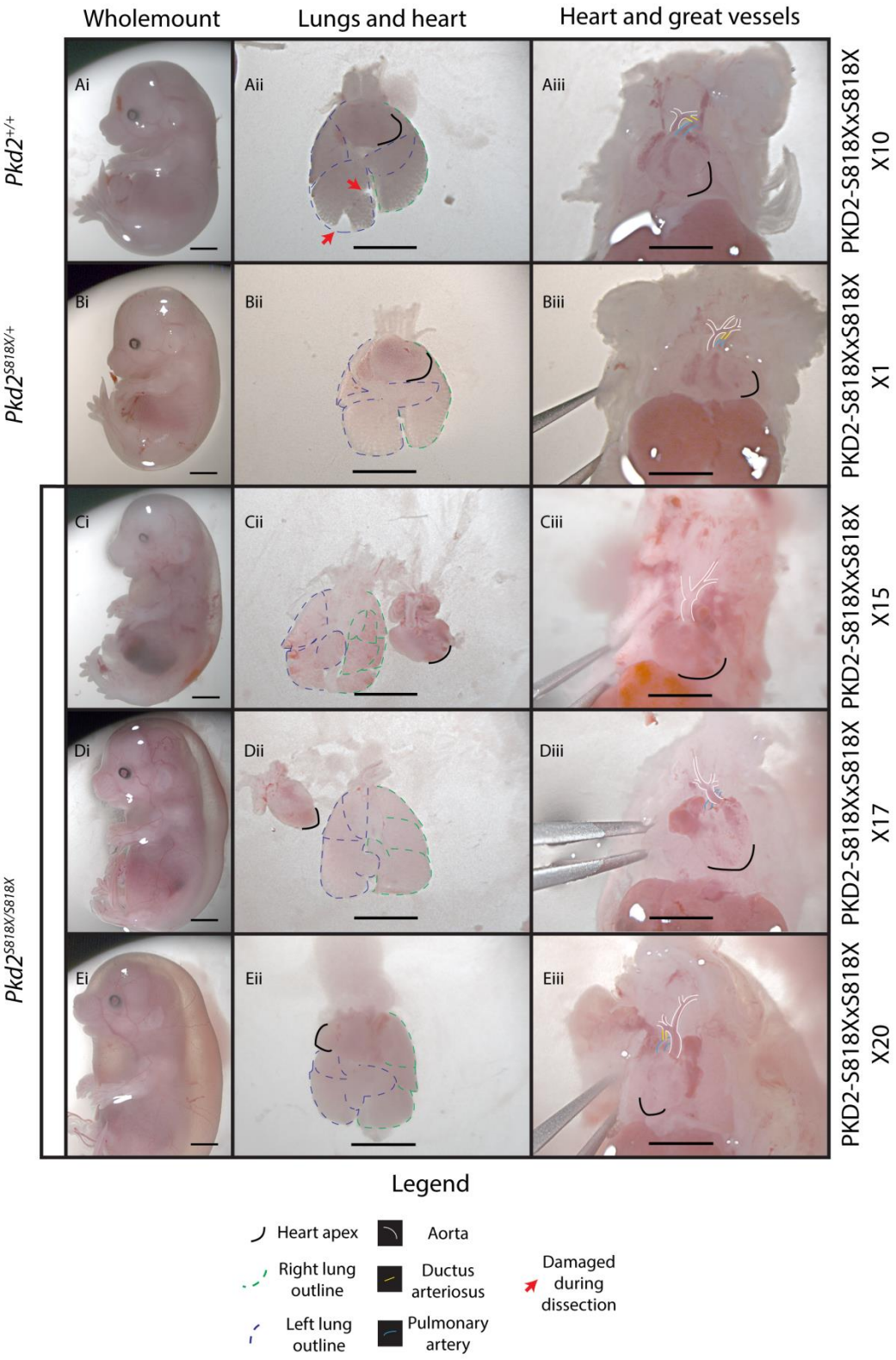


Figure 3.13: Analysis of great vessel and L-R patterning in WT (**A**), *Pkd2*$^{S818X/+}$ (**B**), *Pkd2*$^{S818X/S818X}$ (**C-E**) embryos. Wholemounts are shown in the first column, lung and heart *situs* are shown in the second column, whilst great vessel patterning and positioning is shown in the final column. Sample IDs are given on the right hand side. Scale bar: 2 mm. Unannotated figure is shown in **Appendix 1**, **Fig. A1.9**, page 239**.**

3.2.4.b. Histological sectioning of kidneys

Kidneys were collected and processed as described in section **3.2.2.b**; cysts were assessed in both *Pkd2*$^{S818X/del}$ and *Pkd2*$^{S818X/S818X}$ embryos, alongside WT and *Pkd2*$^{S818X/+}$ samples, as controls. Cysts were not observed in WT (**Fig. 3.14**, **A** and **B**) and heterozygote (*Pkd2*$^{S818X/+}$ shown in **Fig. 3.14**, **C** and **D**, for *Pkd2*$^{del/+}$ see **Fig. 3.6**, **C** and **D**) kidneys. However, all *Pkd2*$^{S818X/del}$ (**Fig. 3.14**, **E** and **F**) and *Pkd2*$^{S818X/S818X}$ kidneys (**Fig. 3.14**, **G** and **H**) were cystic. In terms of renal pathology, the *Pkd2*^{S818X} and *Pkd2*^{del} alleles are indistinguishable, and, as with the *Pkd2*^{fsX7} allele, further work is required to determine whether the *Pkd2*^{S818X} and *Pkd2*^{del} alleles lead to kidney pathologies of different severity (see section **4.2.2**).

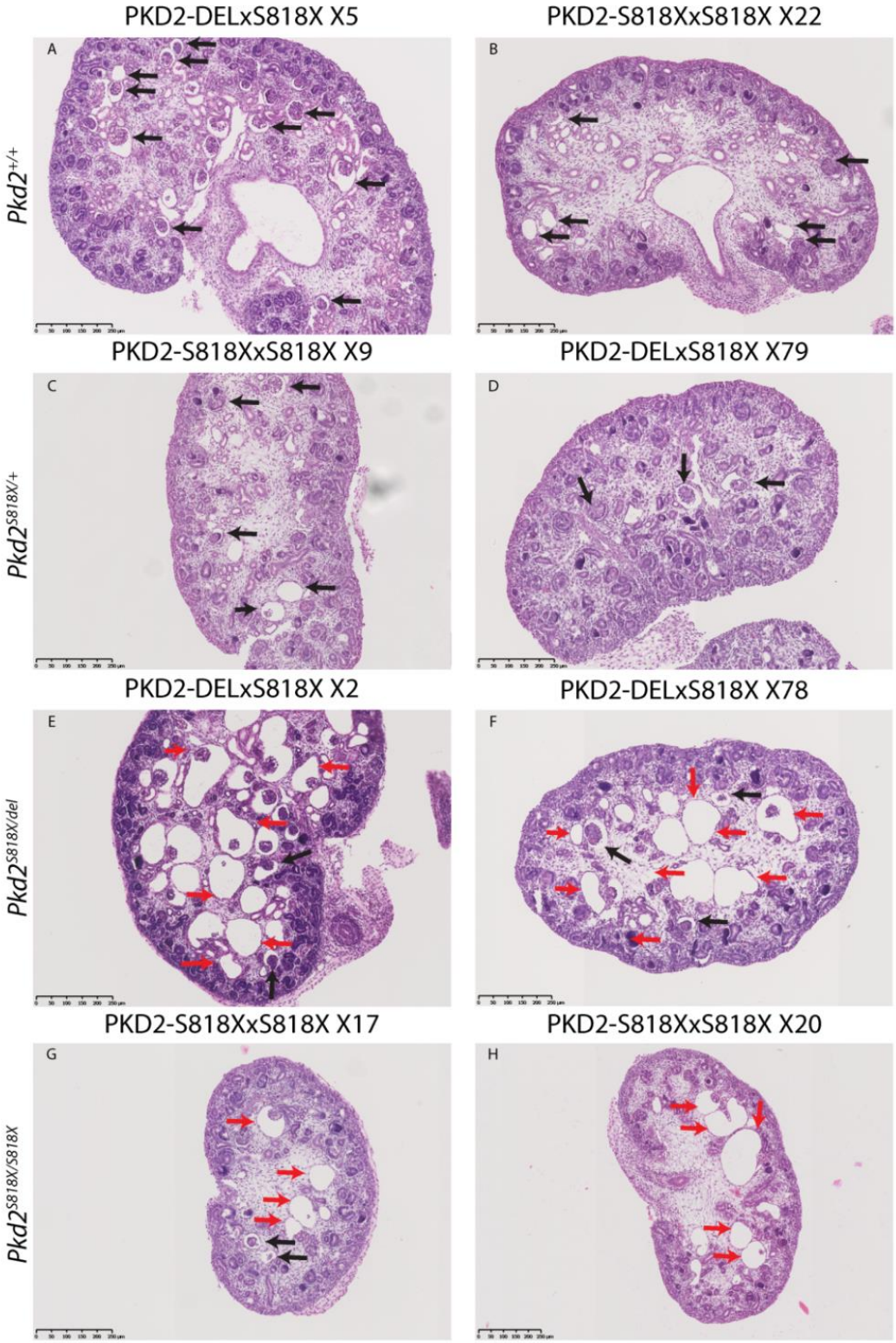


Figure 3.14: Histological sectioning of kidneys from offspring of PKD2-DELxS818X or PKD2-S818XxS818X crosses. WT kidneys are shown in **A-B**, *Pkd2*$^{S818X/+}$ kidneys are shown in **C-D**, *Pkd2*$^{S818X/del}$ kidneys are shown in **E-F**, and *Pkd2*$^{S818X/S818X}$ kidneys are shown in **G-H**. Normal glomeruli are indicated by black arrows, cysts are indicated by red arrows. Sample IDs are given, alongside the matings that produced them, at the top of each image. Scale bar: 250 µm.

3.2.4.c. Phenotypic analysis through µCT

Seven embryos from each genotype, *Pkd2*$^{S818X/del}$ and *Pkd2*$^{S818X/S818X}$, were collected at 15.5-16 dpc and processed as described in section **5.1.3**, in order to perform broad-spectrum phenotypic analysis. Neither WT (**Fig. 3.15**, **Ai**) nor *Pkd2*$^{S818X/+}$ embryos (**Fig. 3.15**, **Bi**) had cystic kidneys, confirming the results from the histological sectioning analysis (**Fig. 3.14**, **A-D**). Both *Pkd2*$^{S818X/del}$ (**Fig. 3.15**, **Ci**, **Di** and **Ei**) and *Pkd2*$^{S818X/S818X}$ embryos (**Fig. 3.17**, **Ci**, **Di** and **Ei**) displayed kidney cysts. As mentioned previously, kidney cysts were less evident in younger animals, closer to 15.5 dpc (see section **3.2.2** and **3.2.3.b**). Pancreatic cysts were also observed in all *Pkd2*$^{S818X/del}$ (**Fig. 3.15**, **Ci**, **Di** and **Ei**) and *Pkd2*$^{S818X/S818X}$ animals (**Fig. 3.17**, **Ci**, **Di** and **Ei**), but not in control embryos. Great vessel patterning and positioning was normal in WT (**Fig. 3.15**, **Ai**) and *Pkd2*$^{S818X/+}$ embryos (**Fig. 3.15**, **Bi**), but a range of abnormal phenotypes was observed in both *Pkd2*$^{S818X/del}$ and *Pkd2*$^{S818X/S818X}$ embryos. Compound heterozygote, *Pkd2*$^{S818X/del}$, embryos displayed normal great vessel patterning (2/13, **Table 3.5**), fusion of the great arteries (2/13, **Fig. 3.15**, **Cii**) and other phenotypes (4/13), including: transposition of the great arteries (**Fig. 3.15**, **Dii**) and DORV (**Fig. 3.15**, **Eii**). *Pkd2*$^{S818X/S818X}$ embryos displayed normal patterning (1/11), IAA (1/11), *situs inversus* (7/11, **Fig. 3.17**, **Cii**, **Dii** and **Eii**), in some samples together with fused, but septated, great vessels (1/11, **Fig. 3.17**, **Dii** and **Eii**; **Fig. 3.23**, **Di** and **Dii**). The fused but septated phenotype means that, from the exterior, the arteries appear to be joined; however, the circulation of the two is separate. Other great vessel phenotypes were also observed in *Pkd2*$^{S818X/S818X}$ embryos (8/11), including transposition of the great arteries (**Table 3.6**). Thymi were also smaller and displaced, compared to WT samples and heterozygous samples, in both *Pkd2*$^{S818X/del}$ (**Fig. 3.15**, **Ciii**, **Diii** and **Eiii**) and *Pkd2*$^{S818X/S818X}$ embryos (**Fig. 3.17**, **Ciii**, **Diii** and **Eiii**). Cleft palate was also seen in *Pkd2*$^{S818X/del}$ embryos (6/7, **Fig. 3.15**, **Civ**, **Div** and **Eiv**), with one sample showing reduced palatal shelf (data not shown); all *Pkd2*$^{S818X/S818X}$ embryos displayed cleft palate (**Fig. 3.17**, **Civ**, **Div** and **Eiv**). This phenotype was not observed in any of the control samples (**Fig. 3.15**, **Aiv** and **Biv**).

A number of nervous system phenotypes were observed in both *Pkd2*$^{S818X/del}$ and *Pkd2*$^{S818X/S818X}$ embryos. Trigeminal ganglia were abnormally-shaped in 6/7 of *Pkd2*$^{S818X/del}$ embryos (**Fig. 3.16**, **Ci**, **Di** and **Ei**) and all *Pkd2*$^{S818X/S818X}$ samples (**Fig. 3.18**, **Ci**, **Di** and **Ei**). The lateral extremities of the fourth ventricle were distended and choroid plexi in the medial part of the fourth ventricle were smaller in all *Pkd2*$^{S818X/del}$ (**Fig. 3.15**, **Cv**, **Dv** and **Ev**) and *Pkd2*$^{S818X/S818X}$ embryos (**Fig. 3.17**, **Cv**, **Dv** and **Ev**). The lateral ventricles were also distended in some embryos of both *Pkd2*$^{S818X/del}$ and *Pkd2*$^{S818X/S818X}$ genotypes (distended: **Fig. 3.15**, **Cv** and **Dv,** normal: **Fig. 3. XVII**, **Dv**); control embryos did not display this phenotype (data not shown).

Atrial abnormalities were also observed in both *Pkd2*$^{S818X/del}$ (6/7) and *Pkd2*$^{S818X/S818X}$ (7/7) embryos. Compound heterozygotes displayed disrupted septation of atria (**Fig. 3.16**, **Ciii**) and abnormal atrio-ventricular connections – R atrium connected to L ventricle or *vice versa* (**Fig. 3.16**, **Diii** and **Eiii**, respectively), whilst *Pkd2*$^{S818X/S818X}$ lacked atrio-ventricular connections (**Fig. 3.18**, **Ciii** and **Eiii**), or had a single atrium (**Fig. 3.18**, **Diii**). When the inferior vena cava was scored to be abnormally positioned, this was also scored as an atrial abnormality, given that normally the right atrium communicates with the inferior vena cava. Heart *situs* was normal (**Fig. 3.16**, **Eii** and **Fig. 3.18**, **Dii**) in 9/18 of *Pkd2*$^{S818X/del}$ embryos and 4/16 of *Pkd2*$^{S818X/S818X}$ embryos, with dextrocardia (**Fig. 3.16**, **Dii** and **Fig. 3.18**, **Cii**) and mesocardia (**Fig. 3.16**, **Cii** and **Fig. 3.18**, **Eii**) being observed in both *Pkd2*$^{S818X/del}$ (5/18 and 4/18, respectively) and *Pkd2*$^{S818X/S818X}$ embryos (10/16 and 2/16, respectively). Lung *situs* was abnormal in *Pkd2*$^{S818X/del}$ embryos, displaying 4:1 (2/17, **Fig. 3.16**, **Div**), 4:4 (5/17, **Fig. 3.16**, **Civ**) and 3:3 R:L lung lobation (1/17, **Fig. 3.16**, **Eiv**). The patterns observed in *Pkd2*$^{S818X/S818X}$ embryos were 1:2 (2/16, **Fig. 3.18**, **Civ**), 4:2 (3/16, **Fig. 3.18**, **Div**) and 4:4 (7/16, **Fig. 3.18**, **Eiv**), but not 4:1. The venous system also showed *situs* abnormalities**;** *Pkd2*$^{S818X/del}$ embryos displayed *situs inversus* for the inferior vena cava (**Fig. 3.16**, **Civ**), duplicated R-sided vena cava (**Fig. 3.16**, **Div**), as well as bilateral inferior vena cava (**Fig. 3XVI, Eiv**), as well as bilateral azygos veins (**Fig. 3.16**, **Div**). *Pkd2*$^{S818X/S818X}$ embryos displayed *situs inversus* for the

inferior vena cava (**Fig. 3.18**, **Civ**) and azygos vein (**Fig. 3.18**, **Eiv**), as well as bilateral inferior vena cava (**Fig. 3.18**, **Eiv**). *Situs* was also assessed for the stomach, spleen and pancreas. *Pkd2*$^{S818X/del}$ embryos showed both normal abdominal organ *situs* (8/17, **Fig. 3.16**, **Dv** and **Ev**), as well as *situs inversus* (9/17, **Fig. 3.16**, **Cv**). Similarly, in *Pkd2*$^{S818X/S818X}$ embryos both normal abdominal *situs* (5/15, **Fig. 3.18**, **Dv**) and *situs inversus* (10/15, **Fig. 3.18**, **Cv** and **Ev**) was observed. In both *Pkd2*$^{S818X/del}$ and *Pkd2*$^{S818X/S818X}$ samples, abnormal liver morphology was encountered even in embryos showing normal *situs*, with livers lacking the caudate lobe (**Fig. 3.16**, **Dv**, **Ev** and **Fig. 3.18**, **Dv**). This indicates that the development of the caudate lobe may only be conditioned by *situs* establishment, but there may be a localised function of *Pkd2* required for the development of the caudate lobe. The abnormal phenotypes observed for *Pkd2*$^{S818X/del}$ and *Pkd2*$^{S818X/S818X}$ embryos are summarised in **Table 3.5** and **Table 3.6**, respectively; full phenotypic analysis data is given in **Appendix 2**, **Table A2.4** and **Table A2.5**, respectively.

The data presented thus far shows differences between the *Pkd2*^{del} and *Pkd2*^{S818X} alleles. The differences reflect the severity of genotypes presented, with *Pkd2*$^{del/del}$ showing the highest incidence of lethality (55.56%, 20/36 embryos), followed by *Pkd2*$^{S818X/del}$ (48.57%, 17/35 embryos) and then *Pkd2*$^{S818X/S818X}$ (36%, 9/25 embryos). The *situs* phenotypes also varied between the three genotypes, with each organ system presenting incidences of particular phenotypes at different frequencies (in between the genotypes). These findings suggest that *Pkd2*^{S818X} is not equivalent to the null allele, *Pkd2*^{del}, but is also different from *Pkd2*^{fsX7}. The data presented in this section invalidates my initial hypothesis with regards to the *Pkd2*^{S818X} allele, as embryos that are homozygous for this allele produce both L-R and kidney cyst phenotypes. However, the presence of both L-R and kidney phenotypes, in the context of the hypothesis described at the end of **Chapter 2**, may be explained by a potential requirement of the CC for PKD2 function in L-R development, but not for interaction with PKD1L1 (see section **4.1.3**).

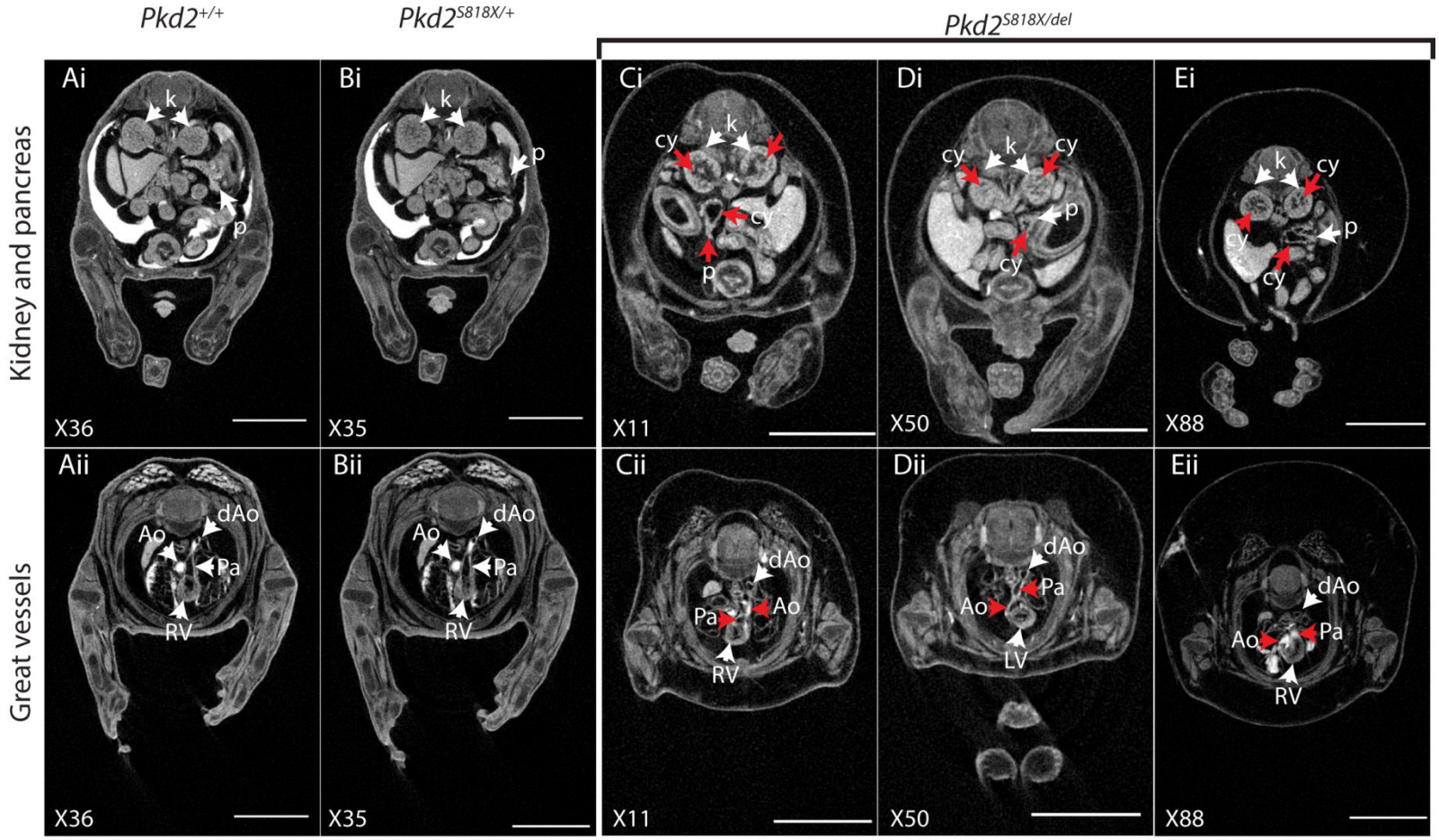


Figure 3.15: µCT sections of WT (**A**), *Pkd2*$^{S818X/+}$ (**B**) and *Pkd2*$^{S818X/del}$ (**C**-**E**) 15.5 dpc embryos, showing most-commonly encountered phenotypes. White arrows: normal phenotypes; red arrows: abnormal phenotypes. Abbreviations (in alphabetical order): Ao – aorta; chp – choroid plexus; cp – cleft palate; cy – cyst; dAo – descending aorta; k – kidney; lav – lateral ventricles; lefv – left extremity of the fourth ventricle; LV – left ventricle; nc – nasal cavity; p – pancreas; Pa – pulmonary artery; RV – right ventricle; sp – soft palate; thy – thymus; to – tongue. Sample IDs are shown bottom left of each section. Scale bar: 2 mm. Unannotated figure is shown in **Appendix 1**, **Fig. A1.10**, pages 240-241.

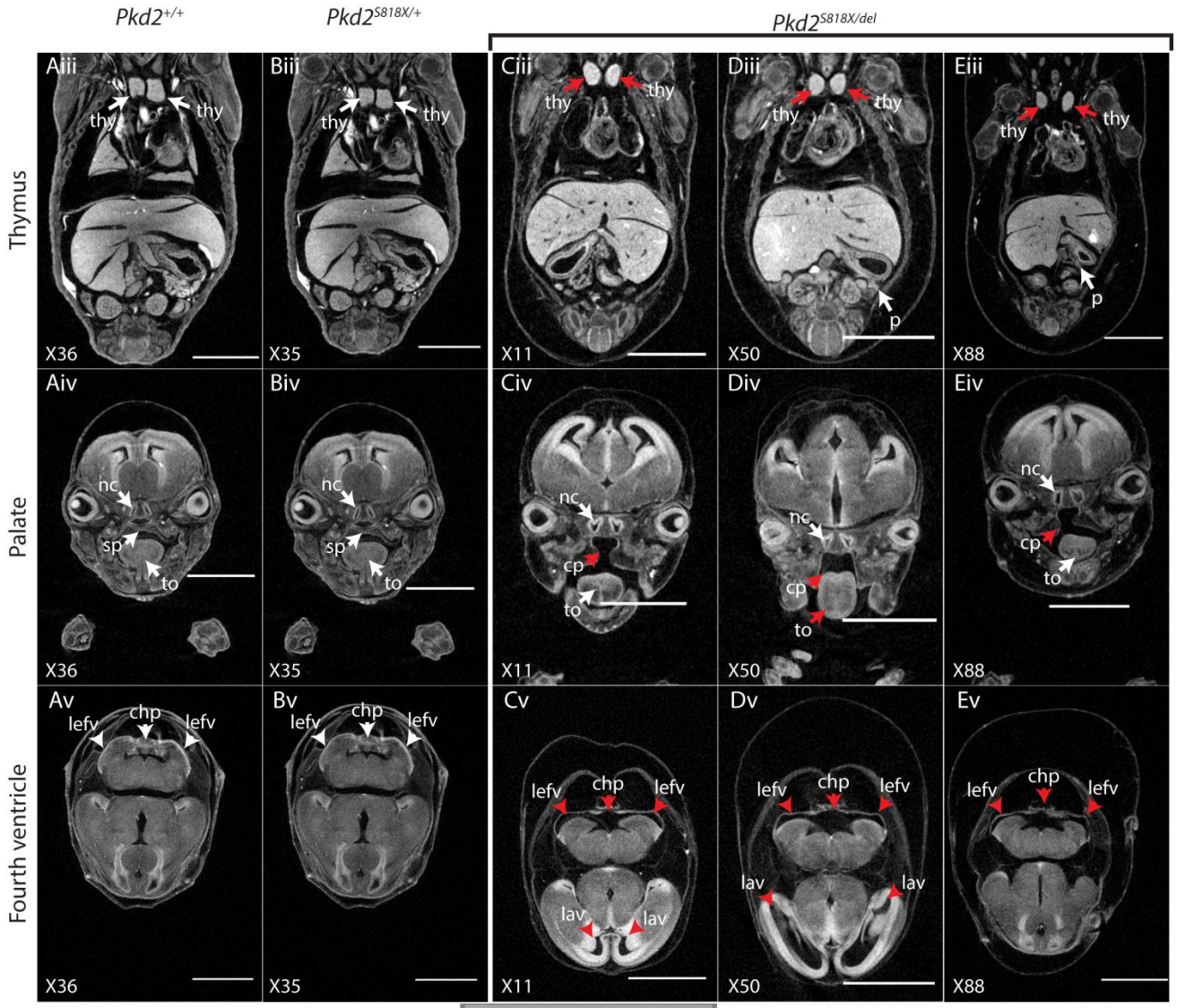


Figure 3.15 (continued)

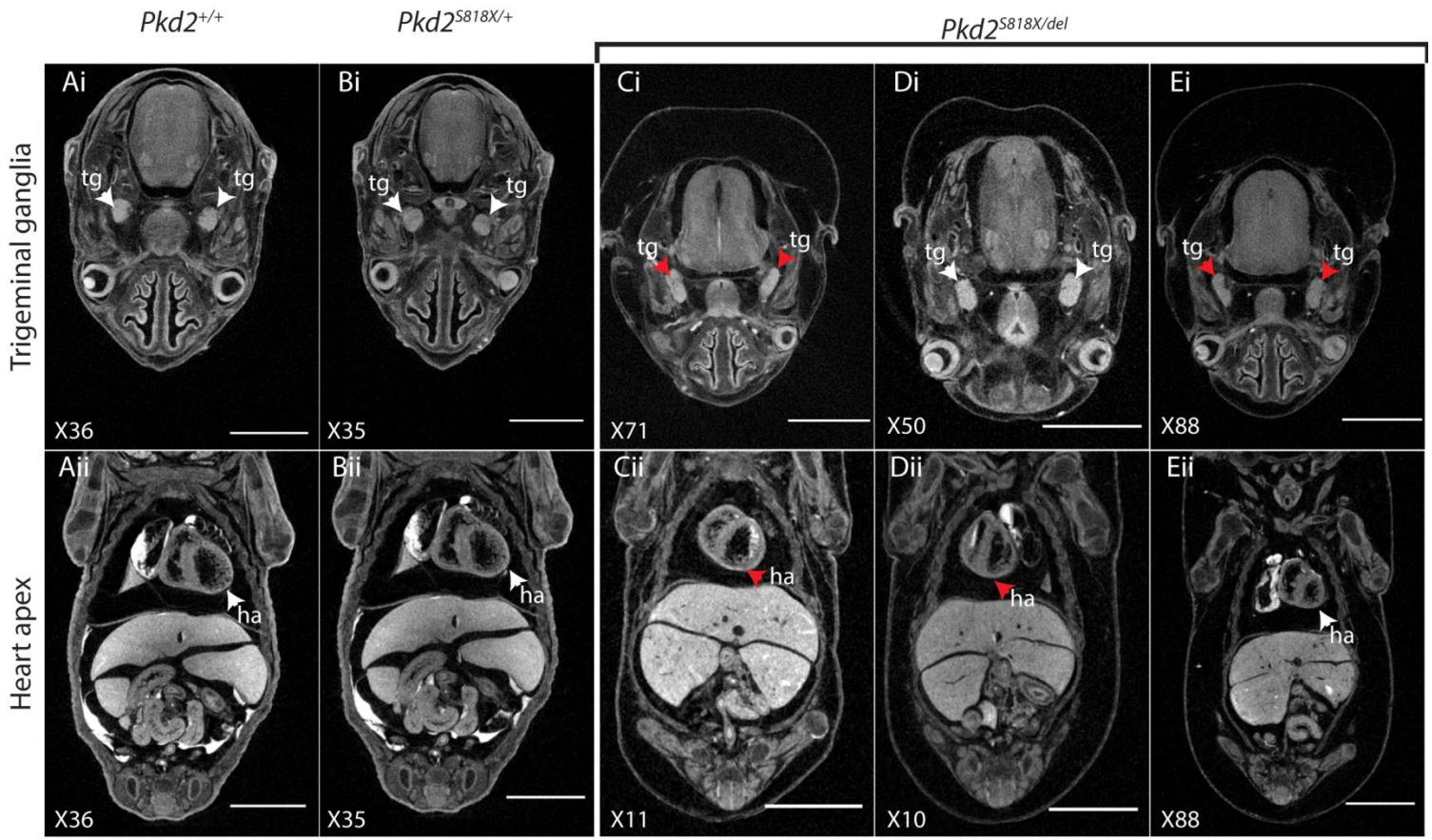


Figure 3.16: µCT sections of WT (**A**), *Pkd2*$^{S818X/+}$ (**B**) and *Pkd2*$^{S818X/del}$ (**C**-**E**) 15.5 dpc embryos, showing phenotypes with variable presentation or penetrance. White arrows: normal phenotypes; red arrows: abnormal phenotypes. Abbreviations (in alphabetical order): al – accessory lobe; av – azygos vein; cal – caudal lobe; cl – cranial lobe; ha – heart apex; ivc – inferior vena cava; lat – left atrium; lll – left lateral lobe; lml – left medial lobe; LV – left ventricle; ml – medial lobe; p – pancreas; pp – papillary process; rat – right atrium; rll – right lateral lobe; rml – right medial lobe; RV – right ventricle; sl – single lobe; spl – spleen; st – stomach; tg – trigeminal ganglion. Sample IDs are shown bottom left of each section. Scale bar: 2 mm. Unannotated figure is shown in **Appendix 1**, **Fig. A1.11**, pages 242-243.

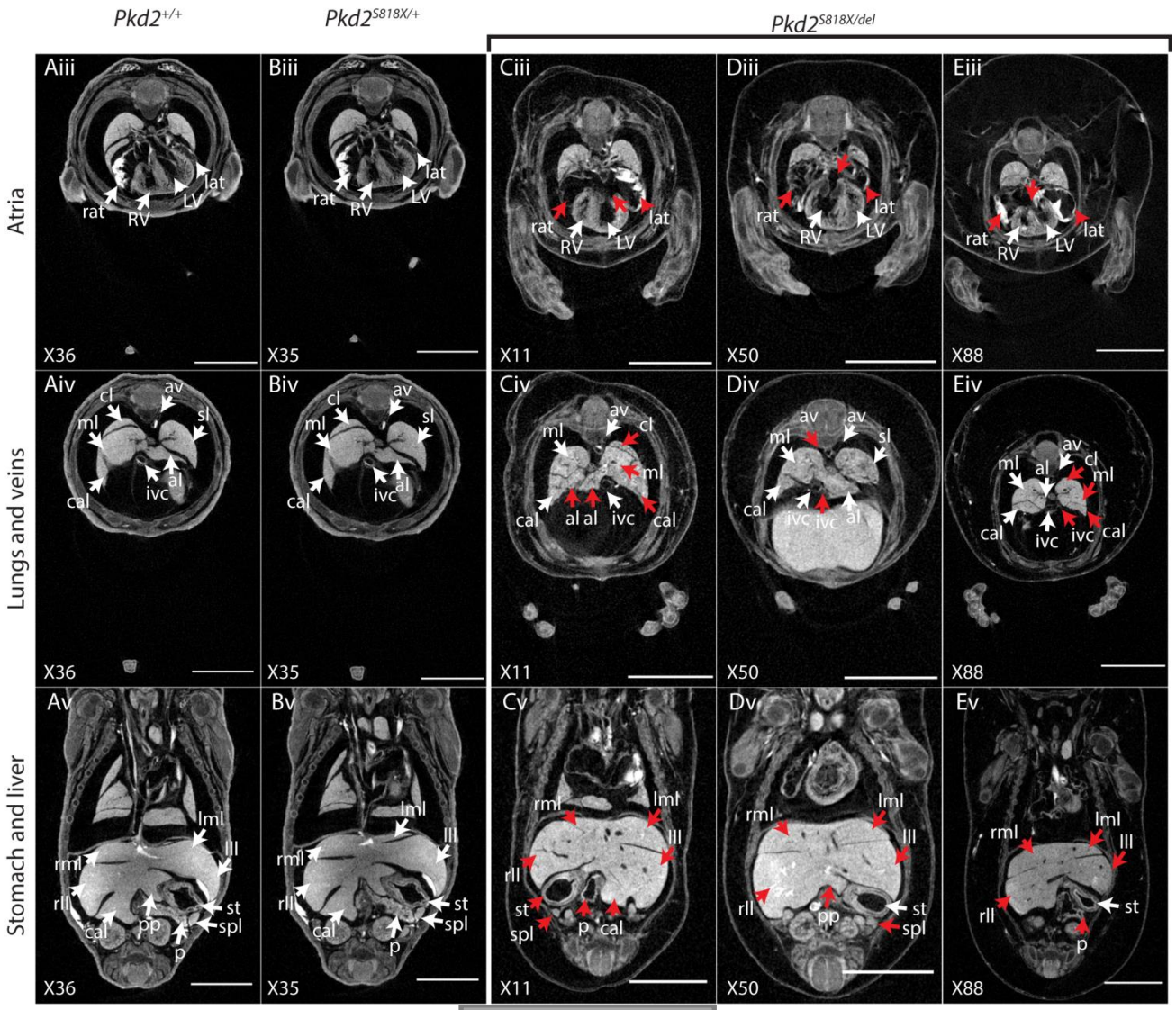


Figure 3.16 (continued)

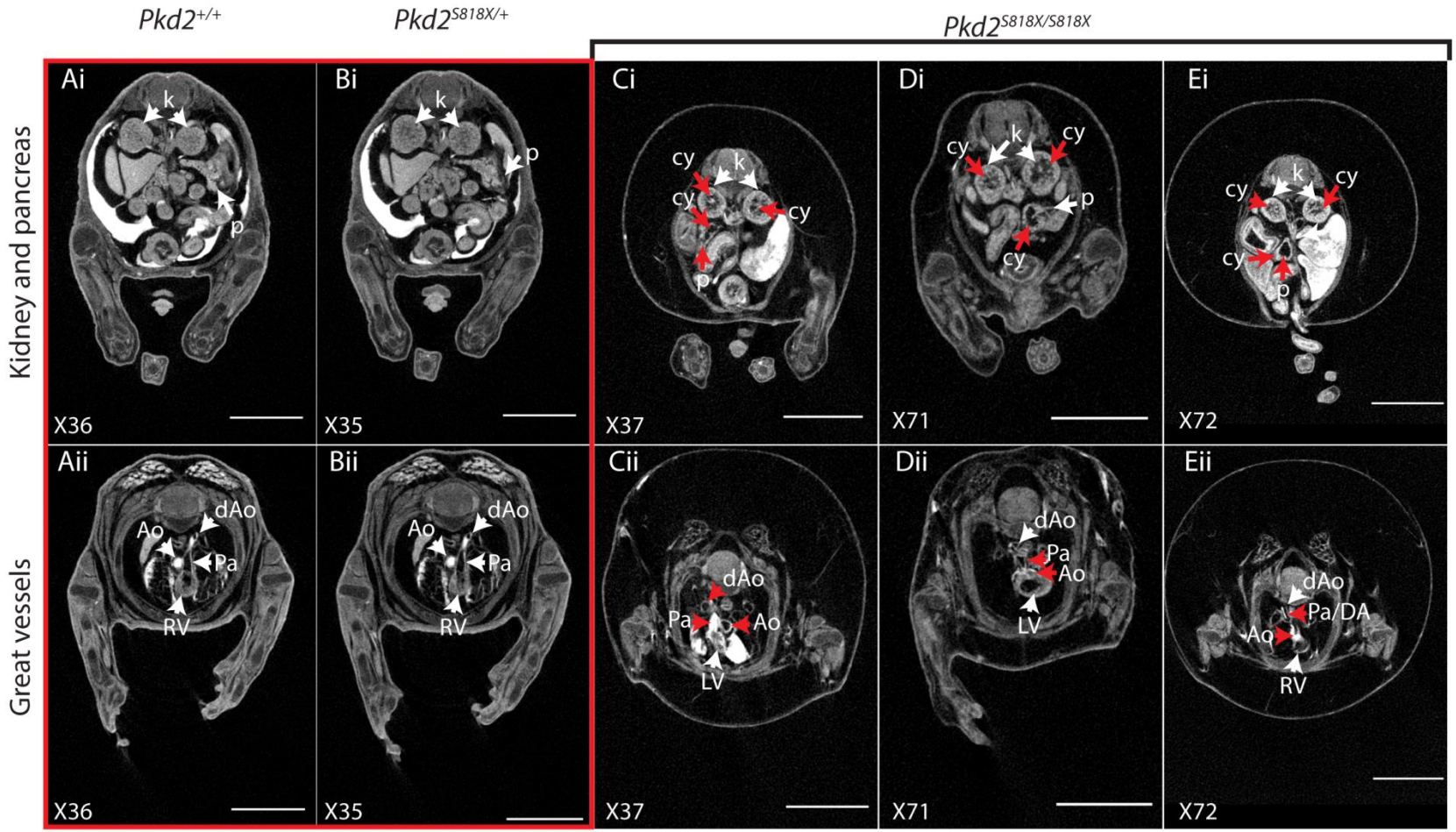


Figure 3.17: µCT sections of WT (**A**), *Pkd2*$^{S818X/+}$ (**B**) and *Pkd2*$^{S818X/S818X}$ (**C**-**E**) 15.5 dpc embryos, showing most-commonly encountered phenotypes. White arrows: normal phenotypes; red arrows: abnormal phenotypes. Abbreviations (in alphabetical order): Ao – aorta; chp – choroid plexus; cp – cleft palate; cy – cyst; dAo – descending aorta; k – kidney; lav – lateral ventricles; lefv – left extremity of the fourth ventricle; LV – left ventricle; nc – nasal cavity; p – pancreas; Pa – pulmonary artery; RV – right ventricle; sp – soft palate; thy – thymus; to – tongue. Sample IDs are shown bottom left of each section. Samples highlighted in red are from a PKD2-DELxS818X cross. Scale bar: 2 mm. Unannotated figure is shown in **Appendix 1**, **Fig. A1.12**, pages 244-245.

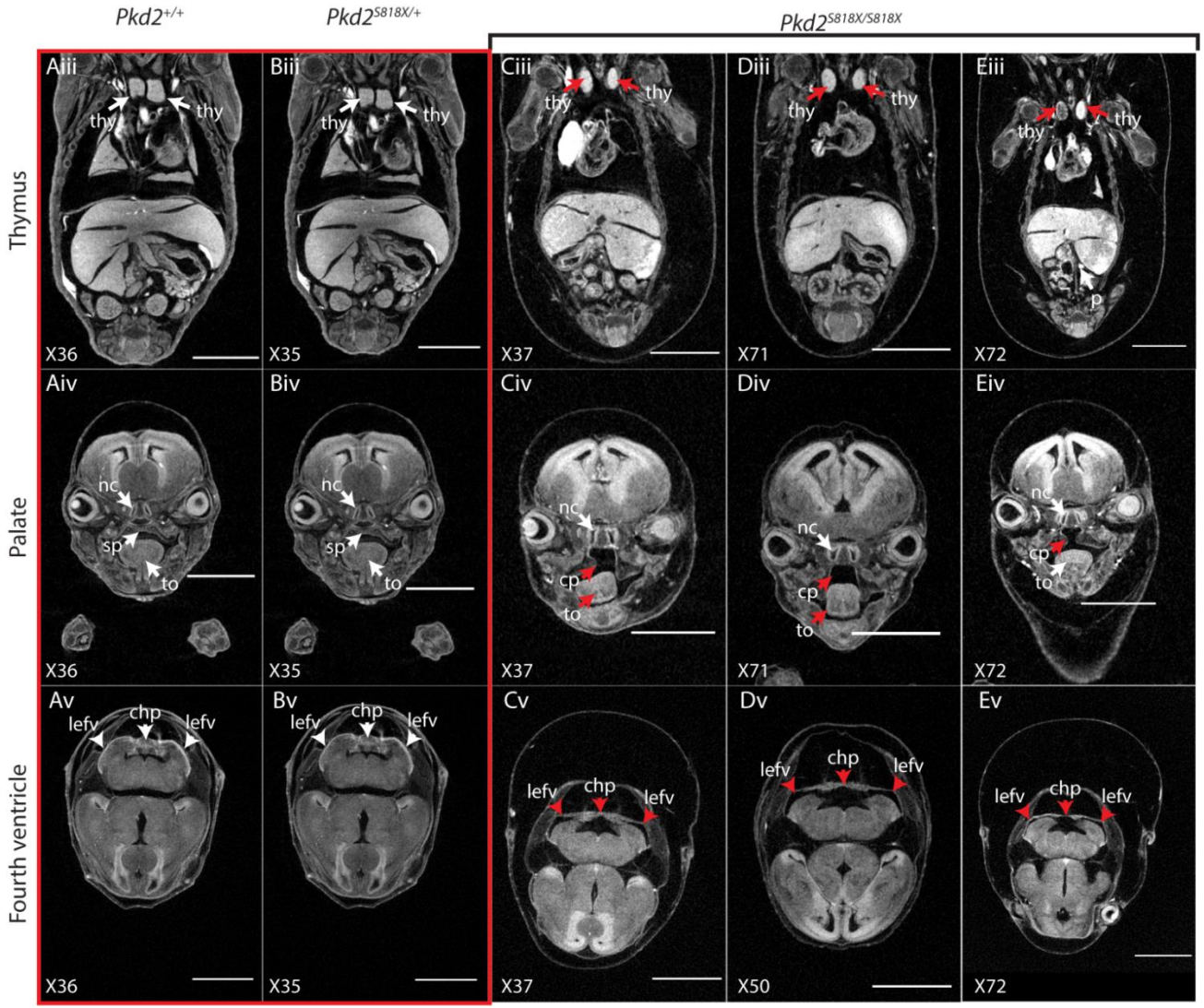


Figure 3.17 (continued)

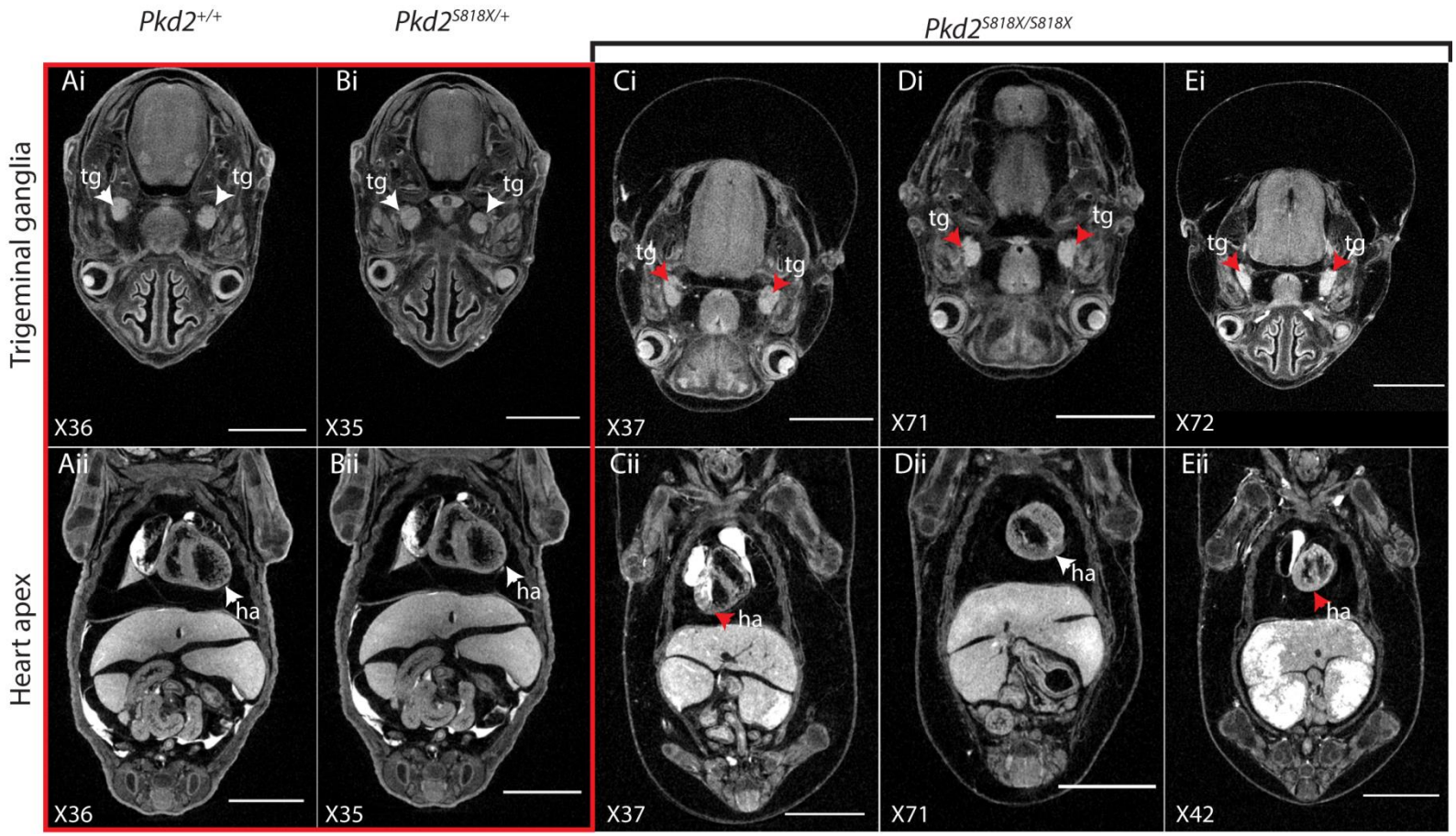


Figure 3.18: µCT sections of WT (**A**), *Pkd2*$^{S818X/+}$ (**B**) and *Pkd2*$^{S818X/S818X}$ (**C**-**E**) 15.5 dpc embryos, showing phenotypes with variable presentation or penetrance. White arrows: normal phenotypes; red arrows: abnormal phenotypes. Abbreviations (in alphabetical order): al – accessory lobe; av – azygos vein; cal – caudal lobe; cl – cranial lobe; ha – heart apex; ivc – inferior vena cava; lat – left atrium; lll – left lateral lobe; lml – left medial lobe; LV – left ventricle; ml – medial lobe; p – pancreas; pp – papillary process; rat – right atrium; rll – right lateral lobe; rml – right medial lobe; RV – right ventricle; sl – single lobe; spl – spleen; st – stomach; tg – trigeminal ganglion. Sample IDs are shown bottom left of each section. Scale bar: 2 mm. Unannotated figure is shown in **Appendix 1**, **Fix. A1.13**, pages 246-247.

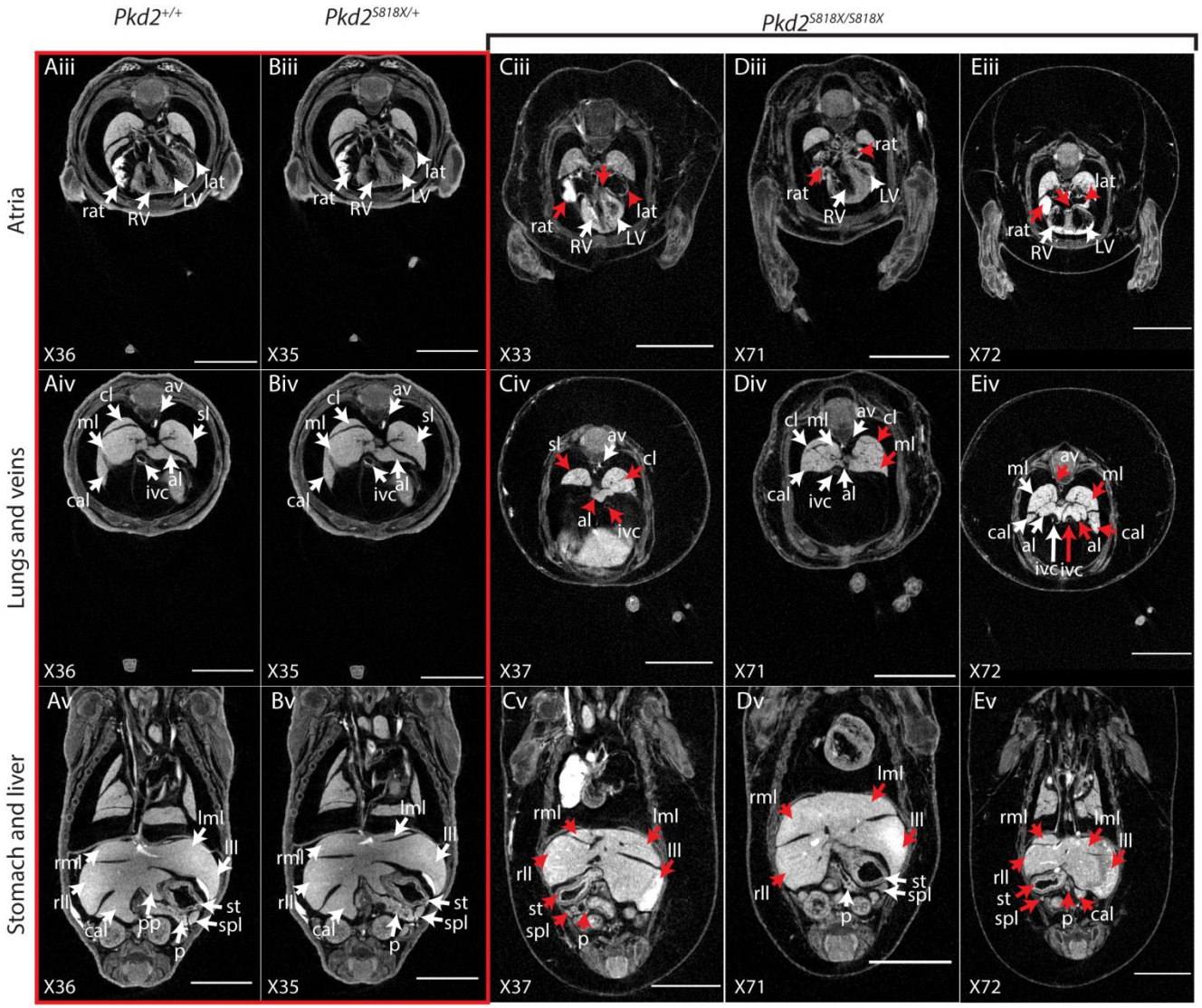


Figure 3.18 (continued)

Table 3.5: Heatmap summary of phenotypes observed in µCT-analysed *Pkd2*$^{S818X/del}$ embryos

Phenotype	PKD2-DELxS818X sample						
	X10	X11	X17	X50	X71	X88	X138
Nervous System							
• Midbrain							
• Mesencephalic vesicle							
• 3rd Ventricle							
• Lateral vesicles							
• Cerebellum							
• CP (in medial 4th ventricle)							
• Lateral extremity of 4th ventricle							
• TG							
• Olfactory lobe							
• Emerging cervical spinal chord							
Cranial							
• Soft palate							
• Submandibular gland							
• C6 vertebra and DRG							
Thoracic							
• Thymus							
• Venous system							
• Ductus arteriosus							
• Lungs	**4:4**	**4:4**			**4:3**	**3:3**	**4:2**
• Aorta							
• Heart apex	**D**	**M**	**M**	**M**			
• Atria							
• Ventricles							
• IVS							
Abdominal							
• Peritoneal cavity							
• Adrenal glands							
• Kidneys	**C**	**C**	**C**	**C**	**C**	**C**	**C**
• Liver lobes							
• Stomach position		**SI**	**SI**				
• Spleen		**SI**	**SI**				
• Pancreas	**C**	**C SI**	**C SI**	**C**	**C**	**C**	**C**
• Ovaries	-			-		-	-
• Testes	**C**	-	-	**C**	-	**C**	**C**
Oedema							
Brown fat							
Spinal shape							

Gray cells represent normal phenotypes, red cells represent abnormal phenotypes. Abbreviations: C – cystic; CP – choroid plexus; D – dextrocardia; DRG – dorsal root ganglia; IVS – interventricular septum; M – mesocardia; SI – *situs inversus*; TG – trigeminal ganglia. Lung lobations are given R:L and are shown only where the lobation is abnormal.

Table 3.6: Heatmap summary of phenotypes observed in µCT-analysed *Pkd2*$^{S818X/S818X}$ embryos

Phenotype	PKD2-S818XxS818X sample						
	X33	X37	X42	X58	X62	X71	X72
Nervous System							
• Midbrain							
• Mesencephalic vesicle							
• 3rd Ventricle							
• Lateral vesicles							
• Cerebellum							
• CP (in medial 4th ventricle)							
• Lateral extremity of 4th ventricle							
• TG							
• Olfactory lobe							
• Emerging cervical spinal chord							
Cranial							
• Soft palate							
• Submandibular gland							
• C6 vertebra and DRG							
Thoracic							
• Thymus							
• Venous system							
• Ductus arteriosus		SI					SI
• Lungs	4:4	1:2	4:4	1:2	4:4	4:2	4:4
• Aorta		SI		SI		SI	SI
• Heart apex	M	D	M	D	D		D
• Atria							
• Ventricles							
• IVS							
Abdominal							
• Peritoneal cavity							
• Adrenal glands							
• Kidneys	C	C	C	C	C	C	C
• Liver lobes							SI
• Stomach position	SI	SI		SI	SI		SI
• Spleen				SI	SI		SI
• Pancreas	C SI	C SI	C	C SI	C SI	C	C SI
• Ovaries		-	-	-	-		-
• Testes	-	C	C	C	C	-	C
Oedema							
Brown fat							
Spinal shape							

Gray cells represent normal phenotypes, red cells represent abnormal phenotypes. Abbreviations: C – cystic; CP – choroid plexus; D – dextrocardia; DRG – dorsal root ganglia; IVS – interventricular septum; M – mesocardia; SI – *situs inversus*; TG – trigeminal ganglia. Lung lobations are given R:L and are shown only where the lobation is abnormal.

3.2.5. Phenotypic analysis of *Pkd2*$^{R870X/R870X}$ embryos at 15.5 dpc

The *Pkd2*^{R870X} allele contains a nonsense mutation, leading to early truncation of PKD2 downstream of the homo-oligomerization sub-region of the CC (**Fig. 3.1**, **B**). Given that this allele likely has a similar effect on protein architecture as the *Pkd2*^{fsX7} allele (see section **3.2.3**), i.e. truncation of the hetero-oligomerization sub-region of the CC, I hypothesised that this allele would produce the same phenotypes as *Pkd2*$^{fsX7/fsX7}$. Specifically, I hypothesised that *Pkd2*$^{R870X/R870X}$ embryos would display kidney cysts, but not L-R phenotypes. Unlike the analyses performed in previous sections, I only analysed *Pkd2*$^{R870X/R870X}$, but not *Pkd2*$^{R870X/del}$ embryos, due to the presumed similarity between the *Pkd2*^{R870X} and *Pkd2*^{fsX7} alleles, in terms of effect on the protein. In addition to this, due to time constraints, fewer homozygous samples were analysed, as compared to the analysis performed for other genotypes.

3.2.5.a. Gross *situs* analysis

Embryos were collected at 15.5-16 dpc to assess for presence of oedema; following this, embryos were sub-dissected for gross *situs* analysis. Neither WT (data not shown, WT from different cross included in **Fig. 3.19**, **Ai**), nor *Pkd2*$^{R870X/+}$ embryos displayed any oedema (**Fig. 3.19**, **Bi**); control embryos also had normal *situs* for the lungs (**Fig. 3.19**, **Aii** and **Bii**, respectively), heart and great vessels (**Fig. 3.19**, **Aiii** and **Biii**, respectively), as well as stomach and spleen (data not shown). In contrast to control embryos, all eight *Pkd2*$^{R870X/R870X}$ embryos analysed (including those used for μCT) displayed severe oedema (**Fig. 3.19**, **Ci** and **Ei**). Lethality up to the point of dissection was also seen in 12/19 embryos (**Fig. 3.19**, **Di** and **Ei**). Ten *Pkd2*$^{R870X/R870X}$ embryos were collected for sub-dissection and gross *situs* analysis; however, considering that some of the samples were dead at the point of dissection, some organs could not be assessed. Homozygotes had either normal heart *situs* (6/16, data not shown) or dextrocardia (6/16, **Fig. 3.19**, **Cii** and **Dii**). Lung lobation patterns were abnormal in all homozygote embryos analysed, showing 4:3 (7/16,

Fig. 3.19, **Cii** and **Dii**), 1:2 (1/16, **Fig. 3.19**, **Eii**), 2:4 (1/16, **Table 3.8**) and 4+:4 (3/16, **Table 3.8**) R:L. Heart great vessels were either normal (4/9, data not shown) in *Pkd2*$^{R870X/R870X}$, or the homozygote embryos displayed *situs inversus* for the aorta and aortic arch (3/9, **Fig. 3.19**, **Ciii**).

Given that lung situs is either randomised, or R-isomeric and R-supernumerary, *Pkd2*^{R870X} exhibits different phenotypes to both *Pkd2*^{del} and *Pkd2*^{fsX7}. The incidence of lethality suggests that the phenotypes produced by *Pkd2*^{R870X} are more severe than those observed in *Pkd2*$^{del/del}$ embryos. The μCT analysis will help further characterise this allele.

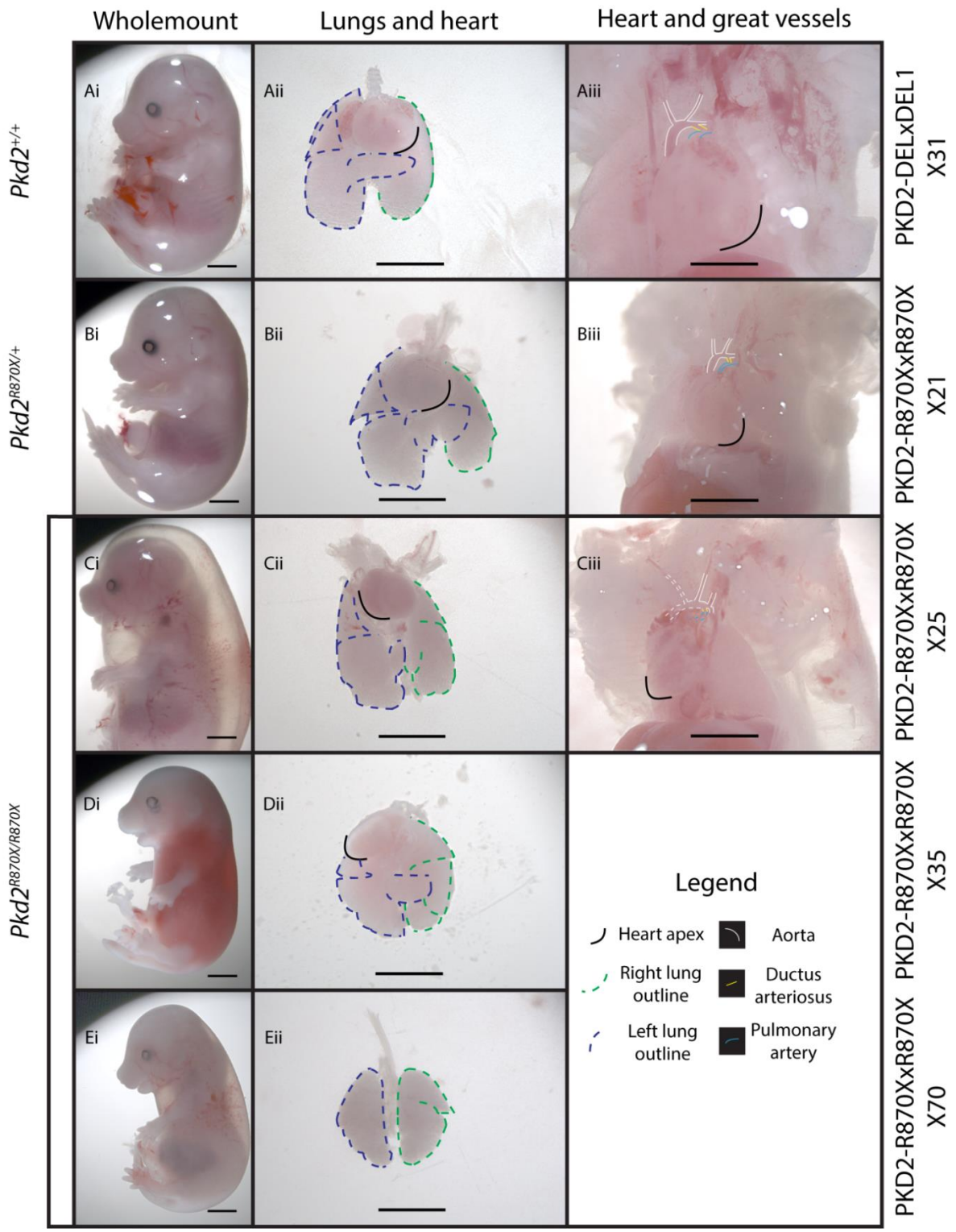


Figure 3.19: Analysis of great vessel and L-R patterning in WT (**A**), *Pkd2*$^{R870X/+}$ (**B**), *Pkd2*$^{R870X/R870X}$ (**C-E**) embryos. Wholemounts are shown in the first column, lung and heart *situs* are shown in the second column, whilst great vessel patterning and positioning is shown in the final column. Sample IDs are given on the right hand side. The WT sample, shown for reference, is derived from a PKD2-DELxDEL1 mating. Scale bar: 2 mm. Unannotated figure is shown in **Appendix 1**, **Fig. A1.14**, page 248**.**

3.2.5.b. Histological sectioning of kidneys

As for previous alleles, kidney phenotypes were assessed by histological sectioning, as described in section **3.2.2.b**. Neither WT nor *Pkd2*$^{R870X/+}$ showed cystic kidneys (**Fig. 3.20**, **A** and **B**). In contrast, cysts were observed in *Pkd2*$^{R870X/R870X}$ kidneys (**Fig. 3.20**, **C**). Due to time constraints, only two homozygote samples were analysed by sectioning, one of which had underdeveloped kidneys; these samples had not developed glomeruli and therefore could not have cysts, as they lacked the structures in which cysts initiate. However, μCT analysis of *Pkd2*$^{R870X/R870X}$ embryos confirmed that this genotype produced kidney cysts in all samples analysed (*vide infra*). This indicates that, with respect to renal pathology, the *Pkd2*^{R870X} allele is similar to the *Pkd2*^{del}, as well as *Pkd2*^{fsX7} and *Pkd2*^{S818X}. As with previous alleles, further work is required to differentiate all of these alleles; this is detailed in section **4.2.2**.

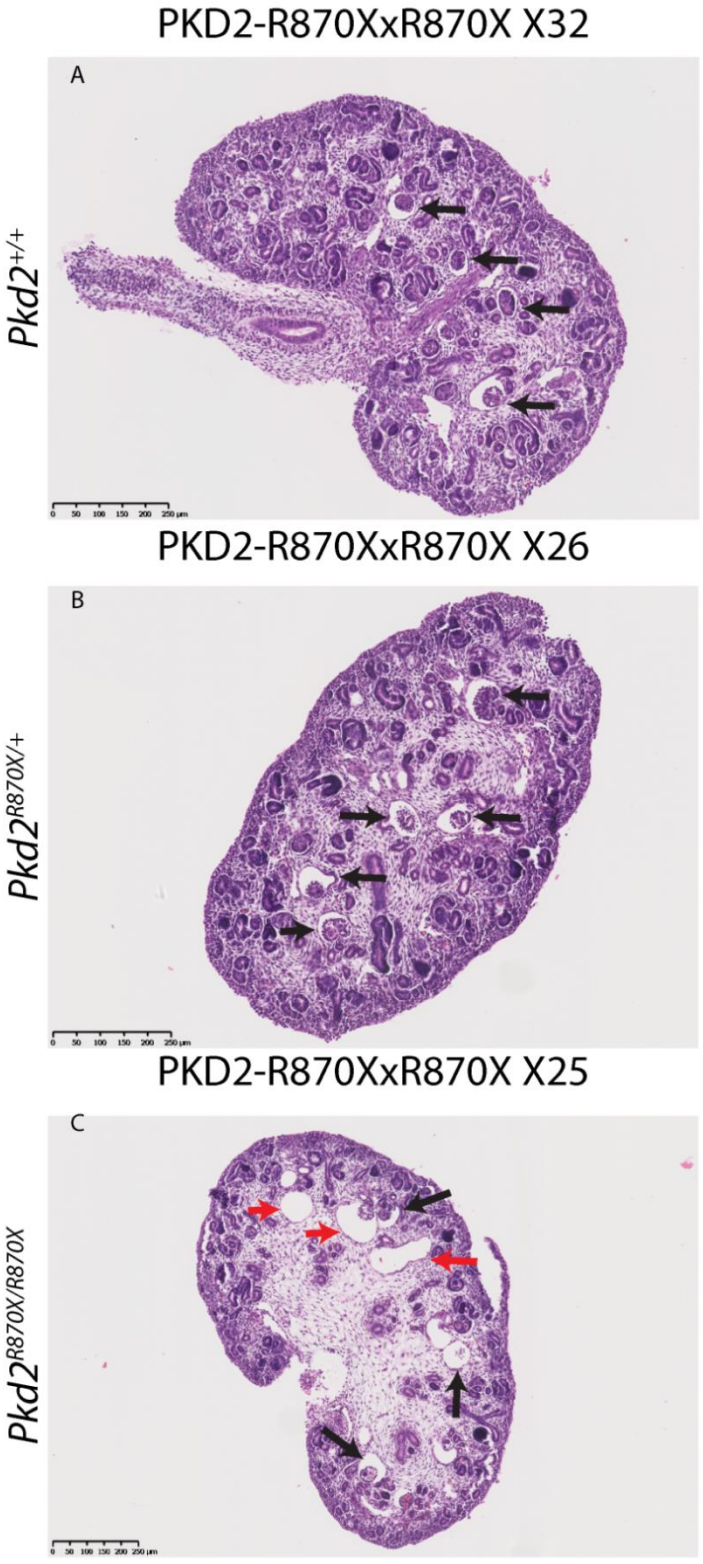


Figure 3.20: Histological sectioning of kidneys from offspring of PKD2-R870XxR870X crosses. WT kidneys are shown in **A**, *Pkd2*$^{R870X/+}$ kidneys are shown in **B**, *Pkd2*$^{R870X/R870X}$ kidneys are shown in **C**. Normal glomeruli are indicated by black arrows, cysts are indicated by red arrows. Sample IDs are given, alongside the matings that produced them, at the top of each image. Scale bar: 250 µm.

3.2.5.c. Phenotypic analysis through µCT

Embryos were collected at 15.5-16 dpc, processed as described in section **5.1.3** and analysed by µCT. Neither WT nor *Pkd2*$^{R870X/+}$ embryos displayed cystic kidneys or pancreas (**Fig. 3.21**, **Ai** and **Bi**). In contrast, all six *Pkd2*$^{R870X/R870X}$ embryos analysed displayed both pancreatic and kidney cysts (**Fig. 3.21**, **Ci**, **Di** and **Ei**). As described previously, kidney cysts were less evident in younger samples (see section **3.2.2**). Great vessel patterning was normal in control embryos (**Fig. 3.21**, **Aii** and **Bii**), as well as a proportion of *Pkd2*$^{R870X/R870X}$ embryos (4/9, **Fig. 3.21**, **Eii**). Homozygote embryos displayed *situs inversus* of the aorta and aortic arch (3/9, **Fig. 3.21**, **Cii**), IAA (1/9, data not shown) or other outflow tract phenotypes (2/9, **Fig. 3.21**, **Cii** and **Dii**), such as transposition with fused, but septated, great arteries (**Fig. 3.21**, **Dii**). The thymi of homozygotes were smaller and displaced in all samples analysed (**Fig. 3.21**, **Ciii**, **Diii** and **Eiii**), a phenotype not observed in WT or heteroygote samples (**Fig. 3.21**, **Aiii** and **Biii**). Cleft palate was observed in all *Pkd2*$^{R870X/R870X}$ samples (**Fig. 3.21**, **Civ**, **Div** and **Eiv**), but not control samples (**Fig. 3.21**, **Aiv** and **Biv**).

No abnormal nervous system phenotypes were observed in any of the control embryos; however, *Pkd2*$^{R870X/R870X}$ embryos displayed a number of abnormalities. The lateral extremity of the fourth ventricle was distended in all homozygote samples (**Fig. 3.21**, **Cv**, **Dv** and **Ev**). The choroid plexi of the medial part of the fourth ventricle were smaller in all the *Pkd2*$^{R870X/R870X}$ samples assessed (**Fig. 3.21**, **Cv**, **Dv** and **Ev**). Trigeminal ganglia were also abnormally shaped in all homozygote samples (**Fig. 3.22**, **Ci**, **Di** and **Ei**). Other nervous system phenotypes observed in *Pkd2*$^{R870X/R870X}$ embryos included abnormal olfactory lobe interlobular space (data not shown) and distended subarachnoid space in the thoracic region (data not shown).

The positioning of the heart was abnormal in *Pkd2*$^{R870X/R870X}$ embryos, but not controls: 4/16 of the homozygote samples had mesocardia (**Fig. 3.22**, **Cii**), 6/16 displayed dextrocardia (**Fig.**

3.22, **Dii**) and 6/16 had levocardia (**Fig. 3.22**, **Eii**). The IVS was interrupted in 4/6 homozygotes (**Fig. 3.22**, **Diii** and **Eiii**) and normal in 2/6 (**Fig. 3.22**, **Ciii**). Atrial abnormalities were also recorded in 5/6 homozygotes (data not shown): abnormal atrioventricular connections, or abnormal atrial-venous connections (drainage of L atrium into a second, abnormally placed, inferior vena cava). Similarly, the venous system displayed abnormal *situs* in 5/6 $Pkd2^{R870X/R870X}$ samples. One sample displayed *situs inversus* for the azygos vein, but normal inferior vena cava (**Fig. 3.22**, **Eiv**), another sample displayed bilateral inferior vena cava only (**Fig. 3.22**, **Div**), whilst a third showed *situs inversus* for the inferior vena cava only (**Fig. 3.22, Civ**); a R-sided duplication of the normal, R-sided, inferior vena cava was also observed in another embryo (**Table A2.6**), as well as a L-sided duplication of a L-sided inferior vena cava, in a different embryo (**Table A2.6**). Lung lobation was abnormal in all homozygote samples**,** showing 3:2 (1/16, **Fig. 3.22**, **Div**), 3:4 (1/16, **Fig. 3.22**, **Civ**) or R-isomeric and R-supernumerary lobation (referred to as 4+:4, 3/16, **Fig. 3.22**, **Eiv**). Stomach, spleen and liver *situs* was either normal (8/16, **Fig. 3.22, Ev**) or inverted (8/16, **Fig. 3.22**, **Cv** and **Dv**). As in the case of the $Pkd2^{S818X}$ allele, the caudate lobe of the liver was missing in samples that showed both normal *situs* and *situs inversus* (see section **3.2.4.b**). The abnormal phenotypes observed for $Pkd2^{R870X/R870X}$ embryos are summarised in **Table 3.7**; full phenotypic analysis data is given in **Appendix 2**, **Table A2.6**. A 3D reconstruction of cardiac great vessel phenotypes observed in $Pkd2^{R870X/R870X}$ embryos, but also $Pkd2^{S818X/del}$ and $Pkd2^{S818X/S818X}$ embryos, is shown in **Fig. 3.23**.

The data presented thus far indicates that the $Pkd2^{R870X}$ allele is the most similar to $Pkd2^{del}$. $Pkd2^{del/del}$ and $Pkd2^{R870X/R870X}$ show similar levels of lethality (55.56% and 63.16%), however, different numbers of embryos were assessed: 20/36 and 12/19, respectively. The incidence of heart and stomach *situs* phenotypes, as well as ventricular septation defects, atrial and venous system abnormalities were also comparable between $Pkd2^{del/del}$ and $Pkd2^{R870X/R870X}$ embryos (**Table 3.8**). However, the two genotypes showed differences in the incidence of great vessel patterning and lung *situs* abnormalities. The data presented in this section invalidates my

initial hypothesis with regards to the *Pkd2*^{R870X} allele, as embryos that are homozygous for this allele produce both L-R and kidney cyst phenotypes, unlike the *Pkd2*^{fsX7} allele. This allele appears to produce phenotypes that are more severe even than those seen in *Pkd2*$^{del/del}$, given the higher incidence of lethality. Further discussion on how the phenotypes of *Pkd2*$^{R870X/R870X}$ embryos could be interpreted through the hypothesis set out at the end of **Chapter 2** is given in section **3.3.5**.

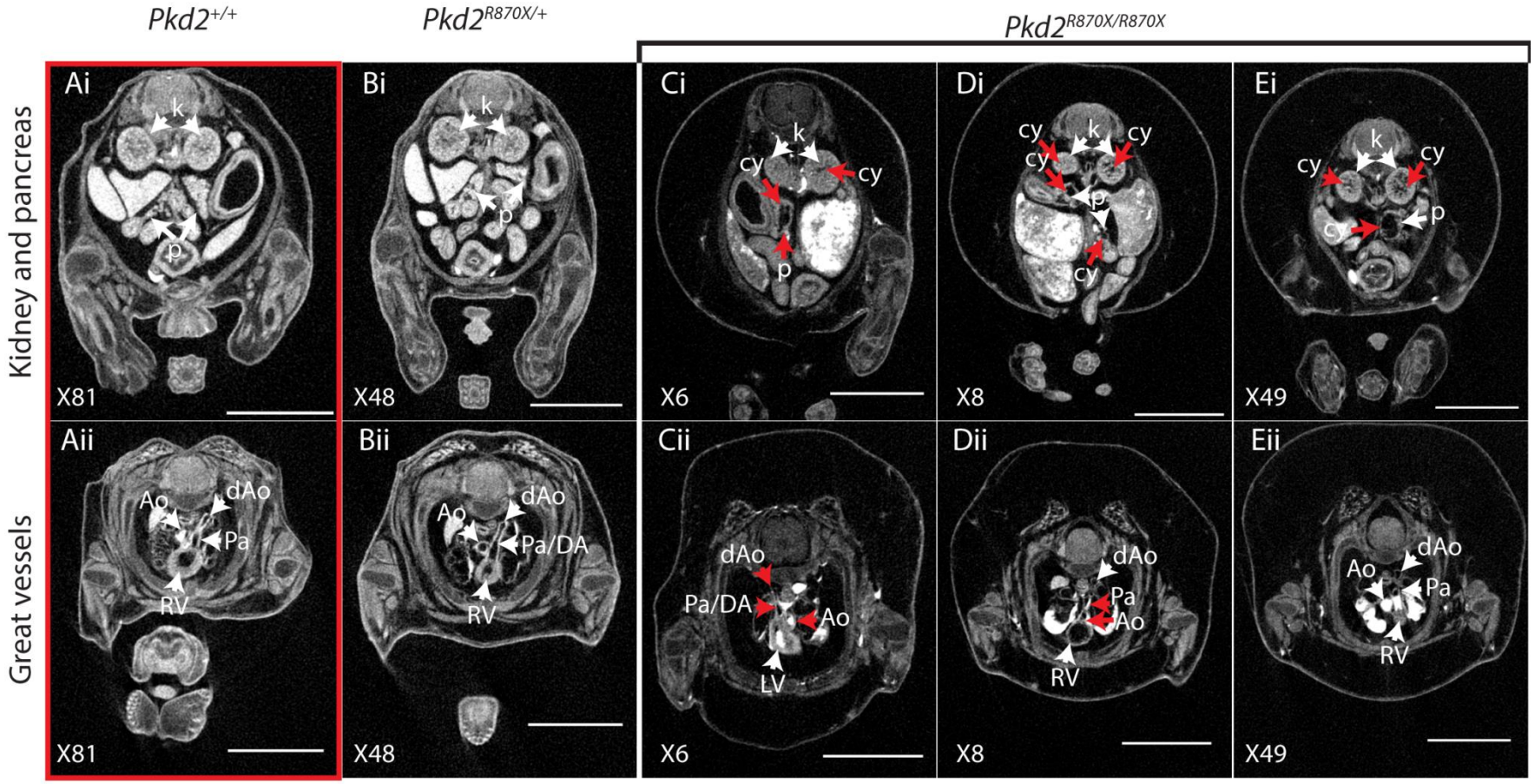


Figure 3.21: µCT sections of WT (**A**), *Pkd2*$^{R870X/+}$ (**B**) and *Pkd2*$^{R870X/R870X}$ (**C**-**E**) 15.5 dpc embryos, showing most commonly-encountered phenotypes. White arrows: normal phenotypes; red arrows: abnormal phenotypes. Abbreviations (in alphabetical order): Ao – aorta; chp – choroid plexus; cp – cleft palate; cy – cyst; dAo – descending aorta; k – kidney; lefv – left extremity of the fourth ventricle; LV – left ventricle; nc – nasal cavity; p – pancreas; Pa – pulmonary artery; Pa/DA – pulmonary artery/ductus arteriosus; RV – right ventricle; sp – soft palate; thy – thymus; to – tongue. Sample IDs are shown bottom left of each section. Sample highlighted in red is derived from a PKD2-S818XxS818X cross. Scale bar: 2 mm. Unannotated figure is shown in **Appendix 1**, **Fig. A1.16**, pages 250-251.

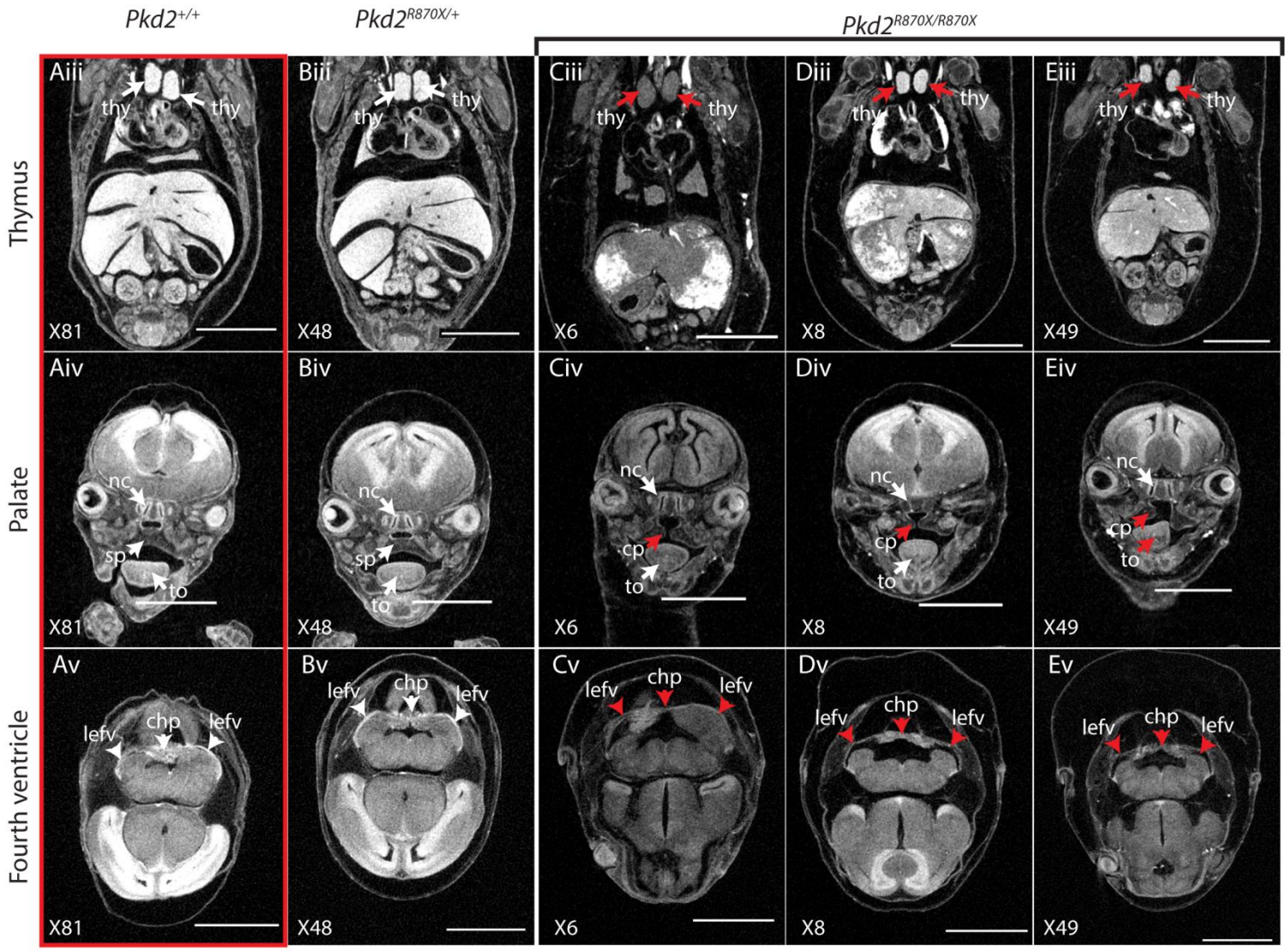


Figure 3.21 (continued)

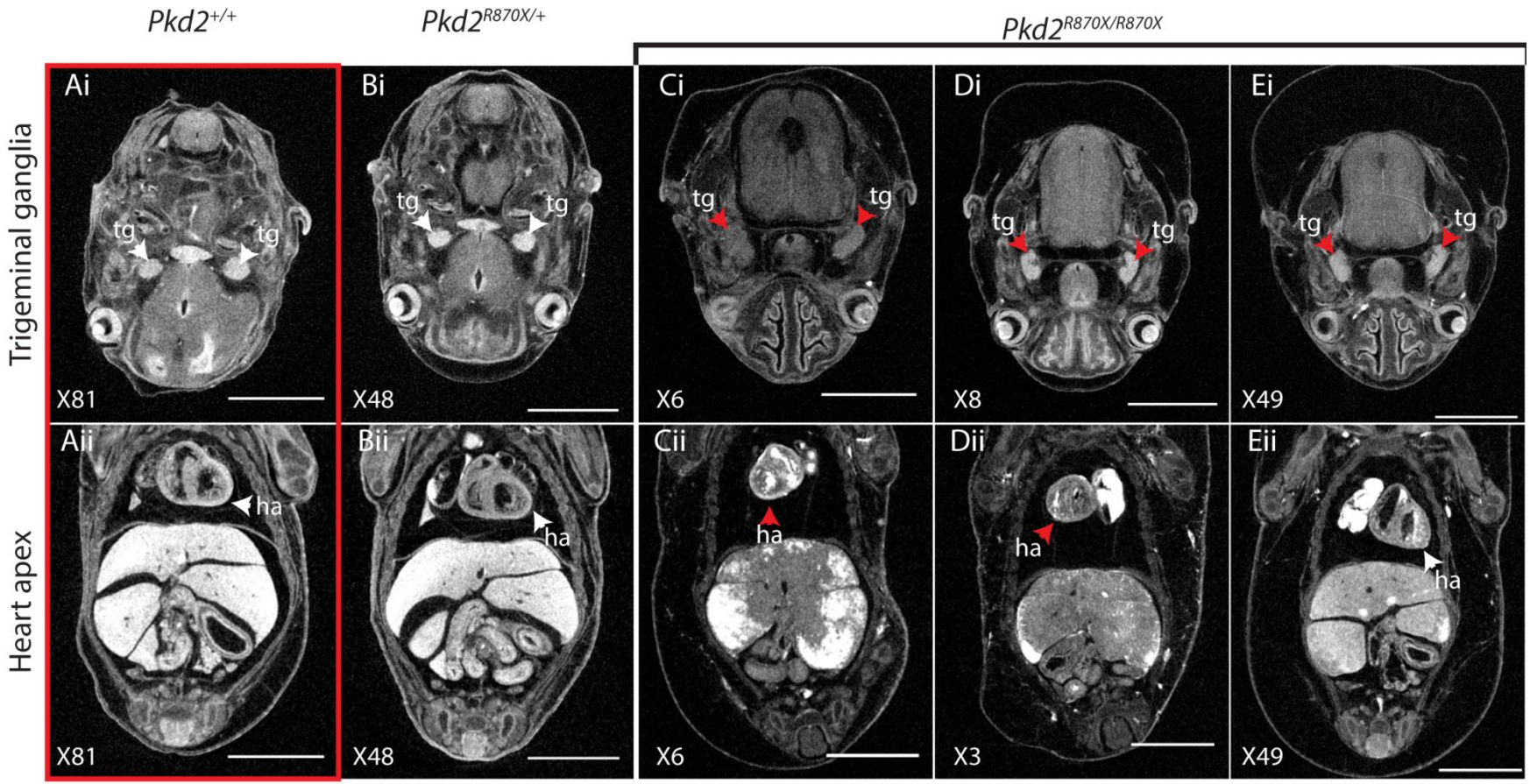


Figure 3.22: µCT sections of WT (**A**), *Pkd2*$^{R870X/+}$ (**B**) and *Pkd2*$^{R870X/R870X}$ (**C**-**E**) 15.5 dpc embryos, showing most commonly-encountered phenotypes. White arrows: normal phenotypes; red arrows: abnormal phenotypes. Abbreviations (in alphabetical order): al – accessory lobe; av – azygos vein; cal – caudal lobe; cl – cranial lobe; ha – heart apex; ivc – inferior vena cava; ivs – interventricular septum; lat – left atrium; lll – left lateral lobe; lml – left medial lobe; LV – left ventricle; ml – medial lobe; p – pancreas; pp – papillary process; rat – right atrium; rll – right lateral lobe; rml – right medial lobe; RV – right ventricle; sl – single lobe; spl – spleen; st – stomach; tg – trigeminal ganglion. Sample IDs are shown bottom left of each section. Sample highlighted in red is derived from a PKD2-S818XxS818X cross. Scale bar: 2 mm. Unannotated figure is shown in **Appendix 1**, **Fig. A1.17**, pages 252-253.

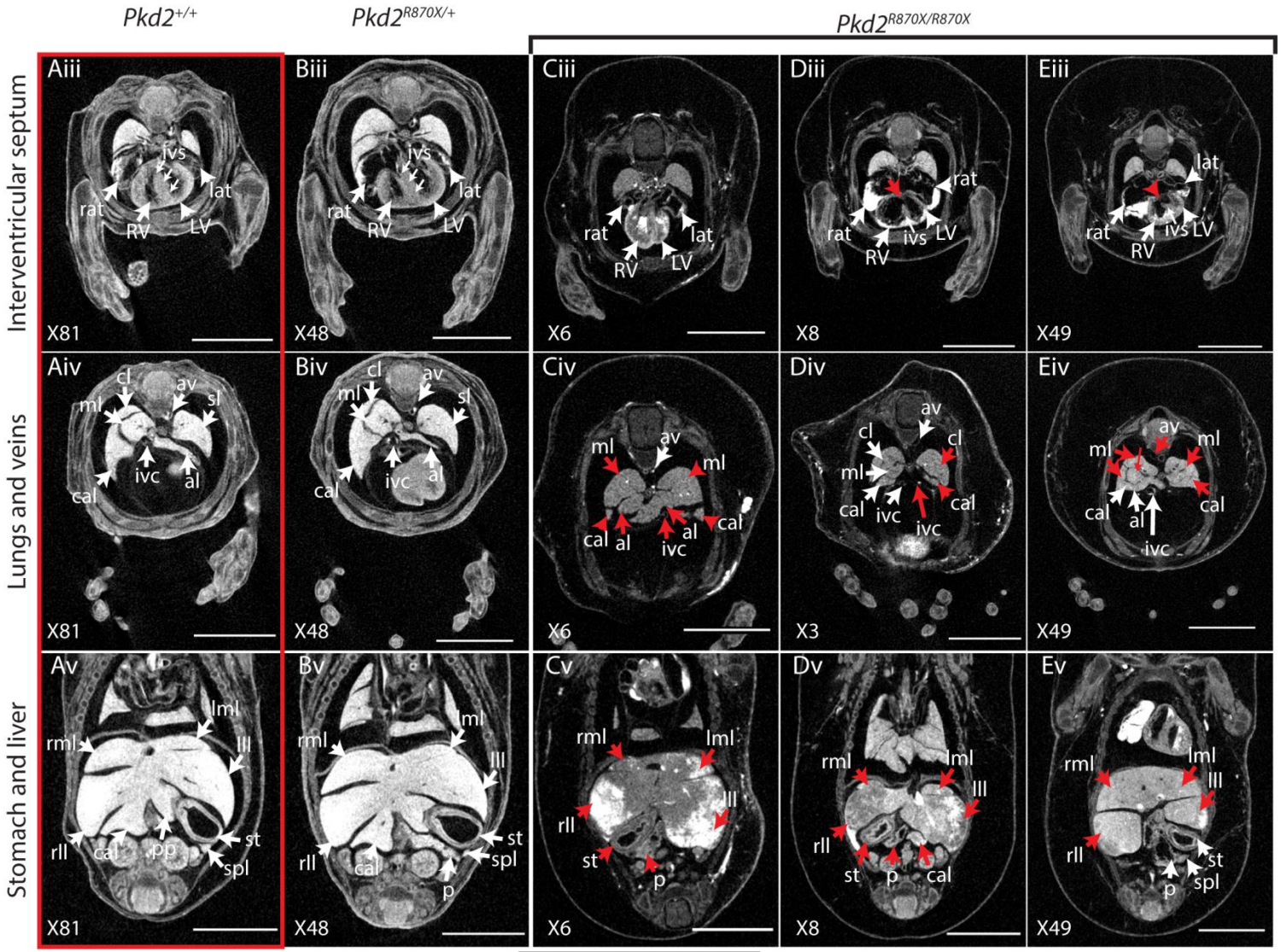


Figure 3.22 (continued)

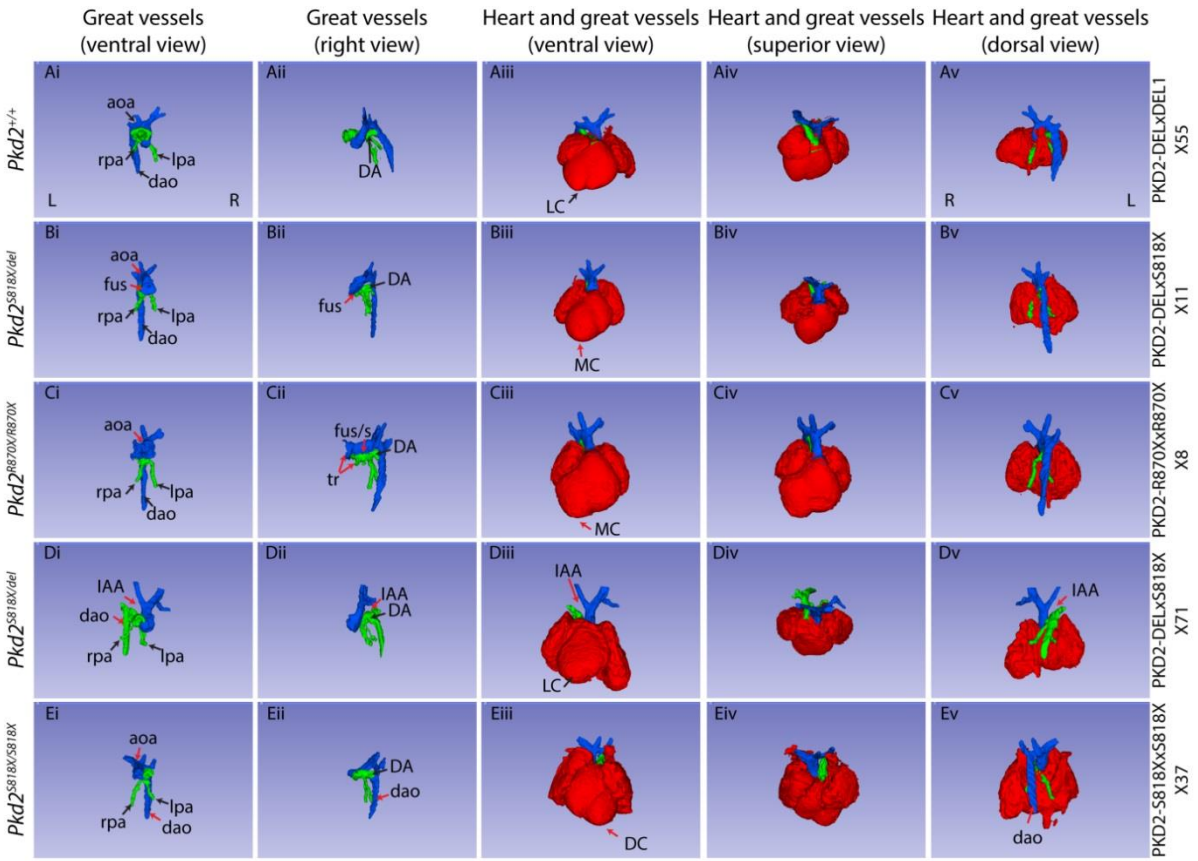


Figure 3.23: 3D reconstruction of cardiac great vessels and heart from WT (**A**), *Pkd2*$^{S818X/del}$ (**B** and **D**), *Pkd2*$^{R870X/R870X}$ (**C**) and *Pkd2*$^{S818X/S818X}$ (**E**) embryos, based on µCT sections. The aorta is shown in blue, the pulmonary artery is shown in green and the heart is shown in red. Normal patterning and positioning is shown in (**A**), fusion of great vessels is shown in (**B**), transposition (with fused, but septated great vessels) is shown in (**C**), IAA is shown in (**D**) and reversed aortic arch is shown in (**E**). Sample IDs are given on the right; genotypes are indicated on the left. L-R orientation indicated in **Ai** applicable to **Ai-iv**, **Bi-iv**, **Ci-iv**, **Di-iv** and **Ei-iv**; L-R sides indicated in **Av** also applicable to **B-Ev**. Black arrows indicate normal structures, red arrows indicate abnormal structures. Abbreviations (in alphabetic order): aoa – aortic arch; DA – ductus arteriosus; dao – descending aorta; DC – dextrocardia; fus – fusion; fus/s – fusion with septation; IAA – interrupted aortic arch; MC – mesocardia; LC – levocardia; lpa – left pulmonary artery; rpa – right pulmonary artery. Figure is shown in larger size in **Appendix 1**, **Fig. A1.15**, page 249.

Table 3.7: Heatmap summary of phenotypes observed in µCT-analysed *Pkd2*$^{R870X/R870X}$ embryos

Phenotype	PKD2-R870XxR870X sample					
	X3	X6	X8	X49	X57	X81
Nervous System						
• Midbrain						
• Mesencephalic vesicle						
• 3rd Ventricle						
• Lateral vesicles						
• Cerebellum						
• CP (in medial 4th ventricle)	-					
• Lateral extremity of 4th ventricle						
• TG						
• Olfactory lobe						
• Emerging cervical spinal chord						
Cranial						
• Soft palate						
• Submandibular gland						
• C6 vertebra and DRG						
Thoracic						
• Thymus						
• Venous system						
• Ductus arteriosus	SI					
• Lungs	3:2	3:4	4:4	4+:4	4:4	4:3
• Aorta		SI				
• Heart apex	D	M	M		M	M
• Atria						
• Ventricles						
• IVS						
Abdominal						
• Peritoneal cavity						
• Adrenal glands						
• Kidneys	C	C	C	C	C	C
• Liver lobes	SI	SI				
• Stomach position	SI	SI	SI			
• Spleen	SI	SI	SI			
• Pancreas	C SI	C SI	C SI	C	C	C
• Ovaries	-					
• Testes	C	-	-	-	-	-
Oedema						
Brown fat						
Spinal shape						

Gray cells represent normal phenotypes, red cells represent abnormal phenotypes. Abbreviations: C – cystic; CP – choroid plexus; D – dextrocardia; DRG – dorsal root ganglia; IVS – interventricular septum; M – mesocardia; SI – *situs inversus*; TG – trigeminal ganglia. Lung lobations are given R:L and are shown only where the lobation is abnormal.

3.2.6. Phenotypic analysis of *Pkd2*$^{ins/ins}$ embryos at 15.5 dpc

The *Pkd2*^{ins} allele consists of an insertion of an arginine residue, in a sequence of 3 repeating R amino acid residues, at the very start of the CC region. Due to the fact that, at the nucleotide level, this single-codon insertion is shared with *Pkd2*^{S818X}, I included the *Pkd2*^{ins} allele in this analysis as a control. This was done to test whether the phenotypes observed in embryos carrying the *Pkd2*^{S818X} allele are due to the truncation of the protein, or due to the insertion of the extra codon and potential effects at the RNA level. Considering the fact that the mutation equates to a duplication of an arginine, in a set of repeating arginine residues, I therefore hypothesised that the *Pkd2*^{ins} allele is unlikely to produce phenotypes, in a homozygous state, that are similar to those produced by *Pkd2*^{S818X}, an allele that truncates the entire CC. Considering that this allele was the last to be analysed and due to time constraints, the analysis described in this sub-section will focus on gross *situs* and histological sectioning of kidneys. Moreover, only a small number of homozygotes were analysed.

3.2.6.a. Gross *situs* analysis

Embryos were collected at 15.5-16 dpc and sub-dissected to assess gross *situs*. Oedema was observed in all three *Pkd2*$^{ins/ins}$ samples (**Fig. 3.24**, **Ci**, **Di** and **Ei**), but not WT (data not shown, WT from different cross included in **Fig. 3.24**, **Ai**) or *Pkd2*$^{ins/+}$ samples (**Fig. 3.24**, **Bi**). Severe oedema was also encountered in all three *Pkd2*$^{ins/ins}$ samples. Similarly, WT and heterozygous samples did not display any lung, heart or great vessel phenotypes (**Fig. 3.24**, **Bii** and **Biii**). *Pkd2*$^{ins/ins}$ embryos showed a range of lung *situs* phenotypes, all of which were abnormal: 4:2 (**Fig. 3.24**, **Cii**), 1:1 (**Fig. 3.24**, **Dii**) and 1:2 (**Fig. 3.24**, **Eii**). Homozygotes either displayed levocardia (**Fig. 3.24**, **Eii**) or dextrocardia (**Fig. 3.24**, **Cii** and **Dii**). Great vessel patterning and positioning in *Pkd2*$^{ins/ins}$ samples was either normal (**Fig. 3.24**, **Eiii**), reversed (**Fig. 3.24**, **Ciii**) or displayed abnormalities such as fusion of the great vessels (**Fig. 3.24**, **Diii**). Finally, lethality was also encountered in *Pkd2*$^{ins/ins}$ samples, but only in one sample

out of the 3 analysed (**Fig. 3.24**, **Di**). Higher numbers will require to be analysed in order to properly compare it to the other CC mutant alleles.

3.2.6.b. Histological sectioning of kidneys

Kidney cysts were assessed by histological sectioning. Cysts were not observed in either WT or *Pkd2*$^{ins/+}$ (**Fig. 3.25**, **A** and **B**); however, kidneys from *Pkd2*$^{ins/ins}$ embryos displayed cysts (**Fig. 3.25**, **C**). Due to time constraints, only two homozygote samples were analysed through sectioning.

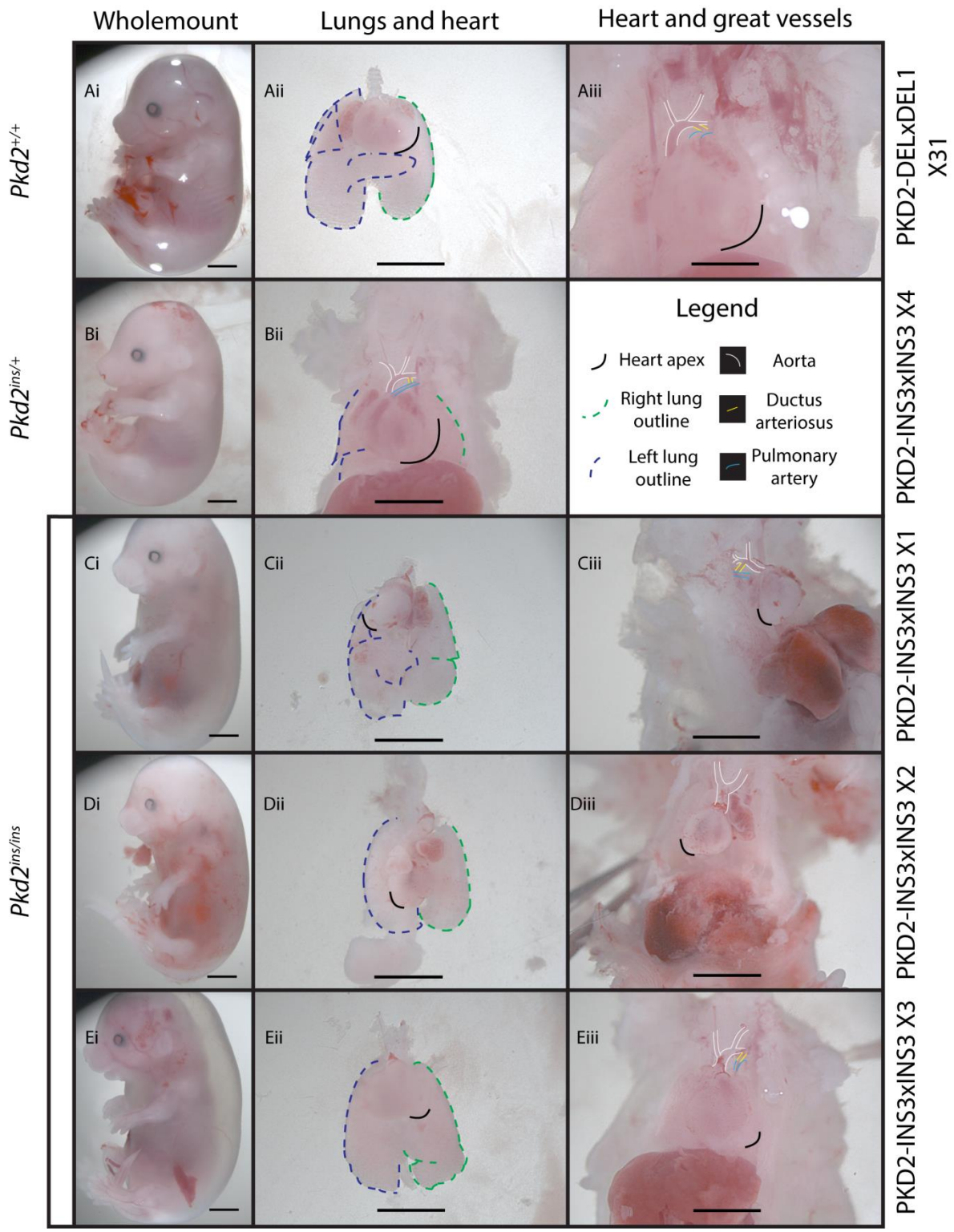


Fig. 3.24: Analysis of great vessel and L-R patterning in WT (**A**), *Pkd2*$^{ins/+}$ (**B**), *Pkd2*$^{ins/ins}$ (**C-E**) embryos. Wholemounts are shown in the first column, lung and heart *situs* are shown in the second column, whilst great vessel patterning and positioning is shown in the final column (with the exception of **B**). Sample IDs are given on the right hand side. The WT sample, shown for reference, is derived from a PKD2-DELxDEL1 mating. Scale bar: 2 mm. Unannotated figure is shown in **Appendix 1**, **Fig. A1.18**, page 254**.**

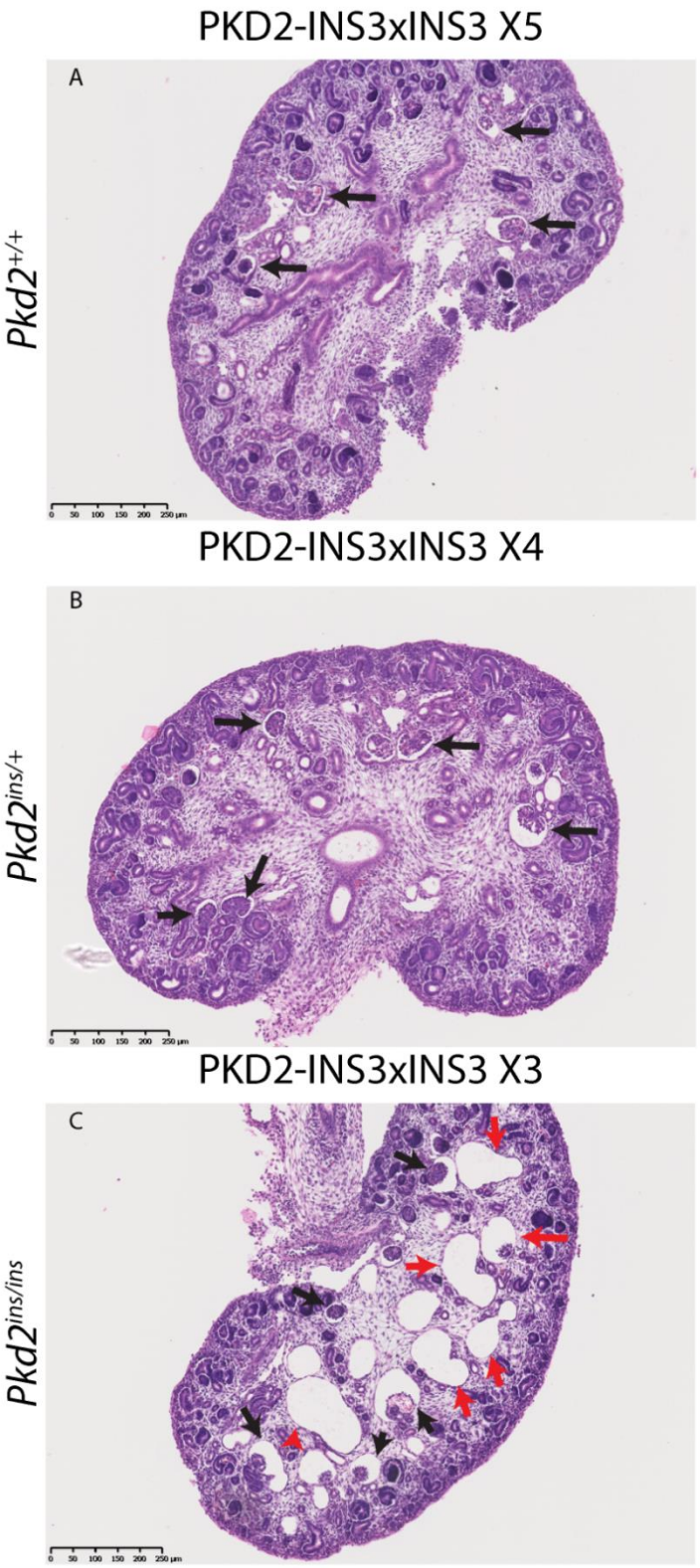


Fig. 3.25: Histological sectioning of kidneys from offspring of PKD2-INS3xINS3 crosses. WT kidneys are shown in **A**, *Pkd2*$^{ins/+}$ kidneys are shown in **B**, *Pkd2*$^{ins/ins}$ kidneys are shown in **C**. Normal glomeruli are indicated by black arrows, cysts are indicated by red arrows. Sample IDs are given, alongside the matings that produced them, at the top of each image. Scale bar: 250 µm.

3.3. Summary of results and discussion

In this chapter, I performed phenotypic analysis on mouse embryos bearing *Pkd2* mutations affecting the region encoding the CC domain. The *in vivo* approach allowed me to address a number of questions. Primarily, this approach allowed me to investigate the role of the PKD2 CC in L-R and kidney development. Secondly, it allowed me to inquire whether or not the CC can be partitioned into two sections with different functions in L-R development, as previously suggested for kidney development (Tsiokas et al., 1997, Tsiokas et al., 1999, Giamarchi et al., 2010). Thirdly, it allowed me to make inferences on the molecular mechanisms behind the interactions of PKD1L1-PKD2, but also PKD1-PKD2 and PKD2 homo-oligomerization. In other words, this approach allowed me to test the validity of the results described in **Chapter 2** by characterising the phenotypes caused by *Pkd2* mutations tested previously. I was particularly interested in whether the mutants analysed display only cystic kidneys, and not *situs* abnormalities; given that the results obtained in **Chapter 2** suggest that the CC is not required for PKD1L1-PKD2 interaction. This situation would support the results obtained in the previous chapter, namely that the PKD1L1-PKD2 interaction differs mechanistically from that of PKD1-PKD2. In contrast, if the mutants display both kidney and L-R phenotypes, this could imply that the ability of PKD2 to interact with binding partners does not guarantee the functionality of the PKD2-based complexes in different contexts (i.e. renal and L-R development), as well as stress the requirement for validating the results described in **Chapter 2**.

3.3.1. Description and predicted impact of CRISPR/Cas9-derived alleles

I initially wanted to analyse two PKD2 truncation mutations described in **Chapter 2**, namely R870X and S818X. The R870X mutation truncates the CC region of PKD2, removing the hetero-oligomerization sub-region, which was previously argued to be required for PKD1-PKD2 interaction (see section **2.1.1**). The equivalent mutation in the human protein, R872X, was previously shown to disrupt the interaction between PKD1 and PKD2 fragments, due to disruption of the PKD2 CC (Qian

et al., 1997). Other mutations, in the hetero-oligomerization sub-region of the PKD2 CC, similarly disrupted the interaction with PKD1 (Tsiokas et al., 1999, Giamarchi et al., 2010). Importantly, the absence of the hetero-oligomerization region did not impede PKD2 homo-oligomerization (Giamarchi et al., 2010). However, the homo-oligomerization sub-region was only shown to be required for PKD2 fragment homo-oligomerization, but not the full-length protein (Giamarchi et al., 2010). Initially, I had predicted that the PKD1L1-PKD2 interaction is similar to that of PKD1-PKD2, given the previous findings arguing for the requirement of the PKD1L1 CC for PKD1L1-PKD2 fragment interaction (Field et al., 2011). However, work presented in **Chapter 2** appears to contradict this, arguing for a difference between the PKD1L1-PKD2 and PKD1-PKD2, in terms of requirement of the CC region for interaction (see section **2.2.3**). The S818X mutation truncates the protein upstream of the CC region, but downstream of the ER localisation signal. Given the data published so far (*vide supra*), this would suggest that, as with the R870X mutation, the presence of the S818X mutation would only disrupt the interaction with PKD1.

A recent study proposed that the first extracellular loop of PKD2, and the equivalent sixth loop of PKD1, behave as interaction domains (Salehi-Najafabadi et al., 2017). This is supported by studies modelling the interaction of PKD1 with PKD2, which also suggest that these extracellular loops come into contact with the interacting partner (Grieben et al., 2017). This study, together with a similar study investigating the structure of PKD2 (Shen et al., 2016), suggest that PKD2 is able to form tetramers in the absence of the CC region. Given these findings, it is possible that the absence of the CC sub-regions will not affect the interaction of PKD2 with itself, PKD1 or PKD1L1. However, Giamarchi and colleagues have suggested that CC mutations in PKD2 affect the capacity of the PKD2-based channel to function properly (Giamarchi et al., 2010). The two truncation mutations, R870X and S818X, are useful tools in testing the involvement of the CC region in interacting with PKD1 and PKD1L1, as well as in investigating the role of the CC in PKD2-based channel function.

Using CRISPR/Cas9, four mutant alleles were generated, two from each attempt to generate the R870X and S818X mutations. The first allele, *Pkd2*^{fsX7}, results in a frameshift and truncates the protein just downstream of the homo-oligomerization sub-region; the second is *Pkd2*^{R870X}; the third is *Pkd2*^{S818X}; and the fourth is *Pkd2*^{ins}, containing an extra amino acid at the beginning of the CC region. The alleles describing these mutations are summarised in **Table 3.1** and the effect of these mutations at the protein level is depicted in **Fig. 3.1**.

3.3.2. Summary and interpretation of *Pkd2*$^{del/del}$ embryo µCT phenotypic analysis

In order to determine whether all of the phenotypes of interest can be assessed using µCT**,** I first performed phenotypic analysis on *Pkd2*$^{del/del}$ embryos, bearing a null allele of *Pkd2.* This allele was adapted from a conditional allele (Garcia-Gonzalez et al., 2010) into a null, and characterised in terms of gross *situs* and kidney phenotypes (Walker, 2016).

Performing phenotypic analysis on *Pkd2*$^{del/del}$ embryos using µCT also provided a baseline for comparison with the CC mutant alleles obtained. The phenotypes previously described for *Pkd2*$^{del/del}$ embryos (Walker, 2016) were observed in µCT-scanned samples: oedema, kidney cysts and *situs* abnormalities (**Fig. 3.3** and **3.4**). This method of analysis also allowed the visualisation of other abnormal phenotypes, not previously described: morphology of brown fat pads, positioning and shape of thymus, cardiac great vessel positioning and patterning, pancreatic cysts, cardiac structure, cranial structure, nervous system, venous system patterning abnormalities and testicular cysts (**Fig. 3.3** and **3.4**).

The L-R patterning abnormalities are known to be linked to *Pkd2* (see section **1.3.3**), however, the extent to which some phenotypes depend on L-R patterning or local roles played by *Pkd2*, such as in the case of cardiac, great vessel and vascular development (*vide infra*), remains to be established. The kidney cyst phenotypes observed are known to be directly linked to *Pkd2* (see section **1.4.1**). Pancreatic cysts have been reported in human ADPKD patients, as well as mouse

models (Wu et al., 2000, Pennekamp et al., 2002, Boucher and Sandford, 2004, Kim et al., 2015). The testicular cysts observed are likely linked to a direct, local role played by *Pkd2* in this tissue, as reported in a previous study examining testicular development in *Pkd2*-deficient mice (Nie and Arend, 2014). In these mice, although cysts were not observed, epididymal duct coiling was delayed and mesonephric tubules/epherent ducts were dilated. Furthermore, male ADPKD patients display a high-incidence of reproductive tract abnormalities, including testicular cysts, as well as infertility (Belet et al., 2002, Manno et al., 2005, Torra et al., 2008, Vora et al., 2008, Kanagarajah et al., 2012, Kim et al., 2015).

The cardiac structure abnormalities have also been previously reported in other *Pkd2* null alleles (Wu et al., 2000, Pennekamp et al., 2002) and are thought to be directly linked to *Pkd2*. However, given that cardiac structure phenotypes observed in the mutants analysed, such as ventricular septation, do not seem to correlate with heart *situs*, this is suggestive that ventricular septation may involve a more localised role of *Pkd2*. The patterning of the cardiac great vessels may be linked to establishment of heart *situs*, given the fact that the great vessels develop in tandem with the heart (Anderson et al., 2003). However, other phenotypes observed, such as fusion of the great vessels (failure to septate) and interrupted aortic arch appear to not correlate with heart *situs*, thereby suggesting that they are caused by a more local role of *Pkd2*. Similarly, given the roles described for *Pkd2* in the circulatory system (see section **1.5.2**), it is likely that the abnormalities seen in terms of venous system patterning are directly linked to the absence of *Pkd2.* Alternatively, the abnormal patterning of the venous system could be an indirect effect stemming from abnormal L-R establishment, due to absence of *Pkd2.* A third option would be that both perturbed *situs* establishment and a local role played by *Pkd2* in vascular patterning result in the phenotypes observed.

Craniofacial abnormalities have been previously reported in conditional alleles of *Pkd2* (Khonsari et al., 2013), lacking *Pkd2* expression in neural crest-derived cells. Interestingly, Khonsari

et alia do not describe a cleft palate phenotype in these embryos, arguing that this is caused by lack of *Pkd2* expression in non-neural crest-derived cranial tissues. Given the expression of both *Pkd1* and *Pkd2* reported at 11.5 dpc in the nervous system (Guillaume and Trudel, 2000), this is also indicative that the phenotypes observed are directly linked to the absence of *Pkd2*. *Pkd2* is known to be expressed in the developing thymus in human embryos (Ong et al., 1999), indicating a potential role in the development of the thymus. However, the abnormal morphology of the brown fat pads may not be a direct effect, resulting from the absence of PKD2, but may be indirectly caused by oedema.

The work described in section **3.2.2** indicates that µCT is a time-efficient method of performing broad-spectrum phenotypic analysis. Moreover, this method is able to detect kidney cysts in embryos older than 15.5 dpc. In samples closer to 15.5 dpc, enhancing the resolution might help better detect the presence of cysts. However, the presence of kidney cysts can be inferred by analysing kidney tissue density in these samples. Alternatively, it could be that the cystic kidney phenotype in embryos at 15.5 dpc is less evident due to developmental delay.

3.3.3. Interpreting *Pkd2*$^{fsX7/del}$ and *Pkd2*$^{fsX7/fsX7}$ embryo phenotypes

The *Pkd2*^{fsX7} allele contains a 1 nucleotide deletion which resulted in a frameshift and truncation after 6 AA. I set out to answer two questions with this allele: to determine whether this allele produces different phenotypes from those observed in *Pkd2*$^{del/del}$ embryos, as well as to test the role of the hetero-oligomerization sub-region of the CC in PKD2 function – which is excluded in the PKD2^{fsX7} protein. I performed phenotypic analysis on both *Pkd2*$^{fsX7/del}$ and *Pkd2*$^{fsX7/fsX7}$ embryos, in order to address these questions. If the *Pkd2*^{fsX7} allele were similar to the null allele, *Pkd2*^{del}, the phenotypes of both *Pkd2*$^{fsX7/del}$ and *Pkd2*$^{fsX7/fsX7}$ embryos would be identical to those observed in *Pkd2*$^{del/del}$ embryos. Considering the results described in **Chapter 2**, which suggest that the CC of PKD2 is not required for the PKD1L1-PKD2 interaction, this would imply that the *Pkd2*^{fsX7} allele will

not lead to L-R phenotypes, but will produce the cystic kidney phenotype due to the requirement of the CC for the PKD1-PKD2 interaction (see section **2.1.1**).

Phenotypic analysis was performed, in tandem for *Pkd2*$^{fsX7/del}$ and *Pkd2*$^{fsX7/fsX7}$ embryos, through one of three methods: dissection using light microscopy (**Fig. 3.5**), for determining gross *situs* phenotype, histological sectioning (**Fig. 3.6**), to assess the presence of kidney cysts, and µCT (**Fig. 3.7**-**3.10**). *Pkd2*$^{fsX7/del}$ embryos displayed different phenotypes from those observed in *Pkd2*$^{del/del}$ embryos, in terms of L-R determination: lower incidence of *situs inversus* for the abdominal viscera, as well as displaying randomisation of lung *situs.* Contrary to what is observed in *Pkd2*$^{del/del}$ embryos, which is a high incidence of right lung isomerism, together with randomisation, but no normal *situs*, *Pkd2*$^{fsX7/del}$ embryos display a high incidence of normal *situs*, as well as low incidences of left isomerism, randomisation and 4+:4 lung lobation. Differences were also observed in terms of cardiac great vessel *situs*: the majority of *Pkd2*$^{fsX7/del}$ embryos showed normal patterning, but not *situs inversus*; in comparison, *Pkd2*$^{del/del}$ embryos showed no normal *situs*, but did show incidence of *situs inversus* (**Table 3.8**). However, it is worth mentioning that only four *Pkd2*$^{del/del}$ embryos were analysed for cardiac great vessel *situs*. Heart apex positioning was normal in *Pkd2*$^{fsX7/del}$ embryos, compared to *Pkd2*$^{del/del}$ showing equal incidences of levocardia (normal) and dextrocardia, as well as mesocardia, in a minority of cases. Similarly to *Pkd2*$^{del/del}$ samples, kidney cysts were observed in *Pkd2*$^{fsX7/del}$ embryos. These phenotypes indicate that the *Pkd2*^{fsX7} and *Pkd2*^{del} alleles differ, as the phenotypes observed in *Pkd2*$^{fsX7/del}$ and *Pkd2*$^{del/del}$ embryos vary. This difference is further supported by the presence of 1:1 R:L lung lobation in *Pkd2*$^{fsX7/del}$ embryos – this phenotype, L-lung isomerism, is the opposite of what is observed in the majority of *Pkd2*$^{del/del}$ embryos, 4:4 R:L lobation, or R-lung isomerism. To date, no incidences of 1:1 R:L lung lobation have been observed in *Pkd2*$^{del/del}$ embryos.

In contrast to both *Pkd2*$^{del/del}$ and *Pkd2*$^{fsX7/del}$ embryos, *Pkd2*$^{fsX7/fsX7}$ displayed no abnormal *situs* phenotypes, but displayed abnormal, cystic kidneys. The absence of L-R phenotypes in *Pkd2*$^{fsX7/fsX7}$ embryos suggest that the homo-oligomerization sub-region of the PKD2 CC, which is

absent in proteins produced by the *Pkd2*^{fsX7} allele, may not be required for L-R determination but is required for normal kidney development. Furthermore, the lack of *situs* phenotypes in *Pkd2*$^{fsX7/fsX7}$ embryos supports the hypothesis that the *Pkd2*^{fsX7} is different from the null. However, given that this analysis only assessed the presence of kidney cysts, further analysis is required to distinguish any differences between the *Pkd2*^{del} and *Pkd2*^{fsX7} on renal pathology (see section **4.2.2**). These findings suggest that, at the molecular level, the PKD2 CC is required for interaction with PKD1, but not PKD1L1. The incidence of abnormal *situs* phenotypes observed in *Pkd2*$^{fsX7/del}$ embryos may be due to a combination of a mild negative effect of the *Pkd2*^{fsX7} allele, preventing the protein from functioning normally, compounded by lower total PKD2 protein levels. Alternatively, the *Pkd2*^{fsX7} allele may also lead to lower levels of total PKD2 protein.

In terms of severity of phenotype, *Pkd2*$^{fsX7/del}$ embryos displayed low incidence of lethality, as compared to *Pkd2*$^{del/del}$ embryos which are lethal in over half of all samples analysed. This suggests that the *Pkd2*^{fsX7} allele is able to rescue the lethality seen in *Pkd2*$^{del/del}$ embryos, and thereby perform some of the normal function associated with the *Pkd2* gene. The absence of lethality in *Pkd2*$^{fsX7/fsX7}$ embryos further supports this.

To conclude, the presence of kidney cysts but not L-R phenotypes in *Pkd2*$^{fsX7/fsX7}$ embryos, support the hypothesis formulated at the end of **Chapter 2**: that the molecular mechanisms involved in the PKD1L1-PKD2 interaction is different from those of the PKD1-PKD2 interaction. More specifically, the absence of the hetero-oligomerization sub-region of the PKD2 CC potentially affects renal, but not L-R, development. This can potentially be accounted for by differences in the requirement of the CC sub-regions between the PKD1-PKD2 interaction, in renal development, and that of PKD1L1-PKD2, in L-R determination.

3.3.4. Interpreting *Pkd2*$^{S818X/del}$ and *Pkd2*$^{S818X/S818X}$ embryo phenotypes

The *Pkd2*^{S818X} allele consists of a truncation mutation upstream of the PKD2 CC region, but directly downstream of the ER retention signal. This allele also contains an in-frame 3 nucleotide insertion downstream of the STOP codon. As with the *Pkd2*^{fsX7} allele, I wanted to investigate whether there are differences or similarities between the *Pkd2*^{S818X} and *Pkd2*^{del} alleles, as well as to test the involvement of the entire CC region in PKD2 function. In order to do this, I analysed both *Pkd2*$^{S818X/del}$ and *Pkd2*$^{S818X/S818X}$ embryos. Similarly to the *Pkd2*^{fsX7} allele (see section **3.3.3**), if the *Pkd2*^{S818X} allele were similar to *Pkd2*^{del}, both *Pkd2*$^{S818X/del}$ and *Pkd2*$^{S818X/S818X}$ embryos would display identical phenotypes to *Pkd2*$^{del/del}$. Moreover, the biochemical results described in **Chapter 2** suggest that these embryos should only display kidney, but not L-R, phenotypes. However, considering that the protein produced by the *Pkd2*^{S818X} allele lacks the CC region entirely, this could affect the function of PKD2-based channels by reducing the efficiency of homo-oligomerization.

Gross *situs* phenotype was determined through dissection using light microscopy for *Pkd2*$^{S818X/del}$ (**Fig. 3.12**) and *Pkd2*$^{S818X/S818X}$ embryos (**Fig. 3.13**), the presence of kidney cysts was assessed through histological sectioning (**Fig. 3.14**) and broad-spectrum phenotypic analysis was performed through μCT (**Fig. 3.15-3.18**). Both *Pkd2*$^{S818X/del}$ and *Pkd2*$^{S818X/S818X}$ embryos displayed abnormal L-R phenotypes, with respect to thoracic and abdominal viscera. However, the presentation and incidence differed from *Pkd2*$^{del/del}$ embryos (**Table 3.8**).

Although at first sight, the presence of both L-R phenotypes and cystic kidneys in *Pkd2*$^{S818X/del}$ and *Pkd2*$^{S818X/S818X}$ embryos appears to contradict the hypothesis proposed at the end of **Chapter 2**, arguing for differences in molecular mechanism of interaction between PKD1-PKD2 and PKD1L1-PKD2, the presence of *situs* phenotypes can potentially be accounted for in these genotypes. Considering that the *Pkd2*^{S818X} allele produces a protein lacking the entirety of the CC region, this

could affect the stability or efficiency of PKD2-based complex formation, and therefore reduced function, in spite of the PKD2^{S818X} being able to interact with PKD1L1.

In terms of severity of genotypes, under half of *Pkd2*$^{S818X/del}$ embryos displayed lethality, whilst a lower incidence of lethality was observed for *Pkd2*$^{S818X/S818X}$. Curiously, the *Pkd2*^{S818X} appears to partially rescue the incidences of abnormal phenotypes observed in *Pkd2*$^{del/del}$ embryos, with *Pkd2*$^{S818X/del}$ embryos showing the highest incidence of normal *situs* for abdominal and thoracic organs. However, *Pkd2*$^{S818X/S818X}$ samples display a higher incidence of randomisation of thoracic and abdominal *situs*, in spite of lower incidence of lethality. These findings also support the hypothesis that the *Pkd2*^{S818X} allele is different from *Pkd2*^{del}. Further work is required to explain these findings, as well as to potentially separate the *Pkd2*$^{S818X/del}$, *Pkd2*$^{S818X/S818X}$ and *Pkd2*$^{del/del}$ genotypes, in terms of renal phenotypes displayed (see section **4.2.2**).

3.3.5. Characterising the *Pkd2*^{R870X} allele

The *Pkd2*^{R870X} allele contains a truncation mutation that removes the hetero-oligomerization sub-region of the CC. The R870X mutation is also the equivalent of one of the most common ADPKD-causing *PKD2* mutations in human (Rossetti et al., 2007, Harris and Rossetti, 2010). This allele was expected to be identical to *Pkd2*^{fsX7}, in terms of phenotypes produced, given the similar effect that the two mutations have on the protein. Similarly to previous alleles, I wanted to investigate two aspects: whether the *Pkd2*^{R870X} allele is different from *Pkd2*^{del} (and similar to *Pkd2*^{fsX7}), and to test the involvement of the hetero-oligomerization sub-region of the CC in PKD2 function.

As with previous alleles, gross *situs* phenotype was determined through dissection and light microscopy (**Fig. 3.19**), histological sectioning was used to test for the presence of kidney cysts (**Fig. 3.20**), whilst µCT was used to perform broad-spectrum phenotypic analysis (**Fig. 3.21** and **3.22**). Unlike *Pkd2*$^{fsX7/fsX7}$ embryos, *Pkd2*$^{R870X/R870X}$ embryos displayed both L-R and kidney phenotypes. In terms of abdominal viscera, heart apex positioning, and incidence of *situs inversus* for cardiac great

vessels, the phenotypes *Pkd2*$^{R870X/R870X}$ embryos argue that the *Pkd2*^{R870X} allele is the most similar to *Pkd2*^{del}. However, *Pkd2*$^{R870X/R870X}$ and *Pkd2*$^{del/del}$ embryos display different incidences of normal patterning of great vessels and lung *situs* phenotypes (**Table 3.8**), suggesting a difference between the two alleles.

A potential explanation for the phenotypes observed could be that the *Pkd2*^{R870X} either produces lower levels of protein (compared to the WT), or the protein produced is degraded. In terms of severity, *Pkd2*$^{R870X/R870X}$ embryos showed the highest incidence of lethality, higher even than *Pkd2*$^{del/del}$. The differences in phenotypes from those of *Pkd2*$^{del/del}$ embryos could potentially be explained if the PKD2^{R870X} protein is antimorphic, or is less functional compared to the WT, in addition to the allele encoding it producing less protein. The antimorphic quality needs to be further tested, given that *Pkd2*$^{R870X/+}$ embryos do not display any abnormal phenotypes (see section **4.2.2**). For example, the PKD2^{R870X} protein could have a higher affinity for binding other PKD2 molecules, and therefore, indirectly, a lower affinity for PKD1L1 or PKD1.

As with the *Pkd2*^{S818X} allele, at first sight the analysis of *Pkd2*$^{R870X/R870X}$ embryos seems to contradict the hypothesis that the PKD1L1-PKD2 interaction is different from PKD1-PKD2. Nonetheless, the data presented for the *Pkd2*$^{R870X/R870X}$ can be explained within the context of this hypothesis (*vide supra*). However, further work is required in order to do this, such as performing phenotypic analysis on *Pkd2*$^{R870X/del}$ embryos, as well as assessing whether *Pkd2*$^{R870X/+}$ adults display cystic kidneys (see section **4.2.2**). The latter would test for a dominant negative quality of the allele, whilst the former would help further differentiate and characterise this allele in comparison to *Pkd2*^{del}.

3.3.6. Preliminary characterisation of the *Pkd2*^{ins} allele

Finally, the last allele to be assessed in terms of phenotypes is *Pkd2*^{ins}. This allele was obtained alongside *Pkd2*^{S818X}, and contains an extra codon, shared with *Pkd2*^{S818X}, at the beginning of

the CC-coding region. In the *Pkd2*^{S818X} allele, this codon is not translated, given that it is downstream of the STOP codon. I had initially predicted that this allele would be unlikely to lead to any phenotypes, as the extra amino acid, an arginine, is within a cluster of three repeating arginine residues. In this scenario, this allele could also be used to test whether the phenotypes caused by the *Pkd2*^{S818X} allele is due to truncation of the protein, or due to potential mRNA-level effects of the extra codon. In addition to this, time constraints and technical difficulties in genotyping these samples prevented me from performing analysis that would be comparable to what was described for previous genotypes.

Unlike the analysis performed for the other CC mutant alleles, only dissection and light microscopy was used to determine gross *situs* phenotypes (**Fig. 3.24**), as well as histological sectioning for determining the presence or absence of kidney cysts (**Fig. 3.25**). Contrary to my prediction, both L-R phenotypes and kidney cysts were observed in all *Pkd2*$^{ins/ins}$ embryos analysed. Given the fact that L-lung isomerism was observed in these embryos, there is a difference between the *Pkd2*^{ins} allele and *Pkd2*^{S818X}. Moreover, the presence of normally-patterned great vessels also argues for a difference between *Pkd2*^{ins} and *Pkd2*^{del}. Lethality was only observed once in *Pkd2*$^{ins/ins}$ embryos.

In order to be able to characterise this allele better, a larger set of *Pkd2*$^{ins/ins}$ embryos needs to be analysed. The phenotypes observed could potentially be explained by disruption of the CC region of the protein, due to the presence of the extra arginine residue. This would mean that *Pkd2*$^{ins/ins}$ embryos should be similar to *Pkd2*$^{S818X/S818X}$ embryos, in terms of incidence of phenotypes, as well as which phenotypes the embryos display. Alternatively, the inserted amino acid may only partially disrupt CC-formation, which could explain differences between *Pkd2*$^{ins/ins}$ and *Pkd2*$^{S818X/S818X}$ phenotypes. The data from *Pkd2*$^{ins/ins}$ embryos is not included in **Table 3.8**.

3.3.7. Novel findings

Although previous studies investigating the phenotypes of *Pkd2* null alleles have described abnormal phenotypes related to PKD2 function, including *situs*, heart structure, kidney and pancreatic cysts (Wu et al., 2000, Pennekamp et al., 2002), the broad-spectrum phenotypic analysis using μCT has revealed a number of novel phenotypes in which PKD2 could play an important role. These phenotypes were observed in both *Pkd2* null homozygotes (see section **3.2.2**), as well as the novel CC mutant alleles (see sections **3.2.3**-**3.2.6**), although the incidence of the novel phenotypes varied in between alleles (see **Appendix 2**).

Nervous system phenotypes were observed, affecting the mesencephalic vesicle, 3rd ventricle, lateral ventricles, cerebellum, choroid plexi, lateral extremities of the 4th ventricle, trigeminal ganglia, olfactory lobe, subarachnoid space and DRG were observed. These phenotypes were present in *Pkd2*$^{del/del}$, *Pkd2*$^{fsX7/del}$, *Pkd2*$^{fsX7/fsX7}$, *Pkd2*$^{S818X/del}$, *Pkd2*$^{S818X/S818X}$ and *Pkd2*$^{R870X/R870X}$ embryos. Notably, the incidence of these phenotypes was reduced in *Pkd2*$^{fsX7/del}$, but more so in *Pkd2*$^{fsX7/fsX7}$ embryos. Submandibular salivary gland, thymus and soft palate abnormalities (including cleft palate) were also observed. In *Pkd2*$^{del/del}$, *Pkd2*$^{S818X/del}$, *Pkd2*$^{S818X/S818X}$ and *Pkd2*$^{R870X/R870X}$, these phenotypes were encountered in all samples; in *Pkd2*$^{fsX7/del}$ and more so in *Pkd2*$^{fsX7/fsX7}$, these phenotypes showed reduced incidence. Although previous studies have identified craniofacial abnormalities in embryos lacking *Pkd2* expression in neural crest-derived tissues (Khonsari et al., 2013), cleft palate in *Pkd2* mutants has not been previously reported. This would argue for a role for PKD2 in craniofacial development, independent of neural crest cells.

Circulatory system abnormalities, aside for heart *situs* and structure defects (atrial and ventricular abnormalities), were also observed, affecting patterning of both cardiac great vessels and the venous system. Abnormal cardiac great vessel patterning was observed in all of the phenotypes investigated aside for *Pkd2*$^{fsX7/fsX7}$, although the exact incidences of particular phenotypes within this

category varied between genotypes. Abnormal patterning of the venous system was similarly observed in all genotypes investigated, but showed reduced incidence in *Pkd2*$^{fsX7/del}$ and *Pkd2*$^{S818X/S818X}$, and was absent in *Pkd2*$^{fsX7/fsX7}$ embryos.

3.3.8. Conclusion

The analysis provided in this chapter shows that µCT is a reliable method that can be employed in performing broad-spectrum phenotypic analysis, particularly targeting kidney cyst and L-R determination phenotypes. Through this method, I have described the phenotypes produced by these alleles in varying genetic contexts: in a homozygous state, as well as compound heterozygous state, in the presence of a null allele. This was done in order to test the similarity of these alleles to that of the null allele described previously (Walker, 2016), as well as to infer on the role played by the PKD2 CC in different contexts.

Aside from the phenotypes observed in *Pkd2*$^{fsX7/fsX7}$ embryos, the results presented in this chapter do not clarify the role of the PKD2 CC region and its sub-regions. However, the results suggest that, within the context of PKD2-based complexes, the CC region may play a role in regulating the function of the complex. The results do suggest, however, that the PKD2 CC appears to be more important in some contexts, such as kidney development. These points are discussed in more detail in section **4.1.4**.

This analysis also provided a comparison in terms of the severity of the phenotypes produced. Based on the incidences of lethality encountered, a hierarchy of genotypes can be produced (**Fig. 3.26**). Differences in lethality between the genotypes also argue that *Pkd2*^{fsX7}, *Pkd2*^{S818X} and *Pkd2*^{R870X} are different from the null allele. The overarching implications of the results described in this chapter for the hypotheses formulated in the previous chapter are discussed in **Chapter 4**.

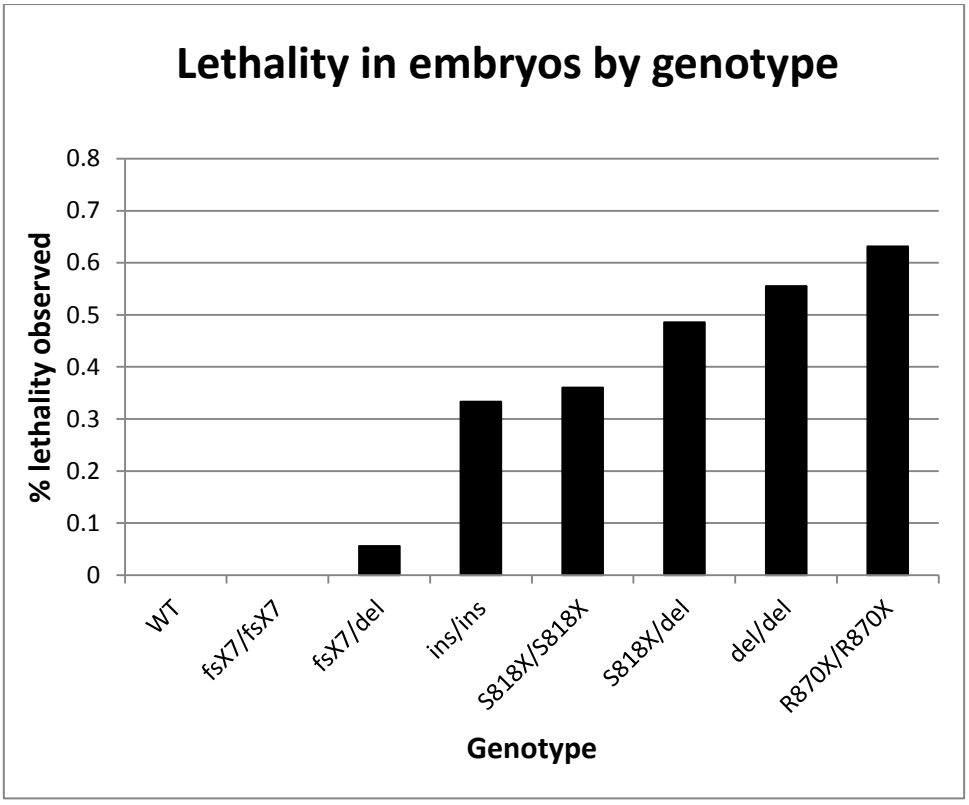


Figure 3.26: Lethality in embryos by genotype. Depicted is the percentage of embryos found dead at the point of dissection, according to genotype. Numbers are given in **Table 3.8**. N.B.: only three embryos were analysed for *Pkd2*$^{ins/ins}$.

Table 3.8: Incidences of phenotypes observed in *Pkd2* mutant embryos

Phenotype	Genotype					
	***Pkd2*$^{del/del}$**	***Pkd2*$^{fsX7/del}$**	***Pkd2*$^{fsX7/fsX7}$**	***Pkd2*$^{R870X/R870X}$**	***Pkd2*$^{S818X/del}$**	***Pkd2*$^{S818X/S818X}$**
Oedema*	16/18 (88.89%)	18/18 (100%)	22/22 (100%)	8/8 (100%)	20/20 (100%)	17/17 (100%)
Severe	4/4 (100%)	12/18 (66.66%)	3/22 (13.63%)	8/8 (100%)	19/20 (95%)	16/17 (94.11%)
Venous system abn.	4/4 (100%)	3/5 (60%)	0/9	5/6 (83.33%)	4/7 (57.14%)	6/7 (85.71%)
Great vessels						
normal	0/4	13/16 (81.25%)	13/13 (100%)	4/9 (44.44%)	2/13 (15.38%)	1/11 (9.09%)
IAA	0/4	2/16 (12.5%)	0/13	1/9 (11.11%)	4/13 (30.77%)	1/11 (9.09%)
Fused vessels	1/4 (25%)	1/16 (6.25%)	0/13	1/9 (11.11%)	2/13 (15.38%)	1/11 (9.09%)
Other**	2/4 (50%)	0/16	0/13	2/9 (22.22%)	4/13 (30.77%)	8/11 (72.72%)
Reversed aortic arch***	2/4 (50%)	0/16	0/13	3/9 (33.33%)	3/13 (23.08%)	7/11 (63.63%)
Lung *situs* (R:L)						
4:1	0/27	13/16 (87.5%)	13/13 (100%)	0/16	2/17 (11.76%)	0/16
1:1	0/27	1/16 (6.25%)	0/13	0/16	0/17	0/16
1:2	0/27	0/16	0/13	1/16 (6.25%)	0/17	2/16 (12.5%)
1:4	1/27 (3.7%)	0/16	0/13	0/16	0/17	0/16
3:2	1/27 (3.7%)	0/16	0/13	1/16 (6.25%)	0/17	0/16
3:3	0/27	0/16	0/13	0/16	1/17 (5.88%)	0/16
3:4	0/27	0/16	0/13	1/16 (6.25%)	0/17	0/16
3:5	0/27	0/16	0/13	0/16	1/17 (5.88%)	0/16
2:1	0/27	1/16 (6.25%)	0/13	0/16	0/17	0/16
2:2	1/27 (3.7%)	0/16	0/13	0/16	0/17	0/16
2:4	0/27	0/16	0/13	1/16 (6.25%)	0/17	0/16
4:2	1/27 (3.7%)	0/16	0/13	0/16	3/17 (17.65%)	3/16 (18.75%)
4:3	2/27 (7.41%)	0/16	0/13	7/16 (43.75%)	5/17 (29.41%)	3/16 (18.75%)
4:4	21/27 (77.78%)	0/16	0/13	2/16 (12.5%)	5/17 (29.41%)	7/16 (43.75%)
4:4+	0/27	0/16	0/13	0/16	0/17	1/16 (6.25%)
4+:4	0/27	1/16 (6.25%)	0/13	3/16 (18.75%)	0/17	0/16

Table 3.8 (continued)

Phenotype	Genotype					
	***Pkd2*$^{del/del}$**	***Pkd2*$^{fsX7/del}$**	***Pkd2*$^{fsX7/fsX7}$**	***Pkd2*$^{R870X/R870X}$**	***Pkd2*$^{S818X/del}$**	***Pkd2*$^{S818X/S818X}$**
Cysts						
Pancreatic cysts	4/4 (100%)	5/5 (100%)	3/9 (33.33%)	6/6 (100%)	7/7 (100%)	7/7 (100%)
Kidney cysts	4/4 (100%)	8/8 (100%)	14/14 (100%)	7/7 (100%)	10/10 (100%)	10/10 (100%)
Heart *situs*						
normal	11/26 (42.31%)	16/16 (100%)	13/13 (100%)	6/16 (37.5%)	9/18 (50%)	4/16 (25%)
dextrocardia	11/26 (42.31%)	0/16	0/13	6/16 (37.5%)	5/18 (27.78%)	10/16 (62.5%)
mesocardia	4/26 (15.38%)	0/16	0/13	4/16 (25%)	4/18 (22.22%)	2/16 (12.5%)
Heart structure						
Ventricular abn.	3/4 (75%)	5/5 (100%)	0/9	4/6 (66.67%)	6/7 (85.71%)	6/7 (85.71%)
Atrial abn.	2/4 (50%)	1/5 (20%)	0/8	5/6 (83.33%)	6/7 (85.71%)	7/7 (100%)
Stomach *situs*						
left	3/7 (42.85%)	15/16 (93.75%)	13/13 (100%)	8/16 (50%)	8/17 (47.06%)	5/15 (33.33%)
right	4/7 (57.15%)	1/16 (6.25%)	0/13	8/16 (50%)	9/17 (52.94%)	10/15 (66.67%)
Lethality****	20/36 (55.56%)	1/18 (5.55%)	0/22	12/19 (63.16%)	17/35 (48.57%)	9/25 (36%)

N.B.: analysis of *Pkd2*$^{del/del}$ embryos includes phenotypes previously described (Walker, 2016). Oedema* was only scored for embryos that were alive or died at the stage of littermates found alive. Other** great vessel abnormalities include transposition of the great arteries and DORV. Reversed aortic arch*** can coincide with other phenotypes observed for the great vessels. Lethality**** was scored if the embryo was found dead at the point of dissection. Normal *situs* categories are bolded and underlined. Abn. short for abnormality.

Chapter 4: Final discussion and further work

4.1. Summary and interpretation of results

4.1.1. Molecular mechanisms of the PKD1L1-PKD2 interaction

In **Chapter 2** I presented work indicating that the molecular mechanisms of PKD1L1-PKD2 interaction differ from those of PKD1-PKD2. Initially, given the homology between PKD1L1 and PKD1, as well as the fact that previous studies had suggested that the interaction of either complex occurs through the CC domains, I had hypothesised that the two complexes interact similarly. However, mutations predicted to disrupt the CC region of PKD2 (see section **2.2.1**) did not abolish the interaction between PKD1L1 and PKD2 fragments (see section **2.2.3**). These findings suggest that the PKD2 CC is not required for PKD1L1-PKD2 interaction. Upon attempting to repeat the experiments which suggested that the CC of PKD1L1 is sufficient for the PKD1L1-PKD2 interaction (Field et al, 2011), I obtained different results from those presented in the previous study (see section **2.2.5**). Considering that the same results were consistently obtained in my hands, under different experimental conditions, the previous study may have reported false positive results. However, the presence of the PKD1L1 CC mutation, previously suggested to disrupt the PKD1L1-PKD2 interaction (Field et al, 2011), did appear to weaken the PKD1L1-PKD2 interaction.

A number of PKD2 fragments of different lengths were generated, in order to test the interaction of PKD1L1-PKD2 in the presence of PKD2 mutations; these mutations were predicted to disrupt the CC domain (see section **2.2.1**). In spite of this prediction, the PKD1L1-PKD2 fragment interaction was disrupted only in the presence of the shortest PKD2 fragment, EFh-COOH, which contains no TMs, but contains the EF-hand and the CC. However, the longer PKD2 fragments, containing TMs, were able to interact with PKD1L1; this could be explained by one of two possibilities. Either the PKD1L1-PKD2 interaction requires membrane anchorage of PKD2, or PKD2 contains a yet-uncharacterised interaction domain in the proximity of the sixth TM. The C630

residue which lies in this region and was previously shown to be required for PKD2 homo-oligomerization, was tested and shown not to be necessary for PKD1L1-PKD2 interaction (see section **2.2.4**). Considering that previous reports have shown that protein fragments of PKD1 and PKD2 consisting only of the CC, but no TMs (see **Table 2.1**), are able to interact, it is unlikely that there is a requirement for PKD2 membrane anchorage, unless there are differences in the molecular mechanisms involved in the PKD1L1-PKD2 interaction.

In spite of the fact that two of the PKD2 fragments generated appeared to interact normally with both full-length PKD2 and a PKD1L1 fragment (see section **2.2.2**), their behaviour was different, when compared to the full-length protein, in terms of interacting with proteins other than PKD1L1. Specifically, the TM5-COOH fragment was prone to purifying a protein which does not interact with PKD2, NPR3, in contrast to the full-length PKD2 protein (see section **2.2.6**). This can potentially be explained by the fact that the protein fragments are prone to artefactual interactions, potentially hydrophobic interactions based on TMs. Given this finding, this could also explain the differences in results, with regards to PKD1-PKD2 interactions (see section **2.2.5**), from those reported in previous studies (see section **2.1.1**). Generally, when attempting to address PKD1-PKD2 interaction, the majority of groups employed different techniques to characterise these interactions – both between different studies, as well as the work presented in **Chapter 2**. These studies also used different protein fragments of both PKD1 and PKD2 in the experiments described. The techniques and fragments used are summarised in **Table 2.1**. Alternatively, the PKD1 protein fragment used to test the interaction with PKD2 in section **2.2.5** may contain other interaction domains yet to be characterised.

In order to test the validity of the results presented in **Chapter 2**, as well as explain differences in results obtained, as compared to previous studies, further work will be required. This is addressed in section **4.2.1**, where I propose experiments to further characterise the mechanisms of PKD1L1-PKD2 interaction, as well as attempt to clarify and reconcile my findings with those of

previous reports. However, if the results presented in **Chapter 2** are valid, it would appear that the molecular mechanisms of PKD1L1-PKD2 interaction are different from those of PKD1-PKD2.

4.1.2. Phenotypic analysis of CC mutants

In order to validate the results obtained in **Chapter 2**, I performed analysis of kidney and L-R phenotypes, on embryos carrying PKD2 mutations analysed through biochemical methods: R870X or S818X. Using CRISPR/Cas9, four alleles of *Pkd2* were generated, henceforth referred to as CC mutant alleles: 1) $Pkd2^{fsX7}$; 2) $Pkd2^{R870X}$; 3) $Pkd2^{S818X}$ and 4) $Pkd2^{ins}$ (see section **3.2.1**). To be able to fully assess whether these mutant alleles produce phenotypes that differ from those observed in *Pkd2* null embryos, I phenotyped $Pkd2^{del/del}$ embryos using µCT. Although $Pkd2^{del/del}$ embryos were previously analysed in terms of gross *situs* and kidney cysts (Walker, 2016), this broad-spectrum morphological analysis allowed me to better assess the differences and similarities between the phenotypes of CC mutant alleles and those of the null allele. Furthermore, performing µCT analysis also showed that this technique can identify kidney cysts, as well as *situs* phenotypes (see section **3.2.2**). The µCT-based analysis was capable of recapitulating the data published in other studies phenotyping *Pkd2* null embryos (Wu et al., 2000, Pennekamp et al., 2002), confirming previously described abnormal phenotypes, but also described novel phenotypes.

4.1.2.a. $Pkd2^{fsX7}$

The $Pkd2^{fsX7}$ allele produces PKD2 protein that lacks the hetero-oligomerization sub-region of the CC; this sub-region was previously shown to be involved in PKD1-PKD2 fragment interaction. The allele was analysed in the context of two genotypes: $Pkd2^{fsX7/del}$ and $Pkd2^{fsX7/fsX7}$. Whilst embryos of both genotypes showed cystic kidneys, only $Pkd2^{fsX7/del}$ embryos displayed L-R phenotypes. However, the phenotypes observed were different from those observed in $Pkd2^{del/del}$ embryos (see section **3.2.3**), arguing that $Pkd2^{fsX7}$ is not a null allele of *Pkd2*. Furthermore, these findings argue that the CC of PKD2 may not be necessary in the interaction with PKD1L1, given the absence of L-R phenotypes

in *Pkd2*$^{fsX7/fsX7}$, and the role played by the PKD1L1-PKD2 complex in L-R determination. The presence of abnormal L-R phenotypes observed in *Pkd2*$^{fsX7/del}$ embryos could be explained by one of two potential mechanisms. On one hand, the PKD2 protein levels could be decreased due to *Pkd2*^{del}, which has previously been shown to not produce any protein (Garcia-Gonzalez et al., 2010, Walker, 2016), as well as the *Pkd2*^{fsX7} allele, to a lesser extent. On the other hand, the L-R phenotypes observed may be caused by a combination of lower protein levels, as well as a mild negative effect of the *Pkd2*^{fsX7} allele (a recessive antimorph), somehow impacting the normal functioning of the PKD2^{fsX7} protein (see section **3.3.3**). These results are consistent with the hypothesis that the interaction of the PKD1L1-PKD2 complex is different to that of PKD1-PKD2, in terms of molecular mechanisms.

4.1.2.b. *Pkd2*^{S818X}

Unlike the *Pkd2*^{fsX7} allele, the *Pkd2*^{S818X} allele produced both L-R and kidney phenotypes, either in the homozygous state, or in the presence of the *Pkd2*^{del} allele. However, the phenotypes observed and the incidence of abnormal phenotypes argue that the *Pkd2*^{S818X} allele is different from *Pkd2*^{del} (see section **3.2.4**); these differences argue that *Pkd2*^{S818X} is not a null allele. *Pkd2*$^{S818X/del}$ embryos display a low incidence of normal *situs* for the cardiac great vessels and lungs, phenotypes that are not observed in *Pkd2*$^{del/del}$ embryos. Moreover, *Pkd2*$^{S818X/del}$ embryos display higher incidence of normal heart and stomach *situs*, as well as lower incidence of lethality, when compared to *Pkd2*$^{del/del}$ embryos. Given these findings, it would appear that the *Pkd2*^{S818X} allele is able to rescue the incidences of abnormal phenotypes observed in *Pkd2*$^{del/del}$ embryos (**Table 3.8**). Curiously, it appears that in *Pkd2*$^{S818X/S818X}$ embryos, some abnormal phenotypes are encountered more often than in *Pkd2*$^{del/del}$ embryos, such as: reversed aortic arch, dextrocardia and *situs inversus* for abdominal viscera (**Table 3.8**). However, it is worth remembering that, for some phenotypes, only a small number of *Pkd2*$^{del/del}$ embryos were assessed. These findings suggest that the effects of the

Pkd2^{S818X} allele may be more prevalent in some organ systems, perhaps affecting roles played by PKD2 that are more specific, or more important, for particular tissues.

The *situs* and kidney phenotypes observed in *Pkd2*$^{S818X/del}$ and *Pkd2*$^{S818X/S818X}$ can be explained by the hypothesis that the PKD1L1-PKD2 interaction is mechanistically different from PKD1-PKD2. Considering that the *Pkd2*^{S818X} allele produces protein lacking the entirety of the CC domain, I predict that either the PKD2-based complexes in *Pkd2*$^{S818X/del}$ and *Pkd2*$^{S818X/S818X}$ embryos are less stable, or the complexes are less likely to form, thereby affecting both PKD1- and PKD1L1-PKD2 complex function. Although Giamarchi and colleagues showed that the CC is not necessary for full-length PKD2 homo-oligomerization, the same study showed that cells expressing homo-oligomerization-deficient PKD2 molecules displayed abnormal Ca^{2+} currents. This potentially occurs by disrupting PKD1-PKD2 complex formation – necessary for inducing the currents (Giamarchi et al., 2010). This would fit with the concept that the stability or function of PKD2-based complexes is affected or compromised in *Pkd2*$^{S818X/S818X}$ and *Pkd2*$^{S818X/del}$ embryos (*vide supra*).

4.1.2.c. *Pkd2*^{R870X}

The *Pkd2*^{R870X} allele was initially expected to produce phenotypes similar to those observed in *Pkd2*^{fsX7}-carrying embryos. This was based on the fact that, like PKD2^{fsX7}, the PKD2^{R870X} protein lacks the hetero-oligomerization sub-region. Contrary to my expectations, *Pkd2*$^{R870X/R870X}$ embryos showed both L-R and kidney phenotypes, unlike *Pkd2*$^{fsX7/fsX7}$ embryos (see section **3.2.5**). Although *Pkd2*$^{R870X/R870X}$ embryos showed comparable incidences of heart and abdominal viscera *situs* phenotypes with *Pkd2*$^{del/del}$, the incidences of abnormal cardiac great vessel and lung *situs* phenotypes were different. Namely, a subset of *Pkd2*$^{R870X/R870X}$ embryos showed normal great vessel patterning, as well as 1:2 R:L lung lobation, which is similar to L-lung isomerism; neither of these phenotypes are observed in *Pkd2*$^{del/del}$ embryos. Furthermore, the *Pkd2*$^{R870X/R870X}$ genotype had a

higher incidence of lethality than any of the other genotypes analysed, including *Pkd2*$^{del/del}$. These findings argue that the *Pkd2*^{R870X} allele is not a null allele, and is different to *Pkd2*^{fsX7} and *Pkd2*^{S818X}.

The phenotypes of *Pkd2*$^{R870X/R870X}$ embryos might result from differing interaction mechanisms between the PKD1L1-PKD2 and PKD1-PKD2 complexes. Specifically, I propose that the *Pkd2*^{R870X} allele produces less protein and leads to impaired PKD2 function. One potential scenario, outlined in section **3.3.5**, is based on the model that PKD1 molecules displace PKD2 molecules in a polycystin tetramer (see section **2.1.2**). In the presence of the *Pkd2*^{R870X} allele, PKD2 levels are lower and the protein produced has a higher affinity for homo-oligomerization. This would only work if PKD1, or a paralog, competes for participation in PKD2-based complexes with other PKD2 molecules. Hypothetically, the inability of PKD1 to displace a PKD2 molecule in order to participate in this complex, due to absence of the hetero-oligomerization sub-region, could explain the kidney phenotypes observed. Similarly, the L-R phenotypes can be explained due to the increased homo-oligomerization affinity of the PKD2^{R870X} molecule, thereby reducing the likelihood of interacting with PKD1L1. Considering that *Pkd2*$^{fsX7/fsX7}$ embryos do not display L-R phenotypes, but *Pkd2*$^{R870X/R870X}$ embryos do, the model described above can also be used to explain the differences between the PKD2^{fsX7} and PKD2^{R870X} proteins. The PKD2^{fsX7} protein could have a disrupted homo-oligomerization sub-region of the CC, impacted by the changes in AA, and therefore lower homo-oligomerization affinity than PKD2^{R870X}. This would also imply that the *Pkd2*^{fsX7} allele rescues the increased homo-oligomerization affinity of the protein, hypothesised for the *Pkd2*^{R870X}. The kidney phenotypes observed in *Pkd2*$^{fsX7/fsX7}$ and *Pkd2*$^{R870X/R870X}$ can still be explained by lack of interaction of PKD2 with PKD1, due to absence of the hetero-oligomerization sub-region.

4.1.2.d. *Pkd2*^{ins}

The *Pkd2*^{ins} allele was not characterised to the same extent as the other *Pkd2* alleles, primarily due to time constraints. This allele was included in the analysis as the mutation it carries is

shared with *Pkd2*^{S818X}. However, in *Pkd2*^{S818X}, the *Pkd2*^{ins} mutation is unlikely to affect the protein, given that the protein is truncated upstream of the insertion of an in-frame codon. It is possible that this might exert an influence at the mRNA level. Although *Pkd2*$^{ins/ins}$ did display, contrary to my expectations, both abnormal kidney and L-R phenotypes (see section **3.2.6**), the embryos displayed left isomerism of the lungs, a phenotype not observed in *Pkd2* null or *Pkd2*$^{S818X/S818X}$ embryos. Ideally, a larger set of *Pkd2*$^{ins/ins}$ embryos should be analysed to further define the *Pkd2*^{ins} phenotype. The effect that the *Pkd2*^{ins} mutation has at the protein level is the insertion of an arginine residue in a stretch of three repeating arginine residues, at the beginning of the CC region. If the CC region is disrupted in PKD2^{ins} proteins, then the incidences of phenotypes and abnormal phenotypes displayed by *Pkd2*$^{ins/ins}$ and *Pkd2*$^{S818X/S818X}$ embryos might be identical. A second possibility is that the PKD2^{ins} protein may only have partially-disrupted the CC region; this might explain potential differences in the phenotypes observed (see section **3.3.6**).

4.1.2.e. Inference of mechanisms

Mechanistically, the *situs* phenotypes observed could be explained primarily by the effects that the CC mutant alleles have on the proper initiation of the L-R genetic pathway (see section **1.3**). The heart and lungs are especially sensitive to abnormal expression of the *Nodal-Pitx2* pathway in the LPM (Ramsdell, 2005). The *situs* of these organs provides a readout of the *Nodal-Pitx2* expression in the LPMs. For the purposes of this analysis, a few categories were defined for determining lung *situs*: normal (4:1), *situs inversus* (1:4), L-lung isomerism (1:1), R-lung isomerism (4:4), R-isomeric and R-supernumerary (4+:4), R-isomeric and L-supernumerary (4:4+) and randomised. These lung morphologies can be used to infer the expression of members of the L-R genetic pathway in the LPM, and by extension, the asymmetric activation of *Cerl2* and *Nodal* around the node, both thought to lie downstream of PKD2 in this tissue (see section **1.3.3**). In essence, the *situs* phenotypes observed could be caused by abnormal PKD2 function, in the CC mutant genotypes of interest, leading to abnormal *Cerl2* and, consequently, *Nodal* activation around the embryonic

node – either spatially (L-R randomised, bilateral, no activation), or temporally (delayed). This then impacts activation of *Nodal-Pitx2* in the LPM, leading to abnormal L-R determination.

The *Pkd2* null embryos largely display R-lung isomerism, a phenotype that indicates lack of *Nodal* in both LPMs (Pennekamp et al., 2002, Walker, 2016). In $Pkd2^{fsX7/del}$ embryos, the majority of embryos display normal lung *situs*; three embryos showed 1:1, 2:1 and 4+:4 R:L lobation. In the first two cases, this morphology is L-isomeric, or similar, indicating bilateral activation of the *Nodal-Pitx2* cascade. The 4+:4 phenotype potentially indicates lack of *Nodal* activation in either LPM. The lung *situs* phenotypes observed in $Pkd2^{S818X/del}$ and $Pkd2^{S818X/S818X}$ embryos mostly consist of R-isomeric lobation patterns (4:4 R:L) or randomised, with a tendency towards R-isomeric (4:3, 4:2 R:L). These can be explained by lack of *Nodal* activation in the left LPM, or low or delayed *Nodal* expression in the left LPM (Norris et al., 2002), respectively. The other abnormal lung lobation phenotypes observed, 3:3, 3:5 R:L in $Pkd2^{S818X/del}$ embryos, or 4:4+ R:L in $Pkd2^{S818X/S818X}$ embryos, can also be potentially explained by reduced or absent *Pitx2* activation in both LPMs. Similarly, the majority of lung lobation phenotypes observed in $Pkd2^{R870X/R870X}$ embryos, 4:3 R:L, as well as the R-isomeric phenotypes, can be explained from the perspective of impacted activation of the *Nodal* cascade in the left LPM. The R- and L- isomerism phenotypes observed are likely caused by absent and bilateral *Nodal* activation around the node, respectively. In contrast, delayed activation and/or abnormal asymmetric activation of *Nodal* around the node could underlie the randomised lung morphologies observed. Both heart and abdominal viscera *situs* were randomised in the genotypes analysed, except for $Pkd2^{fsX7/del}$ and $Pkd2^{fsX7/fsX7}$ embryos.

The phenotypes observed can be explained largely through the activation of the L-R genetic pathway. Other phenotypes, such as patterning of the great vessels and venous system, as well as ventricular and atrial L-R identity, are likely influenced by *Nodal-Pitx2* cascade activation. However, they may also involve a local function, to a greater or lesser extent, played by *Pkd2* in their respective developmental processes. Similarly, differential L-R lung lobation may primarily depend

on *Nodal* cascade activation, but may also involve a localised role for PKD2, which could explain the supernumerary lobation phenotypes observed (4+:4, 4:4+ R:L).

4.1.3. Synthesis

The results presented in **Chapter 2** and **Chapter 3** support the hypothesis that the PKD1L1-PKD2 interaction employs different molecular mechanisms than the PKD1-PKD2 complex. More specifically, the PKD1-PKD2 complex appears to require the CC domains of both proteins, whilst the interaction of PKD1L1 with PKD2 is less reliant on the CC domains. In spite of the apparent lack of requirement of the CC in the PKD1L1-PKD2 interaction, this domain appears to be required for the normal functioning of the complex, as evidenced by mouse mutants lacking this domain. This picture is complicated by the fact that PKD2 CC homo-oligomerization is required for complex formation, when considering interacting partners such as PKD1. Although the CC is not required for PKD2-PKD2 interaction, which can be facilitated by other interaction domains in its absence, the potential impact of CC absence on PKD2 function could explain some of the phenotypes observed in PKD2 CC-deficient embryos.

4.1.4. The role of the PKD2 CC

The work presented in this thesis argues that the CC domain of PKD2 plays more than a simple interaction role. Undoubtedly, at the level of a single PKD2 molecule, the CC of PKD2 participates in the interaction of PKD2 with binding partners, especially other PKD2 molecules, as well as PKD1. However, at the level of PKD2-based complexes, the CC may act to regulate the function of the complex itself – perhaps even channel activity – by mediating interactions with binding partners, such as PKD1L1. These potentially-competitive interactions, between PKD2 molecules and their binding partners, either enhance or downregulate the activity or function of the complex. This model could explain the differences observed in phenotypes, and correlation – or lack of – between L-R, kidney and other phenotypes.

4.2. Future work

4.2.1. Chapter 2

The most important question regarding the results presented in **Chapter 2** is whether or not the data is valid, given the results shown in sections **2.2.6**, as well as **2.2.5**. The PKD2 protein fragments used appear to be more prone to interactions that do not occur when using the full-length protein. In order to validate whether PKD2 is able to interact with PKD1L1, in the presence of CC mutations, the mutations could be tested in the context of the full-length protein. However, given that the PKD1L1-PKD2 interaction likely involves domains other than the CC (Salehi-Najafabadi et al., 2017), further mutational analysis may be required by subsequently testing proteins lacking one or more interaction domains. A different approach would be to test the same interactions using a different technique, such as Förster Resonance Energy Transfer (FRET) – this would allow the study of PKD1L1-PKD2 interaction in the context of a live cell. This approach could be combined with the testing of PKD2 function, by using a genetically-encoded Ca^{2+} sensor. Furthermore, by adding a flow-chamber, the dynamics of the FRET pair-tagged proteins, as well as downstream Ca^{2+} signalling, could be assessed for the PKD1L1-PKD2 complex, in the presence of the mutations of interest. This experiment would allow the dynamics of the PKD1L1-PKD2 interaction, at the molecule level, to be assessed, as well as how the complex reacts in response to flow.

The effect of the CC mutations described in **Chapter 2** on protein localisation could help provide further mechanistic insights into the PKD1L1-PKD2 interaction. For the proteins bearing CC mutations, these localisation experiments can be done *in vivo* and might help better explain the phenotypes observed. Ideally, these experiments would involve the localisation of both PKD2 and PKD1L1. However, in the absence of a reliable antibody for PKD1L1, any localisation experiments targeting the PKD1L1-PKD2 complex can only be performed using exogenous tags, and most likely in overexpression systems.

Considering that the shortest PKD2 fragment analysed (EFh-COOH) is unable to interact with the PKD1L1 fragment, there are two possibilities: either the PKD1L1-PKD2 interaction requires plasma membrane anchorage of PKD2, or there is a yet-uncharacterised interaction domain in the proximity of TM6 of PKD2. In order to test this, a Co-IP experiment can be performed with a recombinant version of the TM6-COOH PKD2 fragment, having the TM replaced with that from a protein which does not interact with PKD1L1 or PKD2. Subsequently, the donor protein would have its TM replaced by TM6 of PKD2, and the interaction of this recombinant protein with PKD1L1 would be tested. Finally, the TM domain of the donor protein can be appended to EFh-COOH, and the interaction of this recombinant protein with PKD1L1 tested, in order to test for plasma membrane anchorage requirement. This exact series of experiments can then be repeated with PKD1. Alternatively, in order to validate the PKD1-PKD2 fragment interactions, fragments of PKD1 from previously published studies can be tested for interaction with PKD2.

4.2.2. Chapter 3

Ideally, higher numbers of *Pkd2*$^{del/del}$ embryos should be analysed by µCT, in order to better characterise this allele in terms of cardiac great vessel and stomach *situs*, as well as heart structure defects. To characterise the *Pkd2*^{ins} allele in a manner comparable to the other CC mutant alleles, µCT analysis should be performed on comparable numbers of embryos. Furthermore, gross *situs*, histological sectioning of kidneys and broad-spectrum phenotyping should be performed on *Pkd2*$^{ins/del}$ embryos. Similarly, the same analysis should be performed on *Pkd2*$^{R870X/del}$ embryos, in order to further assess the differences between the *Pkd2*^{R870X} allele from *Pkd2*^{del}. To test whether any of CC mutant alleles are dominant negative, heterozygous animals should be aged and phenotyped, particularly assessing formation of kidney cysts, as well as cyst formation in other organs.

Analysis of the activity of PKD2 as a channel, in the presence of the CC mutations, will provide further mechanistic insight. Together with the FRET experiment proposed in section **4.2.1**, this will help further test whether the mutations analysed impact PKD2 interactions, and/or have an impact on the activity of the channel. A comparison of PKD2 channel function, in the presence or absence of the CC mutations, as well as interacting partners of PKD2, will help explain the phenotypes observed and further test the model proposed in section **4.1.4**. That is, at the complex level, the PKD2 CC acts to regulate the activity of the channel in response to physically interacting with binding partners, by determining the composition of the channel complex.

To be able to assess the differences or similarities between the CC mutant alleles, in the kidney cyst phenotype, further analysis should be performed to assess cyst volumes, percentage of cystic tissue as compared to total kidney volume, and a comparison between total kidney volumes of WT and mutant samples. Aside for helping to determine and quantify potential differences in mutational impact on renal pathology, this will also test the notion that the PKD2 CC is more important for renal development.

Previous publications have established a link between PKD1 protein level and cystogenesis; mice producing 40% of the WT level of PKD1 protein develop cysts gradually, whilst mice producing 20% of the WT level of PKD1 protein exhibit rapidly-progressing cystic disease (Hopp et al., 2012). The level of PKD2 protein has also been proposed to relate to some of the phenotypes observed in *Pkd2* nulls. For example, in the kidney, the level of PKD2 protein found in $Pkd2^{del/+}$ embryos is 50%, of that in WT kidneys (Walker, 2016). Considering that $Pkd2^{del/+}$ embryos do not display kidney cysts, 50% of the PKD2 protein level appears to be sufficient for renal development. The CC mutant alleles could potentially exhibit abnormal protein levels, due to degradation of the protein or nonsense-mediated decay of the mRNA. Different tissues may require different levels of protein, which could explain the differences in phenotypic severity, and incidence, for some of the genotypes analysed. To test whether the CC mutant alleles lead to lower levels of PKD2 protein, and to further

differentiate these from *Pkd2*^{del}, protein should be extracted from tissues of interest, such as kidneys, thymus, central nervous system, as well as whole embryos, and compared to that in WT samples.

In order to explain why the *Pkd2*^{fsX7} and *Pkd2*^{R870X} produce different phenotypes, the structure of the CC region in these proteins should be assessed and compared to the WT CC. This will address whether these mutations affect the upstream homo-oligomerization sub-region of the CC. As argued in section **4.1.2.c**, the PKD2^{R870X} may have a higher affinity for homo-oligomerization than PKD2^{fsX7}. I suggest that the for the PKD2^{fsX7} protein, the frameshift mutation disrupts the homo-oligomerization sub-region, thereby rescuing the potentially increased affinity for PKD2-PKD2 interactions of the PKD2^{R870X} protein.

As mentioned in section **4.1.2.e**, the *situs* phenotypes displayed by embryos carrying CC mutant alleles can be explained from the perspective of activation of the *Nodal* cascade. However, some of the phenotypes observed also argue for a more localised role played by *Pkd2*. In order to ascertain whether *Pkd2* plays a direct role, an indirect one (by activating the *Nodal* cascade), or both, gene expression studies characterising the L-R asymmetric pathway should be performed on the genotypes of interest at the relevant stages. Although Yoshiba and colleagues established that PKD2 is only required in the node crown cells for normal L-R development, this study only assessed the expression of *Nodal* and *Pitx2* in the LPM (Yoshiba et al., 2012), not L-R development at the level of organ morphology. This will help clarify the roles played by *Pkd2* in the developmental processes involved in the phenotypes observed.

Finally, performing phenotypic analysis in other species, such as zebrafish, using the same mutations will provide information on how well-conserved the PKD1L1-PKD2 function is, in terms of L-R patterning. It will also reveal the conservation in function of other PKD2-based complexes, within other contexts, including kidney development and patterning of the circulatory system.

Furthermore, this approach may potentially provide alternate means of further investigating this interaction, not available in the mouse embryo.

4.3. Conclusion

The data presented across the two chapters suggests that the interaction of PKD1L1 with PKD2 is mechanistically different from that of PKD1-PKD2. Considering the data, this work presents, for the first time, a separation between the roles played by PKD2 in L-R development, and those played in renal development and homeostasis.

The biochemical analysis presented in **Chapter 2** argues that the CC domain of PKD2, a typical protein-protein interaction domain, is not required for the PKD1L1-PKD2 interaction. Although requiring validation, the work presented in this chapter could challenge the mechanisms suggested to underlie PKD1L1-PKD2 interaction, and potentially that of PKD1-PKD2. Furthermore, the work described in this chapter also indicates the involvement of an uncharacterised region of PKD2 in the interaction with PKD1L1 and potentially PKD1.

The phenotypic analysis presented in **Chapter 3** presents a set of novel alleles used in the mouse to better understand the role of *Pkd2* in development. These alleles were initially designed to indirectly test the hypothesis that the molecular mechanisms of PKD1L1-PKD2 interaction are different from those of PKD1-PKD2. The results of phenotyping mice carrying these alleles support this hypothesis of differences, and distinguish the alleles from a null allele of *Pkd2.* Moreover, each of these alleles appears to be unique in terms of the phenotypes presented and their frequency of occurrence, providing tools for further investigating phenotypes in L-R development, patterning of the cardiac great vessels, patterning of the venous system and heart structure development.

Together, this thesis not only advises that there is a difference between the interaction mechanisms of PKD2 with PKD1L1 and PKD1, respectively, but also suggests that the CC region might play different roles under different circumstances. The model that I propose is that, in kidney development, the CC may facilitate the interaction between PKD1 and PKD2, whilst in L-R development, the CC is only required for PKD2 homo-oligomerization. Whilst the data indicates that

the PKD2 CC is necessary for the interaction with PKD1, it appears that the CC plays a different role in the interaction with PKD1L1, perhaps in indirectly regulating the activity of the complex. Considering the pleiotropic nature of the *Pkd2*, as well as its evolutionary conservation, valency as a property of PKD2 domains appears evident and intuitive. The ability of this protein to perform different functions, in distinct contexts, using the same domains, may underlie its pleiotropy, as well as its evolutionary conservation.

Chapter 5: Materials and methods

This section details information regarding mouse work and experimental methods used throughout the study. This section also contains a table with information regarding the composition of solutions referenced in the experimental methods, unless detailed in the relevant subsection – **Table 5.4**, as well as a table with catalogue numbers for the reagents used – **Table 5.5**. Where the work was done in collaboration with other groups or core facilities, this was specified in the relevant subsection.

5.1. Mouse work

All animal work was done in accordance with the Medical Research Council's guidance, published in 'Responsibility in the Use of Animals for Medical Research' (NC3R, 2017) and in accordance with the Animals (Scientific Procedures) Act, 1986. Ethical approval for all studies involving mouse work was obtained as part of the application for the UK Home Office Project Licence; all mice were kept in accordance with UK Home Office welfare guidance and Home Office project licence restrictions. Animals were maintained in controlled 12 hour light/dark cycles, temperature (21 ± 2 ˚C) and humidity (55 ± 10%). Mice had free access to water (10-12 ppm chlorine) and were fed *ad libitum* on a commercial diet (5.3% fat, 21.2% protein, 57.4% carbohydrate, 4.6% fibre; Rat and Mouse Diet No. 3, Special Diet Services, Essex, UK). Housing was provided in IVC cages, under pathogen-free conditions (FELASA screen), in groups of 2-5 mice until the start of the study.

5.1.1. Mouse handling

Adults were culled by cervical dislocation; embryos older than 14.5 dpc were culled through exsanguination in 1x PBS, by cutting the umbilical vein. The ages of the embryos were assessed beginning with the middle of the day when a copulation plug is found, defined as 0.5 dpc. Dissection of embryos and photography was performed using a dissection microscope.

5.1.2. Background and lines

The background of the mutant strains was C57BL/6J. The lines used throughout the study were the following:

i) *Pkd2*^{del}, obtained from a *Pkd2*$^{tm1.2Tjwt}$ allele (Garcia-Gonzalez et al., 2010), in the presence of an *Actin-cre* recombinase allele. The LoxP sites flank exons 11-13; this was obtained by a previous lab member and is described in (Walker, 2016).

ii) *Pkd2*^{em1H}, referred to as *Pkd2*^{fsX7}, in reference to amino acid change, obtained from CRISPR-Cas9 targeted mutagenesis. This allele was obtained as an off-target effect, resulting in the deletion of one nucleotide (c.2600delT); this results in a frameshift, changing the amino acid sequence and prematurely truncating the protein (p.Ile867ThrfsX7).

iii) *Pkd2*^{em2H}, referred to as *Pkd2*^{S818X}, in reference to amino acid change, obtained from CRISPR-Cas9 targeted mutagenesis. This allele contains several nucleotide changes (c.2452A>T, c.2454T>A, c.2467A>C, c.2469G>C, c.2475_2476insAGG), but only one amino acid change (p.Ser818X), leading to the complete truncation of the CC domain.

iv) *Pkd2*^{em3H}, referred to as *Pkd2*^{ins}, in reference to amino acid change, obtained from CRISPR-Cas9 targeted mutagenesis. This allele contains several nucleotide changes, which are shared with *Pkd2*^{em2H}: c.2467A>C, c.2469G>C, c.2475_2476insAGG; the only amino acid change is an insertion of an Arg: p.Arg825_Gly826insArg.

v) *Pkd2*^{em4H}, referred to as *Pkd2*^{R870X}, in reference to amino acid change, obtained from CRISPR-Cas9 targeted mutagenesis. This allele contains several nucleotide changes: c.2598G>A, c.2601C>T, c.2608_2609CG>TA, but only one amino acid change: p.Arg870X.

All lines carrying targeted CRISPR-Cas9 mutations – lines ii) to v) – were designed and engineered at Harwell by the Transgenics core facility.

5.1.3. Histology and µCT

Kidneys were collected from 15.5 dpc embryos and fixed in 4% PFA (w/v) solution for 24 hours, at 4 ˚C. Histological wax sectioning was performed by core services (Histology) of 15.5 dpc embryonic kidneys. The slides were scanned using a Hamamatsu NDP NanoZoomer brightfield scanner, at 20x magnification. For µCT, 15.5-16 dpc embryos were dissected, yolk sac was taken for genotyping and exsanguination was performed by cutting the umbilical artery in 1x PBS and removing the clot every 5 minutes. This process was repeated 3 times in order to remove as much blood as possible. Following exsanguination, embryos were photographed and fixed overnight in 4% PFA (w/v) in 6-well plates, on a rocker at 4 ˚C. Samples were then taken by core services (Transgenics) for further processing and scanning. Data analysis was performed using Fiji (Schindelin et al., 2012) and 3D Slicer (Fedorov et al., 2012). Segmentation was performed using ITK-SNAP (Yushkevich et al., 2006), using a combination of automatic and manual methods.

5.1.4. Genotyping

All genotyping was performed by core services (GEMS), using the following assays:

i) a Taqman wildtype copy count assay is used for genotyping the *Pkd2*^{del}, *Pkd2*^{em2H} (*Pkd2*^{S818X}), *Pkd2*^{em3H} (*Pkd2*^{ins}) and *Pkd2*^{em4H} (*Pkd2*^{R870X}) alleles. A FAM-labelled genotyping assay is run in multiplex with a VIC-labelled *Dot1l* internal control. The primers are described in **Table 5.1**.

ii) a Taqman allelic discrimination assay was used for genotyping the *Pkd2*^{em1H} (*Pkd2*^{fsX7}) allele. A FAM-labelled probe is used for detection of the WT allele, whilst a TET-labelled probe is used for detecting the mutant allele. The primers are described in **Table 5.1**.

N.B.: both genotyping assays were performed using the ABI Sample-to-SNP kit, according to manufacturer's instructions.

5.2. Tissue culture

All tissue culture work was performed using stringent aseptic technique, inside a biosafety cabinet. All consumables and cell stock vials were disinfected with 70% ethanol and/or 1% distel, prior to usage. Cells were maintained in incubators, at 37 ˚C, constant humidity and 5% CO_2, whilst stocks were stored long-term in liquid nitrogen, following freezing. Solutions used in maintenance of cell lines, such as growth media, D-PBS and trypsin, were pre-heated by incubating in a 37 ˚C waterbath prior to use.

5.2.1. Cell thawing

Vials of cell stocks were removed from liquid nitrogen storage and transferred to dry ice before thawing. Each vial was then transferred to a 37 ˚C waterbath, where it was incubated for up to approximately one minute, with gentle swirling, until thawed. Cells were resuspended gently and the volume of stock was transferred to a 10 cm^2 dish or T75 flask, containing pre-warmed growth media. Growth media was changed the following day, or the cells were passaged, if confluent.

5.2.2. Freezing cell stocks

Cells were expanded into as many 10 cm^2 dishes from a founder dish or T75 flask and grown until 90% confluent. Media was aspirated and cells were washed in 1 mL of the appropriate type of trypsin. Following trypsin wash removal, cells were then incubated with 1 mL of trypsin at 37 ˚C until detached. Once detached, trypsin was inactivated with 4 mL of complete growth medium, homogenised and transferred to a 15 mL falcon tube. Cells were pelleted by centrifugation at 120 x g (800 RPM) for 5 minutes. Following supernatant aspiration, cells were gently resuspended in 1 mL freezing medium, transferred to a cryovial and frozen in an isopropanol bath at -80 ˚C. Following freezing or short-term storage at -80 ˚C (2-7 days), cell stocks were transferred to liquid nitrogen for long-term storage.

5.2.3. Counting cells

Trypsinized cells were pelleted by centrifugation at 120 x g (800 RPM) for 5 min and resuspended in 10 mL complete growth medium. After preparation of the haemocytometer, 10 µL of cell suspension was added to the chamber by capillary action. Cells inside the grid, or touching the left or bottom edge of the grid, were counted. Each count was done in a 1 mm^2 area with 0.1 µL volume, four different areas were counted and averaged, to obtain the number of cells/0.1 µL. This was then converted to cells/mL, by multiplying with 10^4.

Table 5.1: Primer and probe sequences for *Pkd2* allele genotyping assays

Assay	Primer name/sequence	Probe name/sequence	Tag
Dot1l internal control	**Dot1L_2F**: TAGTTGGCATCCTTATGCTTCATC **Dot1L_R**: GCCCCAGCACGACCATT	**DotL_2M**: CCAGCTCTCAAGTCG	VIC
Pkd2^{del}	**Pkd2-DelF**: GGATGGCGACCAGGAACT **Pkd2-DelR**: CTCACCCTCTCTTTCTCCAAGTCAT	**Pkd2-DelP**: ACCGAGCGTGAGCATCAACAGATG	FAM
Pkd2^{fsX7}	**Pkd2-fsX7F**: TCCAAGATTGATGCCGTGATTG **Pkd2-fsX7R**: CATCCAGCAGCCGTCCTAAC	**Pkd2-fsX7WT**: TCAAGCTGGAGATCATGG **Pkd2-fsX7M**: TCAAGCTGGAGACATGGA	FAM TET
Pkd2^{ins} and ***Pkd2^{S818X}***	**Pkd2-iF**: AGACAGTGGCCATAGCTCCA **Pkd2-iR**: ATCCCGGTCAGCACAAACCT	**Pkd2-iWT**: TTCCCCTCCTCCTGG	FAM
Pkd2^{R870X}	**Pkd2-R870XF**: CCGTGATTGTCAAGCTGGAG **Pkd2-R870XR**: CGTCCTAACACCTCTCGTCTCTT	**Pkd2-R870XP**: CCCGCTCCATGATCTC	FAM

5.2.4. Passaging

Cells were grown until 80-90% confluent, after which growth media was aspirated and cells were washed with 10 mL pre-warmed D-PBS. Following removal of D-PBS, cells were incubated at 37 ˚C, until detached, in 1 or 2 mL of trypsin, for 10 cm^2 dishes or T75 flasks, respectively. Neutralisation of trypsin was done with 4 volumes of complete growth medium, in which the cells were re-

suspended. A fraction of the volume of cell suspension (splitting ratio) was then used to seed a new dish or flask containing fresh complete growth medium, depending on the growth rate of the cells and experimental requirements. Typically, the splitting ratio varied, between 1:3 to 1:20 (e.g. 4 or 1 mL of a 20 mL total cell suspension volume).

5.2.5. HEK293T line maintenance and handling

HEK293T cells were grown in high glucose, GlutaMAX-I DMEM, supplemented with 10% FBS in T75 flasks, unless used for making stocks or terminal experiments (e.g. CoIP), in which case they were grown in 10 cm^2 dishes. Cells were detached using trypsin-EDTA (0.05% w/v, 0.53 mM, respectively).

For CoIP, 2.5 x 10^6 cells were seeded in 10 cm^2 dishes and left to grow overnight. Transfection of 20 µg of desired expression vectors was performed using JetPEI, according to the manufacturer's specifications. The cells were incubated for 44-48 hours at 37 ˚C, prior to performing CoIP. Each transfection was done in duplicate, for all CoIP experiments.

5.2.6. COS-7 line maintenance and handling

COS-7 cells were grown in high glucose, Na-Pyruvate, GlutaMAX-I DMEM, supplemented with 10% FBS. Cells were maintained in T75 flasks, or grown on coverslips in 6-well plates for immunofluorescence experiments. Cells were detached using trypsin-EDTA (0.25% w/v, 0.53 mM, respectively).

For immunofluorescence, 2.5 x 10^5 cells were seeded in 6-well plates containing 3 coverslips/well and left to settle overnight. Transfection of desired expression vectors was performed using JetPEI, according to the manufacturer's specifications. The cells were incubated for 24 hours at 37 ˚C, prior to performing immunofluorescence.

5.2.7. mIMCD3 line maintenance and handling

mIMCD3 cells were grown in DMEM/F-12 media, supplemented with 10% FBS. Cells were maintained in T75 flasks, or grown on coverslips in 6-well plates for immunofluorescence experiments. Cells were detached using trypsin-EDTA (0.25% w/v, 0.53 mM, respectively).

For immunofluorescence, 2 x 10^5 cells were seeded in 6-well plates containing 3 coverslips/well and left to grow for 48 hours. Transfection of desired expression vectors was performed using Lipofectamine 3000, according to the manufacturer's instructions, and incubated for 24 hours at 37 ˚C. Serum starving was then carried out by replacing the complete growth medium with serum-free DMEM/F12 medium and incubating at 37 ˚C for 24 hours, in order to promote ciliation.

5.3. Immunofluorescence

Growth media was aspirated from each of the wells of the 6-well plate. Cells were fixed with 2 mL of cold (-20 ˚C) 100% methanol per well, by incubation at -20 ˚C for 4 minutes. Fixative was aspirated and samples were rinsed with 2 mL 1x PBS at room temperature. Blocking was done with 4% BSA (w/v) in 1x PBS at room temperature, for 30 minutes.

Primary antibody solutions were prepared in 4% BSA (w/v) in 1x PBS, at the dilutions specified in **Table 5.2.** A sterile parafilm surface was prepared, onto which 30 µL of the primary antibody solution was placed, for each of the coverslips. The coverslips were inverted onto the aliquoted solution and incubated in a dark, humidified chamber at room temperature for 1 hour. The coverslips were then inverted back into wells of a 6-well plate and subjected to three 5 minute washes with 2 mL 1x PBS per well. The same procedure was applied for incubation with secondary antibody-containing solutions (in 4% BSA in 1x PBS).

Following the 1x PBS washes, the coverslips were immersed in 1 mL ddH_2O, after which NucBlue Fixed Cell ReadyProbe reagent (DAPI) was added. After incubation for 1 minute at room temperature, the solution was aspirated and the coverslips were washed with ddH_2O for 5 minutes. The coverslips were then inverted onto Hydromount mounting medium, supplemented with 25 µg/mL DABCO, and left to set overnight at 4 ˚C. Images were taken on a Zeiss Axio Observer.Z1 confocal microscope.

5.4. Biochemistry

5.4.1. Coimmunoprecipitation using sepharose beads

Following 44-48 hours of incubation post-transfection, growth medium was aspirated from each dish and cells were gently rinsed with chilled (4 ˚C) 1x PBS. After aspiration of PBS, dishes were placed on ice and 150 µL of lysis buffer, containing 1x protease inhibitors, was added to each dish.

Duplicate samples were pooled following lysis. The following lysis buffers were used throughout the study:

i) RIPA I buffer (working concentration 1x)

ii) RIPA II buffer

iii) CIP buffer (working concentration 1x)

N.B.: RIPA I buffer was used for the majority of CoIP experiments; CIP and RIPA II buffer were used for comparing WT and mutant PKD1L1-CC-GFP ability to interact with PKD2.

Samples were cleared of cell debris by incubating at 4 ˚C on a rotating wheel for 20 minutes, followed by centrifugation for 10 minutes at 4 ˚C and 18705 x g (13000 RPM). A minimum of 30 µL of the supernatant was set aside for determining protein concentration, via Bradford assay, and use as lysate for later analysis. Protein G-conjugated sepharose beads were aliquoted (20 µL/sample) and

rinsed with lysis buffer, followed by centrifugation at 4 ˚C and 1000 x g for 1 min to pellet beads and remove lysis buffer. The rest of the lysate supernatant was incubated with the beads for 1 hour at 4 ˚C on a rotating wheel. *N.B.*: lysate volume varied between CoIP experiments, ranging from 300 µL to 650 µL; similarly, protein concentration varied both within samples of the same experiment, as well as between experiments, when considering the same sample.

Cleared lysates were spun at 4 ˚C and 1000 x g for 1 min to pellet beads. The supernatant was transferred to a fresh tube and 2 µg of antibody were added for every mg of protein in the pre-cleared lysate. *N.B.*: samples that were precipitated with more than one antibody were distributed, as equal volumes, into different tubes; an equal volume of lysis buffer, supplemented with protease inhibitor, was added to each split sample to reconstitute the original volume. The quantity of protein was determined by rounding off to a whole number. The lysate/antibody mixture was incubated at 4 ˚C on a rotating wheel, either overnight or for 2 hours.

Samples were then incubated with pre-washed sepharose beads for 1 hour at 4 ˚C, on a rotating wheel. Following this, beads were pelleted by centrifugation at 4 ˚C and 1000 x g, for 1 min, and the flowthrough was saved for later analysis, to determine the efficiency of the CoIP reaction. Beads were then washed thrice in 1 mL lysis buffer, at 4 ˚C on a rotating wheel, for 5 minutes. The last of the three washes was done in lysis buffer supplemented with protease inhibitor. After washing, the beads were left in approximately 20 µL of lysis buffer, to which 7.5 µL of LDS sample buffer (4x) and 2.5 µL reducing agent (10x) was added, in preparation for western blotting. Similarly, the lysate and unbound fractions were aliquoted (10 µL) and mixed with 3.75 µL LDS sample buffer (4x) and 1.25 µL reducing agent (10x). Prepared samples were stored at -20 ˚C for up to 3 days.

Table 5.2: Antibodies used throughout experiments

Antibody name	Target	Species	Dilution factor	Wavelength
Dnk-a-Rb650	Rabbit IgG	Donkey	1:400	650 nm
Gt-a-Ms488	Mouse IgG	Goat	1:250 (IF)	488 nm
Gt-a-Ms650	Mouse IgG	Goat	1:250	650 nm
Gt-a-Ms800	Mouse IgG	Goat	1:15000	800 nm
Gt-a-Rb488	Rabbit IgG	Goat	1:250	488 nm
Gt-a-Rb594	Rabbit IgG	Goat	1:400 (IF)	594 nm
Gt-a-Rb680	Rabbit IgG	Goat	1:15000	680 nm
Ms-a-AcTub	Acetylated tubulin	Mouse	1:500	—
Ms-a-GFP	GFP	Mouse	1:4000 (WB)	—
Ms-a-V5	V5	Mouse	1:300 (IF) 1:3000 (WB)	—
Rb-a-PKD2	PKD2	Rabbit	1:200	—
Rb-a-GluTub	Glutamylated tubulin	Rabbit	1:200	—
Rb-a-Myc	c-Myc	Rabbit	1:1000	—

N.B.: Antibody naming is as follows: for primary antibodies, the name contains 'a' and the epitope. For secondary antibodies, the first group of letters represents the species of origin, followed by '-a-', after which the target species or epitope, and emission wavelength for secondary antibodies, are mentioned. The letter 'a' represents 'anti'; Dnk: donkey; Gt: goat; IF: immunofluorescence; Ms: mouse; Rb: rabbit; WB: western blotting.

An alternate protocol was also used for testing the ability of PKD1L1-CC-GFP to interact with the shortest PKD2 fragment (EFh-COOH), or comparing the ability of WT or mutant PKD1L1-CC-GFP to interact with PKD2. The main differences are the following:

i) the buffer used was CIP, not RIPA I

ii) beads were washed before aliquoting for each individual samples – bulk washing

iii) antibody-lysate incubation was shorter (30 min)

iv) supernatant was completely removed from beads, following final wash; beads were resuspended in 80 µL 2x LDS/1x reducing agent (in ddH_2O)

v) lysate and unbound samples were prepared with an equal volume of 2x LDS/1x reducing agent (in ddH_2O)

5.4.2. Coimmunoprecipitation using kit

GFP- and Myc-trap beads were used for CoIP, following the manufacturer's instructions, to purify PKD1-CC-GFP protein complexes. *N.B.:* the lysis buffer recommended by the manufacturer is identical to CIP buffer (*vide supra* – **5.4.1**).

5.4.3. Western blotting

Samples were boiled at 95 ˚C for 10 min prior to loading on gels; 15 µL of each sample was loaded onto each well. Each gel was also loaded with 3 µL of BioRad Precision Plus Dual Color Standards for 4-12% Bis-Tris gels. Gels were run according to the manufacturer's instructions, in 1x MOPS SDS Running buffer or 1x Tris-Acetate SDS Running buffer, respectively. *N.B.*: Given that for CoIP reactions the concentration of protein could not be assessed in the IP fraction, the loading was done with equal volumes of sample. Any other experiments described involve the loading of equal quantity of protein, in 10 µL total volumes, as indicated in the instruction manuals of the gels.

Samples were then transferred using an Invitrogen iBlot Transfer Stack (Nitrocellulose) kit, for 8 minutes at 30 V. Blocking was done in 5% skim milk powder (w/v) in 1x TBST, for a minimum of 1 hour at room temperature with gentle rocking. Antibodies used for protein detection were also prepared in 5% skim milk powder in 1x TBST, at the dilutions specified in **Table 5.2**. Primary antibody incubation was done in 50 mL falcon tubes on a roller, either overnight at 4 ˚C or at room temperature for 2 hours. Membranes were then washed with 1x TBST for 5 minutes at room temperature, thrice, on a rocker. Secondary antibody incubation was done in 5% skim milk powder in 1x TBST for 1 hour at room temperature, in the dark, with gentle rocking. Following three more 5 minute washes in 1x TBST at room temperature, in the dark, membranes were air dried in the dark and scanned using a LI-COR Odyssey Sa.

5.5. Molecular biology

5.5.1. PCR amplification

Desired DNA sequences were amplified using the following reaction conditions: 1x TaqPCR MasterMix, 0.5 µM forward and reverse primers, DNA (variable concentration) and ddH_2O. Reactions were performed on a GStorm thermocycler, according to the TaqPCR MasterMix manufacturer's instructions. Primer sequences are provided in **Table 5.3**. Annealing temperatures were determined by first performing optimisation reactions, across a 10 ˚C temperature gradient (5 ˚C on either side of Tm).

5.5.2. PCR-based mutagenesis

A PCR-based method was employed to mutagenize sequences of interest in multiple reactions. The process is summarised in **Figure 5.1**. The reaction was similar in composition to normal PCR amplification, but also contained Q5 high-fidelity DNA polymerase (1 U) and 0.5x Q5 buffer. Primers used are described in **Table 5.3**.

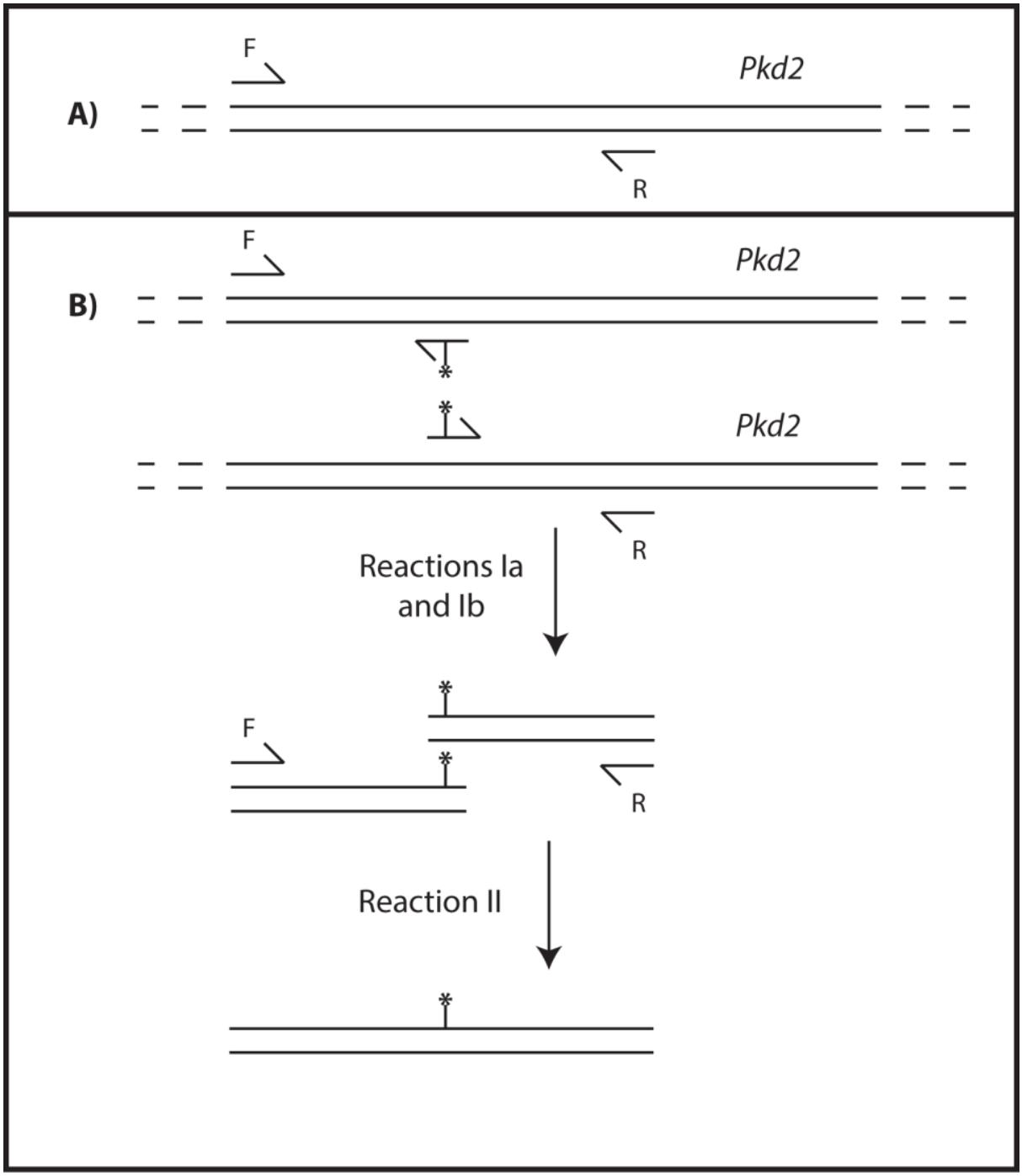


Figure 5.1: PCR strategy used to amplify regions of interest and mutagenize them, here shown for *Pkd2*. **A)** PCR for amplification of entire region of interest; **B)** reactions required for PCR mutagenesis. F and R represent forward and reverse primers for the overall region of interest; mutations are represented by (*). Figure adapted from the author's transfer report.

Table 5.3: Primers used for PCR amplification and mutagenesis

Primer name	Sequence
Amplification	
PKD1-CC_fw	GCCTCGAGATGATTTCCTCTGGTGCTGACAC
PKD1-CC_rv	GCACCGGTTTAGTGCTGCTGGGGTGGACCT
PKD2EFh_fw	GCGTCGACCGCAGAAATGGAACTCTCAGA
PKD2TM5_fw	GCGTCGACCAATTTTAATAGGACCATGAGC
PKD2TM6_fw	GCGTCGACCACCCAGGTCGATGACTTCAG
PKD2_rv	GCGGTACCTTAGGCATGGACGTTGGCACTT
Mutagenesis primers	
PKD2CC_D884A_fw	TTAGGACGGCTGCTGGCTGGC
PKD2CC_D884A_rv	GCCAGCCAGCAGCCGTCCTAA
PKD2CC_L882H_fw	TTAGGACGGCATCTGGATGGC
PKD2CC_L882H_rv	GCCATCCAGATGCCGTCCTAA
PKD2CC_L906P_fw	GCGCCCGGTGCGGGAAGAG
PKD2CC_L906P_rv	CTCTTCCCGCACCGGGCGC
PKD2CC_R872X_fw	TCATGGAGTAGGCCAAGCTGA
PKD2CC_R872X_rv	TCAGCTTGGCCTACTCCATGA
PKD2CC_S818X_fw	TGACGAAGACTGAGGCC
PKD2CC_S818X_rv	GGCCTCAGTCTTCGTCA
PKD2CC_V907D_fw	GCGCCTGGATCGGGAAGAG
PKD2CC_V907D_rv	CTCTTCCCGATCCAGGCGC

Restriction enzyme sites are depicted as follows: SalI, KpnI, XhoI and AgeI. Mutated sites are highlighted in cyan.

5.5.3. Agarose gel electrophoresis

Fragments of DNA were separated by size using 1% (w/v) agarose, 1x TBE gels, containing 200 ng/mL ethidium bromide. Samples containing 1x loading dye were loaded alongside a GeneRuler 1 kb Plus DNA ladder, onto gels submerged in 1x TBE. A constant voltage of 100 V was applied across the gel for 45-60 min. Gels were subsequently analysed using a BioRad Gel Doc XR+ system, or under a long-wave UV lamp if the separated products were later purified.

5.5.4. RNA extraction

Whole kidney and lung was used for extracting RNA. Samples were subjected to DNase treatment using RNase-free DNase Set, and extraction was done using RNeasy Midi kit, by following the manufacturer's instructions.

5.5.5. cDNA generation

Reverse transcription was performed from extracted kidney or lung RNA, using a High-Capacity cDNA Reverse Transcription kit, by following the manufacturer's specifications.

5.5.6. Bacterial transformation

Bacterial transformation using chemically competent *E. coli* DH5α cells was performed by adding 1 µL DNA, or 10 µL for ligation products, to 50 µL of bacteria in pre-chilled culture tubes. After 30 minutes on ice, cells were heat-shocked at 42°C for 45 seconds and incubated on ice for 2 minutes. Following growth for 1 hour in pre-warmed (37°C) liquid LB at 37°C and 225 RPM, cells were plated on selective LB plates (containing 100 µg/mL AMP or 50 µg/mL KAN) and grown overnight. Cells were sub-cultured in 2 mL selective liquid LB (50 µg/mL AMP or KAN) for 8 hours, followed by growth in 50 ml selective liquid LB for 16 hours.

5.5.7. DNA purification

DNA purification for molecular biology applications was done using QIAprep Spin Miniprep Kit, Qiagen Plasmid Midi Kit, QIAquick PCR Purification Kit and QIAquick Gel Extraction Kit, by following the manufacturer's instructions. Constructs used for transfecting cells were purified using PureYield Plasmid Midiprep system, by following the instructions provided with the kit.

5.5.8. Restriction digest

Restriction digestion reactions were performed in 20 µL volume, in 1x Cutsmart buffer, 10-20 U of each restriction enzyme, in ddH_2O. Digestion reactions were performed at 37 ˚C for one hour. Diagnostic digests were also performed following ligation, in order to verify the integration of the insert into the vector backbone. Amplicons and vectors of interest were digested with the following enzymes:

i) pCMV-N-Myc vector and *Pkd2* amplicons were digested using KpnI-HF and SalI-HF

ii) pEGFP-N and *Pkd1* amplicons were digested using XhoI and AgeI-HF

5.5.9. Ligation

Ligation was performed using the Quick Ligation kit, by following the manufacturer's instructions. Digested vector and amplicons were subjected to ligation in two parallel reactions containing different quantities of excess insert, in 1:3 to 1:15 molar ratio.

5.5.10. Sequencing

DNA was analysed by agarose gel electrophoresis to confirm amplification and/or purification of correct products. Sequencing of purified DNA was then performed by GATC biotech, using their SupremeRUN service; sequencing primers were typically the same as those used in PCR amplification, or sequences from the vector backbone.

5.5.11. Constructs used

The following expression constructs were used, from previous studies: PKD2-V5 (gift from R. Sanford), Myc-PKD2 (gift from G. Germino), PKD1L1-CC-GFP (made by D. Grimes), PKD1-FLAG (gift from G. Germino), NPR3-EGFP (gift from C. Esapa).

5.6. Bioinformatics

The probability of coiled coil formation in mouse C-terminal PKD2 sequences was determined using Marcoils and Coiled-coils. Sequences used range from amino acid 815 or 813 to the C terminus of PKD2, for the human and mouse protein, respectively. FinchTV was used for viewing sequencing data. ClustalW was used for alignments for sequence confirmation.

Table 5.4: Composition of solutions used throughout the study

Solution	Composition	Method
CIP	10x: 100mM Tris, 1.5M NaCl, 5mM EDTA, 5% Igepal (v/v), in ddH_2O, final pH 7.4	CoIP
Freezing medium	8.33% DMSO, 41.66% serum-free growth medium, 50% FBS	Freezing cell stocks
Complete growth medium	DMEM or DMEM/F12 containing 10% FBS	Tissue culture
LB (liquid)	10 g/L Bacto-tryptone, 5 g/L yeast extract, 10 g NaCl in ddH_2O; solution is autoclaved prior to use	Bacterial work
LB (solid)	15 g/L agar added to LB (liquid) and dissolved at high temperature	Bacterial work
Loading dye	10x: 20% Ficoll-400 (w/v), 100 mM EDTA and 1.5% (w/v) Orange G	Agarose gel electrophoresis
PBS	1x: 137 mM NaCl, 12 mM phosphate, 2.7 mM KCl in ddH_2O, final pH 7.4	various
RIPA I buffer	10x: 1M NaCl, 1% DOC, 1% SDS (v/v), 10% TritonX-100 (v/v), 0.5mM EGTA, 10 mM EDTA, 100 mM Tris, pH 7.5 in ddH_2O	CoIP
RIPA II buffer	150mM NaCl, 1% Igepal (v/v), 0.5% DOC, 0.1% SDS (v/v), 50mM Tris, pH 7.5 in ddH_2O	CoIP
TBE	10x: 890 mM Tris base, 890 mM boric acid, 20 mM EDTA pH 8 in ddH_2O	Agarose gel electrophoresis
TBST	1x: 1x TBS (v/v), 0.1% Tween (v/v) in ddH_2O	WB

Table 5.5: Reference of reagents, catalogue numbers and supplier, by type of method

Reagent	Catalog number	Supplier/Manufacturer
Antibodies and immunofluorescence		
DABCO	D27802-25G	Sigma-Aldrich
Dnk-a-Rb650	ab96894	Abcam
Gt-a-Ms488	ab96879	Abcam
Gt-a-Ms650	ab96882	Abcam
Gt-a-Ms800	926-32221	LI-COR Biosciences
Gt-a-Rb488	ab96899	Abcam
Gt-a-Rb594	ab96885	Abcam
Gt-a-Rb680	926-32210	LI-COR Biosciences
Hydromount	HS-106	National diagnostics
NucBlue Fixed Cell ReadyProbe reagent	R37606	Thermo Fisher Scientific
Ms-a-AcTub	T7451	Sigma-Aldrich
Ms-a-GFP	11814460001	Roche / Sigma-Aldrich
Ms-a-V5	R9605	Thermo Fisher Scientific
Rb-a-GluTub	ab3201	Millipore
Rb-a-Myc	c3956-.2MG	Sigma-Aldrich
Rb-a-PKD2	sc-25749	Santa Cruz
Biochemistry		
Precision Plus Protein Dual Color Standards	#1610374	Bio Rad
cOmplete EDTA-free Protease Inhibitor cocktail	**04693132001**	Sigma-Aldrich
GFP-trap_A (20 reactions) kit	**gta-20**	Chromotek
iBlot Transfer Stack, Nitrocellulose, Mini	IB301002	Thermo Fisher Scientific
iBlot Transfer Stack, Nitrocellulose, Regular	IB301001	Thermo Fisher Scientific
Invitrogen Novex NuPAGE LDS Sample Buffer (4x)	NP0007	Thermo Fisher Scientific
Invitrogen Novex NuPAGE Sample Reducing Agent (10x)	NP0009	Thermo Fisher Scientific
Myc-trap_A (20 reactions) kit	yta_20	Chromotek
NuPAGE 4-12% Bis-Tris Protein Gels, 1.0 mm, 10 well	NP0321BOX	Thermo Fisher Scientific
NuPAGE 4-12% Bis-Tris Protein Gels, 1.0 mm, 12 well	NP0322BOX	Thermo Fisher Scientific
NuPAGE 4-12% Bis-Tris Protein Gels, 1.5 mm, 15 well	NP0336BOX	Thermo Fisher Scientific
NuPAGE MOPS SDS Running Buffer (20x)	NP0001	Thermo Fisher Scientific
TBS (10x)	#1706435	Bio-Rad

Table 5.5 (continued)

Reagent	Catalog number	Supplier/Manufacturer
Biochemistry		
Protein G Sepharose, Fast Flow	P3296-5ML	Sigma-Aldrich
Molecular biology		
AgeI-HF	R3552S	New England Biolabs
GeneRuler 1 kb Plus DNA Ladder	SM1331	Thermo Fisher Scientific
High-Capacity cDNA Reverse Transcription kit	4368814	Thermo Fisher Scientific
KpnI-HF	R3142S	New Englang Biolabs
PureYield Plasmid Midiprep system	A2495	Promega
Q5 High-Fidelity DNA Polymerase	M0491L	New England Biolabs
Qiagen Plasmid Midi kit	12143	Qiagen
QIAprep Spin Miniprep Kit	27104	Qiagen
QIAquick Gel Extraction Kit	28706	Qiagen
QIAquick PCR Purification Kit	28106	Qiagen
Quick Ligation kit	M2200L	New England Biolabs
RNase-free DNase Set	75142	Qiagen
RNeasy Midi kit	79254	Qiagen
Taq Mastermix	201445	Qiagen
SalI-HF	R3138S	New England Biolabs
XhoI	R0146S	New England Biolabs
Tissue culture		
DMEM + GlutaMAX-I, high glucose	61965026	Thermo Fisher Scientific
DMEM + GlutaMAX-I, high glucose, high pyruvate	31966021	Thermo Fisher Scientific
DMEM/F12	11320033	Thermo Fisher Scientific
D-PBS	14190250	Thermo Fisher Scientific
Heat-inactivated FBS	10500	Thermo Fisher Scientific
Lipofectamine 3000	L300015	Thermo Fisher Scientific
JetPEI	101-10N	Polyplus
Trypsin-EDTA (0.05%), phenol red	25300062	Thermo Fisher Scientific
Trypsin-EDTA (0.25%), phenol red	25200072	Thermo Fisher Scientific

Bibliography

ABOUALAIWI, W. A., TAKAHASHI, M., MELL, B. R., JONES, T. J., RATNAM, S., KOLB, R. J. & NAULI, S. M. 2009. Ciliary polycystin-2 is a mechanosensitive calcium channel involved in nitric oxide signaling cascades. *Circ Res,* 104**,** 860-9.

AFZELIUS, B. A. 2004. Cilia-related diseases. *J Pathol,* 204**,** 470-7.

ANDERSON, R. H., WEBB, S., BROWN, N. A., LAMERS, W. & MOORMAN, A. 2003. Development of the heart: (3) formation of the ventricular outflow tracts, arterial valves, and intrapericardial arterial trunks. *Heart,* 89**,** 1110-8.

ANYATONWU, G. I., ESTRADA, M., TIAN, X., SOMLO, S. & EHRLICH, B. E. 2007. Regulation of ryanodine receptor-dependent calcium signaling by polycystin-2. *Proc Natl Acad Sci U S A,* 104**,** 6454-9.

ARNAOUT, M. A. 2000. The vasculopathy of autosomal dominant polycystic kidney disease: insights from animal models. *Kidney Int,* 58**,** 2599-610.

AVASTHI, P., MASER, R. L. & TRAN, P. V. 2017. Primary Cilia in Cystic Kidney Disease. *Results Probl Cell Differ,* 60**,** 281-321.

BABICH, V., ZENG, W. Z., YEH, B. I., IBRAGHIMOV-BESKROVNAYA, O., CAI, Y., SOMLO, S. & HUANG, C. L. 2004. The N-terminal extracellular domain is required for polycystin-1-dependent channel activity. *J Biol Chem,* 279**,** 25582-9.

BABLER, W. J., PERSING, J. A., WINN, H. R., JANE, J. A. & RODEHEAVER, G. T. 1982. Compensatory growth following premature closure of the coronal suture in rabbits. *J Neurosurg,* 57**,** 535-42.

BADGANDI, H. B., HWANG, S. H., SHIMADA, I. S., LORIOT, E. & MUKHOPADHYAY, S. 2017. Tubby family proteins are adapters for ciliary trafficking of integral membrane proteins. *J Cell Biol,* 216**,** 743-760.

BARR, M. M., DEMODENA, J., BRAUN, D., NGUYEN, C. Q., HALL, D. H. & STERNBERG, P. W. 2001. The Caenorhabditis elegans autosomal dominant polycystic kidney disease gene homologs lov-1 and pkd-2 act in the same pathway. *Curr Biol,* 11**,** 1341-6.

BATAILLE, S., DEMOULIN, N., DEVUYST, O., AUDRÉZET, M. P., DAHAN, K., GODIN, M., FONTÈS, M., PIRSON, Y. & BURTEY, S. 2011. Association of PKD2 (polycystin 2) mutations with left-right laterality defects. *Am J Kidney Dis,* 58**,** 456-60.

BELET, U., DANACI, M., SARIKAYA, S., ODABAŞ, F., UTAŞ, C., TOKGÖZ, B., SEZER, T., TURGUT, T., ERDOĞAN, N. & AKPOLAT, T. 2002. Prevalence of epididymal, seminal vesicle, prostate, and testicular cysts in autosomal dominant polycystic kidney disease. *Urology,* 60**,** 138-41.

BEYER, T., THUMBERGER, T., SCHWEICKERT, A. & BLUM, M. 2012. Connexin26-mediated transfer of laterality cues in Xenopus. *Biol Open,* 1**,** 473-81.

BISGROVE, B. W., SNARR, B. S., EMRAZIAN, A. & YOST, H. J. 2005. Polaris and Polycystin-2 in dorsal forerunner cells and Kupffer's vesicle are required for specification of the zebrafish left-right axis. *Dev Biol,* 287**,** 274-88.

BLUM, M. & OTT, T. 2018. Animal left-right asymmetry. *Curr Biol,* 28**,** R301-R304.

BLUM, M., WEBER, T., BEYER, T. & VICK, P. 2009. Evolution of leftward flow. *Semin Cell Dev Biol,* 20**,** 464-71.

BLÁZQUEZ, E., VELÁZQUEZ, E., HURTADO-CARNEIRO, V. & RUIZ-ALBUSAC, J. M. 2014. Insulin in the brain: its pathophysiological implications for States related with central insulin resistance, type 2 diabetes and Alzheimer's disease. *Front Endocrinol (Lausanne),* 5**,** 161.

BOCA, M., D'AMATO, L., DISTEFANO, G., POLISHCHUK, R. S., GERMINO, G. G. & BOLETTA, A. 2007. Polycystin-1 induces cell migration by regulating phosphatidylinositol 3-kinase-dependent cytoskeletal rearrangements and GSK3beta-dependent cell cell mechanical adhesion. *Mol Biol Cell,* 18**,** 4050-61.

BOUCHER, C. & SANDFORD, R. 2004. Autosomal dominant polycystic kidney disease (ADPKD, MIM 173900, PKD1 and PKD2 genes, protein products known as polycystin-1 and polycystin-2). *Eur J Hum Genet,* 12**,** 347-54.

BOULTER, C., MULROY, S., WEBB, S., FLEMING, S., BRINDLE, K. & SANDFORD, R. 2001. Cardiovascular, skeletal, and renal defects in mice with a targeted disruption of the Pkd1 gene. *Proc Natl Acad Sci U S A,* 98**,** 12174-9.

BRENNAN, J., NORRIS, D. P. & ROBERTSON, E. J. 2002. Nodal activity in the node governs left-right asymmetry. *Genes Dev,* 16**,** 2339-44.

BRUECKNER, M. 2007. Heterotaxia, congenital heart disease, and primary ciliary dyskinesia. *Circulation,* 115**,** 2793-5.

BUTSCHEID, Y., CHUBANOV, V., STEGER, K., MEYER, D., DIETRICH, A. & GUDERMANN, T. 2006. Polycystic kidney disease and receptor for egg jelly is a plasma membrane protein of mouse sperm head. *Mol Reprod Dev,* 73**,** 350-60.

CAI, Y., ANYATONWU, G., OKUHARA, D., LEE, K. B., YU, Z., ONOE, T., MEI, C. L., QIAN, Q., GENG, L., WIZTGALL, R., EHRLICH, B. E. & SOMLO, S. 2004. Calcium dependence of polycystin-2 channel activity is modulated by phosphorylation at Ser812. *J Biol Chem,* 279**,** 19987-95.

CAI, Y., FEDELES, S. V., DONG, K., ANYATONWU, G., ONOE, T., MITOBE, M., GAO, J. D., OKUHARA, D., TIAN, X., GALLAGHER, A. R., TANG, Z., XIE, X., LALIOTI, M. D., LEE, A. H., EHRLICH, B. E. & SOMLO, S. 2014. Altered trafficking and stability of polycystins underlie polycystic kidney disease. *J Clin Invest,* 124**,** 5129-44.

CAI, Y., MAEDA, Y., CEDZICH, A., TORRES, V. E., WU, G., HAYASHI, T., MOCHIZUKI, T., PARK, J. H., WITZGALL, R. & SOMLO, S. 1999. Identification and characterization of polycystin-2, the PKD2 gene product. *J Biol Chem,* 274**,** 28557-65.

CAMPIONE, M., ROS, M. A., ICARDO, J. M., PIEDRA, E., CHRISTOFFELS, V. M., SCHWEICKERT, A., BLUM, M., FRANCO, D. & MOORMAN, A. F. 2001. Pitx2 expression defines a left cardiac lineage of cells: evidence for atrial and ventricular molecular isomerism in the iv/iv mice. *Dev Biol,* 231**,** 252-64.

CARTWRIGHT, J. H., PIRO, N., PIRO, O. & TUVAL, I. 2008. Fluid dynamics of nodal flow and left-right patterning in development. *Dev Dyn,* 237**,** 3477-90.

CARTWRIGHT, J. H., PIRO, O. & TUVAL, I. 2004. Fluid-dynamical basis of the embryonic development of left-right asymmetry in vertebrates. *Proc Natl Acad Sci U S A,* 101**,** 7234-9.

CASUSCELLI, J., SCHMIDT, S., DEGRAY, B., PETRI, E. T., CELIĆ, A., FOLTA-STOGNIEW, E., EHRLICH, B. E. & BOGGON, T. J. 2009. Analysis of the cytoplasmic interaction between polycystin-1 and polycystin-2. *Am J Physiol Renal Physiol,* 297**,** F1310-5.

CELIĆ, A., PETRI, E. T., DEMELER, B., EHRLICH, B. E. & BOGGON, T. J. 2008. Domain mapping of the polycystin-2 C-terminal tail using de novo molecular modeling and biophysical analysis. *J Biol Chem,* 283**,** 28305-12.

CELIĆ, A. S., PETRI, E. T., BENBOW, J., HODSDON, M. E., EHRLICH, B. E. & BOGGON, T. J. 2012. Calcium-induced conformational changes in C-terminal tail of polycystin-2 are necessary for channel gating. *J Biol Chem,* 287**,** 17232-40.

CHAUVET, V., TIAN, X., HUSSON, H., GRIMM, D. H., WANG, T., HIESBERGER, T., HIESEBERGER, T., IGARASHI, P., BENNETT, A. M., IBRAGHIMOV-BESKROVNAYA, O., SOMLO, S. & CAPLAN, M. J. 2004. Mechanical stimuli induce cleavage and nuclear translocation of the polycystin-1 C terminus. *J Clin Invest,* 114**,** 1433-43.

CHEN, X. Z., SEGAL, Y., BASORA, N., GUO, L., PENG, J. B., BABAKHANLOU, H., VASSILEV, P. M., BROWN, E. M., HEDIGER, M. A. & ZHOU, J. 2001. Transport function of the naturally occurring pathogenic polycystin-2 mutant, R742X. *Biochem Biophys Res Commun,* 282**,** 1251-6.

CHEN, Y., ZHANG, Z., LV, X. Y., WANG, Y. D., HU, Z. G., SUN, H., TAN, R. Z., LIU, Y. H., BIAN, G. H., XIAO, Y., LI, Q. W., YANG, Q. T., AI, J. Z., FENG, L., YANG, Y., WEI, Y. Q. & ZHOU, Q. 2008. Expression of Pkd2l2 in testis is implicated in spermatogenesis. *Biol Pharm Bull,* 31**,** 1496-500.

COXAM, B., SABINE, A., BOWER, N. I., SMITH, K. A., PICHOL-THIEVEND, C., SKOCZYLAS, R., ASTIN, J. W., FRAMPTON, E., JAQUET, M., CROSIER, P. S., PARTON, R. G., HARVEY, N. L., PETROVA, T. V., SCHULTE-MERKER, S., FRANCOIS, M. & HOGAN, B. M. 2014. Pkd1 regulates lymphatic vascular morphogenesis during development. *Cell Rep,* 7**,** 623-33.

DECAEN, P. G., DELLING, M., VIEN, T. N. & CLAPHAM, D. E. 2013. Direct recording and molecular identification of the calcium channel of primary cilia. *Nature,* 504**,** 315-8.

DECAEN, P. G., LIU, X., ABIRIA, S. & CLAPHAM, D. E. 2016. Atypical calcium regulation of the PKD2-L1 polycystin ion channel. *Elife,* 5.

DELLING, M., INDZHYKULIAN, A. A., LIU, X., LI, Y., XIE, T., COREY, D. P. & CLAPHAM, D. E. 2016. Primary cilia are not calcium-responsive mechanosensors. *Nature,* 531**,** 656-60.

DELMAS, P., NOMURA, H., LI, X., LAKKIS, M., LUO, Y., SEGAL, Y., FERNÁNDEZ-FERNÁNDEZ, J. M., HARRIS, P., FRISCHAUF, A. M., BROWN, D. A. & ZHOU, J. 2002. Constitutive activation of G-proteins by polycystin-1 is antagonized by polycystin-2. *J Biol Chem,* 277**,** 11276-83.

DELMAS, P., PADILLA, F., OSORIO, N., COSTE, B., RAOUX, M. & CREST, M. 2004. Polycystins, calcium signaling, and human diseases. *Biochem Biophys Res Commun,* 322**,** 1374-83.

DELORENZI, M. & SPEED, T. 2002. An HMM model for coiled-coil domains and a comparison with PSSM-based predictions. *Bioinformatics,* 18**,** 617-25.

DOERR, N., WANG, Y., KIPP, K. R., LIU, G., BENZA, J. J., PLETNEV, V., PAVLOV, T. S., STARUSCHENKO, A., MOHIELDIN, A. M., TAKAHASHI, M., NAULI, S. M. & WEIMBS, T. 2016. Regulation of Polycystin-1 Function by Calmodulin Binding. *PLoS One,* 11**,** e0161525.

DU, J., MA, X., SHEN, B., HUANG, Y., BIRNBAUMER, L. & YAO, X. 2014. TRPV4, TRPC1, and TRPP2 assemble to form a flow-sensitive heteromeric channel. *FASEB J,* 28**,** 4677-85.

ENGLAND, S. J., CAMPBELL, P. C., BANERJEE, S., SWANSON, A. J. & LEWIS, K. E. 2017. Identification and Expression Analysis of the Complete Family of Zebrafish pkd Genes. *Front Cell Dev Biol,* 5**,** 5.

ENGSTRÖM, C., KILIARIDIS, S. & THILANDER, B. 1986. The relationship between masticatory function and craniofacial morphology. II. A histological study in the growing rat fed a soft diet. *Eur J Orthod,* 8**,** 271-9.

ERMAKOV, A., STEVENS, J. L., WHITEHILL, E., ROBSON, J. E., PIELES, G., BROOKER, D., GOGGOLIDOU, P., POWLES-GLOVER, N., HACKER, T., YOUNG, S. R., DEAR, N., HIRST, E., TYMOWSKA-LALANNE, Z., BRISCOE, J., BHATTACHARYA, S. & NORRIS, D. P. 2009. Mouse mutagenesis identifies novel roles for left-right patterning genes in pulmonary, craniofacial, ocular, and limb development. *Dev Dyn,* 238**,** 581-94.

FEDOROV, A., BEICHEL, R., KALPATHY-CRAMER, J., FINET, J., FILLION-ROBIN, J. C., PUJOL, S., BAUER, C., JENNINGS, D., FENNESSY, F., SONKA, M., BUATTI, J., AYLWARD, S., MILLER, J. V., PIEPER, S. & KIKINIS, R. 2012. 3D Slicer as an image computing platform for the Quantitative Imaging Network. *Magn Reson Imaging,* 30**,** 1323-41.

FENG, S., OKENKA, G. M., BAI, C. X., STREETS, A. J., NEWBY, L. J., DECHANT, B. T., TSIOKAS, L., OBARA, T. & ONG, A. C. 2008. Identification and functional characterization of an N-terminal oligomerization domain for polycystin-2. *J Biol Chem,* 283**,** 28471-9.

FENG, S., RODAT-DESPOIX, L., DELMAS, P. & ONG, A. C. 2011. A single amino acid residue constitutes the third dimerization domain essential for the assembly and function of the tetrameric polycystin-2 (TRPP2) channel. *J Biol Chem,* 286**,** 18994-9000.

FIELD, S., RILEY, K. L., GRIMES, D. T., HILTON, H., SIMON, M., POWLES-GLOVER, N., SIGGERS, P., BOGANI, D., GREENFIELD, A. & NORRIS, D. P. 2011. Pkd1l1 establishes left-right asymmetry and physically interacts with Pkd2. *Development,* 138**,** 1131-42.

FOLLIT, J. A., SAN AGUSTIN, J. T., XU, F., JONASSEN, J. A., SAMTANI, R., LO, C. W. & PAZOUR, G. J. 2008. The Golgin GMAP210/TRIP11 anchors IFT20 to the Golgi complex. *PLoS Genet,* 4**,** e1000315.

FOLLIT, J. A., TUFT, R. A., FOGARTY, K. E. & PAZOUR, G. J. 2006. The intraflagellar transport protein IFT20 is associated with the Golgi complex and is required for cilia assembly. *Mol Biol Cell,* 17**,** 3781-92.

FU, X., WANG, Y., SCHETLE, N., GAO, H., PÜTZ, M., VON GERSDORFF, G., WALZ, G. & KRAMER-ZUCKER, A. G. 2008. The subcellular localization of TRPP2 modulates its function. *J Am Soc Nephrol,* 19**,** 1342-51.

GABOW, P. A. 1993. Autosomal dominant polycystic kidney disease. *N Engl J Med,* 329**,** 332-42.

GAINULLIN, V. G., HOPP, K., WARD, C. J., HOMMERDING, C. J. & HARRIS, P. C. 2015. Polycystin-1 maturation requires polycystin-2 in a dose-dependent manner. *J Clin Invest,* 125**,** 607-20.

GALLAGHER, A. R., CEDZICH, A., GRETZ, N., SOMLO, S. & WITZGALL, R. 2000. The polycystic kidney disease protein PKD2 interacts with Hax-1, a protein associated with the actin cytoskeleton. *Proc Natl Acad Sci U S A,* 97**,** 4017-22.

GARCIA-GONZALEZ, M. A., OUTEDA, P., ZHOU, Q., ZHOU, F., MENEZES, L. F., QIAN, F., HUSO, D. L., GERMINO, G. G., PIONTEK, K. B. & WATNICK, T. 2010. Pkd1 and Pkd2 are required for normal placental development. *PLoS One,* 5.

GENG, L., OKUHARA, D., YU, Z., TIAN, X., CAI, Y., SHIBAZAKI, S. & SOMLO, S. 2006. Polycystin-2 traffics to cilia independently of polycystin-1 by using an N-terminal RVxP motif. *J Cell Sci,* 119**,** 1383-95.

GIAMARCHI, A., FENG, S., RODAT-DESPOIX, L., XU, Y., BUBENSHCHIKOVA, E., NEWBY, L. J., HAO, J., GAUDIOSO, C., CREST, M., LUPAS, A. N., HONORÉ, E., WILLIAMSON, M. P., OBARA, T., ONG, A. C. & DELMAS, P. 2010. A polycystin-2 (TRPP2) dimerization domain essential for the function of heteromeric polycystin complexes. *EMBO J,* 29**,** 1176-91.

GONZALEZ-PERRETT, S., BATELLI, M., KIM, K., ESSAFI, M., TIMPANARO, G., MOLTABETTI, N., REISIN, I. L., ARNAOUT, M. A. & CANTIELLO, H. F. 2002. Voltage dependence and pH regulation of human polycystin-2-mediated cation channel activity. *J Biol Chem,* 277**,** 24959-66.

GRIEBEN, M., PIKE, A. C., SHINTRE, C. A., VENTURI, E., EL-AJOUZ, S., TESSITORE, A., SHRESTHA, L., MUKHOPADHYAY, S., MAHAJAN, P., CHALK, R., BURGESS-BROWN, N. A., SITSAPESAN, R., HUISKONEN, J. T. & CARPENTER, E. P. 2017. Structure of the polycystic kidney disease TRP channel Polycystin-2 (PC2). *Nat Struct Mol Biol,* 24**,** 114-122.

GRIMES, D. T. 2012. *The role of the polycystin genes, Pkd1l1 and Pkd2, in the determination of left-right asymmetry.* DPhil, University of Oxford.

GRIMES, D. T., KEYNTON, J. L., BUENAVISTA, M. T., JIN, X., PATEL, S. H., KYOSUKE, S., VIBERT, J., WILLIAMS, D. J., HAMADA, H., HUSSAIN, R., NAULI, S. M. & NORRIS, D. P. 2016. Genetic Analysis Reveals a Hierarchy of Interactions between Polycystin-Encoding Genes and Genes Controlling Cilia Function during Left-Right Determination. *PLoS Genet,* 12**,** e1006070.

GUILLAUME, R. & TRUDEL, M. 2000. Distinct and common developmental expression patterns of the murine Pkd2 and Pkd1 genes. *Mech Dev,* 93**,** 179-83.

HANAOKA, K., QIAN, F., BOLETTA, A., BHUNIA, A. K., PIONTEK, K., TSIOKAS, L., SUKHATME, V. P., GUGGINO, W. B. & GERMINO, G. G. 2000. Co-assembly of polycystin-1 and -2 produces unique cation-permeable currents. *Nature,* 408**,** 990-4.

HARRIS, P. C. & ROSSETTI, S. 2010. Determinants of renal disease variability in ADPKD. *Adv Chronic Kidney Dis,* 17**,** 131-9.

HARRIS, P. C. & TORRES, V. E. 2009. Polycystic kidney disease. *Annu Rev Med,* 60**,** 321-37.

HARRIS, P. C., WARD, C. J., PERAL, B. & HUGHES, J. 1995. Polycystic kidney disease. 1: Identification and analysis of the primary defect. *J Am Soc Nephrol,* 6**,** 1125-33.

HATEBOER, N., V DIJK, M. A., BOGDANOVA, N., COTO, E., SAGGAR-MALIK, A. K., SAN MILLAN, J. L., TORRA, R., BREUNING, M. & RAVINE, D. 1999. Comparison of phenotypes of polycystic kidney disease types 1 and 2. European PKD1-PKD2 Study Group. *Lancet,* 353**,** 103-7.

HELLMICH, U. A. & GAUDET, R. 2014. Structural biology of TRP channels. *Handb Exp Pharmacol,* 223**,** 963-90.

HERRING, S. W. & TENG, S. 2000. Strain in the braincase and its sutures during function. *Am J Phys Anthropol,* 112**,** 575-93.

HIDAKA, S., KÖNECKE, V., OSTEN, L. & WITZGALL, R. 2004. PIGEA-14, a novel coiled-coil protein affecting the intracellular distribution of polycystin-2. *J Biol Chem,* 279**,** 35009-16.

HODGKIN, J. 1998. Seven types of pleiotropy. *Int J Dev Biol,* 42**,** 501-5.

HOENDEROP, J. G., VOETS, T., HOEFS, S., WEIDEMA, F., PRENEN, J., NILIUS, B. & BINDELS, R. J. 2003. Homo- and heterotetrameric architecture of the epithelial Ca2+ channels TRPV5 and TRPV6. *EMBO J,* 22**,** 776-85.

HOFFMEISTER, H., BABINGER, K., GÜRSTER, S., CEDZICH, A., MEESE, C., SCHADENDORF, K., OSTEN, L., DE VRIES, U., RASCLE, A. & WITZGALL, R. 2011. Polycystin-2 takes different routes to the somatic and ciliary plasma membrane. *J Cell Biol,* 192**,** 631-45.

HOFHERR, A., WAGNER, C., FEDELES, S., SOMLO, S. & KÖTTGEN, M. 2014. N-glycosylation determines the abundance of the transient receptor potential channel TRPP2. *J Biol Chem,* 289**,** 14854-67.

HOPP, K., WARD, C. J., HOMMERDING, C. J., NASR, S. H., TUAN, H. F., GAINULLIN, V. G., ROSSETTI, S., TORRES, V. E. & HARRIS, P. C. 2012. Functional polycystin-1 dosage governs autosomal dominant polycystic kidney disease severity. *J Clin Invest,* 122**,** 4257-73.

HOU, B., KOLPAKOVA-HART, E., FUKAI, N., WU, K. & OLSEN, B. R. 2009. The polycystic kidney disease 1 (Pkd1) gene is required for the responses of osteochondroprogenitor cells to midpalatal suture expansion in mice. *Bone,* 44**,** 1121-33.

HUANG, P. & SCHIER, A. F. 2009. Dampened Hedgehog signaling but normal Wnt signaling in zebrafish without cilia. *Development,* 136**,** 3089-98.

HUGHES, J., WARD, C. J., ASPINWALL, R., BUTLER, R. & HARRIS, P. C. 1999. Identification of a human homologue of the sea urchin receptor for egg jelly: a polycystic kidney disease-like protein. *Hum Mol Genet,* 8**,** 543-9.

INOUE, Y., SOHARA, E., KOBAYASHI, K., CHIGA, M., RAI, T., ISHIBASHI, K., HORIE, S., SU, X., ZHOU, J., SASAKI, S. & UCHIDA, S. 2014. Aberrant glycosylation and localization of polycystin-1 cause polycystic kidney in an AQP11 knockout model. *J Am Soc Nephrol,* 25**,** 2789-99.

ISHIMARU, Y., INADA, H., KUBOTA, M., ZHUANG, H., TOMINAGA, M. & MATSUNAMI, H. 2006. Transient receptor potential family members PKD1L3 and PKD2L1 form a candidate sour taste receptor. *Proc Natl Acad Sci U S A,* 103**,** 12569-74.

ISHIMARU, Y., KATANO, Y., YAMAMOTO, K., AKIBA, M., MISAKA, T., ROBERTS, R. W., ASAKURA, T., MATSUNAMI, H. & ABE, K. 2010. Interaction between PKD1L3 and PKD2L1 through their transmembrane domains is required for localization of PKD2L1 at taste pores in taste cells of circumvallate and foliate papillae. *FASEB J,* 24**,** 4058-67.

KAMURA, K., KOBAYASHI, D., UEHARA, Y., KOSHIDA, S., IIJIMA, N., KUDO, A., YOKOYAMA, T. & TAKEDA, H. 2011. Pkd1l1 complexes with Pkd2 on motile cilia and functions to establish the left-right axis. *Development,* 138**,** 1121-9.

KANAGARAJAH, P., AYYATHURAI, R. & LYNNE, C. M. 2012. Male infertility and adult polycystic kidney disease--revisited: case report and current literature review. *Andrologia,* 44 Suppl 1**,** 838-41.

KANAI-AZUMA, M., KANAI, Y., GAD, J. M., TAJIMA, Y., TAYA, C., KUROHMARU, M., SANAI, Y., YONEKAWA, H., YAZAKI, K., TAM, P. P. & HAYASHI, Y. 2002. Depletion of definitive gut endoderm in Sox17-null mutant mice. *Development,* 129**,** 2367-79.

KARCHER, C., FISCHER, A., SCHWEICKERT, A., BITZER, E., HORIE, S., WITZGALL, R. & BLUM, M. 2005. Lack of a laterality phenotype in Pkd1 knock-out embryos correlates with absence of polycystin-1 in nodal cilia. *Differentiation,* 73**,** 425-32.

KARTAGENER 1935. Mitteilung: Bronchiektasienbei Situs viscerum inversus. *Beitr Klin Tuberk,* 83**,** 489-501.

KHONSARI, R. H., OHAZAMA, A., RAOUF, R., KAWASAKI, M., KAWASAKI, K., PORNTAVEETUS, T., GHAFOOR, S., HAMMOND, P., SUTTIE, M., ODRI, G. A., SANDFORD, R. N., WOOD, J. N. & SHARPE, P. T. 2013. Multiple postnatal craniofacial anomalies are characterized by conditional loss of polycystic kidney disease 2 (Pkd2). *Hum Mol Genet,* 22**,** 1873-85.

KIM, H., JEONG, W., AHN, K., AHN, C. & KANG, S. 2004. Siah-1 interacts with the intracellular region of polycystin-1 and affects its stability via the ubiquitin-proteasome pathway. *J Am Soc Nephrol,* 15**,** 2042-9.

KIM, H., XU, H., YAO, Q., LI, W., HUANG, Q., OUTEDA, P., CEBOTARU, V., CHIARAVALLI, M., BOLETTA, A., PIONTEK, K., GERMINO, G. G., WEINMAN, E. J., WATNICK, T. & QIAN, F. 2014. Ciliary membrane proteins traffic through the Golgi via a Rabep1/GGA1/Arl3-dependent mechanism. *Nat Commun,* 5**,** 5482.

KIM, I., FU, Y., HUI, K., MOECKEL, G., MAI, W., LI, C., LIANG, D., ZHAO, P., MA, J., CHEN, X. Z., GEORGE, A. L., COFFEY, R. J., FENG, Z. P. & WU, G. 2008. Fibrocystin/polyductin modulates renal tubular formation by regulating polycystin-2 expression and function. *J Am Soc Nephrol,* 19**,** 455-68.

KIM, J. A., BLUMENFELD, J. D. & PRINCE, M. R. 2015. Seminal Vesicles in Autosomal Dominant Polycystic Kidney Disease. *In:* X, L. (ed.) *Polycystic Kidney Disease.* Brisbane, Australia: Codon Publications.

KIM, K., DRUMMOND, I., IBRAGHIMOV-BESKROVNAYA, O., KLINGER, K. & ARNAOUT, M. A. 2000. Polycystin 1 is required for the structural integrity of blood vessels. *Proc Natl Acad Sci U S A,* 97**,** 1731-6.

KNOBEL, K. M., PEDEN, E. M. & BARR, M. M. 2008. Distinct protein domains regulate ciliary targeting and function of C. elegans PKD-2. *Exp Cell Res,* 314**,** 825-33.

KOBORI, T., SMITH, G. D., SANDFORD, R. & EDWARDSON, J. M. 2009. The transient receptor potential channels TRPP2 and TRPC1 form a heterotetramer with a 2:2 stoichiometry and an alternating subunit arrangement. *J Biol Chem,* 284**,** 35507-13.

KOLPAKOVA-HART, E., MCBRATNEY-OWEN, B., HOU, B., FUKAI, N., NICOLAE, C., ZHOU, J. & OLSEN, B. R. 2008. Growth of cranial synchondroses and sutures requires polycystin-1. *Dev Biol,* 321**,** 407-19.

KOULEN, P., CAI, Y., GENG, L., MAEDA, Y., NISHIMURA, S., WITZGALL, R., EHRLICH, B. E. & SOMLO, S. 2002. Polycystin-2 is an intracellular calcium release channel. *Nat Cell Biol,* 4**,** 191-7.

KUO, I. Y., KEELER, C., CORBIN, R., ĆELIĆ, A., PETRI, E. T., HODSDON, M. E. & EHRLICH, B. E. 2014. The number and location of EF hand motifs dictates the calcium dependence of polycystin-2 function. *FASEB J,* 28**,** 2332-46.

KURBEGOVIC, A., KIM, H., XU, H., YU, S., CRUANÈS, J., MASER, R. L., BOLETTA, A., TRUDEL, M. & QIAN, F. 2014. Novel functional complexity of polycystin-1 by GPS cleavage in vivo: role in polycystic kidney disease. *Mol Cell Biol,* 34**,** 3341-53.

KÖTTGEN, M., BENZING, T., SIMMEN, T., TAUBER, R., BUCHHOLZ, B., FELICIANGELI, S., HUBER, T. B., SCHERMER, B., KRAMER-ZUCKER, A., HÖPKER, K., SIMMEN, K. C., TSCHUCKE, C. C., SANDFORD, R., KIM, E., THOMAS, G. & WALZ, G. 2005. Trafficking of TRPP2 by PACS proteins represents a novel mechanism of ion channel regulation. *EMBO J,* 24**,** 705-16.

KÖTTGEN, M., BUCHHOLZ, B., GARCIA-GONZALEZ, M. A., KOTSIS, F., FU, X., DOERKEN, M., BOEHLKE, C., STEFFL, D., TAUBER, R., WEGIERSKI, T., NITSCHKE, R., SUZUKI, M., KRAMER-ZUCKER, A., GERMINO, G. G., WATNICK, T., PRENEN, J., NILIUS, B., KUEHN, E. W. & WALZ,

G. 2008. TRPP2 and TRPV4 form a polymodal sensory channel complex. *J Cell Biol,* 182**,** 437-47.

LEHTONEN, S., ORA, A., OLKKONEN, V. M., GENG, L., ZERIAL, M., SOMLO, S. & LEHTONEN, E. 2000. In vivo interaction of the adapter protein CD2-associated protein with the type 2 polycystic kidney disease protein, polycystin-2. *J Biol Chem,* 275**,** 32888-93.

LI, A., TIAN, X., SUNG, S. W. & SOMLO, S. 2003. Identification of two novel polycystic kidney disease-1-like genes in human and mouse genomes. *Genomics,* 81**,** 596-608.

LI, M., YU, Y. & YANG, J. 2011. Structural biology of TRP channels. *Adv Exp Med Biol,* 704**,** 1-23.

LI, X., LUO, Y., STARREMANS, P. G., MCNAMARA, C. A., PEI, Y. & ZHOU, J. 2005a. Polycystin-1 and polycystin-2 regulate the cell cycle through the helix-loop-helix inhibitor Id2. *Nat Cell Biol,* 7**,** 1202-12.

LI, Y., KLENA, N. T., GABRIEL, G. C., LIU, X., KIM, A. J., LEMKE, K., CHEN, Y., CHATTERJEE, B., DEVINE, W., DAMERLA, R. R., CHANG, C., YAGI, H., SAN AGUSTIN, J. T., THAHIR, M., ANDERTON, S., LAWHEAD, C., VESCOVI, A., PRATT, H., MORGAN, J., HAYNES, L., SMITH, C. L., EPPIG, J. T., REINHOLDT, L., FRANCIS, R., LEATHERBURY, L., GANAPATHIRAJU, M. K., TOBITA, K., PAZOUR, G. J. & LO, C. W. 2015. Global genetic analysis in mice unveils central role for cilia in congenital heart disease. *Nature,* 521**,** 520-4.

LI, Y., WRIGHT, J. M., QIAN, F., GERMINO, G. G. & GUGGINO, W. B. 2005b. Polycystin 2 interacts with type I inositol 1,4,5-trisphosphate receptor to modulate intracellular Ca2+ signaling. *J Biol Chem,* 280**,** 41298-306.

LIU, C., LIU, W., LU, M. F., BROWN, N. A. & MARTIN, J. F. 2001. Regulation of left-right asymmetry by thresholds of Pitx2c activity. *Development,* 128**,** 2039-48.

LIU, X., VIEN, T., DUAN, J., SHEU, S. H., DECAEN, P. G. & CLAPHAM, D. E. 2018. Polycystin-2 is an essential ion channel subunit in the primary cilium of the renal collecting duct epithelium. *Elife,* 7.

LU, W., PEISSEL, B., BABAKHANLOU, H., PAVLOVA, A., GENG, L., FAN, X., LARSON, C., BRENT, G. & ZHOU, J. 1997. Perinatal lethality with kidney and pancreas defects in mice with a targetted Pkd1 mutation. *Nat Genet,* 17**,** 179-81.

LU, W., SHEN, X., PAVLOVA, A., LAKKIS, M., WARD, C. J., PRITCHARD, L., HARRIS, P. C., GENEST, D. R., PEREZ-ATAYDE, A. R. & ZHOU, J. 2001. Comparison of Pkd1-targeted mutants reveals that loss of polycystin-1 causes cystogenesis and bone defects. *Hum Mol Genet,* 10**,** 2385-96.

LUPAS, A., VAN DYKE, M. & STOCK, J. 1991. Predicting coiled coils from protein sequences. *Science,* 252**,** 1162-4.

MA, L., XU, M., FORMAN, J. R., CLARKE, J. & OBERHAUSER, A. F. 2009. Naturally occurring mutations alter the stability of polycystin-1 polycystic kidney disease (PKD) domains. *J Biol Chem,* 284**,** 32942-9.

MACKENZIE, F. E., ROMERO, R., WILLIAMS, D., GILLINGWATER, T., HILTON, H., DICK, J., RIDDOCH-CONTRERAS, J., WONG, F., IRESON, L., POWLES-GLOVER, N., RILEY, G., UNDERHILL, P., HOUGH, T., ARKELL, R., GREENSMITH, L., RIBCHESTER, R. R. & BLANCO, G. 2009. Upregulation of PKD1L2 provokes a complex neuromuscular disease in the mouse. *Hum Mol Genet,* 18**,** 3553-66.

MALHAS, A. N., ABUKNESHA, R. A. & PRICE, R. G. 2002. Interaction of the leucine-rich repeats of polycystin-1 with extracellular matrix proteins: possible role in cell proliferation. *J Am Soc Nephrol,* 13**,** 19-26.

MANNO, M., MARCHESAN, E., TOMEI, F., CICUTTO, D., MARUZZI, D., MAIERON, A. & TURCO, A. 2005. Polycystic kidney disease and infertility: case report and literature review. *Arch Ital Urol Androl,* 77**,** 25-8.

MARKOFF, A., BOGDANOVA, N., KNOP, M., RÜFFER, C., KENIS, H., LUX, P., REUTELINGSPERGER, C., TODOROV, V., DWORNICZAK, B., HORST, J. & GERKE, V. 2007. Annexin A5 interacts with

polycystin-1 and interferes with the polycystin-1 stimulated recruitment of E-cadherin into adherens junctions. *J Mol Biol,* 369**,** 954-66.
MARQUES, S., BORGES, A. C., SILVA, A. C., FREITAS, S., CORDENONSI, M. & BELO, J. A. 2004. The activity of the Nodal antagonist Cerl-2 in the mouse node is required for correct L/R body axis. *Genes Dev,* 18**,** 2342-7.
MARSZALEK, J. R., RUIZ-LOZANO, P., ROBERTS, E., CHIEN, K. R. & GOLDSTEIN, L. S. 1999. Situs inversus and embryonic ciliary morphogenesis defects in mouse mutants lacking the KIF3A subunit of kinesin-II. *Proc Natl Acad Sci U S A,* 96**,** 5043-8.
MCGRATH, J., SOMLO, S., MAKOVA, S., TIAN, X. & BRUECKNER, M. 2003. Two populations of node monocilia initiate left-right asymmetry in the mouse. *Cell,* 114**,** 61-73.
MERRICK, D., CHAPIN, H., BAGGS, J. E., YU, Z., SOMLO, S., SUN, Z., HOGENESCH, J. B. & CAPLAN, M. J. 2012. The γ-secretase cleavage product of polycystin-1 regulates TCF and CHOP-mediated transcriptional activation through a p300-dependent mechanism. *Dev Cell,* 22**,** 197-210.
MIO, K., OGURA, T., KIYONAKA, S., MORI, Y. & SATO, C. 2007. Subunit dissociation of TRPC3 ion channel under high-salt condition. *J Electron Microsc (Tokyo),* 56**,** 111-7.
MIYAKAWA, A., IBARRA, C., MALMERSJÖ, S., APERIA, A., WIKLUND, P. & UHLÉN, P. 2013. Intracellular calcium release modulates polycystin-2 trafficking. *BMC Nephrol,* 14**,** 34.
MOCHIZUKI, T., WU, G., HAYASHI, T., XENOPHONTOS, S. L., VELDHUISEN, B., SARIS, J. J., REYNOLDS, D. M., CAI, Y., GABOW, P. A., PIERIDES, A., KIMBERLING, W. J., BREUNING, M. H., DELTAS, C. C., PETERS, D. J. & SOMLO, S. 1996. PKD2, a gene for polycystic kidney disease that encodes an integral membrane protein. *Science,* 272**,** 1339-42.
MOLLAND, K. L., NARAYANAN, A., BURGNER, J. W. & YERNOOL, D. A. 2010. Identification of the structural motif responsible for trimeric assembly of the C-terminal regulatory domains of polycystin channels PKD2L1 and PKD2. *Biochem J,* 429**,** 171-83.
MONIS, W. J., FAUNDEZ, V. & PAZOUR, G. J. 2017. BLOC-1 is required for selective membrane protein trafficking from endosomes to primary cilia. *J Cell Biol,* 216**,** 2131-2150.
MOSS, M. L. 1960. Inhibition and stimulation of sutural fusion in the rat calvaria. *Anat Rec,* 136**,** 457-67.
MOY, G. W., MENDOZA, L. M., SCHULZ, J. R., SWANSON, W. J., GLABE, C. G. & VACQUIER, V. D. 1996. The sea urchin sperm receptor for egg jelly is a modular protein with extensive homology to the human polycystic kidney disease protein, PKD1. *J Cell Biol,* 133**,** 809-17.
MURRAY, S. A. & GRIDLEY, T. 2006. Snail family genes are required for left-right asymmetry determination, but not neural crest formation, in mice. *Proc Natl Acad Sci U S A,* 103**,** 10300-4.
NAKAMURA, T., MINE, N., NAKAGUCHI, E., MOCHIZUKI, A., YAMAMOTO, M., YASHIRO, K., MENO, C. & HAMADA, H. 2006. Generation of robust left-right asymmetry in the mouse embryo requires a self-enhancement and lateral-inhibition system. *Dev Cell,* 11**,** 495-504.
NAKAMURA, T., SAITO, D., KAWASUMI, A., SHINOHARA, K., ASAI, Y., TAKAOKA, K., DONG, F., TAKAMATSU, A., BELO, J. A., MOCHIZUKI, A. & HAMADA, H. 2012. Fluid flow and interlinked feedback loops establish left-right asymmetric decay of Cerl2 mRNA. *Nat Commun,* 3**,** 1322.
NAULI, S. M., ALENGHAT, F. J., LUO, Y., WILLIAMS, E., VASSILEV, P., LI, X., ELIA, A. E., LU, W., BROWN, E. M., QUINN, S. J., INGBER, D. E. & ZHOU, J. 2003. Polycystins 1 and 2 mediate mechanosensation in the primary cilium of kidney cells. *Nat Genet,* 33**,** 129-37.
NAULI, S. M., KAWANABE, Y., KAMINSKI, J. J., PEARCE, W. J., INGBER, D. E. & ZHOU, J. 2008. Endothelial cilia are fluid shear sensors that regulate calcium signaling and nitric oxide production through polycystin-1. *Circulation,* 117**,** 1161-71.
NAULI, S. M. & ZHOU, J. 2004. Polycystins and mechanosensation in renal and nodal cilia. *Bioessays,* 26**,** 844-56.

NC3R. 2017. *Responsibility in the use of animals in bioscience research* [Online]. Available: https://www.nc3rs.org.uk/responsibility-use-animals-bioscience-research [Accessed 12 April 2018].
NEWBY, L. J., STREETS, A. J., ZHAO, Y., HARRIS, P. C., WARD, C. J. & ONG, A. C. 2002. Identification, characterization, and localization of a novel kidney polycystin-1-polycystin-2 complex. *J Biol Chem,* 277**,** 20763-73.
NIE, X. & AREND, L. J. 2014. Novel roles of Pkd2 in male reproductive system development. *Differentiation,* 87**,** 161-71.
NILIUS, B. & OWSIANIK, G. 2011. The transient receptor potential family of ion channels. *Genome Biol,* 12**,** 218.
NIMS, N., VASSMER, D. & MASER, R. L. 2003. Transmembrane domain analysis of polycystin-1, the product of the polycystic kidney disease-1 (PKD1) gene: evidence for 11 membrane-spanning domains. *Biochemistry,* 42**,** 13035-48.
NISHIO, S., HATANO, M., NAGATA, M., HORIE, S., KOIKE, T., TOKUHISA, T. & MOCHIZUKI, T. 2005. Pkd1 regulates immortalized proliferation of renal tubular epithelial cells through p53 induction and JNK activation. *J Clin Invest,* 115**,** 910-8.
NOMURA, H., TURCO, A. E., PEI, Y., KALAYDJIEVA, L., SCHIAVELLO, T., WEREMOWICZ, S., JI, W., MORTON, C. C., MEISLER, M., REEDERS, S. T. & ZHOU, J. 1998. Identification of PKDL, a novel polycystic kidney disease 2-like gene whose murine homologue is deleted in mice with kidney and retinal defects. *J Biol Chem,* 273**,** 25967-73.
NONAKA, S., SHIRATORI, H., SAIJOH, Y. & HAMADA, H. 2002. Determination of left-right patterning of the mouse embryo by artificial nodal flow. *Nature,* 418**,** 96-9.
NONAKA, S., TANAKA, Y., OKADA, Y., TAKEDA, S., HARADA, A., KANAI, Y., KIDO, M. & HIROKAWA, N. 1998. Randomization of left-right asymmetry due to loss of nodal cilia generating leftward flow of extraembryonic fluid in mice lacking KIF3B motor protein. *Cell,* 95**,** 829-37.
NORRIS, D. P. 2012. Cilia, calcium and the basis of left-right asymmetry. *BMC Biol,* 10**,** 102.
NORRIS, D. P., BRENNAN, J., BIKOFF, E. K. & ROBERTSON, E. J. 2002. The Foxh1-dependent autoregulatory enhancer controls the level of Nodal signals in the mouse embryo. *Development,* 129**,** 3455-68.
OBARA, T., MANGOS, S., LIU, Y., ZHAO, J., WIESSNER, S., KRAMER-ZUCKER, A. G., OLALE, F., SCHIER, A. F. & DRUMMOND, I. A. 2006. Polycystin-2 immunolocalization and function in zebrafish. *J Am Soc Nephrol,* 17**,** 2706-18.
OCAÑA, O. H., COSKUN, H., MINGUILLÓN, C., MURAWALA, P., TANAKA, E. M., GALCERÁN, J., MUÑOZ-CHÁPULI, R. & NIETO, M. A. 2017. A right-handed signalling pathway drives heart looping in vertebrates. *Nature,* 549**,** 86-90.
OKADA, Y., TAKEDA, S., TANAKA, Y., IZPISÚA BELMONTE, J. C. & HIROKAWA, N. 2005. Mechanism of nodal flow: a conserved symmetry breaking event in left-right axis determination. *Cell,* 121**,** 633-44.
OKI, S., HASHIMOTO, R., OKUI, Y., SHEN, M. M., MEKADA, E., OTANI, H., SAIJOH, Y. & HAMADA, H. 2007. Sulfated glycosaminoglycans are necessary for Nodal signal transmission from the node to the left lateral plate in the mouse embryo. *Development,* 134**,** 3893-904.
OLBRICH, H., HÄFFNER, K., KISPERT, A., VÖLKEL, A., VOLZ, A., SASMAZ, G., REINHARDT, R., HENNIG, S., LEHRACH, H., KONIETZKO, N., ZARIWALA, M., NOONE, P. G., KNOWLES, M., MITCHISON, H. M., MEEKS, M., CHUNG, E. M., HILDEBRANDT, F., SUDBRAK, R. & OMRAN, H. 2002. Mutations in DNAH5 cause primary ciliary dyskinesia and randomization of left-right asymmetry. *Nat Genet,* 30**,** 143-4.
ONG, A. C., WARD, C. J., BUTLER, R. J., BIDDOLPH, S., BOWKER, C., TORRA, R., PEI, Y. & HARRIS, P. C. 1999. Coordinate expression of the autosomal dominant polycystic kidney disease

proteins, polycystin-2 and polycystin-1, in normal and cystic tissue. *Am J Pathol,* 154**,** 1721-9.

OUTEDA, P., HUSO, D. L., FISHER, S. A., HALUSHKA, M. K., KIM, H., QIAN, F., GERMINO, G. G. & WATNICK, T. 2014. Polycystin signaling is required for directed endothelial cell migration and lymphatic development. *Cell Rep,* 7**,** 634-44.

PAABY, A. B. & ROCKMAN, M. V. 2013. The many faces of pleiotropy. *Trends Genet,* 29**,** 66-73.

PAN, Z., YANG, H. & REINACH, P. S. 2011. Transient receptor potential (TRP) gene superfamily encoding cation channels. *Hum Genomics,* 5**,** 108-16.

PARNELL, S. C., MAGENHEIMER, B. S., MASER, R. L., RANKIN, C. A., SMINE, A., OKAMOTO, T. & CALVET, J. P. 1998. The polycystic kidney disease-1 protein, polycystin-1, binds and activates heterotrimeric G-proteins in vitro. *Biochem Biophys Res Commun,* 251**,** 625-31.

PARNELL, S. C., MAGENHEIMER, B. S., MASER, R. L., ZIEN, C. A., FRISCHAUF, A. M. & CALVET, J. P. 2002. Polycystin-1 activation of c-Jun N-terminal kinase and AP-1 is mediated by heterotrimeric G proteins. *J Biol Chem,* 277**,** 19566-72.

PATEL, A., DELMAS, P. & HONORÉ , E. 2007. Mechano- and Chemo-sensory Polycystins. *In:* MARTINAC, B. (ed.) *Sensing with Ion Channels.* Springer Science & Business Media.

PATEL, K., ISAAC, A. & COOKE, J. 1999. Nodal signalling and the roles of the transcription factors SnR and Pitx2 in vertebrate left-right asymmetry. *Curr Biol,* 9**,** 609-12.

PEETERS, H. & DEVRIENDT, K. 2006. Human laterality disorders. *Eur J Med Genet,* 49**,** 349-62.

PENNEKAMP, P., KARCHER, C., FISCHER, A., SCHWEICKERT, A., SKRYABIN, B., HORST, J., BLUM, M. & DWORNICZAK, B. 2002. The ion channel polycystin-2 is required for left-right axis determination in mice. *Curr Biol,* 12**,** 938-43.

PETRACCA, Y. L., SARTORETTI, M. M., DI BELLA, D. J., MARIN-BURGIN, A., CARCAGNO, A. L., SCHINDER, A. F. & LANUZA, G. M. 2016. The late and dual origin of cerebrospinal fluid-contacting neurons in the mouse spinal cord. *Development,* 143**,** 880-91.

PETRI, E. T., CELIC, A., KENNEDY, S. D., EHRLICH, B. E., BOGGON, T. J. & HODSDON, M. E. 2010. Structure of the EF-hand domain of polycystin-2 suggests a mechanism for Ca2+-dependent regulation of polycystin-2 channel activity. *Proc Natl Acad Sci U S A,* 107**,** 9176-81.

QIAN, F., BOLETTA, A., BHUNIA, A. K., XU, H., LIU, L., AHRABI, A. K., WATNICK, T. J., ZHOU, F. & GERMINO, G. G. 2002. Cleavage of polycystin-1 requires the receptor for egg jelly domain and is disrupted by human autosomal-dominant polycystic kidney disease 1-associated mutations. *Proc Natl Acad Sci U S A,* 99**,** 16981-6.

QIAN, F., GERMINO, F. J., CAI, Y., ZHANG, X., SOMLO, S. & GERMINO, G. G. 1997. PKD1 interacts with PKD2 through a probable coiled-coil domain. *Nat Genet,* 16**,** 179-83.

QIAN, Q., HUNTER, L. W., LI, M., MARIN-PADILLA, M., PRAKASH, Y. S., SOMLO, S., HARRIS, P. C., TORRES, V. E. & SIECK, G. C. 2003. Pkd2 haploinsufficiency alters intracellular calcium regulation in vascular smooth muscle cells. *Hum Mol Genet,* 12**,** 1875-80.

QIU, N., XIAO, Z., CAO, L., BUECHEL, M. M., DAVID, V., ROAN, E. & QUARLES, L. D. 2012. Disruption of Kif3a in osteoblasts results in defective bone formation and osteopenia. *J Cell Sci,* 125**,** 1945-57.

RAMSDELL, A. F. 2005. Left-right asymmetry and congenital cardiac defects: getting to the heart of the matter in vertebrate left-right axis determination. *Dev Biol,* 288**,** 1-20.

ROSSETTI, S., CONSUGAR, M. B., CHAPMAN, A. B., TORRES, V. E., GUAY-WOODFORD, L. M., GRANTHAM, J. J., BENNETT, W. M., MEYERS, C. M., WALKER, D. L., BAE, K., ZHANG, Q. J., THOMPSON, P. A., MILLER, J. P., HARRIS, P. C. & CONSORTIUM, C. 2007. Comprehensive molecular diagnostics in autosomal dominant polycystic kidney disease. *J Am Soc Nephrol,* 18**,** 2143-60.

ROXO-ROSA, M., JACINTO, R., SAMPAIO, P. & LOPES, S. S. 2015. The zebrafish Kupffer's vesicle as a model system for the molecular mechanisms by which the lack of Polycystin-2 leads to stimulation of CFTR. *Biol Open,* 4**,** 1356-66.

SALEHI-NAJAFABADI, Z., LI, B., VALENTINO, V., NG, C., MARTIN, H., YU, Y., WANG, Z. & KASHYAP, P. 2017. Extracellular Loops Are Essential for the Assembly and Function of Polycystin Receptor-Ion Channel Complexes. *J Biol Chem,* 292**,** 4210-4221.

SAUND, R. S., KANAI-AZUMA, M., KANAI, Y., KIM, I., LUCERO, M. T. & SAIJOH, Y. 2012. Gut endoderm is involved in the transfer of left-right asymmetry from the node to the lateral plate mesoderm in the mouse embryo. *Development,* 139**,** 2426-35.

SCHINDELIN, J., ARGANDA-CARRERAS, I., FRISE, E., KAYNIG, V., LONGAIR, M., PIETZSCH, T., PREIBISCH, S., RUEDEN, C., SAALFELD, S., SCHMID, B., TINEVEZ, J. Y., WHITE, D. J., HARTENSTEIN, V., ELICEIRI, K., TOMANCAK, P. & CARDONA, A. 2012. Fiji: an open-source platform for biological-image analysis. *Nat Methods,* 9**,** 676-82.

SCHRÖDER, S., FRATERNALI, F., QUAN, X., SCOTT, D., QIAN, F. & PFUHL, M. 2011. When a module is not a domain: the case of the REJ module and the redefinition of the architecture of polycystin-1. *Biochem J,* 435**,** 651-60.

SCHUMANN, F., HOFFMEISTER, H., BADER, R., SCHMIDT, M., WITZGALL, R. & KALBITZER, H. R. 2009a. Ca2+-dependent conformational changes in a C-terminal cytosolic domain of polycystin-2. *J Biol Chem,* 284**,** 24372-83.

SCHUMANN, F. H., HOFFMEISTER, H., SCHMIDT, M., BADER, R., BESL, E., WITZGALL, R. & KALBITZER, H. R. 2009b. NMR-assignments of a cytosolic domain of the C-terminus of polycystin-2. *Biomol NMR Assign,* 3**,** 141-4.

SHEN, P. S., YANG, X., DECAEN, P. G., LIU, X., BULKLEY, D., CLAPHAM, D. E. & CAO, E. 2016. The Structure of the Polycystic Kidney Disease Channel PKD2 in Lipid Nanodiscs. *Cell,* 167**,** 763-773.e11.

SHUTE, R., JEELANI, O., LEE, L., BRENNAN, E., BOCKENHAUER, D., BARNICOAT, A. & SHROFF, R. 2014. Rapid head growth in a baby with autosomal dominant polycystic kidney disease (ADPKD): questions. *Pediatr Nephrol,* 29**,** 217-8, 219-21.

STEARNS, F. W. 2010. One hundred years of pleiotropy: a retrospective. *Genetics,* 186**,** 767-73.

STREETS, A. J., MOON, D. J., KANE, M. E., OBARA, T. & ONG, A. C. 2006. Identification of an N-terminal glycogen synthase kinase 3 phosphorylation site which regulates the functional localization of polycystin-2 in vivo and in vitro. *Hum Mol Genet,* 15**,** 1465-73.

STREETS, A. J., NEWBY, L. J., O'HARE, M. J., BUKANOV, N. O., IBRAGHIMOV-BESKROVNAYA, O. & ONG, A. C. 2003. Functional analysis of PKD1 transgenic lines reveals a direct role for polycystin-1 in mediating cell-cell adhesion. *J Am Soc Nephrol,* 14**,** 1804-15.

SU, X., WU, M., YAO, G., EL-JOUNI, W., LUO, C., TABARI, A. & ZHOU, J. 2015. Regulation of polycystin-1 ciliary trafficking by motifs at its C-terminus and polycystin-2 but not by cleavage at the GPS site. *J Cell Sci,* 128**,** 4063-73.

SUTHERLAND, M. J. & WARE, S. M. 2009. Disorders of left-right asymmetry: heterotaxy and situs inversus. *Am J Med Genet C Semin Med Genet,* 151C**,** 307-17.

SUTTON, K. A., JUNGNICKEL, M. K. & FLORMAN, H. M. 2008. A polycystin-1 controls postcopulatory reproductive selection in mice. *Proc Natl Acad Sci U S A,* 105**,** 8661-6.

TAKEDA, S., YONEKAWA, Y., TANAKA, Y., OKADA, Y., NONAKA, S. & HIROKAWA, N. 1999. Left-right asymmetry and kinesin superfamily protein KIF3A: new insights in determination of laterality and mesoderm induction by kif3A-/- mice analysis. *J Cell Biol,* 145**,** 825-36.

TANAKA, Y., OKADA, Y. & HIROKAWA, N. 2005. FGF-induced vesicular release of Sonic hedgehog and retinoic acid in leftward nodal flow is critical for left-right determination. *Nature,* 435**,** 172-7.

TORRA, R., SARQUELLA, J., CALABIA, J., MARTÍ, J., ARS, E., FERNÁNDEZ-LLAMA, P. & BALLARIN, J. 2008. Prevalence of cysts in seminal tract and abnormal semen parameters in patients with autosomal dominant polycystic kidney disease. *Clin J Am Soc Nephrol,* 3**,** 790-3.

TORRES, V. E. & HARRIS, P. C. 2009. Autosomal dominant polycystic kidney disease: the last 3 years. *Kidney Int,* 76**,** 149-68.

TORRES, V. E., HARRIS, P. C. & PIRSON, Y. 2007. Autosomal dominant polycystic kidney disease. *Lancet,* 369**,** 1287-301.

TSIOKAS, L., ARNOULD, T., ZHU, C., KIM, E., WALZ, G. & SUKHATME, V. P. 1999. Specific association of the gene product of PKD2 with the TRPC1 channel. *Proc Natl Acad Sci U S A,* 96**,** 3934-9.

TSIOKAS, L., KIM, E., ARNOULD, T., SUKHATME, V. P. & WALZ, G. 1997. Homo- and heterodimeric interactions between the gene products of PKD1 and PKD2. *Proc Natl Acad Sci U S A,* 94**,** 6965-70.

TURCO, A. E., PADOVANI, E. M., CHIAFFONI, G. P., PEISSEL, B., ROSSETTI, S., MARCOLONGO, A., GAMMARO, L., MASCHIO, G. & PIGNATTI, P. F. 1993. Molecular genetic diagnosis of autosomal dominant polycystic kidney disease in a newborn with bilateral cystic kidneys detected prenatally and multiple skeletal malformations. *J Med Genet,* 30**,** 419-22.

VARJOSALO, M. & TAIPALE, J. 2008. Hedgehog: functions and mechanisms. *Genes Dev,* 22**,** 2454-72.

VELDHUISEN, B., SPRUIT, L., DAUWERSE, H. G., BREUNING, M. H. & PETERS, D. J. 1999. Genes homologous to the autosomal dominant polycystic kidney disease genes (PKD1 and PKD2). *Eur J Hum Genet,* 7**,** 860-72.

VETRINI, F., D'ALESSANDRO, L. C., AKDEMIR, Z. C., BRAXTON, A., AZAMIAN, M. S., ELDOMERY, M. K., MILLER, K., KOIS, C., SACK, V., SHUR, N., RIJHSINGHANI, A., CHANDARANA, J., DING, Y., HOLTZMAN, J., JHANGIANI, S. N., MUZNY, D. M., GIBBS, R. A., ENG, C. M., HANCHARD, N. A., HAREL, T., ROSENFELD, J. A., BELMONT, J. W., LUPSKI, J. R. & YANG, Y. 2016. Bi-allelic Mutations in PKD1L1 Are Associated with Laterality Defects in Humans. *Am J Hum Genet,* 99**,** 886-893.

VIOTTI, M., NIU, L., SHI, S. H. & HADJANTONAKIS, A. K. 2012. Role of the gut endoderm in relaying left-right patterning in mice. *PLoS Biol,* 10**,** e1001276.

VOGEL, P., READ, R., HANSEN, G. M., FREAY, L. C., ZAMBROWICZ, B. P. & SANDS, A. T. 2010. Situs inversus in Dpcd/Poll-/-, Nme7-/- , and Pkd1l1-/- mice. *Vet Pathol,* 47**,** 120-31.

VORA, N., PERRONE, R. & BIANCHI, D. W. 2008. Reproductive issues for adults with autosomal dominant polycystic kidney disease. *Am J Kidney Dis,* 51**,** 307-18.

WALKER, R. V. 2016. *Investigating the role of ciliary localisation of the TRPP channel, Polycystin2 (PKD2), on development and progression of Polycystic Kidney Disease.* DPhil, University of Oxford.

WARD, C. J., TURLEY, H., ONG, A. C., COMLEY, M., BIDDOLPH, S., CHETTY, R., RATCLIFFE, P. J., GATTNER, K. & HARRIS, P. C. 1996. Polycystin, the polycystic kidney disease 1 protein, is expressed by epithelial cells in fetal, adult, and polycystic kidney. *Proc Natl Acad Sci U S A,* 93**,** 1524-8.

WARD, H. H., BROWN-GLABERMAN, U., WANG, J., MORITA, Y., ALPER, S. L., BEDRICK, E. J., GATTONE, V. H., DERETIC, D. & WANDINGER-NESS, A. 2011. A conserved signal and GTPase complex are required for the ciliary transport of polycystin-1. *Mol Biol Cell,* 22**,** 3289-305.

WHEELER, G. L. & BROWNLEE, C. 2008. Ca2+ signalling in plants and green algae--changing channels. *Trends Plant Sci,* 13**,** 506-14.

WILKES, M., MADEJ, M. G., KREUTER, L., RHINOW, D., HEINZ, V., DE SANCTIS, S., RUPPEL, S., RICHTER, R. M., JOOS, F., GRIEBEN, M., PIKE, A. C., HUISKONEN, J. T., CARPENTER, E. P.,

KÜHLBRANDT, W., WITZGALL, R. & ZIEGLER, C. 2017. Molecular insights into lipid-assisted Ca2+ regulation of the TRP channel Polycystin-2. *Nat Struct Mol Biol,* 24**,** 123-130.

WILSON, P. D. 2004. Polycystic kidney disease: new understanding in the pathogenesis. *Int J Biochem Cell Biol,* 36**,** 1868-73.

WU, G., D'AGATI, V., CAI, Y., MARKOWITZ, G., PARK, J. H., REYNOLDS, D. M., MAEDA, Y., LE, T. C., HOU, H., KUCHERLAPATI, R., EDELMANN, W. & SOMLO, S. 1998a. Somatic inactivation of Pkd2 results in polycystic kidney disease. *Cell,* 93**,** 177-88.

WU, G., HAYASHI, T., PARK, J. H., DIXIT, M., REYNOLDS, D. M., LI, L., MAEDA, Y., CAI, Y., COCA-PRADOS, M. & SOMLO, S. 1998b. Identification of PKD2L, a human PKD2-related gene: tissue-specific expression and mapping to chromosome 10q25. *Genomics,* 54**,** 564-8.

WU, G., MARKOWITZ, G. S., LI, L., D'AGATI, V. D., FACTOR, S. M., GENG, L., TIBARA, S., TUCHMAN, J., CAI, Y., PARK, J. H., VAN ADELSBERG, J., HOU, H., KUCHERLAPATI, R., EDELMANN, W. & SOMLO, S. 2000. Cardiac defects and renal failure in mice with targeted mutations in Pkd2. *Nat Genet,* 24**,** 75-8.

WU, G., TIAN, X., NISHIMURA, S., MARKOWITZ, G. S., D'AGATI, V., PARK, J. H., YAO, L., LI, L., GENG, L., ZHAO, H., EDELMANN, W. & SOMLO, S. 2002. Trans-heterozygous Pkd1 and Pkd2 mutations modify expression of polycystic kidney disease. *Hum Mol Genet,* 11**,** 1845-54.

WU, L. J., SWEET, T. B. & CLAPHAM, D. E. 2010. International Union of Basic and Clinical Pharmacology. LXXVI. Current progress in the mammalian TRP ion channel family. *Pharmacol Rev,* 62**,** 381-404.

XIAO, Z., CAO, L., LIANG, Y., HUANG, J., STERN, A. R., DALLAS, M., JOHNSON, M. & QUARLES, L. D. 2014. Osteoblast-specific deletion of Pkd2 leads to low-turnover osteopenia and reduced bone marrow adiposity. *PLoS One,* 9**,** e114198.

XIAO, Z., ZHANG, S., CAO, L., QIU, N., DAVID, V. & QUARLES, L. D. 2010. Conditional disruption of Pkd1 in osteoblasts results in osteopenia due to direct impairment of bone formation. *J Biol Chem,* 285**,** 1177-87.

XIAO, Z., ZHANG, S., MAGENHEIMER, B. S., LUO, J. & QUARLES, L. D. 2008. Polycystin-1 regulates skeletogenesis through stimulation of the osteoblast-specific transcription factor RUNX2-II. *J Biol Chem,* 283**,** 12624-34.

XIAO, Z., ZHANG, S., MAHLIOS, J., ZHOU, G., MAGENHEIMER, B. S., GUO, D., DALLAS, S. L., MASER, R., CALVET, J. P., BONEWALD, L. & QUARLES, L. D. 2006. Cilia-like structures and polycystin-1 in osteoblasts/osteocytes and associated abnormalities in skeletogenesis and Runx2 expression. *J Biol Chem,* 281**,** 30884-95.

XIAO, Z. S. & QUARLES, L. D. 2010. Role of the polycytin-primary cilia complex in bone development and mechanosensing. *Ann N Y Acad Sci,* 1192**,** 410-21.

XU, J. X., LU, T. S., LI, S., WU, Y., DING, L., DENKER, B. M., BONVENTRE, J. V. & KONG, T. 2015. Polycystin-1 and Gα12 regulate the cleavage of E-cadherin in kidney epithelial cells. *Physiol Genomics,* 47**,** 24-32.

XU, M., MA, L., BUJALOWSKI, P. J., QIAN, F., SUTTON, R. B. & OBERHAUSER, A. F. 2013. Analysis of the REJ Module of Polycystin-1 Using Molecular Modeling and Force-Spectroscopy Techniques. *J Biophys,* 2013**,** 525231.

XU, Y., STREETS, A. J., HOUNSLOW, A. M., TRAN, U., JEAN-ALPHONSE, F., NEEDHAM, A. J., VILARDAGA, J. P., WESSELY, O., WILLIAMSON, M. P. & ONG, A. C. 2016. The Polycystin-1, Lipoxygenase, and α-Toxin Domain Regulates Polycystin-1 Trafficking. *J Am Soc Nephrol,* 27**,** 1159-73.

YANG, Y. & EHRLICH, B. E. 2016. Structural studies of the C-terminal tail of polycystin-2 (PC2) reveal insights into the mechanisms used for the functional regulation of PC2. *J Physiol,* 594**,** 4141-9.

YANG, Y., HODSDON, M. E., LOLIS, E. J. & EHRLICH, B. E. 2016. Conformational dynamics of Ca2+-dependent responses in the polycystin-2 C-terminal tail. *Biochem J,* 473**,** 285-96.

YANG, Y., KEELER, C., KUO, I. Y., LOLIS, E. J., EHRLICH, B. E. & HODSDON, M. E. 2015. Oligomerization of the polycystin-2 C-terminal tail and effects on its Ca2+-binding properties. *J Biol Chem,* 290**,** 10544-54.

YOSHIBA, S., SHIRATORI, H., KUO, I. Y., KAWASUMI, A., SHINOHARA, K., NONAKA, S., ASAI, Y., SASAKI, G., BELO, J. A., SASAKI, H., NAKAI, J., DWORNICZAK, B., EHRLICH, B. E., PENNEKAMP, P. & HAMADA, H. 2012. Cilia at the node of mouse embryos sense fluid flow for left-right determination via Pkd2. *Science,* 338**,** 226-31.

YU, M., RIVA, L., XIE, H., SCHINDLER, Y., MORAN, T. B., CHENG, Y., YU, D., HARDISON, R., WEISS, M. J., ORKIN, S. H., BERNSTEIN, B. E., FRAENKEL, E. & CANTOR, A. B. 2009. Insights into GATA-1-mediated gene activation versus repression via genome-wide chromatin occupancy analysis. *Mol Cell,* 36**,** 682-95.

YU, Y., ULBRICH, M. H., LI, M. H., DOBBINS, S., ZHANG, W. K., TONG, L., ISACOFF, E. Y. & YANG, J. 2012. Molecular mechanism of the assembly of an acid-sensing receptor ion channel complex. *Nat Commun,* 3**,** 1252.

YUAN, S., ZHAO, L., BRUECKNER, M. & SUN, Z. 2015. Intraciliary calcium oscillations initiate vertebrate left-right asymmetry. *Curr Biol,* 25**,** 556-67.

YUASA, T., TAKAKURA, A., DENKER, B. M., VENUGOPAL, B. & ZHOU, J. 2004. Polycystin-1L2 is a novel G-protein-binding protein. *Genomics,* 84**,** 126-38.

YUASA, T., VENUGOPAL, B., WEREMOWICZ, S., MORTON, C. C., GUO, L. & ZHOU, J. 2002. The sequence, expression, and chromosomal localization of a novel polycystic kidney disease 1-like gene, PKD1L1, in human. *Genomics,* 79**,** 376-86.

YUSHKEVICH, P. A., PIVEN, J., HAZLETT, H. C., SMITH, R. G., HO, S., GEE, J. C. & GERIG, G. 2006. User-guided 3D active contour segmentation of anatomical structures: significantly improved efficiency and reliability. *Neuroimage,* 31**,** 1116-28.

ZHANG, P., LUO, Y., CHASAN, B., GONZÁLEZ-PERRETT, S., MONTALBETTI, N., TIMPANARO, G. A., CANTERO, M. E. R., RAMOS, A. J., GOLDMANN, W. H., ZHOU, J. & CANTIELLO, H. F. 2009. The multimeric structure of polycystin-2 (TRPP2): structural-functional correlates of homo- and hetero-multimers with TRPC1. *Hum Mol Genet,* 18**,** 1238-51.

ZHU, J., YU, Y., ULBRICH, M. H., LI, M. H., ISACOFF, E. Y., HONIG, B. & YANG, J. 2011. Structural model of the TRPP2/PKD1 C-terminal coiled-coil complex produced by a combined computational and experimental approach. *Proc Natl Acad Sci U S A,* 108**,** 10133-8.

NEC PLVS VLTRA

Appendix 1: Figures

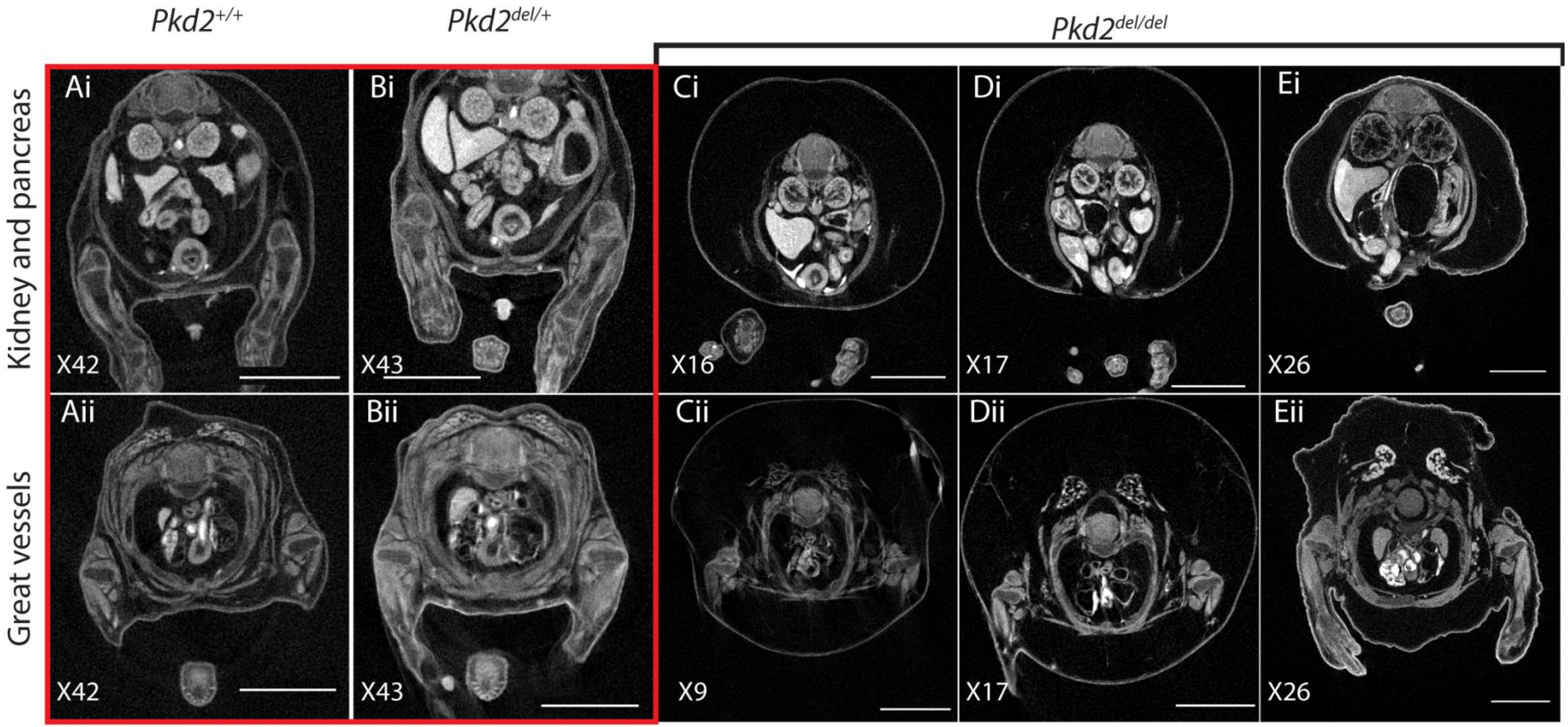


Figure A1.1: Unannotated **Fig. 3.3**, see **Chapter 3**, pages 92-93.

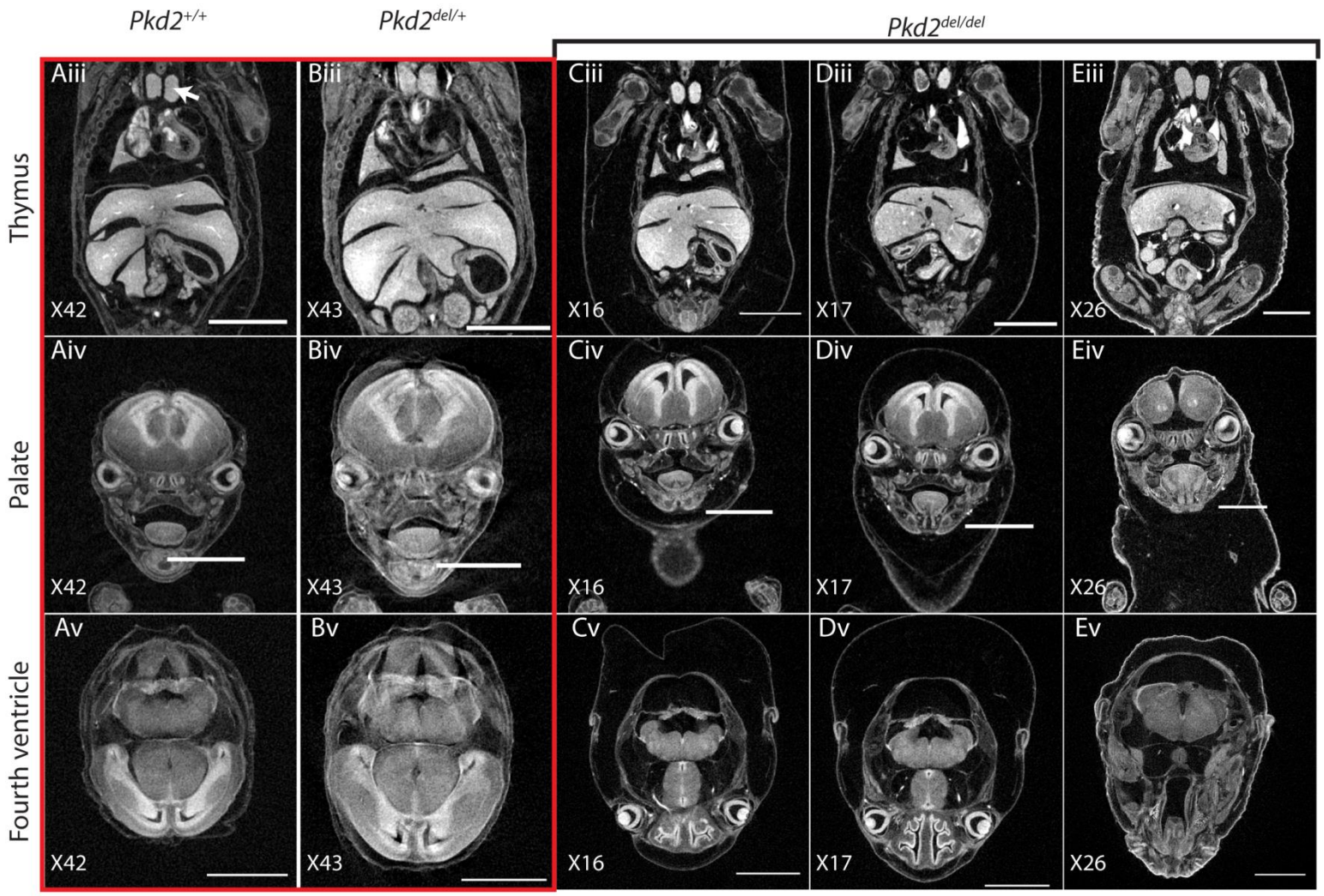


Figure A1.1 (continued)

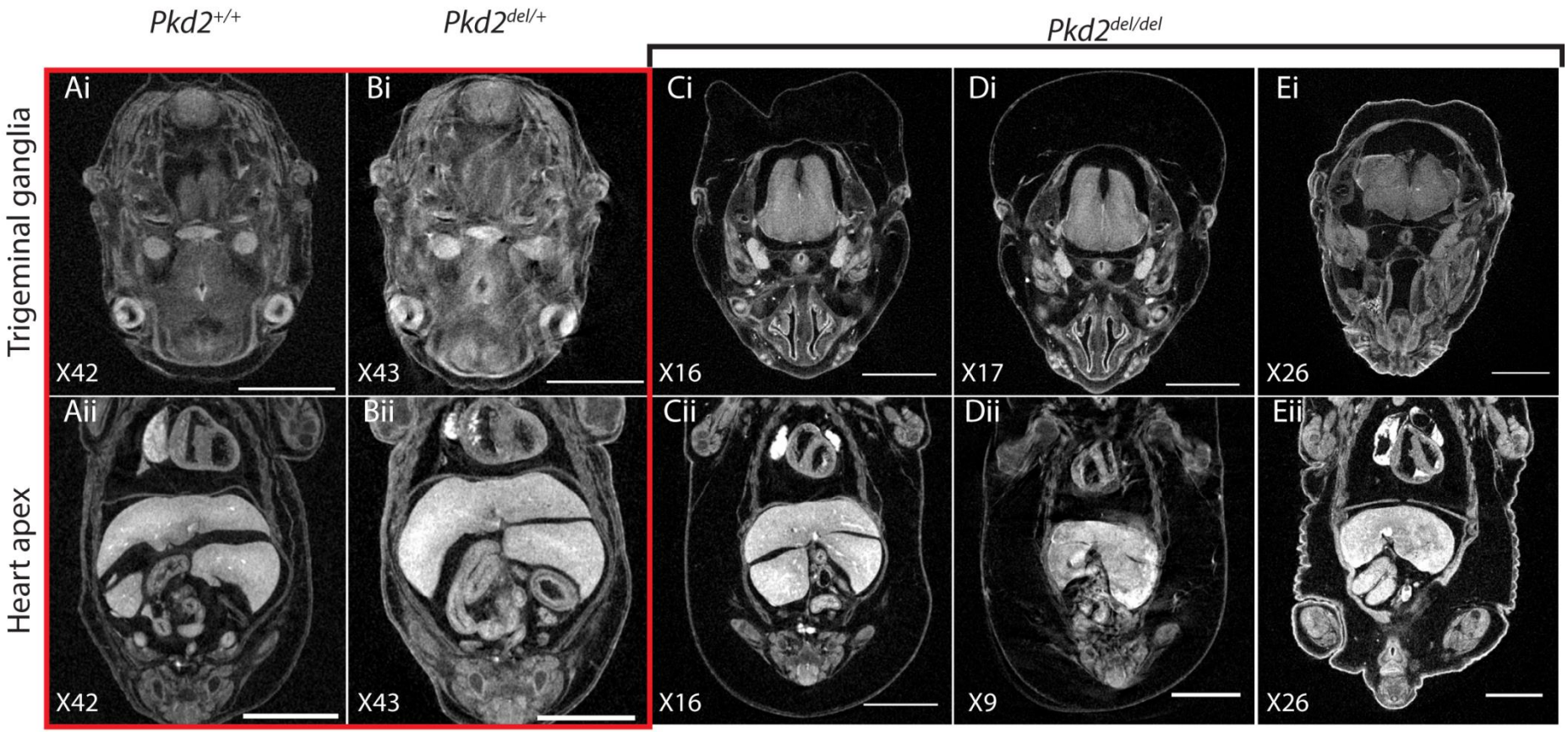


Figure A1.2: Unannotated **Fig. 3.4**, see **Chapter 3**, pages 96-97.

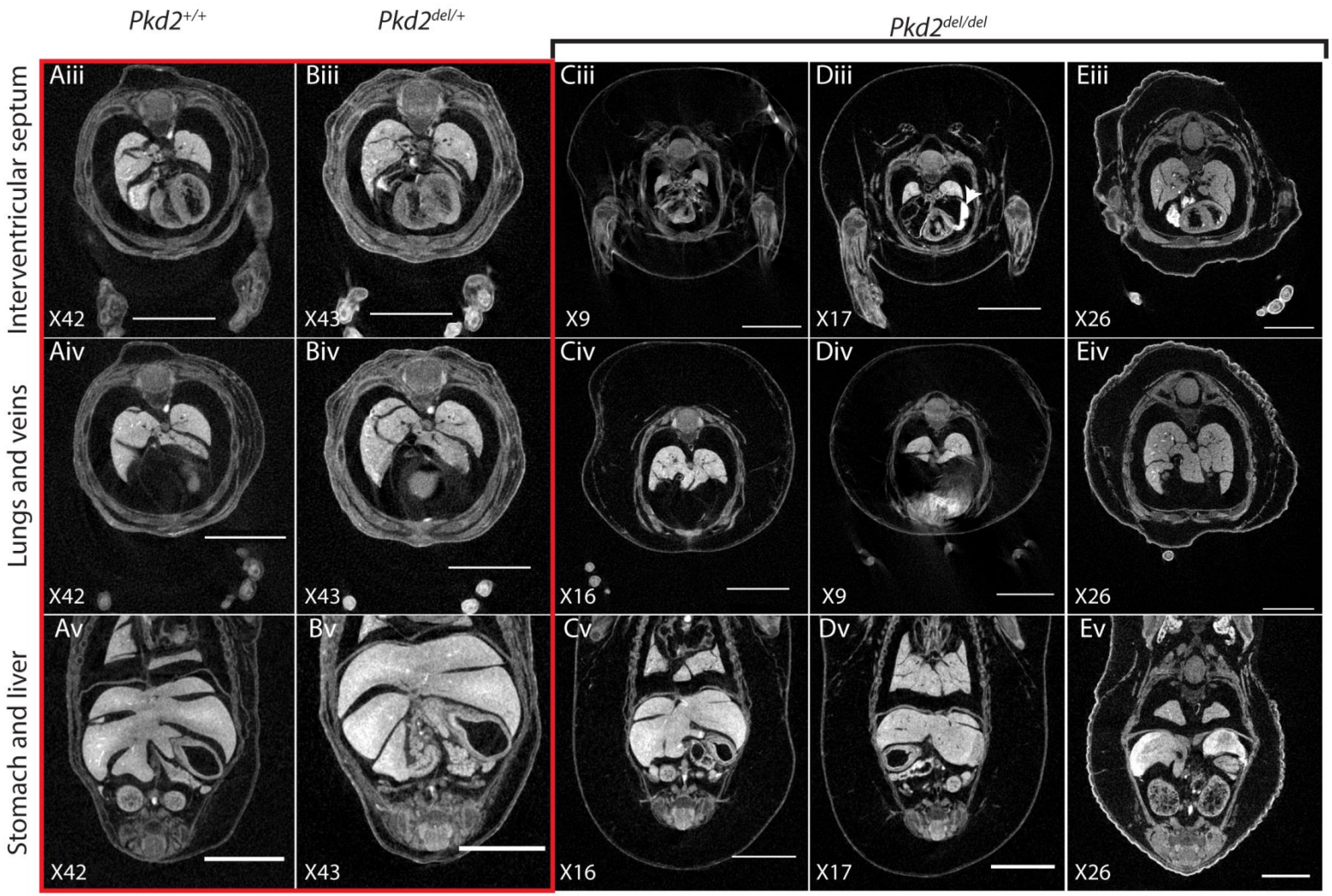


Figure A1.2 (continued)

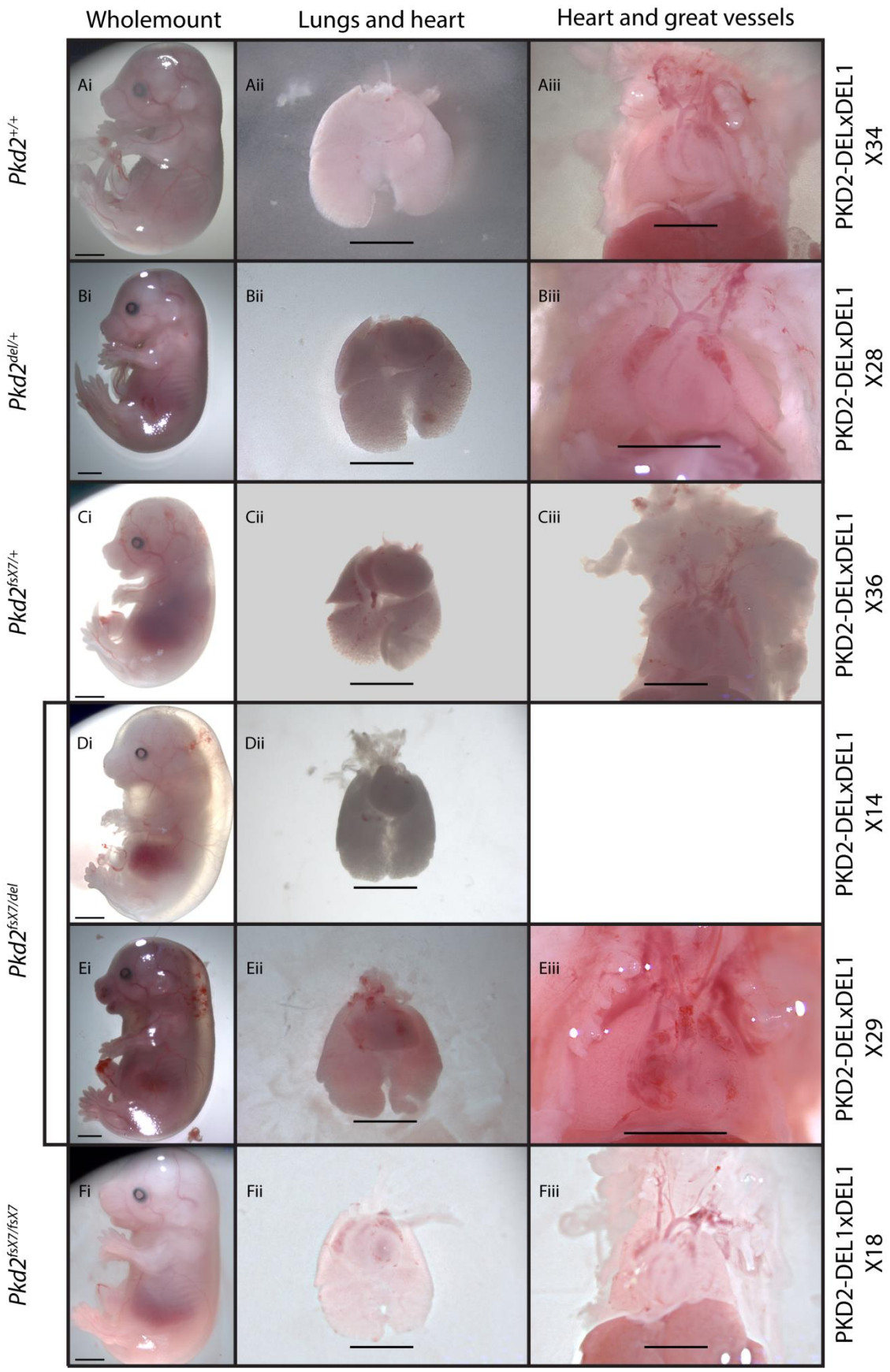


Figure A1.3: Unannotated **Fig. 3.5**, see **Chapter 3**, page 100.

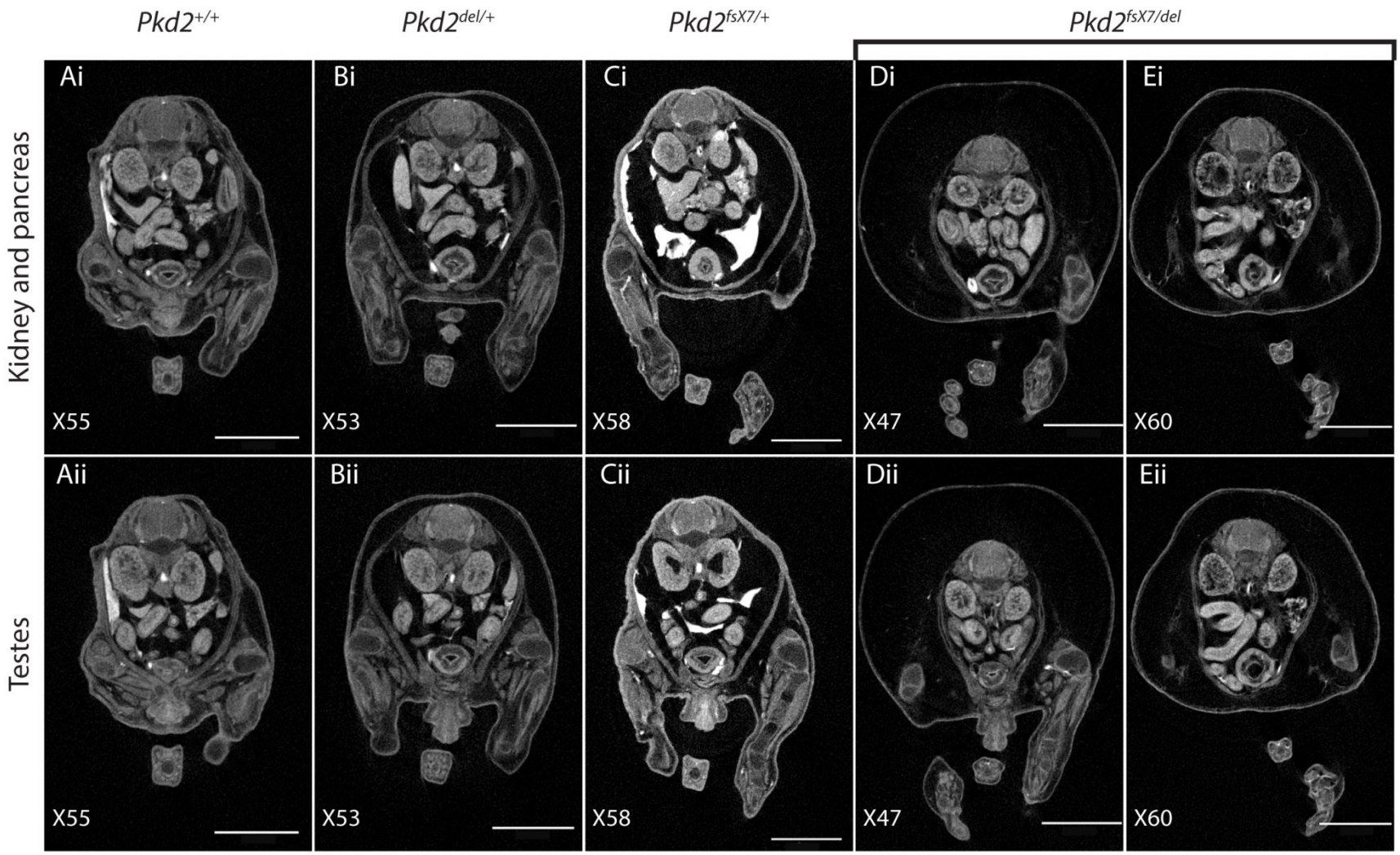


Figure A1.4: Unannotated **Fig. 3.7**, see **Chapter 3**, pages 106-107.

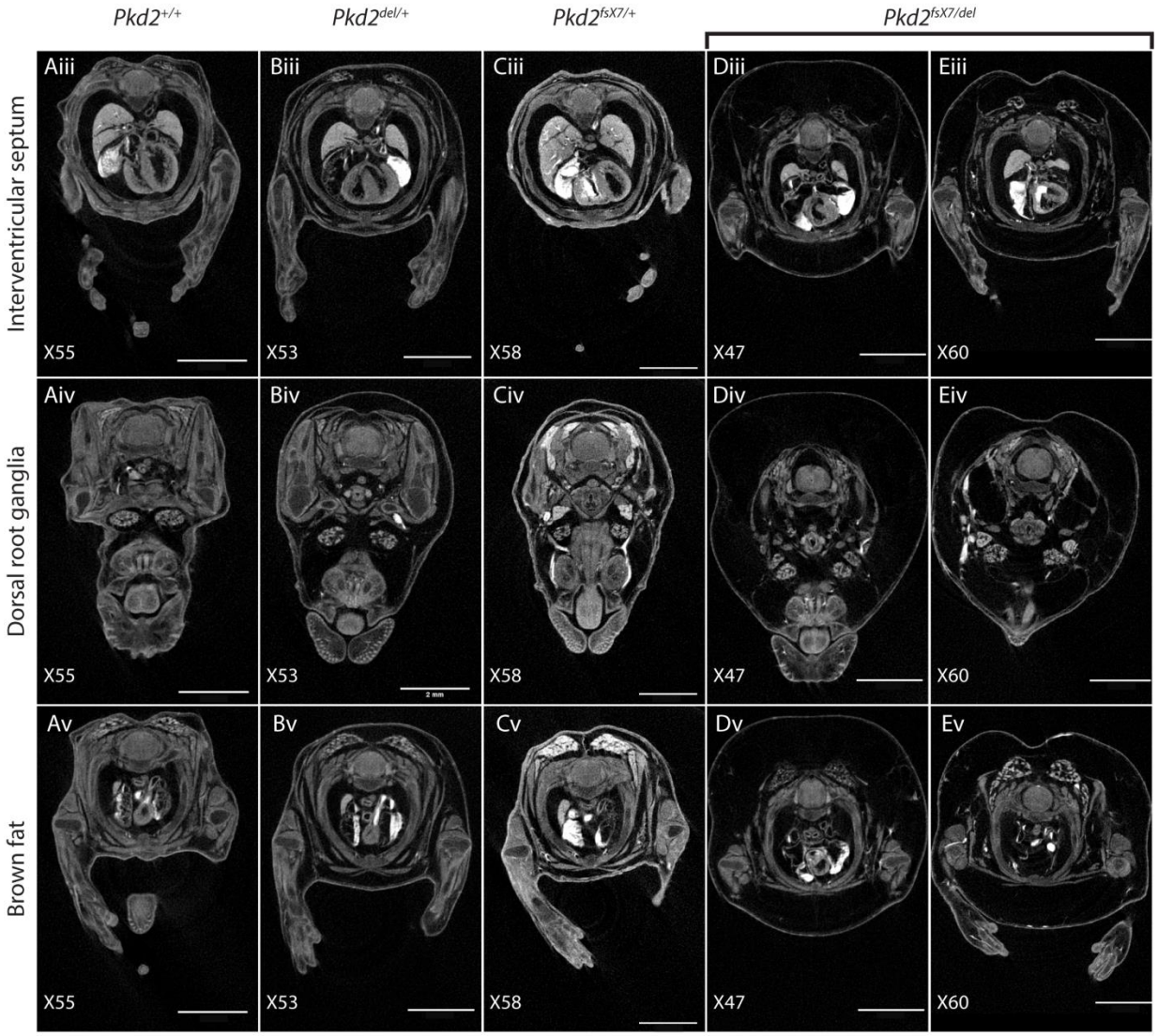


Figure A1.4 (continued)

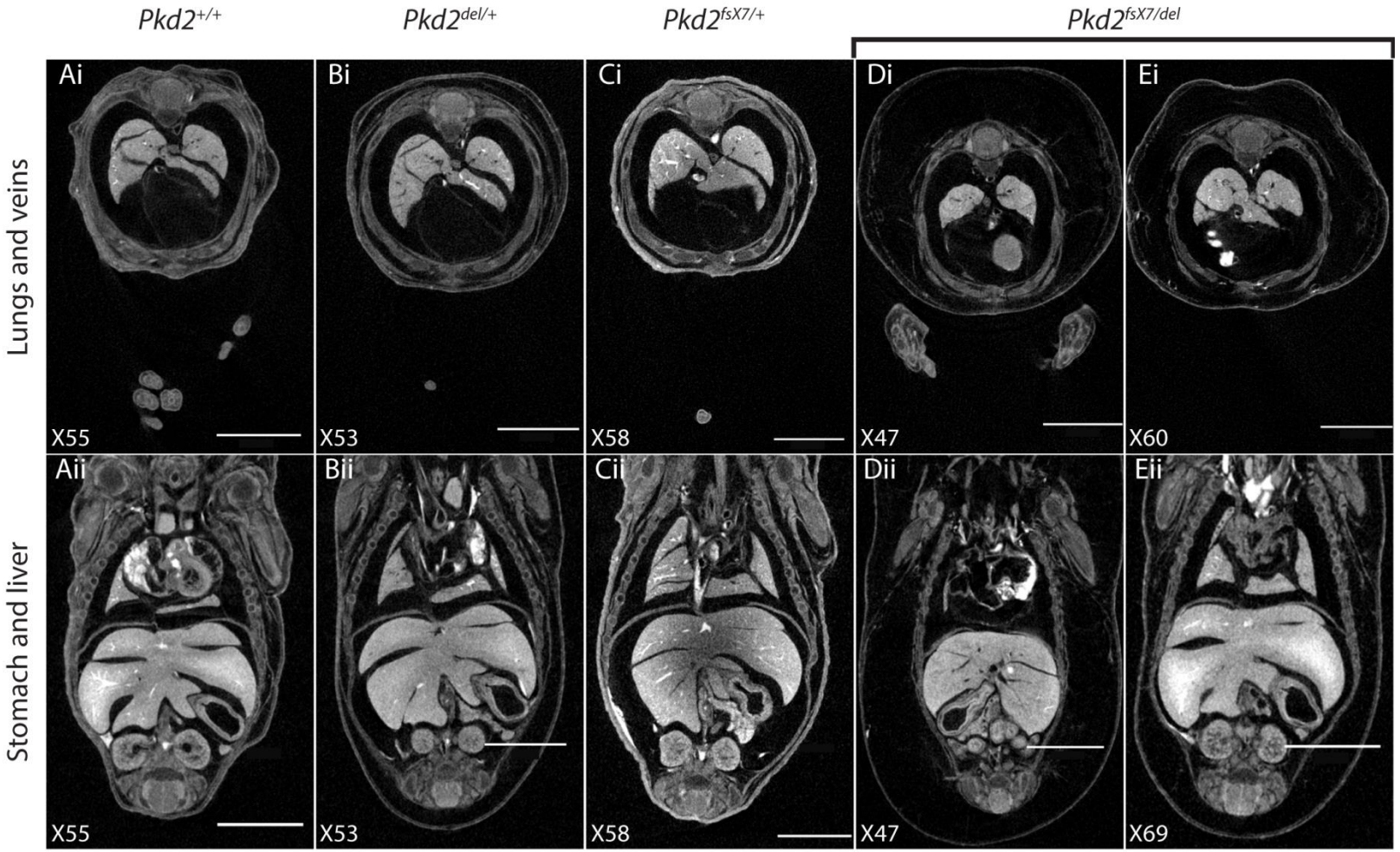


Figure A1.5: Unannotated **Fig. 3.8**, see **Chapter 3**, pages 108-109.

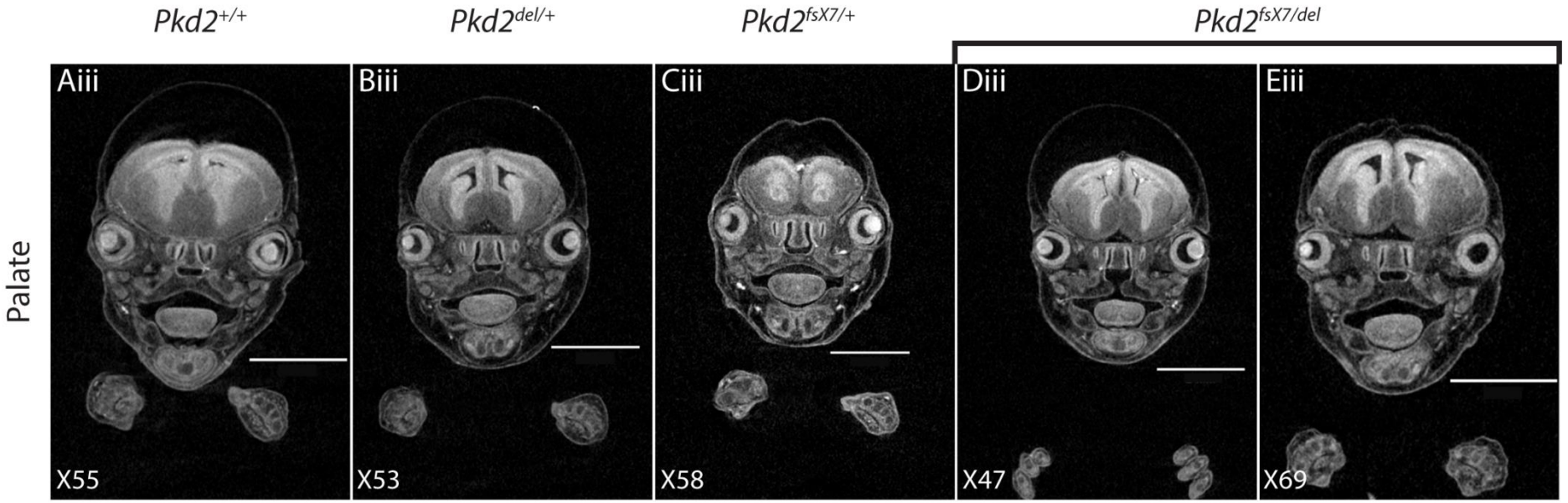


Figure A1.5 (continued)

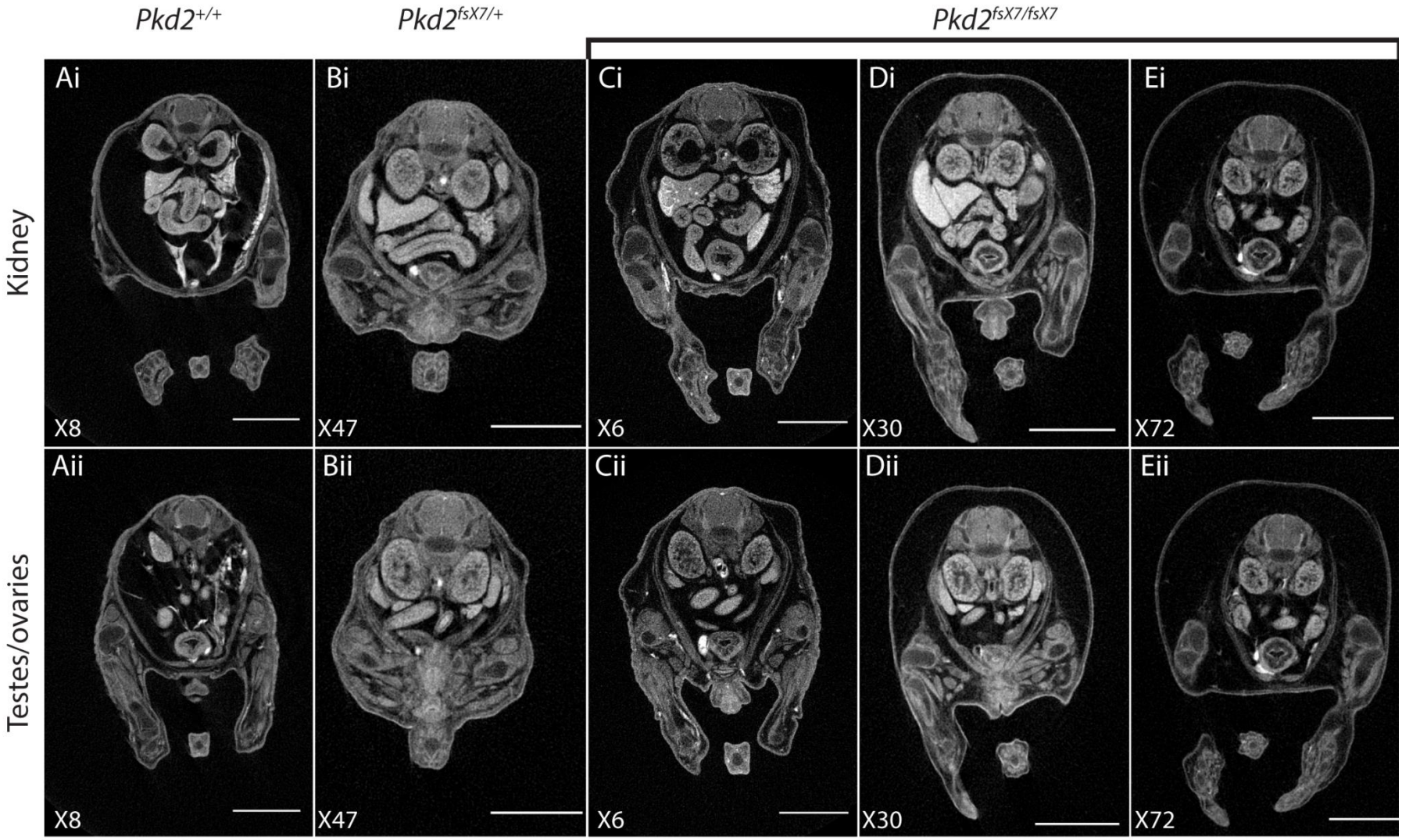


Figure A1.6: Unannotated **Fig. 3.9**, see **Chapter 3**, pages 110-111.

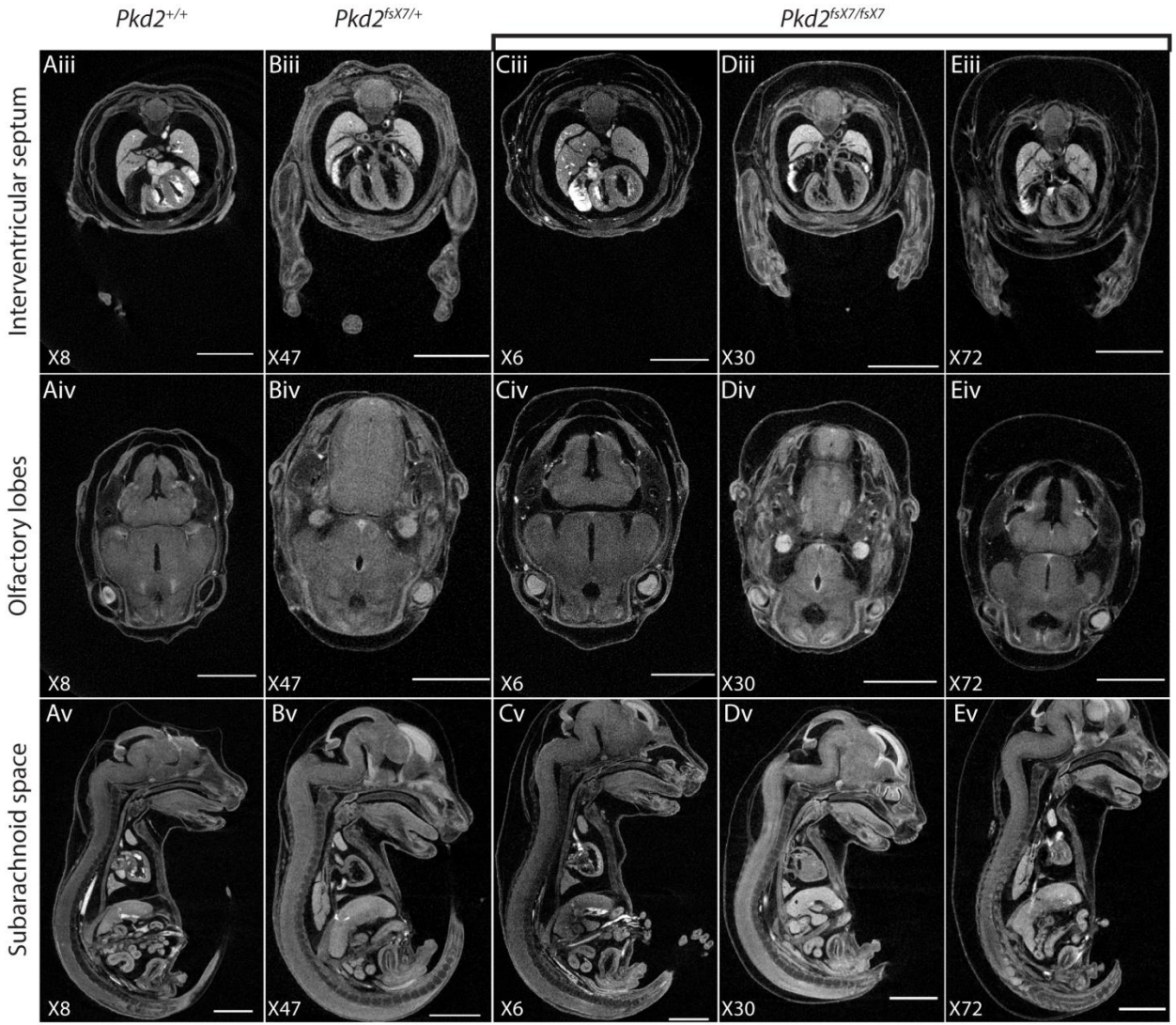


Figure A1.6 (continued)

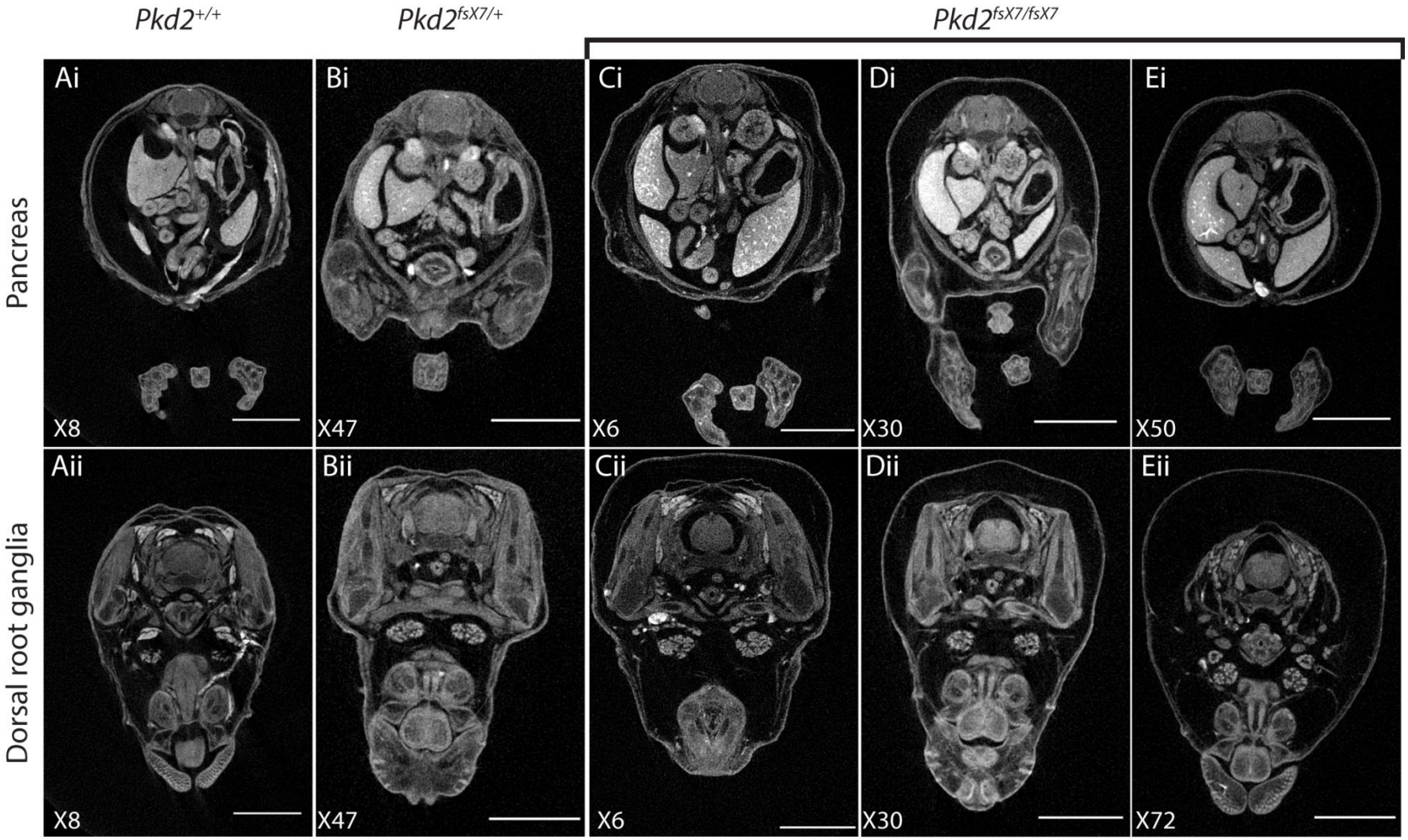


Figure A1.7: Unannotated **Fig. 3.10**, see **Chapter 3**, pages 112-113.

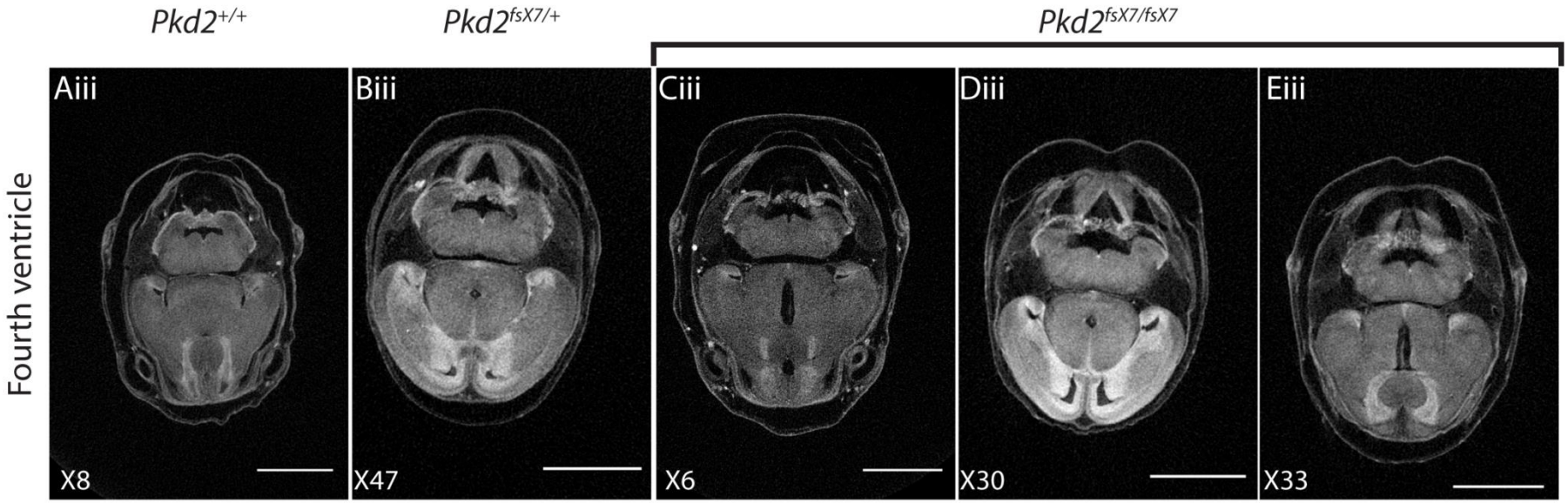


Figure A1.7 (continued)

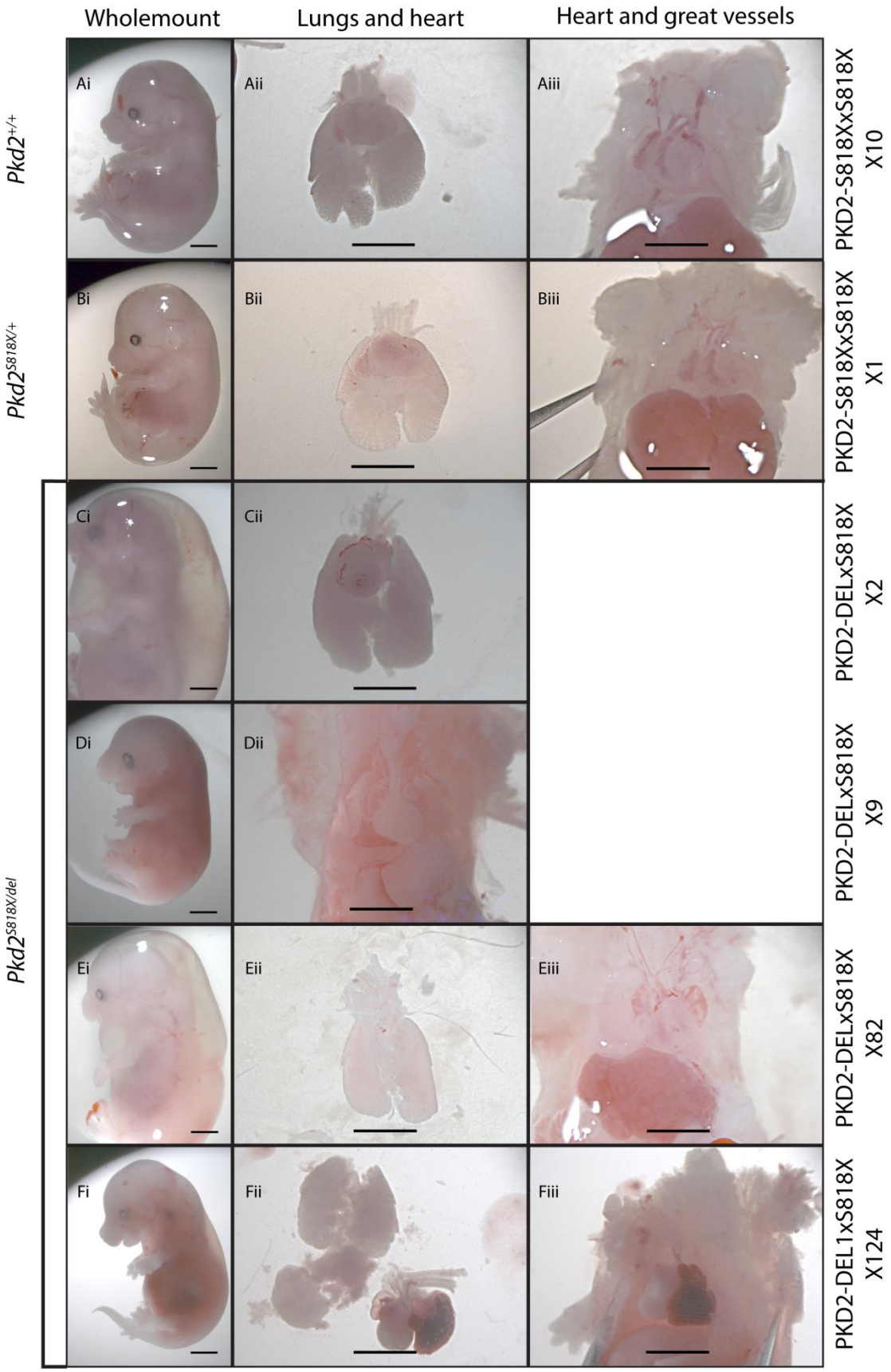


Figure A1.8: Unannotated **Fig. 3.12**, see **Chapter 3**, page 120.

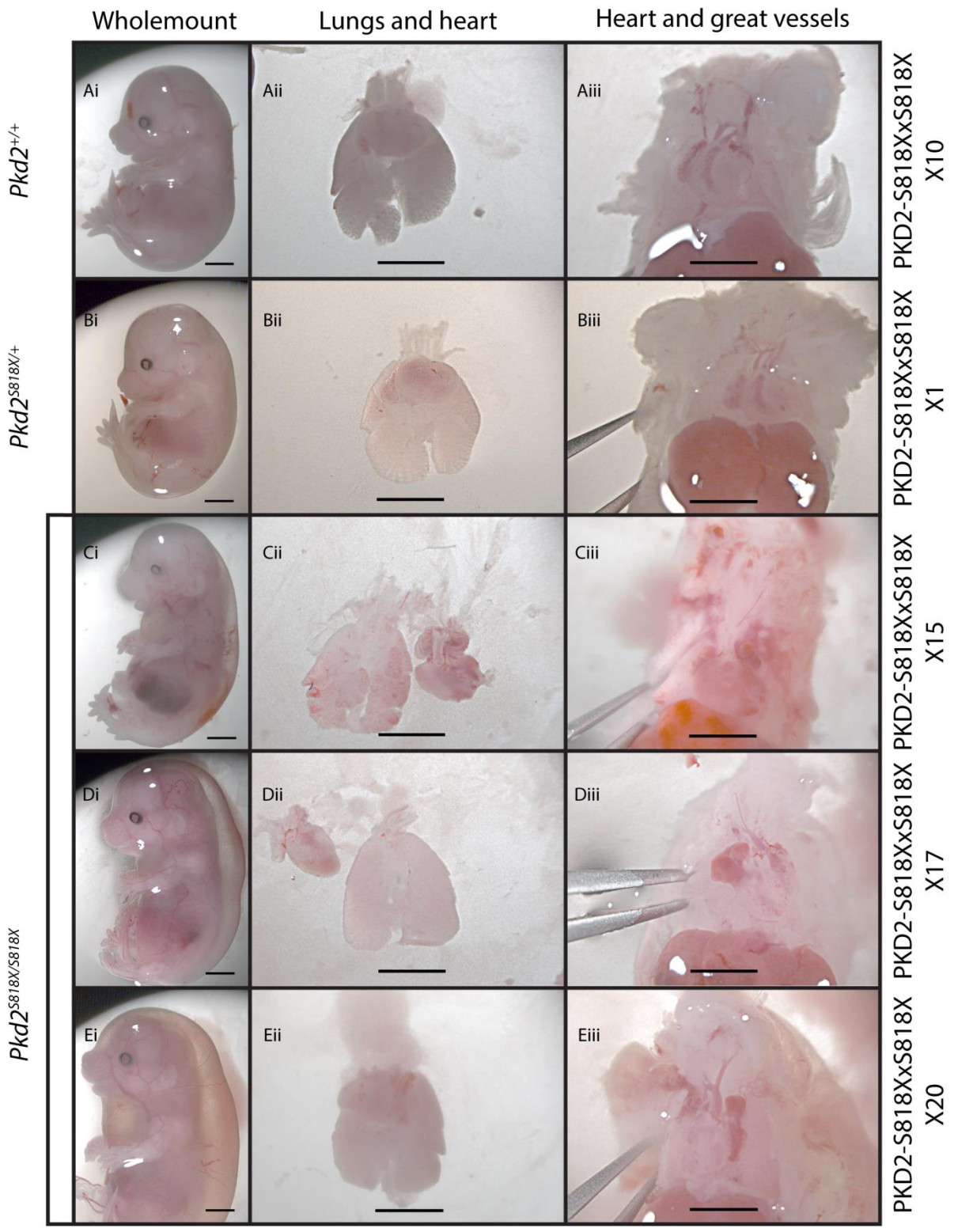


Figure A1.9: Unannotated **Fig. 3.13**, see **Chapter 3**, page 121.

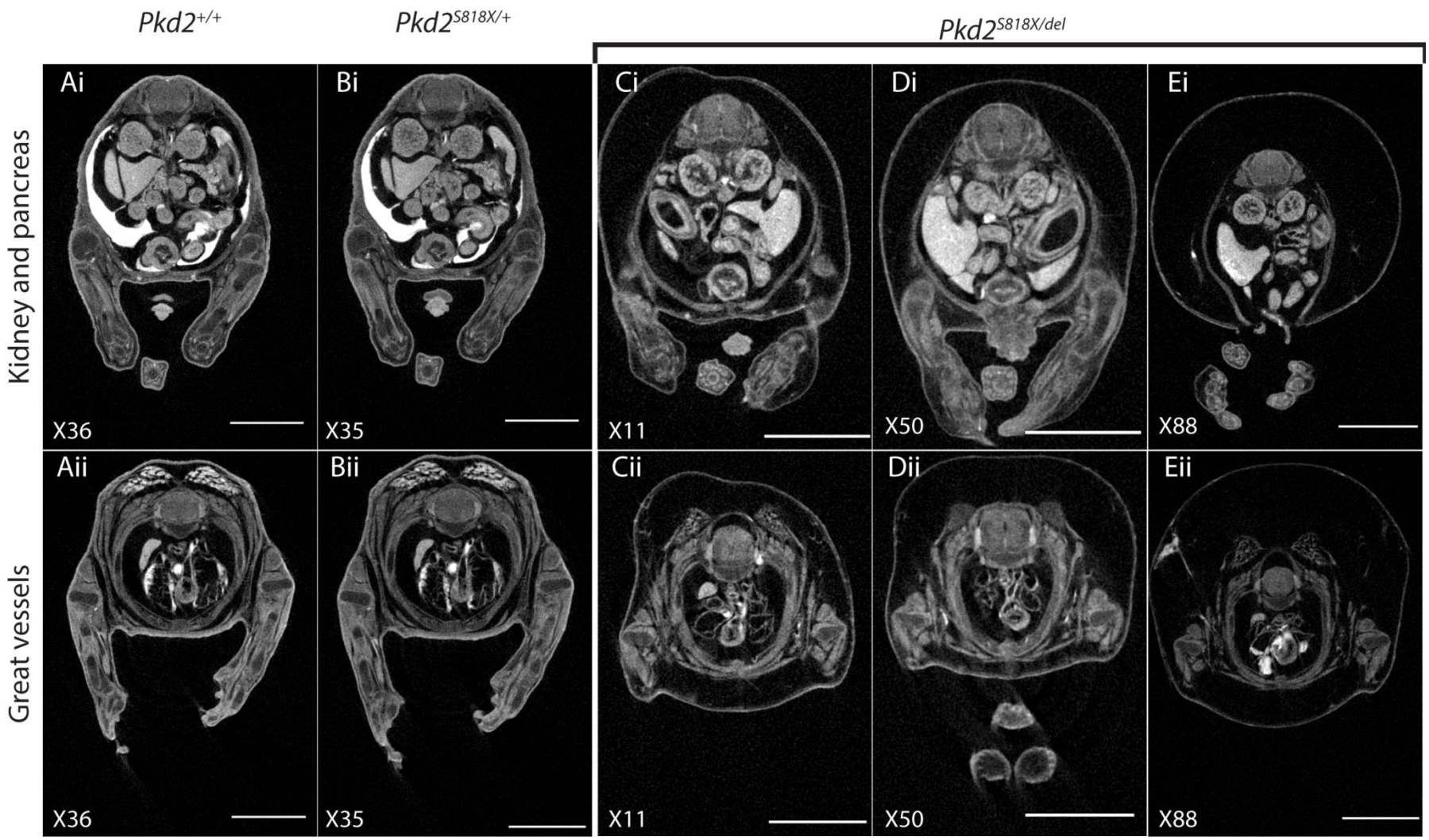


Figure A1.10: Unannotated **Fig. 3.15**, see **Chapter 3**, pages 128-129.

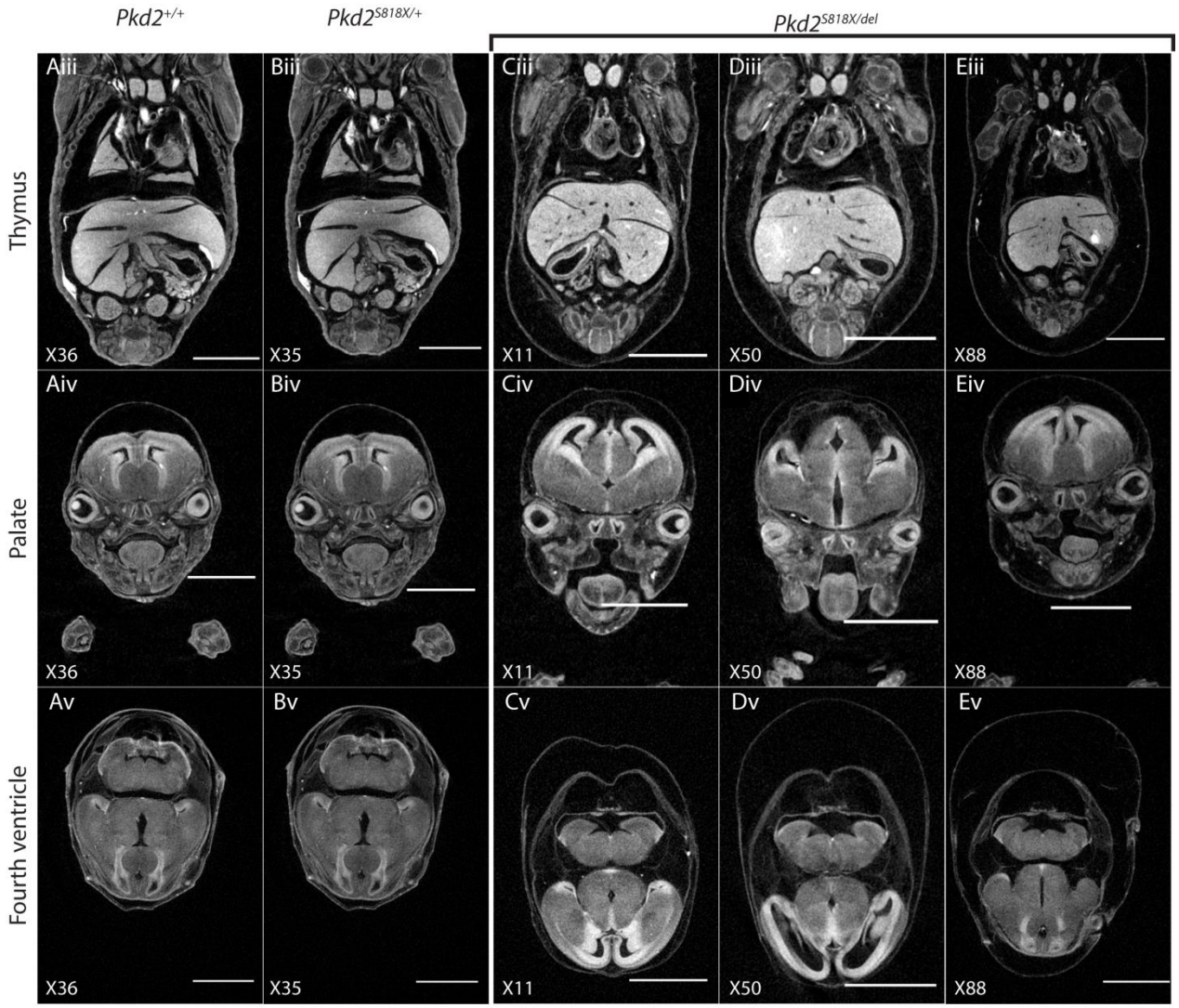


Figure A1.10 (continued)

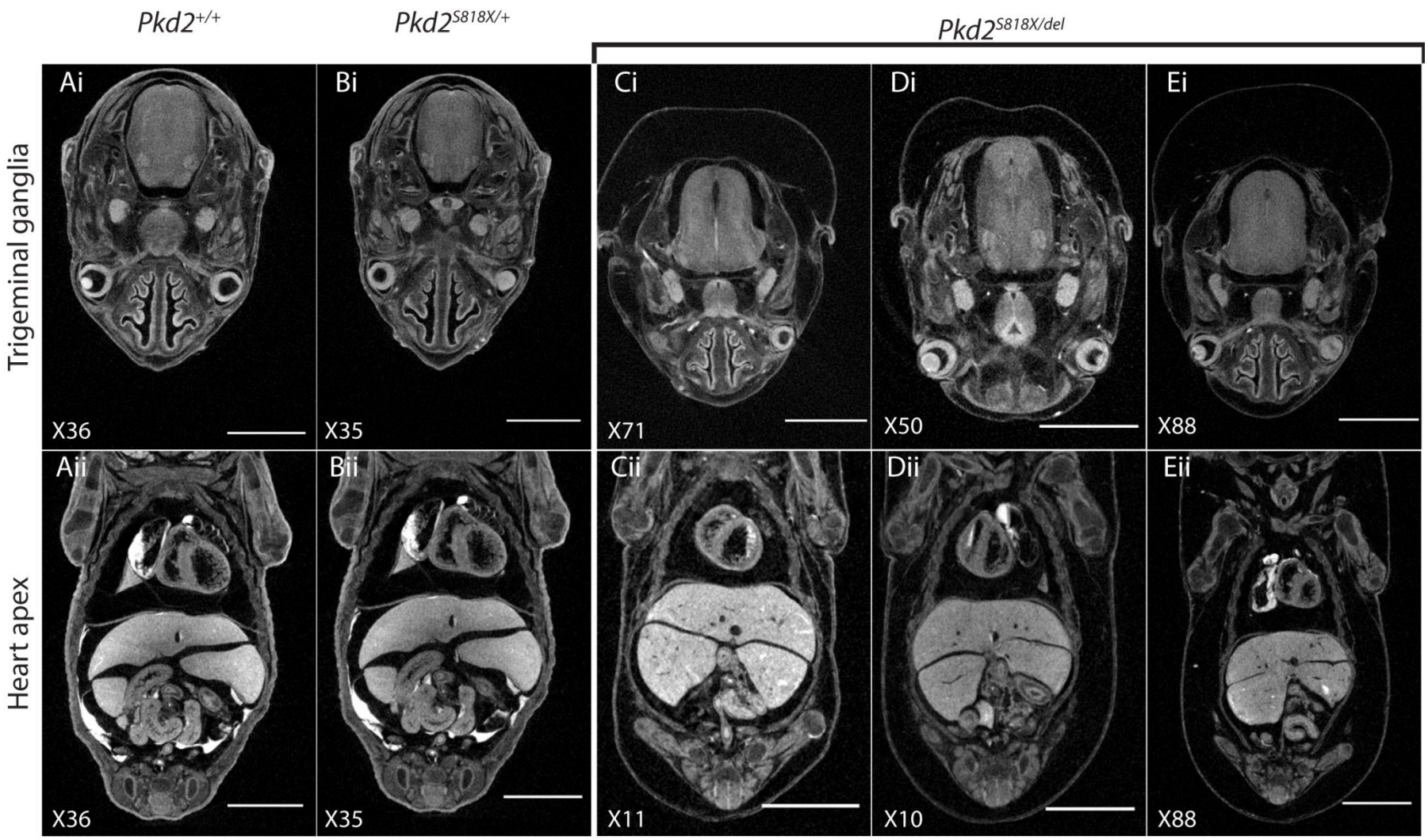


Figure A1.11: Unannotated **Fig. 3.16**, see **Chapter 3**, pages 130-131.

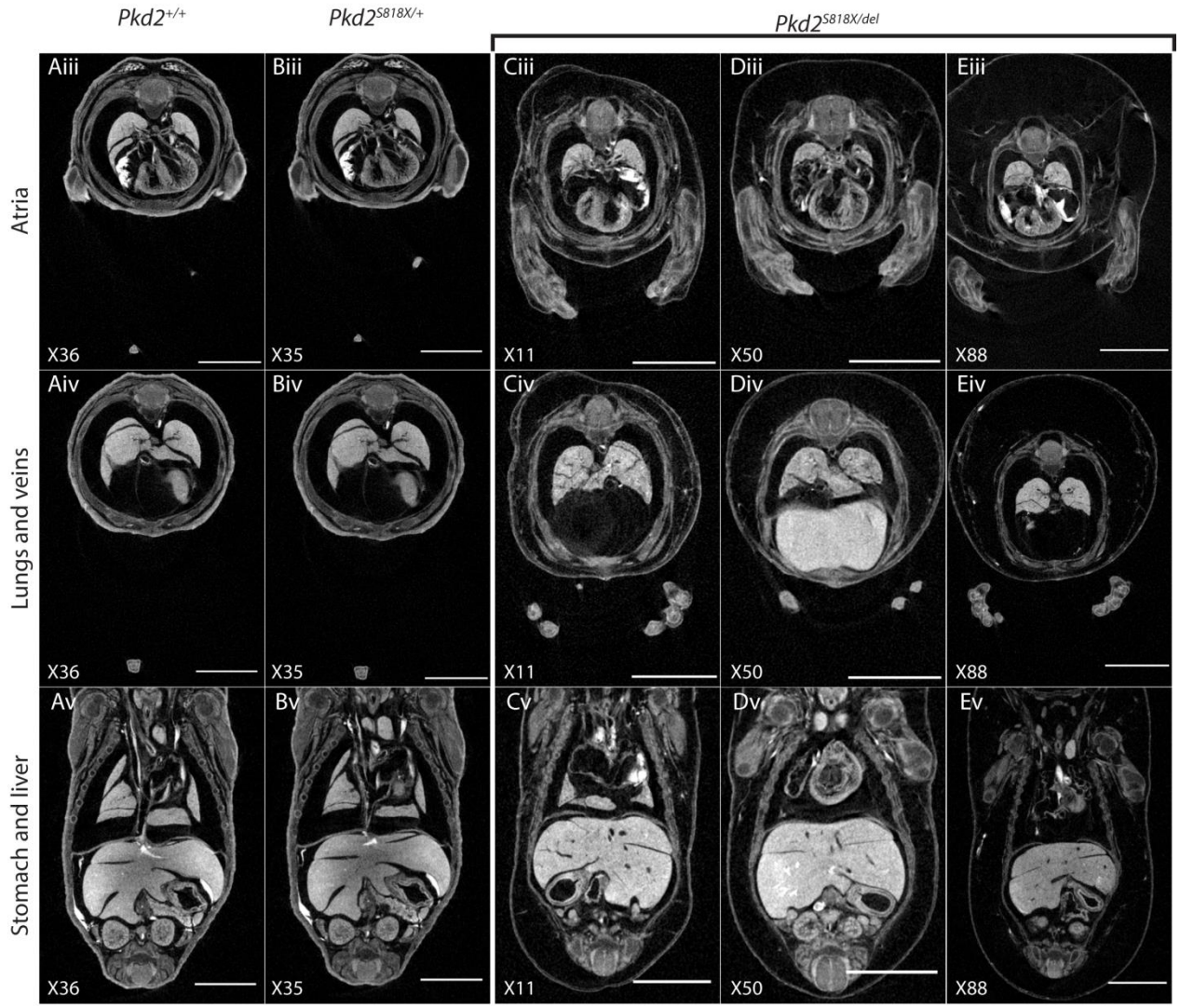


Figure A1.11 (continued)

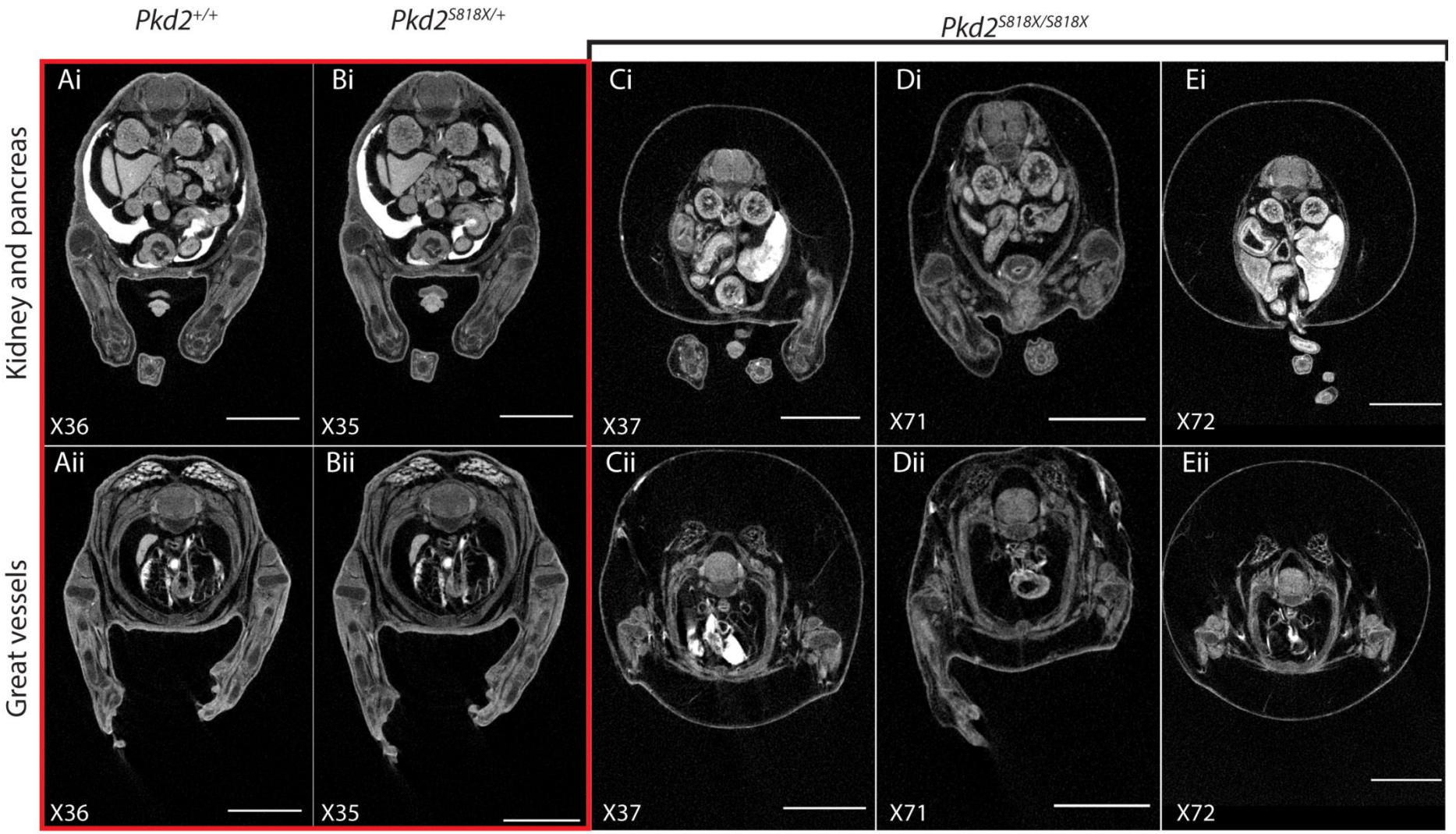


Figure A1.12: Unannotated **Fig. 3.17**, see **Chapter 3**, pages 132-133.

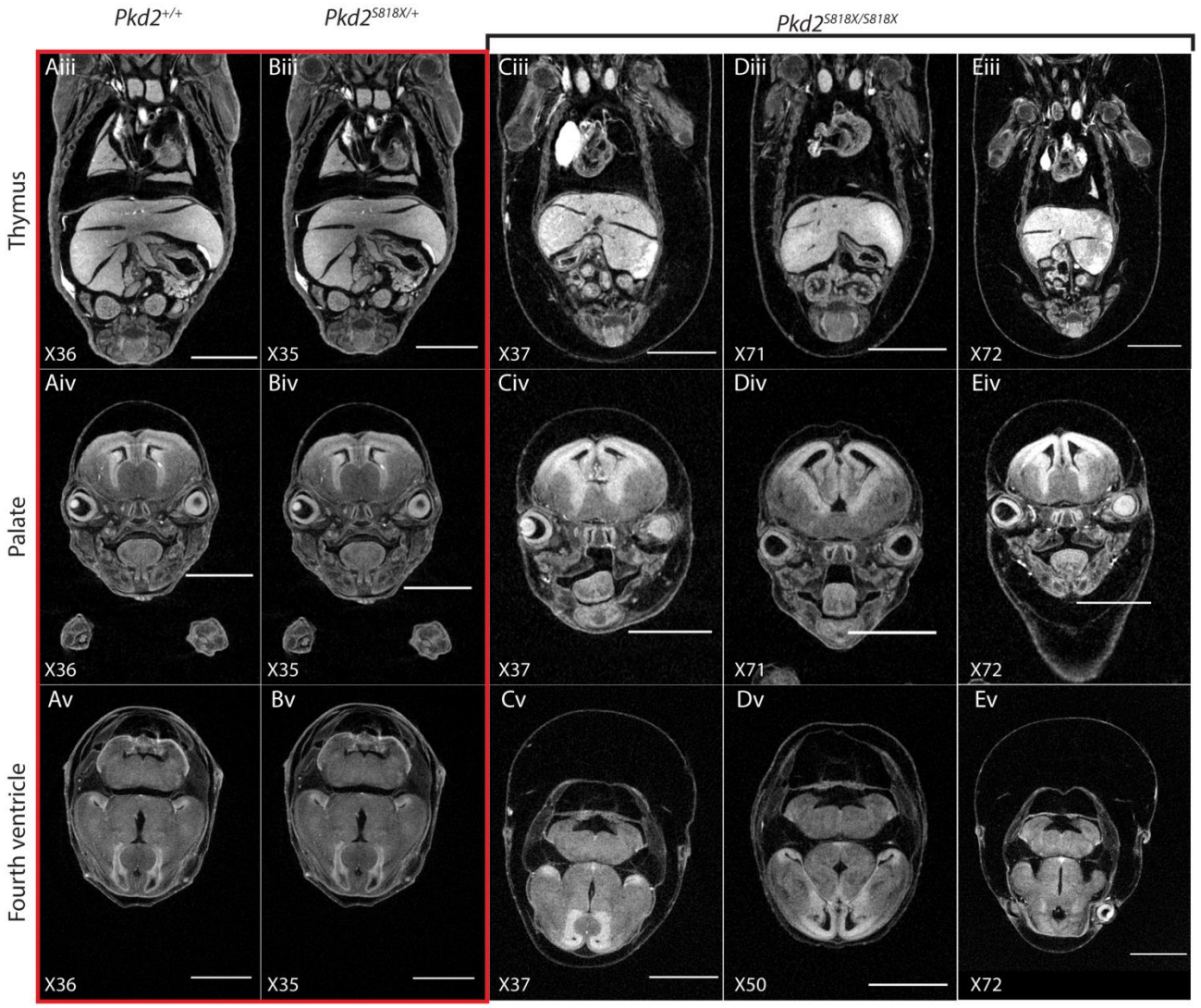


Figure A1.12 (continued)

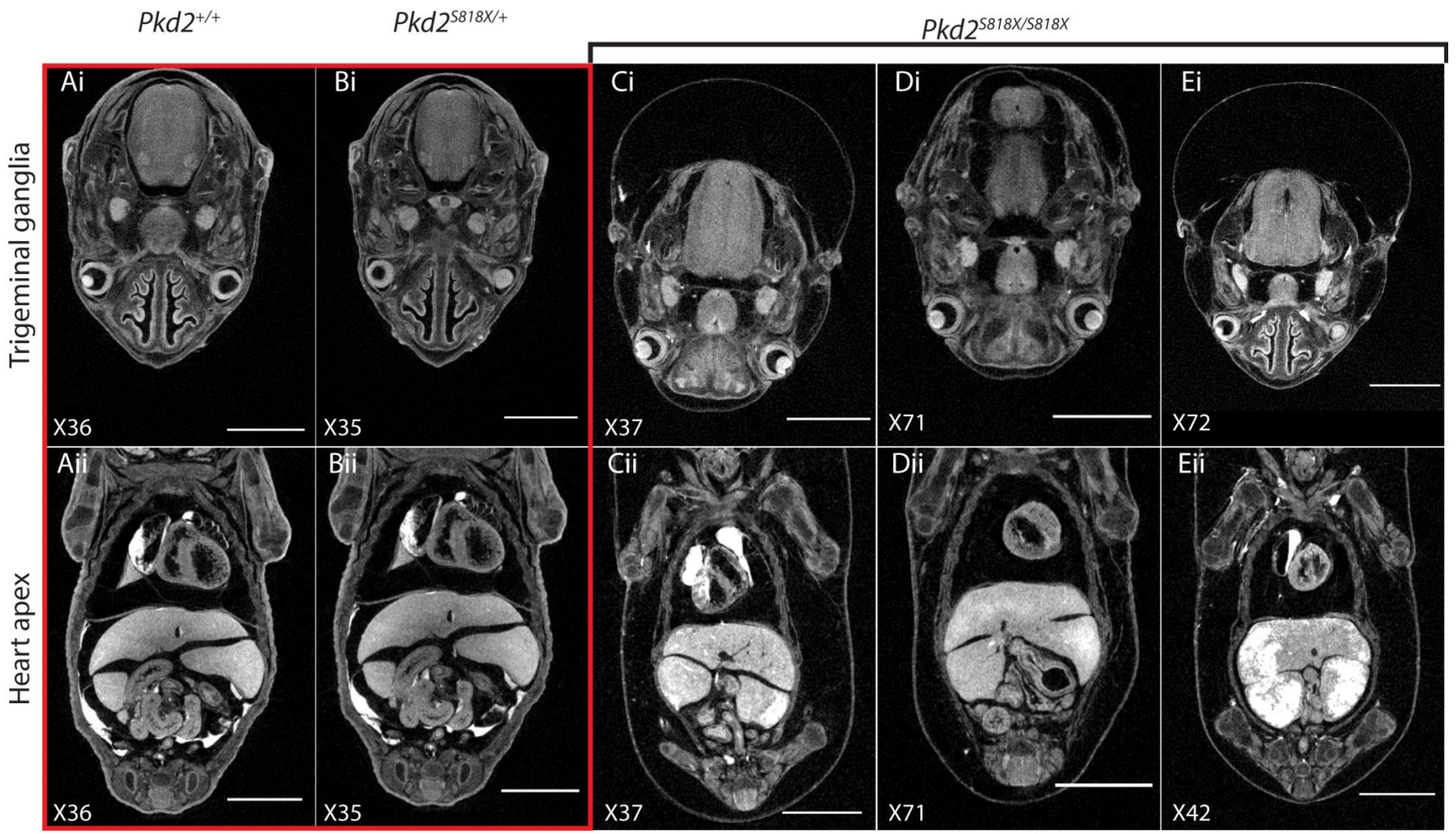


Figure A1.13: Unannotated **Fig. 3.18**, see **Chapter 3**, pages 134-135.

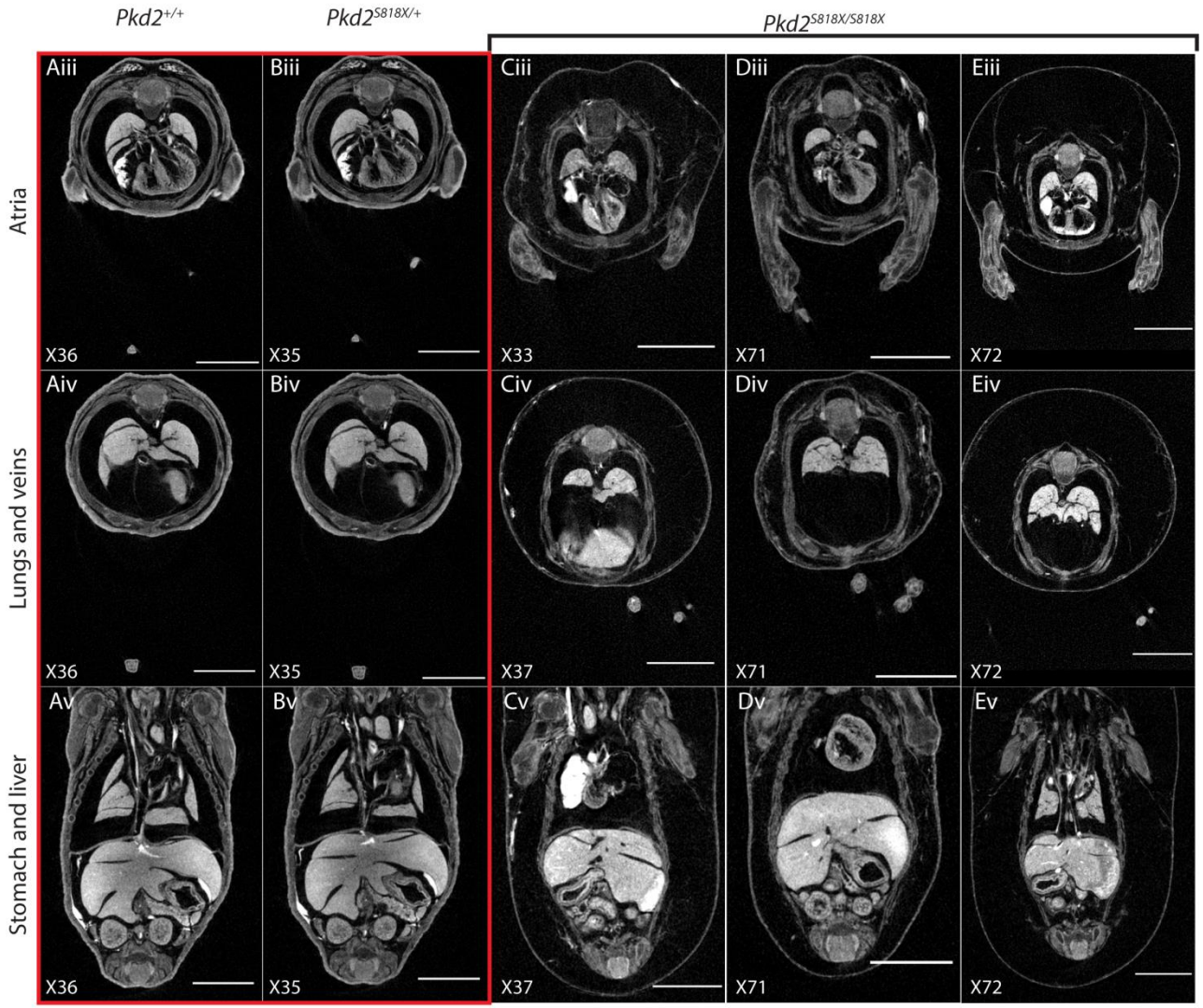


Figure A1.13 (continued)

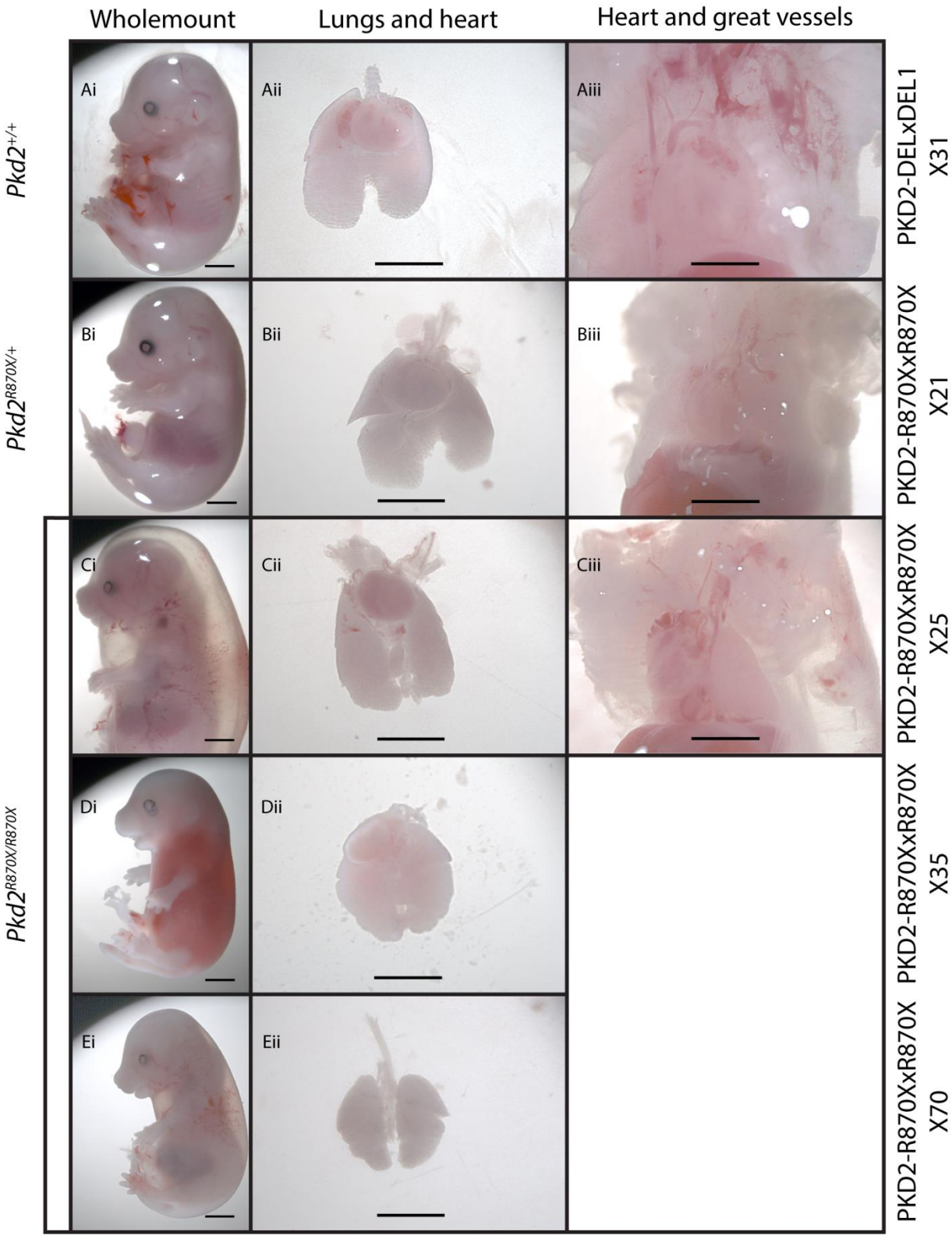


Figure A1.14: Unannotated **Fig. 3.19**, see **Chapter 3**, page 140.

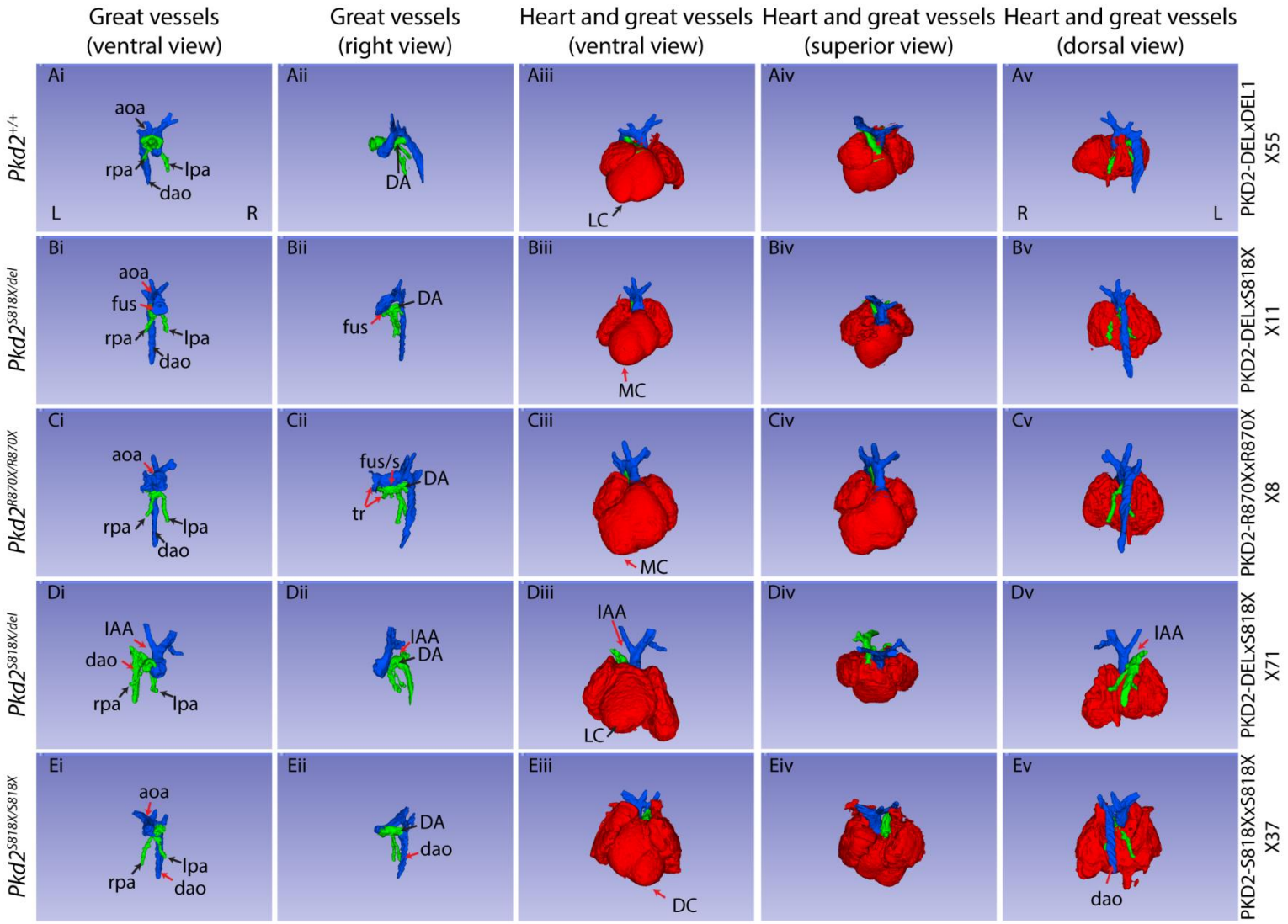


Figure A1.15: Unannotated **Fig. 3.23**, see **Chapter 3**, page 150.

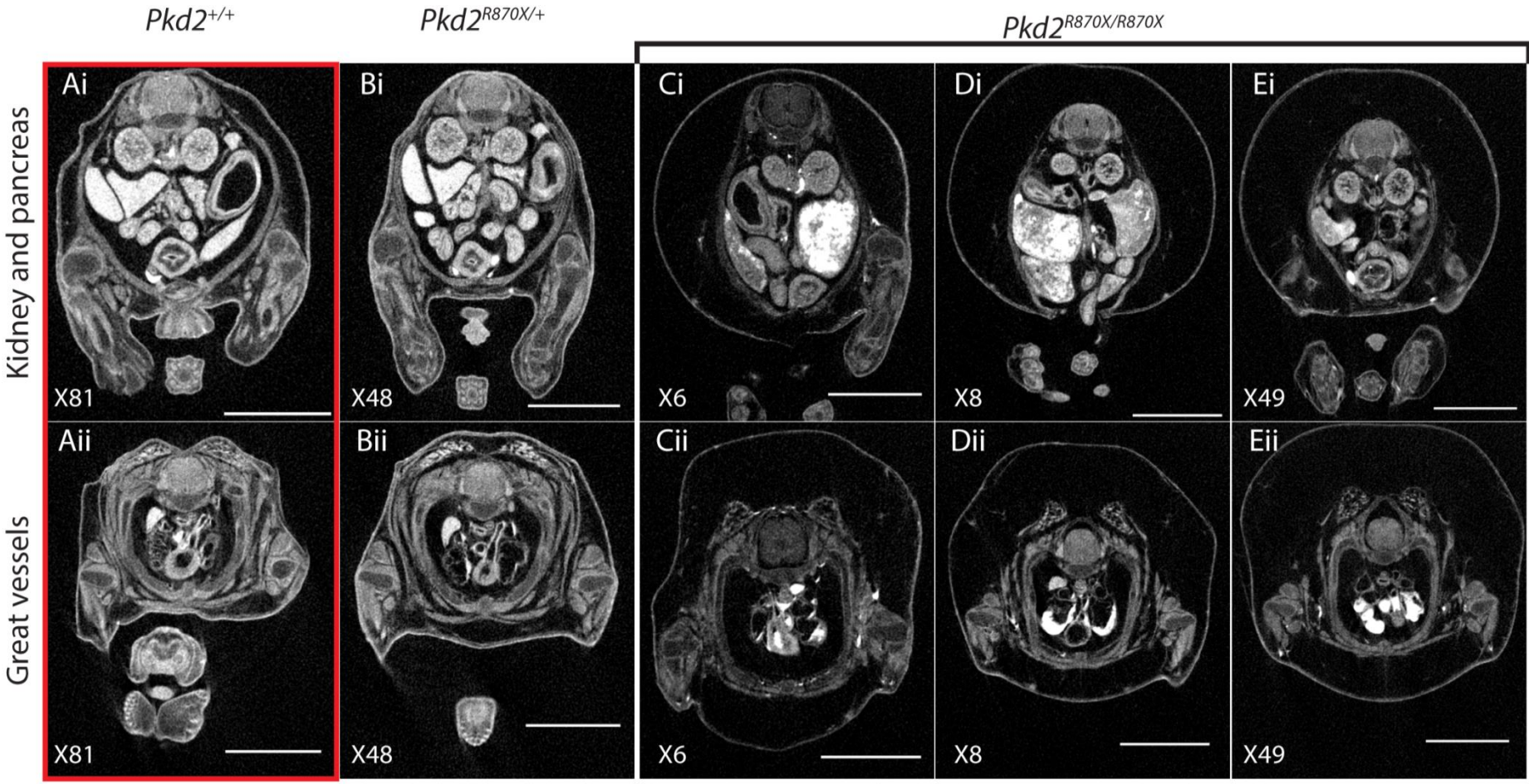


Figure A1.16: Unannotated **Fig. 3. 21**, see **Chapter 3**, pages 146-147.

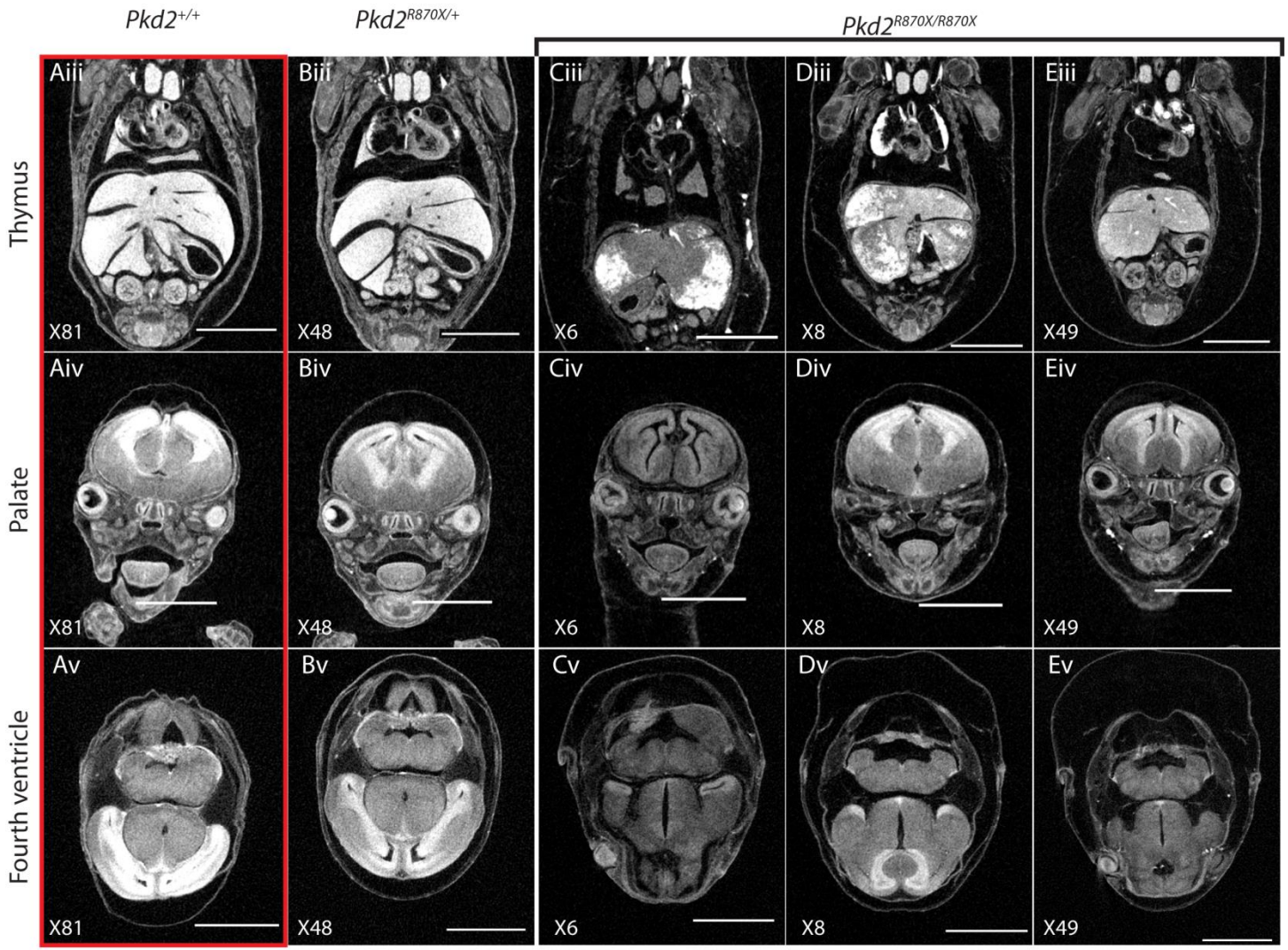


Figure A1.16 (continued)

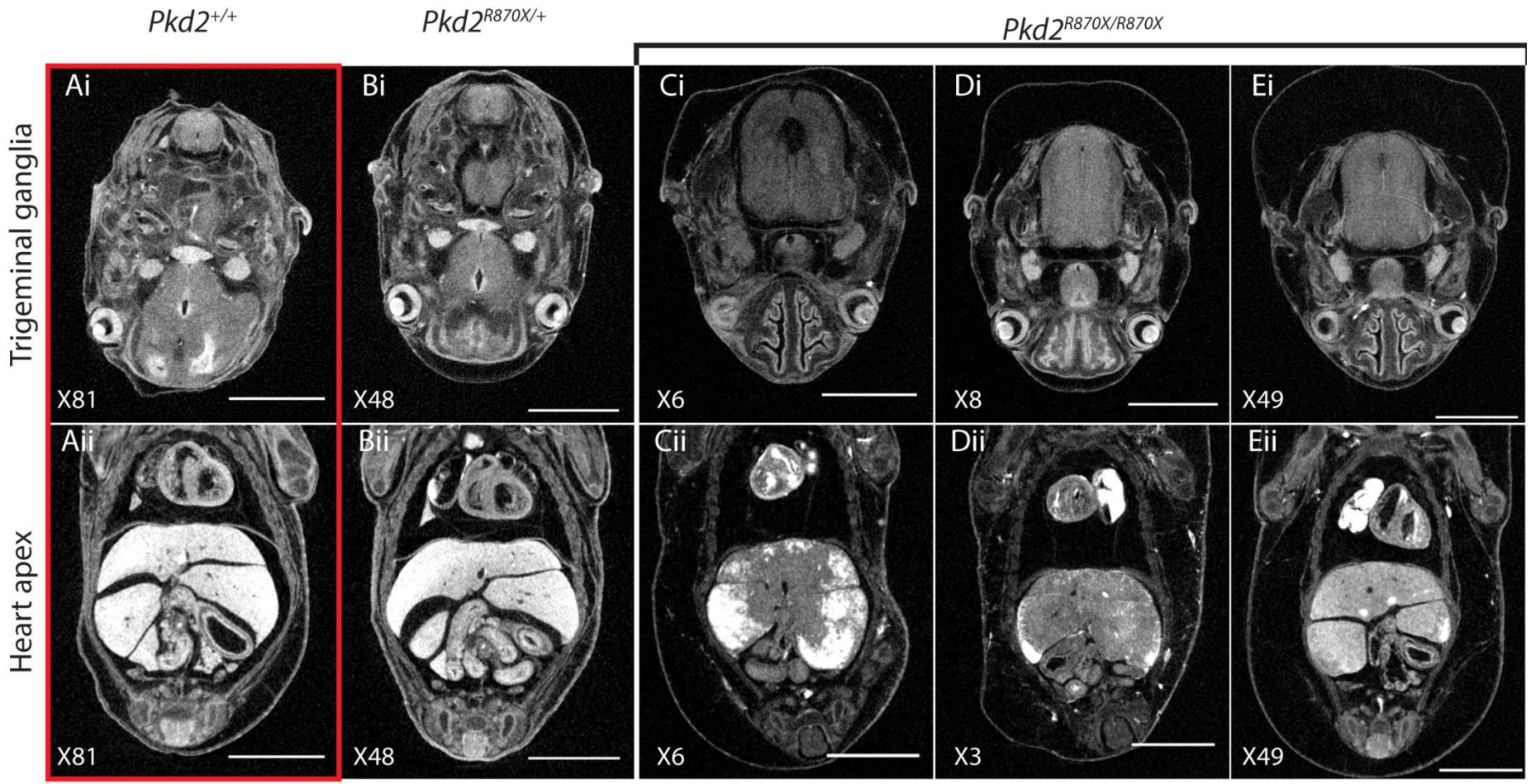


Figure A1.17: Unannotated **Fig. 3.22**, see **Chapter 3**, pages 148-149.

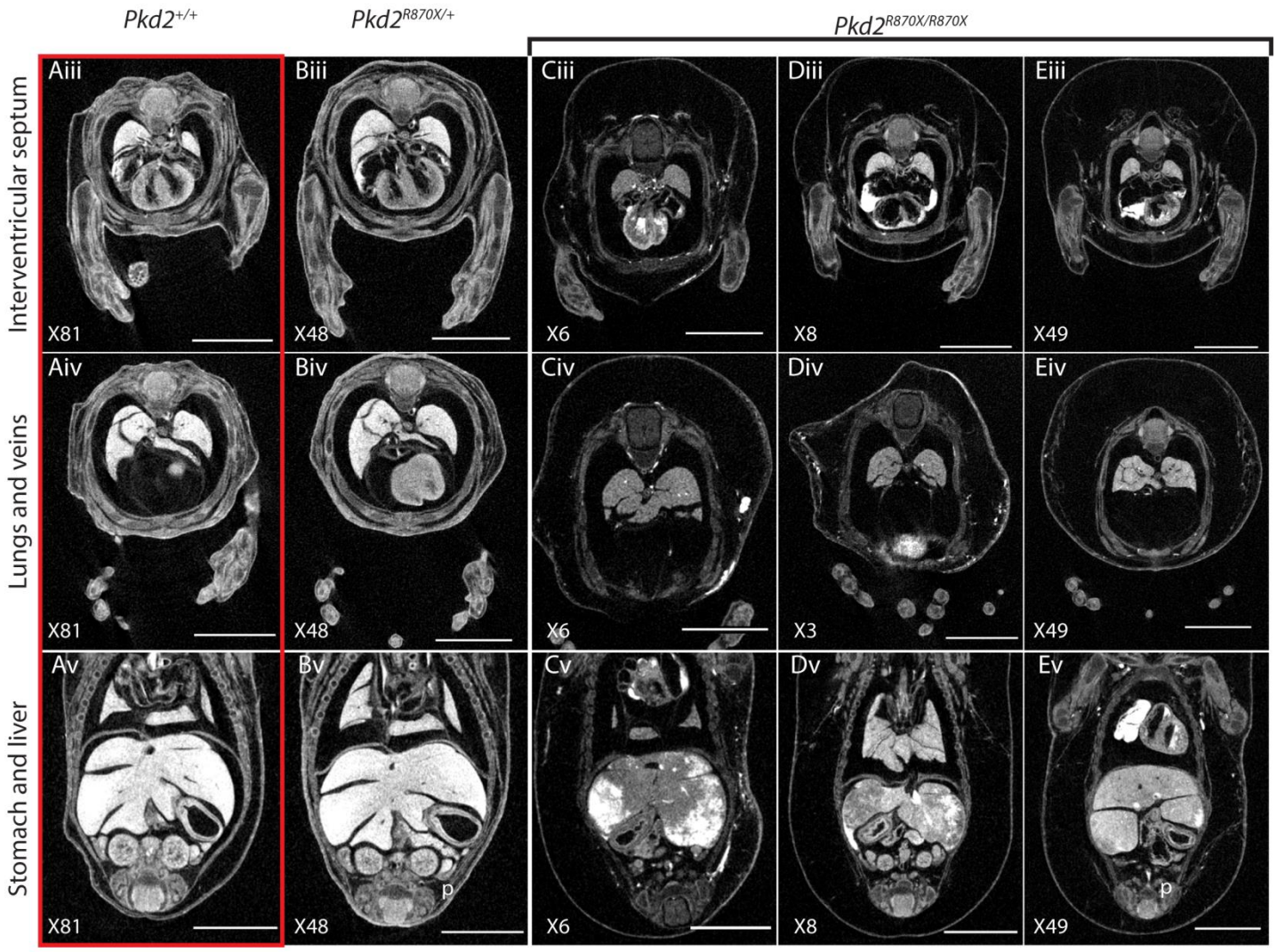


Figure A1.17 (continued)

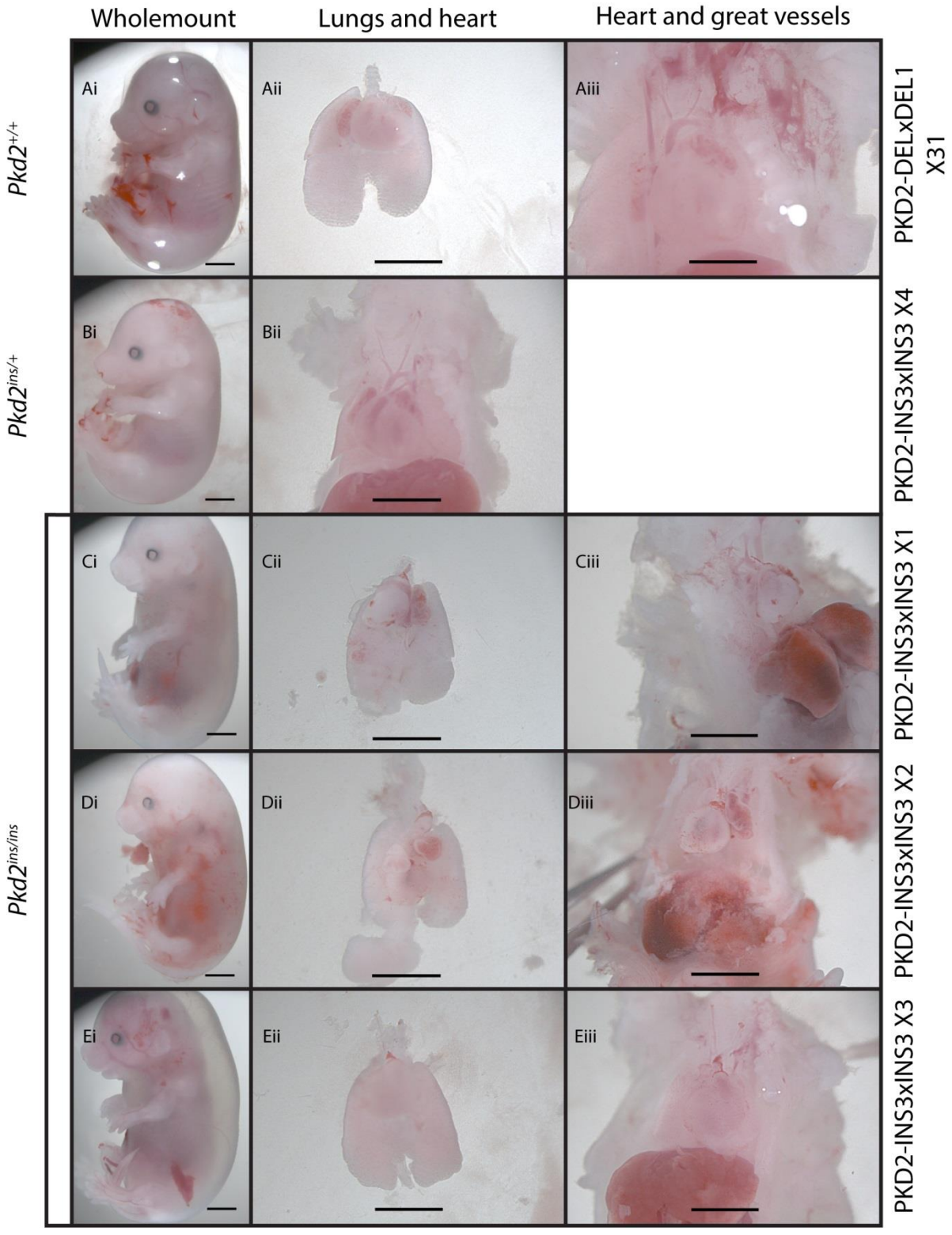


Figure A1.18: Unannotated **Fig. 3.24**, see **Chapter 3**, page 154.

Appendix 2: Tables for µCT data

Table A2.1: µCT data from PKD-DELxDEL embryos

BRAIN - CNS	**PKD2-DELxDEL X9_HOM**	**PKD2-DELxDEL X16_HOM**	**PKD2-DELxDEL X17_HOM**	**PKD2-DELxDEL X26_HOM**
Midbrain (roof)	normal	normal	normal	normal
Mesencephalic vesicle (4th)	normal	abnormal - constricted	abnormal - constricted	abnormal - constricted
Midbrain	normal	normal	normal	normal
3rd Ventricle	normal	normal	normal	abnormal - constricted
Lateral vesicles (R/L-emerging)	normal	abnormal - distended	abnormal - distended	normal
Cerebellum	abnormal - smaller?	abnormal - smaller	abnormal - smaller	abnormal - smaller
Choroid Plexus (in lateral vesicles)	normal	normal	normal	normal
CP (med. 4th V)	abnormal - smaller?	abnormal - smaller?	abnormal - smaller?	abnormal - smaller?
Semicircular canal (R/L)	normal	normal	normal	normal
4th V + median sulcus	abnormal - distended laterally	abnormal - distended laterally	abnormal - distended laterally	abnormal shape
Trigeminal V G. (R/L)	abnormal shape	abnormal shape	abnormal shape	abnormal shaped and positioned
Olfactory lobe	abnormally spaced	abnormally spaced	abnormally spaced	abnormally spaced
Rathke's pouch	normal	normal	normal	normal
Emerging cervical spinal cord	abnormal - distended subarachn. Space	abnormal - distended subarachn. Space	abnormal - distended subarachn. Space	abnormal - distended subarachn. Space
FACE (Ear, Nose, Eye)	**PKD2-DELxDEL X9_HOM**	**PKD2-DELxDEL X16_HOM**	**PKD2-DELxDEL X17_HOM**	**PKD2-DELxDEL X26_HOM**
Cochlea (R/L)	normal	normal	normal	normal
Pinna (R/L)	normal	normal	normal	normal
Nasal septum (primordium)	normal	normal	normal	normal
Nasal cavity	normal	normal	normal	normal
Vibrissae	normal	normal	normal	normal
Intra retinal space	normal	normal	normal	abnormal structure
Hyaloid cavity	normal	normal	normal	abnormal - constricted
Lens	normal	normal	normal	normal
Eyelids	normal	normal	normal	normal

Table A2.1 (continued)

FACE (Mouth)	**PKD2-DELxDEL X9_HOM**	**PKD2-DELxDEL X16_HOM**	**PKD2-DELxDEL X17_HOM**	**PKD2-DELxDEL X26_HOM**
Eustachian tube	normal	normal	normal	normal
Soft palate	abnormal - cleft palate	abnormal - cleft palate	abnormal - smaller palatal shelf	abnormal - cleft palate
Epiglottis	normal	normal	normal	normal
Tongue	normal	normal	normal	normal
Lower molar tooth (R/L)	normal	normal	normal	normal
Upper molar tooth (R/L)	normal	normal	normal	normal
Thyroid (R/L)	normal	normal	normal	normal
Submandibular gland (R/L)	abnormal - smaller and different shape	abnormal - smaller and different shape	abnormal - different shape	abnormal - different shape
C6 vertebra +DRG	abnormal - displaced	abnormal - displaced	abnormal - displaced	abnormal - displaced
Oeseophagus	normal	normal	normal	normal
Trachea	normal	normal	normal	normal
HEART-LUNGS	**PKD2-DELxDEL X9_HOM**	**PKD2-DELxDEL X16_HOM**	**PKD2-DELxDEL X17_HOM**	**PKD2-DELxDEL X26_HOM**
Thymus (R/L)	abnormal - smaller and displaced	abnormal - smaller	abnormal - smaller and displaced	abnormal - smaller and displaced
Vena cava (R/L)	abnormal - bilateral inf. Vena cava	abnormal - bilateral azygos (L sided very small)	abnormal - R sided azygos	abnormal - R sided azygos
Sternum primordium	normal	normal	normal	normal
First rib	normal	normal	normal	normal
Ductus Arteriosus	abnormal - reversed	normal	abnormal - reversed	normal
DA wall	hard to asses	normal	normal	normal
Lung: cranial lobe (R/L)	abnormal 2:2	abnormal 4:4	abnormal 4:4	abnormal 4:4
Main bronchus (R/L)	normal	normal	normal	normal
Aorta	abnormal - reversed and fused to PA	abnormal - DORV	abnormal - reversed, transposed (PA first out of L ventricle; Ao out of R)	abnormal - transposed (PA first out of L ventricle; Ao out of R)

Table A2.1 (continued)

HEART-LUNGS	**PKD2-DELxDEL X9_HOM**	**PKD2-DELxDEL X16_HOM**	**PKD2-DELxDEL X17_HOM**	**PKD2-DELxDEL X26_HOM**
Atrium (R/L)	abnormal - bilateral inf. Vena cava	normal	abnormal - L+R atria opening into L ventricle	normal
Ventricles (R/L)	abnormal - joined	abnormal - joined	abnormal - joined	normal
Lung: Middle lobes (R/L)	abnormal 2:2	abnormal 4:4	abnormal 4:4	abnormal 4:4
Tricuspid valve (R Ventricle)	hard to asses	abnormal - missing	abnormal - missing	normal
Mitral valve (L Ventricle)	normal	normal	normal	normal
Interventricular Septum	abnormal - communication between Vs	abnormal - communication between Vs	abnormal - communication between Vs	normal
Heart apex	Dextrocardia	Mesocardia	Mesocardia	Mesocardia
Lung: Accesory R lung	abnormal 2:2	abnormal 4:4	abnormal 4:4	abnormal 4:4
Lung: Caudate lobe	abnormal 2:2	abnormal 4:4	abnormal 4:4	abnormal 4:4
LIVER-GUT	**PKD2-DELxDEL X9_HOM**	**PKD2-DELxDEL X16_HOM**	**PKD2-DELxDEL X17_HOM**	**PKD2-DELxDEL X26_HOM**
Diaphragm (R/L domes)	normal	normal	normal	normal
Peritoneal cavity	abnormal - constricted	abnormal - constricted	abnormal - constricted	abnormal - constricted
Liver (R/L lobes)	abnormal - reversed	normal	abnormal - reversed	normal
Interlobular space	abnormal	abnormal	abnormal	normal
Caudate lobe	abnormal - missing	normal	abnormal - missing	abnormal - small and displaced
Stomach pyloric antrum	abnormal - R side	normal	abnormal - R side	normal
Stomach fundus	normal	normal	normal	normal
Stomach lumen	abnormal - constricted	abnormal - constricted	abnormal - constricted	abnormal - constricted
Pancreas	abnormal - R side; cystic	abnormal - R lobe displaced centrally; cystic	abnormal - R side; cystic; L lobe displaced centrally	abnormal - extremely large cysts occupying 1/2 of peritoneum
Small intestine	abnormal - reversed	normal	abnormal - reversed	abnormal - displaced by pancreatic cyst

Table A2.1 (continued)

KIDNEY-GONADS	PKD2-DELxDEL X9_HOM	PKD2-DELxDEL X16_HOM	PKD2-DELxDEL X17_HOM	PKD2-DELxDEL X26_HOM
Adrenals (R/L)	hard to asses	normal	normal	normal
Kidney: upper pole (R/L)	abnormal - cystic	abnormal - cystic	abnormal - cystic	abnormal - V large cysts
Kidney: pelvic region (R/L)	abnormal - filled	abnormal - filled	abnormal - filled	normal
Bladder	normal	normal	normal	normal
Spleen (L)	abnormal - R side	abnormal - smaller	abnormal - smaller	abnormal - displaced by pancreatic cyst
Ovaries (R/L)	-	normal	normal	-
Testes (post L "higher" vs R)	abnormal - small cysts on L testis	-	-	abnormal - small cysts, displaced by pancreas
OTHER	**PKD2-DELxDEL X9_HOM**	**PKD2-DELxDEL X16_HOM**	**PKD2-DELxDEL X17_HOM**	**PKD2-DELxDEL X26_HOM**
Brown fat	abnormal	abnormal	abnormal	abnormal
Digits	normal	normal	normal	normal
Tail	normal	normal	normal	normal
Oedema	Yes - severe	Yes - severe	Yes - severe	Yes - severe
Spinal shape	normal	normal	normal	abnormal

Table A2.2: µCT data from PKD-DELxDEL1 embryos

BRAIN - CNS	**PKD2-DELxDEL1 X40_cHet**	**PKD2-DELxDEL1 X41_fsX7-HET**	**PKD2-DELxDEL1 X42_WT**	**PKD2-DELxDEL1 X43_del-HET**
Midbrain (roof)	normal	normal	normal	normal
Mesencephalic vesicle (4th)	normal	normal	normal	normal
Midbrain	normal	normal	normal	normal
3rd Ventricle	normal	normal	normal	normal
Lateral vesicles (R/L-emerging)	normal	normal	normal	normal
Cerebellum	normal	normal	normal	normal
Choroid Plexus (in lateral vesicles)	normal	normal	normal	normal
CP (med. 4th V)	normal	normal	normal	normal
Semicircular canal (R/L)	normal	normal	normal	normal
4th V + median sulcus	abnormal - slightly distended laterally	normal	normal	normal
Trigeminal V G. (R/L)	normal	normal	normal	normal
Olfactory lobe	abnormal space between/undern eath	normal	normal	normal
Rathke's pouch	normal	normal	normal	normal
Emerging cervical spinal cord	abnormal - distended subarachn. space, dorsally	normal	normal	normal
FACE (Ear, Nose, Eye)	**PKD2-DELxDEL1 X40_cHet**	**PKD2-DELxDEL1 X41_fsX7-HET**	**PKD2-DELxDEL1 X42_WT**	**PKD2-DELxDEL1 X43_del-HET**
Cochlea (R/L)	normal	normal	normal	normal
Pinna (R/L)	normal	normal	normal	normal
Nasal septum (primordium)	normal	normal	normal	normal
Nasal cavity	normal	normal	normal	abnormal - constricted
Vibrissae	normal	normal	normal	normal
Intra retinal space	abnormal?	abnormal?	normal	normal
Hyaloid cavity	normal	normal	normal	normal
Lens	normal	normal	normal	normal
Eyelids	normal	normal	normal	normal

Table A2.2 (continued)

FACE (Mouth)	**PKD2-DELxDEL1 X40_cHet**	**PKD2-DELxDEL1 X41_fsX7-HET**	**PKD2-DELxDEL1 X42_WT**	**PKD2-DELxDEL1 X43_del-HET**
Eustachian tube	normal	normal	normal	normal
Soft palate	normal	normal	normal	hard to assess
Epiglottis	normal	normal	normal	normal
Tongue	normal	normal	normal	normal
Lower molar tooth (R/L)	normal	normal	normal	hard to assess
Upper molar tooth (R/L)	normal	normal	normal	normal
Thyroid (R/L)	normal	normal	normal	hard to assess
Submandibular gland (R/L)	normal	normal	normal	normal
C6 vertebra +DRG	abnormal - displaced DRG due to expansion in the subarachn. space?	normal	normal	normal
Oeseophagus	normal	normal	normal	normal
Trachea	normal	normal	normal	normal
HEART-LUNGS	**PKD2-DELxDEL1 X40_cHet**	**PKD2-DELxDEL1 X41_fsX7-HET**	**PKD2-DELxDEL1 X42_WT**	**PKD2-DELxDEL1 X43_del-HET**
Thymus (R/L)	normal	normal	normal	normal
Vena cava (R/L)	normal	normal	normal	normal
Sternum primordium	normal	normal	normal	normal
First rib	normal	normal	normal	normal
Ductus Arteriosus	normal	normal	normal	normal
DA wall	normal	normal	normal	normal
Lung: cranial lobe (R/L)	normal	normal	normal	normal
Main bronchus (R/L)	normal	normal	normal	normal
Aorta	normal	normal	normal	normal

Table A2.2 (continued)

HEART-LUNGS	**PKD2-DELxDEL1 X40_cHet**	**PKD2-DELxDEL1 X41_fsX7-HET**	**PKD2-DELxDEL1 X42_WT**	**PKD2-DELxDEL1 X43_del-HET**
Atrium (R/L)	normal	normal	normal	normal
Ventricles (R/L)	abnormal	normal	normal	normal
Lung: Middle lobes (R/L)	normal	normal	normal	normal
Tricuspid valve (R Ventricle)	NA	normal	normal	normal
Mitral valve (L Ventricle)	NA	normal	normal	normal
Interventricular Septum	abnormal	normal	normal	normal
Heart apex	normal	normal	normal	normal
Lung: Accesory R lung	normal	normal	normal	normal
Lung: Caudate lobe	normal	normal	normal	normal
LIVER-GUT	**PKD2-DELxDEL1 X40_cHet**	**PKD2-DELxDEL1 X41_fsX7-HET**	**PKD2-DELxDEL1 X42_WT**	**PKD2-DELxDEL1 X43_del-HET**
Diaphragm (R/L domes)	normal	normal	normal	normal
Peritoneal cavity	abnormal, shrunk	abnormal, enlarged	normal	normal
Liver (R/L lobes)	normal	normal	normal	normal
Interlobular space	abnormal, enlarged	abnormal?	normal	normal
Caudate lobe	normal	normal	normal	normal
Stomach pyloric antrum	normal	normal	normal	normal
Stomach fundus	normal	normal	normal	abnormal? - smooth
Stomach lumen	normal	normal	normal	normal
Pancreas	Abnormal, cysts in duct?	normal	normal	normal
Small intestine	normal	normal	normal	normal

Table A2.2 (continued)

KIDNEY-GONADS	PKD2-DELxDEL1 X40_cHet	PKD2-DELxDEL1 X41_fsX7-HET	PKD2-DELxDEL1 X42_WT	PKD2-DELxDEL1 X43_del-HET
Adrenals (R/L)	normal	normal	normal	normal
Kidney: upper pole (R/L)	abnormal	normal	normal	normal
Kidney: pelvic region (R/L)	abnormal	normal	normal	abnormal? - constricted
Bladder	normal	normal	normal	normal
Spleen (L)	normal	normal	normal	normal
Ovaries (R/L)	-	normal	-	normal
Testes (post L "higher" vs R)	abnormal	-	normal	-
OTHER	**PKD2-DELxDEL1 X40_cHet**	**PKD2-DELxDEL1 X41_fsX7-HET**	**PKD2-DELxDEL1 X42_WT**	**PKD2-DELxDEL1 X43_del-HET**
Brown fat	abnormal	normal	normal	normal
Digits	normal	normal	normal	normal
Tail	normal	normal	normal	normal
Oedema	Yes	normal	mild	normal
Spinal shape	normal	normal	normal	normal

Table A2.2 (continued)

BRAIN - CNS	**PKD2-DELxDEL1 X46_del-HET**	**PKD2-DELxDEL1 X47_cHet**	**PKD2-DELxDEL1 X48_fsX7-HET**	**PKD2-DELxDEL1 X53_del-HET**
Midbrain (roof)	normal	normal	normal	normal
Mesencephalic vesicle (4th)	normal	abnormal - distended lateral extremities	normal	normal
Midbrain	normal	normal	normal	normal
3rd Ventricle	normal	abnormal - fluid filled near CP	normal	normal
Lateral vesicles (R/L-emerging)	normal	abnormal - fluid filled near CP	normal	normal
Cerebellum	normal	normal	normal	normal
Choroid Plexus (in lateral vesicles)	normal	abnormal - fluid filled near CP	normal	normal
CP (med. 4th V)	normal	normal	normal	normal
Semicircular canal (R/L)	normal	normal	normal	normal
4th V + median sulcus	normal	abnormal - distended	normal	normal
Trigeminal V G. (R/L)	normal	normal	normal	normal
Olfactory lobe	normal	abnormal space between/undern eath	normal	normal
Rathke's pouch	normal	normal	normal	normal
Emerging cervical spinal cord	normal	abnormal - distended subarachn. space, dorsally	normal	normal
FACE (Ear, Nose, Eye)	**PKD2-DELxDEL1 X46_del-HET**	**PKD2-DELxDEL1 X47_cHet**	**PKD2-DELxDEL1 X48_fsX7-HET**	**PKD2-DELxDEL1 X53_del-HET**
Cochlea (R/L)	normal	normal	normal	normal
Pinna (R/L)	abnormal - detached	abnormal - detached	normal	normal
Nasal septum (primordium)	normal	normal	normal	normal
Nasal cavity	abnormal - constricted	normal	normal	normal
Vibrissae	normal	normal	normal	normal
Intra retinal space	normal	normal	normal	normal
Hyaloid cavity	abnormal - constricted	normal	normal	normal
Lens	abnormal - cysts?	abnormal - cysts?	abnormal - cysts?	normal
Eyelids	normal	normal	normal	normal

Table A2.2 (continued)

FACE (Mouth)	**PKD2-DELxDEL1 X46_del-HET**	**PKD2-DELxDEL1 X47_cHet**	**PKD2-DELxDEL1 X48_fsX7-HET**	**PKD2-DELxDEL1 X53_del-HET**
Eustachian tube	normal	normal	normal	normal
Soft palate	normal	abnormal - cleft palate	normal	normal
Epiglottis	normal	normal	normal	normal
Tongue	normal	normal	normal	normal
Lower molar tooth (R/L)	normal	normal	normal	normal
Upper molar tooth (R/L)	normal	normal	normal	normal
Thyroid (R/L)	normal	normal	normal	normal
Submandibular gland (R/L)	normal	abnormal - smaller?	normal	normal
C6 vertebra +DRG	normal	abnormal - displaced DRG due to expansion in the subarachn. space?	normal	normal
Oeseophagus	normal	normal	normal	normal
Trachea	normal	normal	normal	normal
HEART-LUNGS	**PKD2-DELxDEL1 X46_del-HET**	**PKD2-DELxDEL1 X47_cHet**	**PKD2-DELxDEL1 X48_fsX7-HET**	**PKD2-DELxDEL1 X53_del-HET**
Thymus (R/L)	normal	abnormal - smaller?	normal	normal
Vena cava (R/L)	normal	abnormal - bilateral inferior, R-sided smaller, bilateral azygos vein	normal	normal
Sternum primordium	normal	normal	normal	normal
First rib	normal	normal	normal	normal
Ductus Arteriosus	normal	normal	normal	normal
DA wall	normal	normal	normal	normal
Lung: cranial lobe (R/L)	normal	1:1 lung lobation (2x LEFT)	normal	normal
Main bronchus (R/L)	normal	normal	normal	normal
Aorta	normal	normal	normal	normal

Table A2.2 (continued)

HEART-LUNGS	**PKD2-DELxDEL1 X46_del-HET**	**PKD2-DELxDEL1 X47_cHet**	**PKD2-DELxDEL1 X48_fsX7-HET**	**PKD2-DELxDEL1 X53_del-HET**
Atrium (R/L)	normal	abnormal - 2 x IVC	normal	normal
Ventricles (R/L)	normal	abnormal - VSD	normal	normal
Lung: Middle lobes (R/L)	normal	1:1 lung lobation (2x LEFT)	normal	normal
Tricuspid valve (R Ventricle)	normal	normal	normal	normal
Mitral valve (L Ventricle)	normal	normal	normal	normal
Interventricular Septum	normal	abnormal - communication between Vs	normal	normal
Heart apex	normal	normal	normal	normal
Lung: Accesory R lung	normal	1:1 lung lobation (2x LEFT)	normal	normal
Lung: Caudate lobe	normal	1:1 lung lobation (2x LEFT) - odd shape	normal	normal
LIVER-GUT	**PKD2-DELxDEL1 X46_del-HET**	**PKD2-DELxDEL1 X47_cHet**	**PKD2-DELxDEL1 X48_fsX7-HET**	**PKD2-DELxDEL1 X53_del-HET**
Diaphragm (R/L domes)	normal	normal	normal	normal
Peritoneal cavity	normal	Abnormal, shrunk	abnormal - enlarged?	normal
Liver (R/L lobes)	normal	Abnormal- reversed abnormally patterned?	normal	normal
Interlobular space	normal	normal	normal	normal
Caudate lobe	normal	abnormal - missing due to position of stomach	normal	normal
Stomach pyloric antrum	normal	reversed stomach - right side	normal	normal
Stomach fundus	abnormal? - smooth	reversed position	normal	normal
Stomach lumen	normal	normal	normal	normal
Pancreas	normal	abnormal - cystic	normal	normal
Small intestine	normal	abnormal - mirror image?	normal	normal

Table A2.2 (continued)

KIDNEY-GONADS	**PKD2-DELxDEL1 X46_del-HET**	**PKD2-DELxDEL1 X47_cHet**	**PKD2-DELxDEL1 X48_fsX7-HET**	**PKD2-DELxDEL1 X53_del-HET**
Adrenals (R/L)	normal	abnormal - displaced by R-sided azygos	normal	normal
Kidney: upper pole (R/L)	normal	Abnormal, cystic	normal	normal
Kidney: pelvic region (R/L)	abnormal? - constricted	normal	abnormal - constricted	abnormal - constricted
Bladder	normal	normal	normal	normal
Spleen (L)	normal	abnormal - abnormal shaped and reversed.	normal	normal
Ovaries (R/L)	normal	-	-	-
Testes (post L "higher" vs R)	-	L higher than R, maybe cystic?	normal	normal
OTHER	**PKD2-DELxDEL1 X46_del-HET**	**PKD2-DELxDEL1 X47_cHet**	**PKD2-DELxDEL1 X48_fsX7-HET**	**PKD2-DELxDEL1 X53_del-HET**
Brown fat	normal	abnormal	normal	normal
Digits	normal	normal	normal	normal
Tail	normal	normal	normal	normal
Oedema	some oedema	Yes - severe	mild oedema on posterior side and head	some oedema
Spinal shape	normal	normal	normal	normal

Table A2.2 (continued)

BRAIN - CNS	**PKD2-DELxDEL1 X55_WT**	**PKD2-DELxDEL1 X56_WT**	**PKD2-DELxDEL1 X58_fsX7-HET**	**PKD2-DELxDEL1 X59_WT**
Midbrain (roof)	normal	normal	normal	normal
Mesencephalic vesicle (4th)	normal	normal	normal	normal
Midbrain	normal	normal	normal	normal
3rd Ventricle	normal	normal	normal	normal
Lateral vesicles (R/L-emerging)	normal	normal	normal	normal
Cerebellum	normal	normal	normal	normal
Choroid Plexus (in lateral vesicles)	normal	normal	normal	normal
CP (med. 4th V)	normal	normal	normal	normal
Semicircular canal (R/L)	normal	normal	normal	normal
4th V + median sulcus	normal	normal	normal	normal
Trigeminal V G. (R/L)	normal	normal	normal	normal
Olfactory lobe	normal	normal	normal	normal
Rathke's pouch	normal	normal	normal	normal
Emerging cervical spinal cord	normal	normal	normal	normal
FACE (Ear, Nose, Eye)	**PKD2-DELxDEL1 X55_WT**	**PKD2-DELxDEL1 X56_WT**	**PKD2-DELxDEL1 X58_fsX7-HET**	**PKD2-DELxDEL1 X59_WT**
Cochlea (R/L)	normal	normal	normal	normal
Pinna (R/L)	normal	normal	normal	normal
Nasal septum (primordium)	normal	normal	normal	normal
Nasal cavity	normal	normal	normal	normal
Vibrissae	normal	normal	normal	normal
Intra retinal space	constricted	constricted	normal	normal
Hyaloid cavity	abnormal in left eye	normal	normal	normal
Lens	abnormal in left eye	normal	normal	normal
Eyelids	normal	normal	normal	normal

Table A2.2 (continued)

FACE (Mouth)	**PKD2-DELxDEL1 X55_WT**	**PKD2-DELxDEL1 X56_WT**	**PKD2-DELxDEL1 X58_fsX7-HET**	**PKD2-DELxDEL1 X59_WT**
Eustachian tube	normal	normal	normal	normal
Soft palate	normal	normal	normal	normal
Epiglottis	normal	normal	normal	normal
Tongue	normal	normal	normal	normal
Lower molar tooth (R/L)	normal	normal	normal	normal
Upper molar tooth (R/L)	normal	normal	normal	normal
Thyroid (R/L)	normal	normal	normal	normal
Submandibular gland (R/L)	normal	normal	normal	normal
C6 vertebra +DRG	normal	normal	normal	normal
Oeseophagus	normal	normal	normal	normal
Trachea	normal	normal	normal	normal
HEART-LUNGS	**PKD2-DELxDEL1 X55_WT**	**PKD2-DELxDEL1 X56_WT**	**PKD2-DELxDEL1 X58_fsX7-HET**	**PKD2-DELxDEL1 X59_WT**
Thymus (R/L)	normal	normal	normal	normal
Vena cava (R/L)	normal	normal	normal	normal
Sternum primordium	normal	normal	normal	normal
First rib	normal	normal	normal	normal
Ductus Arteriosus	normal	normal	normal	normal
DA wall	normal	normal	normal	normal
Lung: cranial lobe (R/L)	normal	normal	normal	normal
Main bronchus (R/L)	normal	normal	normal	normal
Aorta	normal	normal	normal	normal

Table A2.2 (continued)

HEART-LUNGS	**PKD2-DELxDEL1 X55_WT**	**PKD2-DELxDEL1 X56_WT**	**PKD2-DELxDEL1 X58_fsX7-HET**	**PKD2-DELxDEL1 X59_WT**
Atrium (R/L)	normal	normal	normal	hard to assess - filled with blood
Ventricles (R/L)	normal	normal	normal	normal
Lung: Middle lobes (R/L)	normal	normal	normal	normal
Tricuspid valve (R Ventricle)	normal	normal	normal	hard to assess - filled with blood
Mitral valve (L Ventricle)	normal	normal	normal	hard to assess - filled with blood
Interventricular Septum	normal	normal	normal	normal
Heart apex				
Lung: Accesory R lung	normal	normal	normal	normal
Lung: Caudate lobe	normal	normal	normal	normal
LIVER-GUT	**PKD2-DELxDEL1 X55_WT**	**PKD2-DELxDEL1 X56_WT**	**PKD2-DELxDEL1 X58_fsX7-HET**	**PKD2-DELxDEL1 X59_WT**
Diaphragm (R/L domes)	normal	normal	normal	normal
Peritoneal cavity	normal	normal	normal	normal
Liver (R/L lobes)	normal	normal	normal	normal
Interlobular space	normal	normal	normal	normal
Caudate lobe	normal	normal	normal	normal
Stomach pyloric antrum	normal	normal	normal	normal
Stomach fundus	normal	normal	normal	normal
Stomach lumen	normal	normal	normal	normal
Pancreas	normal	normal	normal	normal
Small intestine	normal	normal	normal	normal

Table A2.2 (continued)

KIDNEY-GONADS	PKD2-DELxDEL1 X55_WT	PKD2-DELxDEL1 X56_WT	PKD2-DELxDEL1 X58_fsX7-HET	PKD2-DELxDEL1 X59_WT
Adrenals (R/L)	normal	normal	normal	normal
Kidney: upper pole (R/L)	normal	normal	normal	normal
Kidney: pelvic region (R/L)	normal	normal	normal	normal
Bladder	normal	normal	normal	normal
Spleen (L)	normal	normal	normal	normal
Ovaries (R/L)	-	normal	-	normal
Testes (post L "higher" vs R)	abnormal - R higher than L	-	normal	-
OTHER	**PKD2-DELxDEL1 X55_WT**	**PKD2-DELxDEL1 X56_WT**	**PKD2-DELxDEL1 X58_fsX7-HET**	**PKD2-DELxDEL1 X59_WT**
Brown fat	normal	normal	normal	normal
Digits	normal	normal	normal	normal
Tail	normal	normal	normal	normal
Oedema	normal	normal	normal	normal
Spinal shape	normal	normal	normal	normal

Table A2.2 (continued)

BRAIN - CNS	**PKD2-DELxDEL1 X60_cHet**	**PKD2-DELxDEL1 X61_cHet**	**PKD2-DELxDEL1 X69_cHet**
Midbrain (roof)	normal	normal	normal
Mesencephalic vesicle (4th)	normal	normal	normal
Midbrain	normal	normal	normal
3rd Ventricle	abnormal - constricted	normal	normal
Lateral vesicles (R/L-emerging)	normal	normal	normal
Cerebellum	normal	normal	normal
Choroid Plexus (in lateral vesicles)	normal	normal	normal
CP (med. 4th V)	normal	normal	normal
Semicircular canal (R/L)	normal	normal	normal
4th V + median sulcus	abnormal - distended laterally	abnormal - distended	abnormal - distended laterally
Trigeminal V G. (R/L)	abnormal shape - elongated	abnormal shape - elongated	abnormal shape - elongated
Olfactory lobe	abnormal space between/underneath	abnormal space between/underneath	abnormal space between/underneath
Rathke's pouch	normal	normal	normal
Emerging cervical spinal cord	abnormal - distended dorsally	abnormal - distended dorsally	abnormal - distended dorsally
FACE (Ear, Nose, Eye)	**PKD2-DELxDEL1 X60_cHet**	**PKD2-DELxDEL1 X61_cHet**	**PKD2-DELxDEL1 X69_cHet**
Cochlea (R/L)	normal	normal	normal
Pinna (R/L)	normal	normal	normal
Nasal septum (primordium)	normal	normal	normal
Nasal cavity	abnormal - constricted	abnormal - constricted	abnormal - constricted
Vibrissae	normal	normal	normal
Intra retinal space	normal	normal	normal
Hyaloid cavity	normal	normal	normal
Lens	normal	normal	normal
Eyelids	normal	normal	normal

Table A2.2 (continued)

FACE (Mouth)	**PKD2-DELxDEL1 X60_cHet**	**PKD2-DELxDEL1 X61_cHet**	**PKD2-DELxDEL1 X69_cHet**
Eustachian tube	normal	normal	normal
Soft palate	abnormal - cleft palate	normal	normal
Epiglottis	normal	normal	normal
Tongue	normal	normal	normal
Lower molar tooth (R/L)	normal	normal	normal
Upper molar tooth (R/L)	normal	normal	normal
Thyroid (R/L)	normal	normal	normal
Submandibular gland (R/L)	abnormal - odd shape	abnormal - odd shape	abnormal - odd shape
C6 vertebra +DRG	Abnormal - detached?	Abnormal - detached?	Abnormal - detached?
Oeseophagus	normal	normal	normal
Trachea	normal	normal	normal
HEART-LUNGS	**PKD2-DELxDEL1 X60_cHet**	**PKD2-DELxDEL1 X61_cHet**	**PKD2-DELxDEL1 X69_cHet**
Thymus (R/L)	abnormal - displaced	normal	abnormal - smaller and displaced
Vena cava (R/L)	normal	abnormal - vessel descending from L sup. Vena cava, passing through L adrenal	normal
Sternum primordium	normal	normal	normal
First rib	normal	normal	normal
Ductus Arteriosus	normal	normal	normal
DA wall	abnormal - smaller?	abnormal - smaller?	normal
Lung: cranial lobe (R/L)	abnormal - odd shape?	abnormal L - 5:4 segmentation	normal
Main bronchus (R/L)	normal	normal	normal
Aorta	normal	normal	normal

Table A2.2 (continued)

HEART-LUNGS	**PKD2-DELxDEL1 X60_cHet**	**PKD2-DELxDEL1 X61_cHet**	**PKD2-DELxDEL1 X69_cHet**
Atrium (R/L)	abnormal - enlarged R atrium	normal	normal
Ventricles (R/L)	abnormal - joined	abnormal - joined	abnormal - small hole in septum
Lung: Middle lobes (R/L)	abnormal - odd shape?	abnormal L - 5:4 segmentation	normal
Tricuspid valve (R Ventricle)	hard to assess	normal	normal
Mitral valve (L Ventricle)	hard to assess	normal	normal
Interventricular Septum	abnormal - communication between Vs	abnormal - communication between Vs	abnormal - communication between Vs
Heart apex			
Lung: Accesory R lung	abnormal - smaller	abnormal L - 5:4 segmentation	normal
Lung: Caudate lobe	abnormal - odd shape	abnormal L - 5:4 segmentation	normal
LIVER-GUT	**PKD2-DELxDEL1 X60_cHet**	**PKD2-DELxDEL1 X61_cHet**	**PKD2-DELxDEL1 X69_cHet**
Diaphragm (R/L domes)	normal	normal	normal
Peritoneal cavity	Abnormal, shrunk	Abnormal, shrunk	Abnormal, shrunk
Liver (R/L lobes)	normal	normal	normal
Interlobular space	abnormal	abnormal	normal
Caudate lobe	abnormal	abnormal	normal
Stomach pyloric antrum	normal	abnormal - stomach constricted	normal
Stomach fundus	normal	normal	normal
Stomach lumen	abnormal - constricted?	abnormal - constricted?	normal
Pancreas	abnormal - cystic	abnormal - cystic	abnormal - cystic
Small intestine	normal	normal	normal

Table A2.2 (continued)

KIDNEY-GONADS	**PKD2-DELxDEL1 X60_cHet**	**PKD2-DELxDEL1 X61_cHet**	**PKD2-DELxDEL1 X69_cHet**
Adrenals (R/L)	abnormal - Left adrenal separate from kidney, displaced by azygos vein	abnormal - displaced by azygos vein	normal
Kidney: upper pole (R/L)	Abnormal, cystic	Abnormal, cystic	Abnormal, cystic
Kidney: pelvic region (R/L)	Abnormal, enlarged?	Abnormal, enlarged?	normal
Bladder	normal	normal	normal
Spleen (L)	normal	normal	normal
Ovaries (R/L)	-	normal	-
Testes (post L "higher" vs R)	Abnormal, cystic	-	abnromal - cystic? And displaced
OTHER	**PKD2-DELxDEL1 X60_cHet**	**PKD2-DELxDEL1 X61_cHet**	**PKD2-DELxDEL1 X69_cHet**
Brown fat	abnormal shape	abnormal shape	abnormal shape
Digits	normal	normal	normal
Tail	normal	normal	normal
Oedema	Yes	Yes	Yes
Spinal shape	normal	normal	normal

Table A2.3: µCT data from PKD-DEL1xDEL1 embryos

BRAIN - CNS	**PKD2-DEL1xDEL1 X3_fsX7-HET**	**PKD2-DEL1xDEL1 X4_WT**	**PKD2-DEL1xDEL1 X5_fsX7-HET**	**PKD2-DEL1xDEL1 X6_HOM**
Midbrain (roof)	normal	normal	normal	normal
Mesencephalic vesicle (4th)	normal	normal	normal	normal
Midbrain	normal	normal	normal	normal
3rd Ventricle	normal	normal	normal	normal
Lateral vesicles (R/L-emerging)	normal	normal	normal	normal
Cerebellum	normal	normal	normal	normal
Choroid Plexus (in lateral vesicles)	normal	normal	normal	normal
CP (med. 4th V)	normal	normal	normal	normal
Semicircular canal (R/L)	normal	normal	normal	normal
4th V + median sulcus	normal	normal	normal	abnormal - slightly distended laterally
Trigeminal V G. (R/L)	normal	normal	normal	normal
Olfactory lobe	normal	normal	normal	abnormal - enlarged gap between lobes
Rathke's pouch	normal	normal	normal	normal
Emerging cervical spinal cord	normal	normal	normal	Abnormal - enlarged subarachn. space
FACE (Ear, Nose, Eye)	**PKD2-DEL1xDEL1 X3_fsX7-HET**	**PKD2-DEL1xDEL1 X4_WT**	**PKD2-DEL1xDEL1 X5_fsX7-HET**	**PKD2-DEL1xDEL1 X6_HOM**
Cochlea (R/L)	normal	normal	normal	normal
Pinna (R/L)	normal	normal	normal	normal
Nasal septum (primordium)	normal	normal	normal	normal
Nasal cavity	normal	normal	normal	normal
Vibrissae	normal	normal	normal	normal
Intra retinal space	normal	normal	normal	normal
Hyaloid cavity	normal	normal	normal	normal
Lens	normal	normal	normal	normal
Eyelids	normal	normal	normal	normal

Table A2.3 (continued)

FACE (Mouth)	**PKD2-DEL1xDEL1 X3_fsX7-HET**	**PKD2-DEL1xDEL1 X4_WT**	**PKD2-DEL1xDEL1 X5_fsX7-HET**	**PKD2-DEL1xDEL1 X6_HOM**
Eustachian tube	normal	normal	normal	normal
Soft palate	normal	normal	normal	normal
Epiglottis	normal	normal	normal	normal
Tongue	normal	normal	normal	normal
Lower molar tooth (R/L)	normal	normal	normal	normal
Upper molar tooth (R/L)	normal	normal	normal	normal
Thyroid (R/L)	normal	normal	normal	normal
Submandibular gland (R/L)	normal	normal	normal	normal
C6 vertebra +DRG	normal	normal	normal	abnormal - displaced
Oeseophagus	normal	normal	normal	normal
Trachea	normal	normal	normal	normal
HEART-LUNGS	**PKD2-DEL1xDEL1 X3_fsX7-HET**	**PKD2-DEL1xDEL1 X4_WT**	**PKD2-DEL1xDEL1 X5_fsX7-HET**	**PKD2-DEL1xDEL1 X6_HOM**
Thymus (R/L)	normal	normal	normal	normal
Vena cava (R/L)	normal	normal	normal	normal
Sternum primordium	normal	normal	normal	normal
First rib	normal	normal	normal	normal
Ductus Arteriosus	normal	normal	normal	normal
DA wall	normal	normal	normal	normal
Lung: cranial lobe (R/L)	normal	normal	normal	normal
Main bronchus (R/L)	normal	normal	normal	normal
Aorta	normal	normal	normal	normal

Table A2.3 (continued)

HEART-LUNGS	**PKD2-DEL1xDEL1 X3_fsX7-HET**	**PKD2-DEL1xDEL1 X4_WT**	**PKD2-DEL1xDEL1 X5_fsX7-HET**	**PKD2-DEL1xDEL1 X6_HOM**
Atrium (R/L)	normal	normal	normal	normal
Ventricles (R/L)	normal	normal	normal	normal
Lung: Middle lobes (R/L)	normal	normal	normal	normal
Tricuspid valve (R Ventricle)	hard to assess	hard to assess	normal	hard to assess
Mitral valve (L Ventricle)	hard to assess	hard to assess	normal	hard to assess
Interventricular Septum	normal	normal	normal	normal
Heart apex	normal	normal	normal	normal
Lung: Accesory R lung	normal	normal	normal	normal
Lung: Caudate lobe	normal	normal	normal	normal
LIVER-GUT	**PKD2-DEL1xDEL1 X3_fsX7-HET**	**PKD2-DEL1xDEL1 X4_WT**	**PKD2-DEL1xDEL1 X5_fsX7-HET**	**PKD2-DEL1xDEL1 X6_HOM**
Diaphragm (R/L domes)	normal	normal	normal	normal
Peritoneal cavity	normal	normal	normal	Abnormal, shrunk
Liver (R/L lobes)	normal	normal	normal	normal
Interlobular space	abnormal, enlarged	abnormal, enlarged	normal	normal
Caudate lobe	normal	normal	normal	normal
Stomach pyloric antrum	normal	normal	normal	normal
Stomach fundus	normal	normal	normal	normal
Stomach lumen	normal	normal	normal	normal
Pancreas	normal	normal	normal	abnormal - small cysts on L and R lobes
Small intestine	normal	normal	normal	normal

Table A2.3 (continued)

KIDNEY-GONADS	PKD2-DEL1xDEL1 X3_fsX7-HET	PKD2-DEL1xDEL1 X4_WT	PKD2-DEL1xDEL1 X5_fsX7-HET	PKD2-DEL1xDEL1 X6_HOM
Adrenals (R/L)	normal	normal	normal	normal
Kidney: upper pole (R/L)	normal	normal	normal	Abnormal, cystic
Kidney: pelvic region (R/L)	normal	normal	normal	Abnormal, enlarged
Bladder	normal	normal	normal	normal
Spleen (L)	normal	normal	normal	normal
Ovaries (R/L)	-	normal	-	normal
Testes (post L "higher" vs R)	normal	-	normal	-
OTHER	**PKD2-DEL1xDEL1 X3_fsX7-HET**	**PKD2-DEL1xDEL1 X4_WT**	**PKD2-DEL1xDEL1 X5_fsX7-HET**	**PKD2-DEL1xDEL1 X6_HOM**
Brown fat	normal	normal	normal	abnormal - different shape
Digits	normal	normal	normal	normal
Tail	normal	normal	normal	normal
Oedema	normal	mild	normal	Yes
Spinal shape	normal	normal	normal	normal

Table A2.3 (continued)

BRAIN - CNS	**PKD2-DEL1xDEL1 X8_WT**	**PKD2-DEL1xDEL1 X29_HOM**	**PKD2-DEL1xDEL1 X30_HOM**	**PKD2-DEL1xDEL1 X33_HOM**
Midbrain (roof)	normal	normal	normal	normal
Mesencephalic vesicle (4th)	normal	normal	normal	normal
Midbrain	normal	normal	normal	normal
3rd Ventricle	normal	normal	normal	normal
Lateral vesicles (R/L-emerging)	normal	normal	normal	normal
Cerebellum	normal	normal	normal	normal
Choroid Plexus (in lateral vesicles)	normal	normal	normal	normal
CP (med. 4th V)	normal	normal	normal	normal
Semicircular canal (R/L)	normal	normal	normal	normal
4th V + median sulcus	normal	abnormal - enlarged	abnormal - distended laterally	normal
Trigeminal V G. (R/L)	normal	normal	normal	normal
Olfactory lobe	normal	abnormal - gap between lobes	abnormal - gap between lobes	abnormal - gap between lobes
Rathke's pouch	normal	normal	normal	normal
Emerging cervical spinal cord	normal	abnormal - enlarged subarachn. Space	abnormal - enlarged subarachn. Space	abnormal - enlarged subarachn. Space
FACE (Ear, Nose, Eye)	**PKD2-DEL1xDEL1 X8_WT**	**PKD2-DEL1xDEL1 X29_HOM**	**PKD2-DEL1xDEL1 X30_HOM**	**PKD2-DEL1xDEL1 X33_HOM**
Cochlea (R/L)	normal	normal	normal	normal
Pinna (R/L)	normal	normal	normal	normal
Nasal septum (primordium)	normal	normal	normal	normal
Nasal cavity	normal	abnormal - constricted	abnormal - constricted	abnormal - constricted
Vibrissae	normal	normal	normal	normal
Intra retinal space	normal	normal	normal	normal
Hyaloid cavity	normal	normal	normal	normal
Lens	normal	abnormal - small cysts?	abnormal - small cysts?	abnormal - small cysts?
Eyelids	normal	normal	normal	normal

Table A2.3 (continued)

FACE (Mouth)	**PKD2-DEL1xDEL1 X8_WT**	**PKD2-DEL1xDEL1 X29_HOM**	**PKD2-DEL1xDEL1 X30_HOM**	**PKD2-DEL1xDEL1 X33_HOM**
Eustachian tube	normal	normal	normal	normal
Soft palate	normal	normal	normal	normal
Epiglottis	normal	normal	normal	normal
Tongue	normal	normal	normal	normal
Lower molar tooth (R/L)	normal	normal	normal	normal
Upper molar tooth (R/L)	normal	normal	normal	normal
Thyroid (R/L)	normal	normal	normal	normal
Submandibular gland (R/L)	normal	normal	normal	normal
C6 vertebra +DRG	normal	normal	normal	R ganglion slightly displaced
Oeseophagus	normal	normal	normal	normal
Trachea	normal	normal	normal	normal
HEART-LUNGS	**PKD2-DEL1xDEL1 X8_WT**	**PKD2-DEL1xDEL1 X29_HOM**	**PKD2-DEL1xDEL1 X30_HOM**	**PKD2-DEL1xDEL1 X33_HOM**
Thymus (R/L)	normal	normal	normal	normal
Vena cava (R/L)	normal	normal	normal	normal
Sternum primordium	normal	normal	normal	normal
First rib	normal	normal	normal	normal
Ductus Arteriosus	normal	normal	normal	normal
DA wall	normal	normal	normal	normal
Lung: cranial lobe (R/L)	normal	normal	normal	normal
Main bronchus (R/L)	normal	normal	normal	normal
Aorta	normal	normal	normal	normal

Table A2.3 (continued)

HEART-LUNGS	**PKD2-DEL1xDEL1 X8_WT**	**PKD2-DEL1xDEL1 X29_HOM**	**PKD2-DEL1xDEL1 X30_HOM**	**PKD2-DEL1xDEL1 X33_HOM**
Atrium (R/L)	normal	normal	normal	normal
Ventricles (R/L)	normal	normal	normal	normal
Lung: Middle lobes (R/L)	normal	normal	normal	normal
Tricuspid valve (R Ventricle)	normal	normal	normal	normal
Mitral valve (L Ventricle)	normal	normal	normal	normal
Interventricular Septum	normal	normal	normal	normal
Heart apex				
Lung: Accesory R lung	normal	normal	normal	normal
Lung: Caudate lobe	normal	normal	normal	normal
LIVER-GUT	**PKD2-DEL1xDEL1 X8_WT**	**PKD2-DEL1xDEL1 X29_HOM**	**PKD2-DEL1xDEL1 X30_HOM**	**PKD2-DEL1xDEL1 X33_HOM**
Diaphragm (R/L domes)	normal	normal	normal	normal
Peritoneal cavity	normal	Abnormal, shrunk	Abnormal, shrunk	Abnormal, shrunk
Liver (R/L lobes)	normal	normal	normal	normal
Interlobular space	normal	normal	normal	normal
Caudate lobe	normal	normal	normal	normal
Stomach pyloric antrum	normal	normal	normal	normal
Stomach fundus	normal	normal	normal	normal
Stomach lumen	normal	normal	normal	normal
Pancreas	normal	normal	normal	normal
Small intestine	normal	normal	normal	normal

Table A2.3 (continued)

KIDNEY-GONADS	PKD2-DEL1xDEL1 X8_WT	PKD2-DEL1xDEL1 X29_HOM	PKD2-DEL1xDEL1 X30_HOM	PKD2-DEL1xDEL1 X33_HOM
Adrenals (R/L)	normal	normal	normal	normal
Kidney: upper pole (R/L)	normal	Abnormal, cystic	Abnormal, cystic	Abnormal, cystic
Kidney: pelvic region (R/L)	normal	Abnormal, cystic	Abnormal, cystic	Abnormal, cystic
Bladder	normal	normal	normal	normal
Spleen (L)	normal	normal	normal	normal
Ovaries (R/L)	-	-	normal	-
Testes (post L "higher" vs R)	normal	abnormal - small cysts?	-	abnormal - small cysts?
OTHER	**PKD2-DEL1xDEL1 X8_WT**	**PKD2-DEL1xDEL1 X29_HOM**	**PKD2-DEL1xDEL1 X30_HOM**	**PKD2-DEL1xDEL1 X33_HOM**
Brown fat	normal	abnormal - different shape	abnormal - different shape	abnormal - different shape
Digits	normal	normal	normal	normal
Tail	normal	normal	normal	normal
Oedema	normal	Yes	Yes	Yes
Spinal shape	normal	normal	normal	normal

Table A2.3 (continued)

BRAIN - CNS	**PKD2-DEL1xDEL1 X35_HOM**	**PKD2-DEL1xDEL1 X47_fsX7-HET**	**PKD2-DEL1xDEL1 X49_HOM**	**PKD2-DEL1xDEL1 X50_HOM**
Midbrain (roof)	normal	normal	normal	normal
Mesencephalic vesicle (4th)	normal	normal	abnormal structures in vesicle	normal
Midbrain	normal	normal	normal	normal
3rd Ventricle	normal	normal	abnormal structures in vesicle	normal
Lateral vesicles (R/L-emerging)	normal	normal	normal	normal
Cerebellum	normal	normal	normal	normal
Choroid Plexus (in lateral vesicles)	normal	normal	normal	normal
CP (med. 4th V)	normal	normal	normal	normal
Semicircular canal (R/L)	normal	normal	normal	normal
4th V + median sulcus	abnormal - distended laterally	normal	abnormal - slightly distended laterally	abnormal - slightly distended laterally
Trigeminal V G. (R/L)	normal	normal	normal	normal
Olfactory lobe	abnormal - gap between lobes	normal	abnormal - gap between lobes	abnormal - gap between lobes
Rathke's pouch	normal	normal	normal	normal
Emerging cervical spinal cord	abnormal - enlarged subarachn. Space	normal	abnormal - enlarged subarachn. Space	abnormal - enlarged subarachn. Space
FACE (Ear, Nose, Eye)	**PKD2-DEL1xDEL1 X35_HOM**	**PKD2-DEL1xDEL1 X47_fsX7-HET**	**PKD2-DEL1xDEL1 X49_HOM**	**PKD2-DEL1xDEL1 X50_HOM**
Cochlea (R/L)	normal	normal	normal	normal
Pinna (R/L)	normal	normal	normal	normal
Nasal septum (primordium)	normal	normal	normal	normal
Nasal cavity	normal	normal	normal	normal
Vibrissae	normal	normal	normal	normal
Intra retinal space	normal	normal	normal	normal
Hyaloid cavity	normal	normal	normal	normal
Lens	abnormal - small cysts?	abnormal - small cysts?	abnormal - small cysts?	abnormal - small cysts?
Eyelids	normal	normal	normal	normal

Table A2.3 (continued)

FACE (Mouth)	**PKD2-DEL1xDEL1 X35_HOM**	**PKD2-DEL1xDEL1 X47_fsX7-HET**	**PKD2-DEL1xDEL1 X49_HOM**	**PKD2-DEL1xDEL1 X50_HOM**
Eustachian tube	normal	normal	normal	normal
Soft palate	normal	normal	normal	normal
Epiglottis	normal	normal	normal	normal
Tongue	normal	normal	normal	normal
Lower molar tooth (R/L)	normal	normal	normal	normal
Upper molar tooth (R/L)	normal	normal	normal	normal
Thyroid (R/L)	normal	normal	normal	normal
Submandibular gland (R/L)	normal	normal	normal	normal
C6 vertebra +DRG	normal	normal	abnormal - displaced DRG	abnormal - displaced DRG
Oeseophagus	normal	normal	normal	normal
Trachea	normal	normal	normal	normal
HEART-LUNGS	**PKD2-DEL1xDEL1 X35_HOM**	**PKD2-DEL1xDEL1 X47_fsX7-HET**	**PKD2-DEL1xDEL1 X49_HOM**	**PKD2-DEL1xDEL1 X50_HOM**
Thymus (R/L)	normal	normal	abnormal - displaced	abnormal - displaced
Vena cava (R/L)	normal	normal	normal	normal
Sternum primordium	normal	normal	normal	normal
First rib	normal	normal	normal	normal
Ductus Arteriosus	normal	normal	normal	normal
DA wall	normal	normal	normal	normal
Lung: cranial lobe (R/L)	normal	normal	normal	normal
Main bronchus (R/L)	normal	normal	normal	normal
Aorta	normal	normal	normal	normal

Table A2.3 (continued)

HEART-LUNGS	**PKD2-DEL1xDEL1 X35_HOM**	**PKD2-DEL1xDEL1 X47_fsX7-HET**	**PKD2-DEL1xDEL1 X49_HOM**	**PKD2-DEL1xDEL1 X50_HOM**
Atrium (R/L)	normal	normal	normal	normal
Ventricles (R/L)	normal	normal	normal	normal
Lung: Middle lobes (R/L)	normal	normal	normal	normal
Tricuspid valve (R Ventricle)	hard to assess	normal	normal	normal
Mitral valve (L Ventricle)	normal	normal	normal	normal
Interventricular Septum	hard to assess	normal	normal	normal
Heart apex	normal	normal	normal	normal
Lung: Accesory R lung	normal	normal	normal	normal
Lung: Caudate lobe	normal	normal	normal	normal
LIVER-GUT	**PKD2-DEL1xDEL1 X35_HOM**	**PKD2-DEL1xDEL1 X47_fsX7-HET**	**PKD2-DEL1xDEL1 X49_HOM**	**PKD2-DEL1xDEL1 X50_HOM**
Diaphragm (R/L domes)	normal	normal	normal	normal
Peritoneal cavity	Abnormal, shrunk	normal	Abnormal, shrunk	Abnormal, shrunk
Liver (R/L lobes)	normal	normal	normal	normal
Interlobular space	normal	normal	normal	normal
Caudate lobe	normal	normal	normal	normal
Stomach pyloric antrum	normal	normal	normal	normal
Stomach fundus	normal	normal	normal	normal
Stomach lumen	normal	normal	normal	normal
Pancreas	abnormal - small cysts?	normal	normal	abnormal - cystic?
Small intestine	normal	normal	normal	normal

Table A2.3 (continued)

KIDNEY-GONADS	PKD2-DEL1xDEL1 X35_HOM	PKD2-DEL1xDEL1 X47_fsX7-HET	PKD2-DEL1xDEL1 X49_HOM	PKD2-DEL1xDEL1 X50_HOM
Adrenals (R/L)	normal	normal	normal	normal
Kidney: upper pole (R/L)	Abnormal, cystic	normal	Abnormal, cystic	Abnormal, cystic
Kidney: pelvic region (R/L)	Abnormal, cystic	normal	Abnormal, cystic	Abnormal, cystic
Bladder	normal	normal	normal	normal
Spleen (L)	normal	normal	normal	normal
Ovaries (R/L)	normal	normal	-	normal
Testes (post L "higher" vs R)	-	-	abnormal - small cysts on R testis?	-
OTHER	**PKD2-DEL1xDEL1 X35_HOM**	**PKD2-DEL1xDEL1 X47_fsX7-HET**	**PKD2-DEL1xDEL1 X49_HOM**	**PKD2-DEL1xDEL1 X50_HOM**
Brown fat	abnormal - different shape	normal	abnormal - different shape	abnormal - different shape
Digits	normal	normal	normal	normal
Tail	normal	normal	normal	normal
Oedema	Yes	normal	Yes	Yes
Spinal shape	normal	normal	normal	normal

Table A2.3 (continued)

BRAIN - CNS	**PKD2-DEL1xDEL1 X67_HOM**	**PKD2-DEL1xDEL1 X72_HOM**
Midbrain (roof)	normal	normal
Mesencephalic vesicle (4th)	normal	normal
Midbrain	normal	normal
3rd Ventricle	normal	normal
Lateral vesicles (R/L-emerging)	normal	normal
Cerebellum	normal	normal
Choroid Plexus (in lateral vesicles)	normal	normal
CP (med. 4th V)	normal	normal
Semicircular canal (R/L)	normal	normal
4th V + median sulcus	abnormal - slightly distended laterally	abnormal - slightly distended laterally
Trigeminal V G. (R/L)	abnormal shape - elongated	abnormal shape - elongated
Olfactory lobe	abnormal - gap between lobes	abnormal - gap between lobes
Rathke's pouch	normal	normal
Emerging cervical spinal cord	abnormal - enlarged subarachn. Space	abnormal - enlarged subarachn. Space
FACE (Ear, Nose, Eye)	**PKD2-DEL1xDEL1 X67_HOM**	**PKD2-DEL1xDEL1 X72_HOM**
Cochlea (R/L)	normal	normal
Pinna (R/L)	normal	normal
Nasal septum (primordium)	normal	normal
Nasal cavity	normal	abnormal - slightly constricted
Vibrissae	normal	normal
Intra retinal space	normal	normal
Hyaloid cavity	normal	normal
Lens	normal	abnormal - small cysts?
Eyelids	normal	normal

Table A2.3 (continued)

FACE (Mouth)	**PKD2-DEL1xDEL1 X67_HOM**	**PKD2-DEL1xDEL1 X72_HOM**
Eustachian tube	normal	normal
Soft palate	normal	normal
Epiglottis	normal	normal
Tongue	normal	normal
Lower molar tooth (R/L)	normal	normal
Upper molar tooth (R/L)	normal	normal
Thyroid (R/L)	normal	normal
Submandibular gland (R/L)	abnormal shape	abnormal shape
C6 vertebra +DRG	abnormal - displaced DRG	abnormal - displaced DRG
Oeseophagus	normal	normal
Trachea	normal	normal
HEART-LUNGS	**PKD2-DEL1xDEL1 X67_HOM**	**PKD2-DEL1xDEL1 X72_HOM**
Thymus (R/L)	abnormal - displaced?	abnormal - displaced?
Vena cava (R/L)	normal	normal
Sternum primordium	normal	normal
First rib	normal	normal
Ductus Arteriosus	normal	normal
DA wall	normal	normal
Lung: cranial lobe (R/L)	Abnormal – uneven surface	normal
Main bronchus (R/L)	normal	normal
Aorta	normal	normal

Table A2.3 (continued)

HEART-LUNGS	**PKD2-DEL1xDEL1 X67_HOM**	**PKD2-DEL1xDEL1 X72_HOM**
Atrium (R/L)	L atrium contracted - hard to assess	normal
Ventricles (R/L)	normal	normal
Lung: Middle lobes (R/L)	Abnormal – uneven surface	normal
Tricuspid valve (R Ventricle)	normal	normal
Mitral valve (L Ventricle)	normal	normal
Interventricular Septum	normal	normal
Heart apex	normal	normal
Lung: Accesory R lung	Abnormal – uneven surface	normal
Lung: Caudate lobe	Abnormal – uneven surface	normal
LIVER-GUT	**PKD2-DEL1xDEL1 X67_HOM**	**PKD2-DEL1xDEL1 X72_HOM**
Diaphragm (R/L domes)	normal	normal
Peritoneal cavity	Abnormal, shrunk	Abnormal, shrunk
Liver (R/L lobes)	normal	normal
Interlobular space	normal	normal
Caudate lobe	normal	normal
Stomach pyloric antrum	normal	normal
Stomach fundus	normal	normal
Stomach lumen	normal	normal
Pancreas	normal	normal
Small intestine	normal	normal
KIDNEY-GONADS	**PKD2-DEL1xDEL1 X67_HOM**	**PKD2-DEL1xDEL1 X72_HOM**
Adrenals (R/L)	normal	normal
Kidney: upper pole (R/L)	Abnormal, cystic	Abnormal, cystic
Kidney: pelvic region (R/L)	Abnormal, cystic	Abnormal - constricted
Bladder	normal	normal
Spleen (L)	normal	normal
Ovaries (R/L)	normal	-
Testes (post L "higher" vs R)	-	abnormal - small cysts?
OTHER	**PKD2-DEL1xDEL1 X67_HOM**	**PKD2-DEL1xDEL1 X72_HOM**
Brown fat	abnormal - different shape	abnormal - different shape
Digits	normal	normal
Tail	normal	normal
Oedema	Yes	Yes
Spinal shape	normal	normal

Table A2.4: µCT data from PKD-DELxS818X embryos

BRAIN - CNS	**PKD2-DELxS818X X10_cHet**	**PKD2-DELxS818X X11_cHet**	**PKD2-DELxS818X X17_cHet**	**PKD2-DELxS818X X18_S818X-HET**
Midbrain (roof)	normal	normal	normal	normal
Mesencephalic vesicle (4th)	normal	normal	normal	normal
Midbrain	normal	normal	normal	normal
3rd Ventricle	normal	normal	normal	normal
Lateral vesicles (R/L-emerging)	abnormal - distended	abnormal - distended	abnormal - distended	normal
Cerebellum	normal	normal	normal	normal
Choroid Plexus (in lateral vesicles)	normal	normal	normal	normal
CP (med. 4th V)	abnormal	abnormal	abnormal	normal
Semicircular canal (R/L)	normal	normal	normal	normal
4th V + median sulcus	abnormal - distended laterally	abnormal - distended laterally	abnormal - distended laterally	normal
Trigeminal V G. (R/L)	abnormal shape	abnormal shape	abnormal shape	normal
Olfactory lobe	abnormally spaced	abnormally spaced	abnormally spaced	normal
Rathke's pouch	normal	normal	normal	normal
Emerging cervical spinal cord	abnormal - distended	abnormal - distended	abnormal - distended	normal
FACE (Ear, Nose, Eye)	**PKD2-DELxS818X X10_cHet**	**PKD2-DELxS818X X11_cHet**	**PKD2-DELxS818X X17_cHet**	**PKD2-DELxS818X X18_S818X-HET**
Cochlea (R/L)	normal	normal	normal	normal
Pinna (R/L)	normal	normal	normal	normal
Nasal septum (primordium)	normal	normal	normal	normal
Nasal cavity	abnormal - constricted	abnormal - constricted	abnormal - constricted	abnormal - constricted
Vibrissae	normal	normal	normal	normal
Intra retinal space	normal	normal	normal	normal
Hyaloid cavity	normal	normal	normal	normal
Lens	abnormal - cysts?	abnormal - cysts?	abnormal - cysts?	abnormal - cysts?
Eyelids	normal	normal	normal	normal

Table A2.4 (continued)

FACE (Mouth)	**PKD2-DELxS818X X10_cHet**	**PKD2-DELxS818X X11_cHet**	**PKD2-DELxS818X X17_cHet**	**PKD2-DELxS818X X18_S818X-HET**
Eustachian tube	normal	normal	normal	normal
Soft palate	abnormal - cleft palate	abnormal - cleft palate	abnormal - cleft palate	normal
Epiglottis	normal	normal	normal	normal
Tongue	normal	normal	normal	normal
Lower molar tooth (R/L)	normal	normal	normal	normal
Upper molar tooth (R/L)	absent?	absent?	normal	normal
Thyroid (R/L)	normal	normal	normal	normal
Submandibular gland (R/L)	abnormal - smaller?	abnormal - smaller?	abnormal - smaller?	abnormal - compacted?
C6 vertebra +DRG	abnormal - displaced DRG	abnormal - displaced DRG	abnormal - displaced DRG	normal
Oeseophagus	normal	normal	normal	normal
Trachea	normal	normal	normal	normal
HEART-LUNGS	**PKD2-DELxS818X X10_cHet**	**PKD2-DELxS818X X11_cHet**	**PKD2-DELxS818X X17_cHet**	**PKD2-DELxS818X X18_S818X-HET**
Thymus (R/L)	abnormal - smaller	abnormal - smaller	abnormal - smaller	normal
Vena cava (R/L)	normal	L-sided inferior	L- and R- inferior	normal
Sternum primordium	normal	normal	normal	normal
First rib	normal	normal	normal	normal
Ductus Arteriosus	abnormal - fused aorta/pulmonary artery	abnormal - fused aorta/pulmonary artery	normal	normal
DA wall	abnormal - fused aorta/pulmonary artery	abnormal - fused aorta/pulmonary artery	normal	normal
Lung: cranial lobe (R/L)	abnormal - 4:4	abnormal - 4:4	normal	normal
Main bronchus (R/L)	normal	normal	normal	normal
Aorta	abnormal - fused aorta/pulmonary artery. R-sided descending	abnormal - fused aorta/pulmonary artery	abnormal - transposition?	normal

Table A2.4 (continued)

HEART-LUNGS	PKD2-DELxS818X X10_cHet	PKD2-DELxS818X X11_cHet	PKD2-DELxS818X X17_cHet	PKD2-DELxS818X X18_S818X-HET
Atrium (R/L)	abnormal L atrium - no A-V septum	abnormal	abnormal	normal
Ventricles (R/L)	abnormal L ventricle - no IVS, no A-V septum	Abnormal - interrupted	no IVS	normal
Lung: Middle lobes (R/L)	abnormal - 4:4	abnormal - 4:4	abnormal - 4:4	normal
Tricuspid valve (R Ventricle)	hard to assess	normal	normal	normal
Mitral valve (L Ventricle)	normal	normal	normal	normal
Interventricular Septum	abnormal - IVS interrupted?	abnormal - IVS interrupted	abnormal - IVS interrupted	normal
Heart apex	Dextrocardia	Mesocardia	Mesocardia	normal
Lung: Accesory R lung	abnormal - 4:4	abnormal - 4:4	abnormal - 4:4	normal
Lung: Caudate lobe	abnormal - 4:4	abnormal - 4:4	abnormal - 4:4	normal
LIVER-GUT	**PKD2-DELxS818X X10_cHet**	**PKD2-DELxS818X X11_cHet**	**PKD2-DELxS818X X17_cHet**	**PKD2-DELxS818X X18_S818X-HET**
Diaphragm (R/L domes)	normal	normal	normal	normal
Peritoneal cavity	abnormal, shrunk	abnormal, shrunk	abnormal, shrunk	normal
Liver (R/L lobes)	normal	normal	abnormal - reversed	normal
Interlobular space	normal	abnormal?	abnormal?	normal
Caudate lobe	normal	abnormal - L-side	abnormal - missing	normal
Stomach pyloric antrum	normal	reversed stomach - right side	reversed stomach - right side	normal
Stomach fundus	abnormal - smooth?	reversed position, smooth	reversed position, smooth	normal
Stomach lumen	abnormal - smooth?	abnormal - smooth?	abnormal - smooth?	abnormal - smooth?
Pancreas	Abnormal - cystic	Abnormal - cystic, R-side	Abnormal - cystic, R-side	normal
Small intestine	normal	reversed	reversed	normal

Table A2.4 (continued)

KIDNEY-GONADS	PKD2-DELxS818X X10_cHet	PKD2-DELxS818X X11_cHet	PKD2-DELxS818X X17_cHet	PKD2-DELxS818X X18_S818X-HET
Adrenals (R/L)	normal	normal	normal	normal
Kidney: upper pole (R/L)	abnormal - cystic	abnormal - cystic	abnormal - cystic	normal
Kidney: pelvic region (R/L)	normal	normal	normal	normal
Bladder	normal	normal	normal	normal
Spleen (L)	normal	R-side	R-side	normal
Ovaries (R/L)	-	normal	normal	-
Testes (post L "higher" vs R)	abnormal - cystic?	-	-	R higher than L
OTHER	**PKD2-DELxS818X X10_cHet**	**PKD2-DELxS818X X11_cHet**	**PKD2-DELxS818X X17_cHet**	**PKD2-DELxS818X X18_S818X-HET**
Brown fat	abnormal	abnormal	abnormal	normal
Digits	normal	normal	normal	normal
Tail	ND	normal	normal	normal
Oedema	Yes - severe	Yes	Yes - severe	normal
Spinal shape	normal	normal	normal	normal

Table A2.4 (continued)

BRAIN - CNS	**PKD2-DELxS818X X19_S818X-HET**	**PKD2-DELxS818X X35_S818X-HET**	**PKD2-DELxS818X X36_WT**	**PKD2-DELxS818X X50_cHET**
Midbrain (roof)	normal	normal	normal	normal
Mesencephalic vesicle (4th)	normal	normal	normal	normal
Midbrain	normal	normal	normal	normal
3rd Ventricle	normal	normal	normal	abnormal - distended
Lateral vesicles (R/L-emerging)	normal	normal	normal	abnormal - distended, communicate with 3rd V
Cerebellum	normal	normal	normal	normal
Choroid Plexus (in lateral vesicles)	normal	normal	normal	normal
CP (med. 4th V)	normal	normal	normal	abnormal
Semicircular canal (R/L)	normal	normal	normal	normal
4th V + median sulcus	normal	normal	normal	abnormal - distended laterally
Trigeminal V G. (R/L)	normal	normal	normal	normal
Olfactory lobe	normal	normal	normal	abnormally spaced
Rathke's pouch	normal	normal	normal	normal
Emerging cervical spinal cord	normal	normal	normal	abnormal - distended subarachn. space
FACE (Ear, Nose, Eye)	**PKD2-DELxS818X X19_S818X-HET**	**PKD2-DELxS818X X35_S818X-HET**	**PKD2-DELxS818X X36_WT**	**PKD2-DELxS818X X50_cHET**
Cochlea (R/L)	normal	normal	normal	normal
Pinna (R/L)	normal	normal	normal	normal
Nasal septum (primordium)	normal	normal	normal	normal
Nasal cavity	abnormal - constricted	normal	normal	abnormal - constricted
Vibrissae	normal	normal	normal	normal
Intra retinal space	normal	normal	normal	normal
Hyaloid cavity	normal	normal	normal	normal
Lens	abnormal - cysts?	abnormal - cysts?	normal	abnormal - cysts?
Eyelids	normal	normal	normal	normal

Table A2.4 (continued)

FACE (Mouth)	**PKD2-DELxS818X X19_S818X-HET**	**PKD2-DELxS818X X35_S818X-HET**	**PKD2-DELxS818X X36_WT**	**PKD2-DELxS818X X50_cHET**
Eustachian tube	normal	normal	normal	normal
Soft palate	normal	normal	normal	abnormal - cleft palate
Epiglottis	normal	normal	normal	normal
Tongue	normal	normal	normal	abnormal shape
Lower molar tooth (R/L)	normal	normal	normal	hard to assess
Upper molar tooth (R/L)	normal	normal	normal	hard to assess
Thyroid (R/L)	hard to assess	normal	normal	normal
Submandibular gland (R/L)	hard to assess	normal	normal	abnormal - smaller?
C6 vertebra +DRG	normal	normal	normal	abnormal - displaced DRG
Oeseophagus	normal	normal	normal	normal
Trachea	normal	normal	normal	normal
HEART-LUNGS	**PKD2-DELxS818X X19_S818X-HET**	**PKD2-DELxS818X X35_S818X-HET**	**PKD2-DELxS818X X36_WT**	**PKD2-DELxS818X X50_cHET**
Thymus (R/L)	normal	normal	normal	abnormal - smaller and abnormally positioned
Vena cava (R/L)	normal	normal	normal	bilateral azygos, bilateral inf. Vena cava
Sternum primordium	normal	normal	normal	normal
First rib	normal	normal	normal	normal
Ductus Arteriosus	normal	normal	normal	normal
DA wall	normal	normal	normal	normal
Lung: cranial lobe (R/L)	normal	normal	normal	abnormal shape
Main bronchus (R/L)	normal	normal	normal	normal
Aorta	normal	normal	normal	abnormal - transposed great arteries

Table A2.4 (continued)

HEART-LUNGS	**PKD2-DELxS818X X19_S818X-HET**	**PKD2-DELxS818X X35_S818X-HET**	**PKD2-DELxS818X X36_WT**	**PKD2-DELxS818X X50_cHET**
Atrium (R/L)	normal	normal	normal	L atrium into R ventricle
Ventricles (R/L)	normal	normal	normal	no IVS
Lung: Middle lobes (R/L)	normal	normal	normal	abnormal shape
Tricuspid valve (R Ventricle)	normal	normal	normal	abnormal - both valves opening into R ventricle
Mitral valve (L Ventricle)	normal	normal	normal	abnormal - both valves opening into R ventricle
Interventricular Septum	normal	normal	normal	Abnormal - interrupted
Heart apex	normal	normal	normal	Mesocardia
Lung: Accesory R lung	normal	normal	normal	abnormal shape
Lung: Caudate lobe	normal	normal	normal	abnormal shape
LIVER-GUT	**PKD2-DELxS818X X19_S818X-HET**	**PKD2-DELxS818X X35_S818X-HET**	**PKD2-DELxS818X X36_WT**	**PKD2-DELxS818X X50_cHET**
Diaphragm (R/L domes)	normal	normal	normal	normal
Peritoneal cavity	abnormal, shrunk	normal	normal	abnormal, shrunk
Liver (R/L lobes)	normal	normal	normal	normal
Interlobular space	normal	normal	normal	abnormal?
Caudate lobe	normal	normal	normal	abnormal - missing
Stomach pyloric antrum	normal	normal	normal	normal
Stomach fundus	normal	normal	normal	abnormal - smooth?
Stomach lumen	hard to assess	normal	normal	abnormal - smaller
Pancreas	normal	normal	normal	Abnormal - cystic
Small intestine	normal	normal	normal	normal

Table A2.4 (continued)

KIDNEY-GONADS	PKD2-DELxS818X X19_S818X-HET	PKD2-DELxS818X X35_S818X-HET	PKD2-DELxS818X X36_WT	PKD2-DELxS818X X50_cHET
Adrenals (R/L)	normal	normal	normal	abnormal - vessel passing through R adrenal
Kidney: upper pole (R/L)	normal	normal	normal	abnormal - cystic
Kidney: pelvic region (R/L)	normal	normal	normal	normal
Bladder	normal	normal	normal	normal
Spleen (L)	normal	normal	normal	abnormally shaped/positioned
Ovaries (R/L)	-	normal	-	normal
Testes (post L "higher" vs R)	R higher than L	-	small cysts in R testis? L higher than R	-
OTHER	**PKD2-DELxS818X X19_S818X-HET**	**PKD2-DELxS818X X35_S818X-HET**	**PKD2-DELxS818X X36_WT**	**PKD2-DELxS818X X50_cHET**
Brown fat	normal	normal	normal	abnormal
Digits	normal	normal	normal	normal
Tail	normal	normal	normal	normal
Oedema	normal	normal	mild	Yes
Spinal shape	normal	normal	normal	normal

Table A2.4 (continued)

BRAIN - CNS	**PKD2-DELxS818X X71_cHet**	**PKD2-DELxS818X X88_cHet**	**PKD2-DELxS818X X138_cHet**
Midbrain (roof)	normal	normal	normal
Mesencephalic vesicle (4th)	normal	normal	abnormal - constricted
Midbrain	normal	normal	normal
3rd Ventricle	normal	abnormal - constricted	abnormal - constricted
Lateral vesicles (R/L-emerging)	abnormal - distended	abnormal - distended	abnormal - distended, communicate with 3rd V
Cerebellum	normal	normal	normal
Choroid Plexus (in lateral vesicles)	normal	normal	normal
CP (med. 4th V)	abnormal	abnormal	abnormal
Semicircular canal (R/L)	normal	normal	normal
4th V + median sulcus	abnormal - distended laterally	abnormal - distended laterally	abnormal - distended laterally
Trigeminal V G. (R/L)	abnormal shape	abnormal shape	abnormal shape
Olfactory lobe	abnormally spaced	abnormally spaced	abnormally spaced
Rathke's pouch	normal	normal	normal
Emerging cervical spinal cord	abnormal - distended	abnormal - distended subarachn. space	abnormal - distended subarachn. space
FACE (Ear, Nose, Eye)	**PKD2-DELxS818X X71_cHet**	**PKD2-DELxS818X X88_cHet**	**PKD2-DELxS818X X138_cHet**
Cochlea (R/L)	normal	normal	normal
Pinna (R/L)	normal	normal	normal
Nasal septum (primordium)	normal	normal	normal
Nasal cavity	abnormal - constricted	normal	abnormal - constricted
Vibrissae	normal	normal	normal
Intra retinal space	normal	normal	normal
Hyaloid cavity	normal	normal	normal
Lens	abnormal - cysts?	abnormal - cysts?	normal
Eyelids	normal	normal	abnormal - open; delay?

Table A2.4 (continued)

FACE (Mouth)	**PKD2-DELxS818X X71_cHet**	**PKD2-DELxS818X X88_cHet**	**PKD2-DELxS818X X138_cHet**
Eustachian tube	normal	normal	normal
Soft palate	abnormal - cleft palate	abnormal - cleft palate	abnormal - smaller palatal shelf
Epiglottis	abnormal - smaller?	normal	normal
Tongue	normal	normal	normal
Lower molar tooth (R/L)	normal	normal	normal
Upper molar tooth (R/L)	normal	normal	normal
Thyroid (R/L)	normal	normal	normal
Submandibular gland (R/L)	abnormal - smaller?	abnormal - smaller?	abnormal - smaller?
C6 vertebra +DRG	abnormal - displaced DRG	abnormal - displaced DRG	abnormal - displaced DRG cranialmost
Oeseophagus	normal	normal	normal
Trachea	normal	normal	normal
HEART-LUNGS	**PKD2-DELxS818X X71_cHet**	**PKD2-DELxS818X X88_cHet**	**PKD2-DELxS818X X138_cHet**
Thymus (R/L)	abnormal - smaller and abnormally positioned	abnormal - smaller and abnormally positioned	abnormal - smaller and abnormally positioned
Vena cava (R/L)	normal	abnormal - bilateral inf. Vena cava	normal
Sternum primordium	normal	normal	normal
First rib	normal	normal	normal
Ductus Arteriosus	normal	abnormal - smaller	normal
DA wall	normal	abnormal - thinner	normal
Lung: cranial lobe (R/L)	abnormal - 4:3	abnormal - 3:3 - missing R cranial	abnormal - 4:2
Main bronchus (R/L)	normal	normal	normal
Aorta	abnormal - IAA	abnormal - DORV	normal

Table A2.4 (continued)

HEART-LUNGS	**PKD2-DELxS818X X71_cHet**	**PKD2-DELxS818X X88_cHet**	**PKD2-DELxS818X X138_cHet**
Atrium (R/L)	R atrium into L ventricle	R atrium into L ventricle	normal
Ventricles (R/L)	no IVS	interrupted IVS	normal
Lung: Middle lobes (R/L)	abnormal - 4:3	abnormal - 3:3 - missing R cranial	abnormal - 4:2
Tricuspid valve (R Ventricle)	normal	normal	normal
Mitral valve (L Ventricle)	normal	normal	hard to assess
Interventricular Septum	Abnormal - interrupted	Abnormal - interrupted	normal
Heart apex	normal	normal	normal
Lung: Accesory R lung	abnormal - smaller?	abnormal - smaller	normal
Lung: Caudate lobe	abnormal - 4:3	abnormal - 3:3 - missing R cranial	abnormal - 4:2
LIVER-GUT	**PKD2-DELxS818X X71_cHet**	**PKD2-DELxS818X X88_cHet**	**PKD2-DELxS818X X138_cHet**
Diaphragm (R/L domes)	normal	normal	normal
Peritoneal cavity	abnormal, shrunk	abnormal, shrunk	abnormal, shrunk
Liver (R/L lobes)	normal	normal	normal
Interlobular space	abnormal?	abnormal?	normal
Caudate lobe	abnormal - missing	abnormal - missing	normal
Stomach pyloric antrum	normal	normal	normal
Stomach fundus	abnormal - smooth?	normal	normal
Stomach lumen	normal	abnormal - smaller	abnormal - smaller
Pancreas	Abnormal - cystic	Abnormal - cystic	Abnormal - cystic
Small intestine	normal	normal	normal

Table A2.4 (continued)

KIDNEY-GONADS	**PKD2-DELxS818X X71_cHet**	**PKD2-DELxS818X X88_cHet**	**PKD2-DELxS818X X138_cHet**
Adrenals (R/L)	normal	abnormal - vessel passing through R adrenal	normal
Kidney: upper pole (R/L)	abnormal - cystic	abnormal - cystic	abnormal - cystic
Kidney: pelvic region (R/L)	normal	normal	normal
Bladder	abnormal - cystic?	normal	abnormal - constricted
Spleen (L)	missing?	abnormally shaped/positioned	normal
Ovaries (R/L)	normal	-	-
Testes (post L "higher" vs R)	-	abnormal - small cysts?	abnormal - cystic
OTHER	**PKD2-DELxS818X X71_cHet**	**PKD2-DELxS818X X88_cHet**	**PKD2-DELxS818X X138_cHet**
Brown fat	abnormal	abnormal	abnormal
Digits	normal	normal	normal
Tail	normal	normal	abnormal - small and oedemic
Oedema	Yes - severe	Yes - severe	Yes - severe
Spinal shape	normal	normal	normal

Table A2.5: µCT data from PKD-S818XxS818X embryos

BRAIN - CNS	**PKD2-S818XxS818X X33_HOM**	**PKD2-S818XxS818X X37_HOM**	**PKD2-S818XxS818X X42_HOM**	**PKD2-S818XxS818X X58_HOM**
Midbrain (roof)	normal	normal	normal	normal
Mesencephalic vesicle (4th)	normal	normal	abnormal - distended	normal
Midbrain	normal	normal	normal	normal
3rd Ventricle	abnormal - distended; communicates with lateral V	normal	abnormal - distended; communicates with lateral V	normal
Lateral vesicles (R/L-emerging)	abnormal - distended;	normal	abnormal - distended;	normal
Cerebellum	normal	normal	normal	normal
Choroid Plexus (in lateral vesicles)	abnormal - missing?	normal	abnormal - missing?	normal
CP (med. 4th V)	abnormal - smaller	abnormal - smaller	abnormal - smaller/missing	abnormal - smaller
Semicircular canal (R/L)	normal	normal	normal	normal
4th V + median sulcus	abnormal - distended laterally	abnormal - distended laterally	abnormal - distended laterally	abnormal - distended laterally
Trigeminal V G. (R/L)	abnormal shape	abnormal shape	abnormal shape	abnormal shape
Olfactory lobe	abnormally spaced - hole between/underneath	abnormally spaced - hole between/underneath	abnormally spaced - hole between/underneath	abnormally spaced - hole between/underneath
Rathke's pouch	normal	normal	normal	normal
Emerging cervical spinal cord	abnormal - distended subarachn. Space	abnormal - distended subarachn. Space; hindbrain/pons abnormal	abnormal - distended subarachn. Space; hindbrain/pons abnormal	abnormal - distended subarachn. Space; hindbrain/pons abnormal
FACE (Ear, Nose, Eye)	**PKD2-S818XxS818X X33_HOM**	**PKD2-S818XxS818X X37_HOM**	**PKD2-S818XxS818X X42_HOM**	**PKD2-S818XxS818X X58_HOM**
Cochlea (R/L)	normal	normal	normal	normal
Pinna (R/L)	normal	normal	normal	normal
Nasal septum (primordium)	normal	normal	normal	normal
Nasal cavity	abnormal - constricted	normal	abnormal - constricted	abnormal - constricted
Vibrissae	normal	normal	normal	normal

Table A2.5 (continued)

FACE (Ear, Nose, Eye)	**PKD2-S818XxS818XX33_HOM**	**PKD2-S818XxS818XX37_HOM**	**PKD2-S818XxS818XX42_HOM**	**PKD2-S818XxS818XX58_HOM**
Intra retinal space	normal	normal	normal	normal
Hyaloid cavity	normal	normal	normal	normal
Lens	abnormal - small cysts?	abnormal - large cysts?	abnormal - small cysts R lens	abnormal - large cysts?
Eyelids	normal	normal	normal	normal
FACE (Mouth)	**PKD2-S818XxS818XX33_HOM**	**PKD2-S818XxS818XX37_HOM**	**PKD2-S818XxS818XX42_HOM**	**PKD2-S818XxS818XX58_HOM**
Eustachian tube	constricted	normal	constricted	constricted
Soft palate	abnormal - cleft palate	abnormal - cleft palate	abnormal - cleft palate	abnormal - cleft palate
Epiglottis	abnormal - smaller?	normal	abnormal - smaller?	abnormal - smaller?
Tongue	abnormal shape?	abnormal shape?	normal	normal
Lower molar tooth (R/L)	hard to assess	normal	normal	normal
Upper molar tooth (R/L)	hard to assess	normal	normal	normal
Thyroid (R/L)	normal	normal	normal	normal
Submandibular gland (R/L)	abnormal size/shape	abnormal size/shape	abnormal size/shape	abnormal size/shape
C6 vertebra +DRG	normal	abnormal - displaced DRG	normal	abnormal - displaced DRG
Oeseophagus	normal	normal	normal	normal
Trachea	normal	normal	normal	normal
HEART-LUNGS	**PKD2-S818XxS818XX33_HOM**	**PKD2-S818XxS818XX37_HOM**	**PKD2-S818XxS818XX42_HOM**	**PKD2-S818XxS818XX58_HOM**
Thymus (R/L)	abnormal - displaced/smaller	abnormal - displaced/smaller	abnormal - displaced/smaller	abnormal - displaced/smaller
Vena cava (R/L)	2x inferior vena cava; 2x azygos	L-sided inf. Vena cava; azygos vein switches sides around aorta	2x inferior vena cava, L larger; R-sided azygos	2x inferior vena cava, L larger
Sternum primordium	normal	normal	normal	normal
First rib	normal	normal	normal	normal
Ductus Arteriosus	absent (no pulm. Artery)	inverted	normal	normal
DA wall	absent (no pulm. Artery)	normal	normal	normal

Table A2.5 (continued)

HEART-LUNGS	**PKD2-S818XxS818XX33_HOM**	**PKD2-S818XxS818XX37_HOM**	**PKD2-S818XxS818XX42_HOM**	**PKD2-S818XxS818XX58_HOM**
Lung: cranial lobe (R/L)	abnormal shape; 4:4 lungs	abnormal shape; 1:2 lungs	abnormal shape; 4:4 lungs	abnormal shape; 1:2 lungs
Main bronchus (R/L)	normal	normal	normal	normal
Aorta	abnormal; single vessel out of L ventricle, small in size	inverted	abnormal - transposed?	abnormal - transposed/inverted
Atrium (R/L)	Abnormal L - missing mitral/separate from L V	abnormal - L atrium -> inf. V. cava	abnormal - L atrium -> inf. V. cava	abnormal - L atrium -> inf. V. cava
Ventricles (R/L)	Abnormal - interrupted	Abnormal - interrupted	abnormal - constricted?	normal
Lung: Middle lobes (R/L)	abnormal shape; 4:4 lungs	abnormal shape; 1:2 lungs	abnormal shape; 4:4 lungs	abnormal shape; 1:2 lungs
Tricuspid valve (R Ventricle)	normal	normal	hard to assess	normal
Mitral valve (L Ventricle)	abnormal - missing?	normal	hard to assess	normal
Interventricular Septum	abnormal - interrupted	abnormal - interrupted	abnormal - interrupted	normal
Heart apex	Mesocardia	Dextrocardia	Mesocardia	Dextrocardia
Lung: Accesory R lung	abnormal shape; 4:4 lungs	abnormal shape; 1:2 lungs	abnormal shape; 4:4 lungs	abnormal shape; 1:2 lungs
Lung: Caudate lobe	abnormal shape; 4:4 lungs	abnormal shape; 1:2 lungs	abnormal shape; 4:4 lungs	abnormal shape; 1:2 lungs
LIVER-GUT	**PKD2-S818XxS818XX33_HOM**	**PKD2-S818XxS818XX37_HOM**	**PKD2-S818XxS818XX42_HOM**	**PKD2-S818XxS818XX58_HOM**
Diaphragm (R/L domes)	normal	normal	abnormal - missing L dome?	normal
Peritoneal cavity	abnormal - constricted	abnormal - constricted	abnormal - constricted	abnormal - constricted
Liver (R/L lobes)	abnormal - inverted	abnormal - inverted	normal	abnormal - inverted
Interlobular space	abnormal	abnormal	normal	abnormal
Caudate lobe	abnormal - missing?	abnormal - missing?	abnormal - missing?	abnormal - missing?
Stomach pyloric antrum	abnormal - R side	abnormal - R side	normal	abnormal - R side
Stomach fundus	abnormal - smooth	normal	abnormal - smooth	normal

Table A2.5 (continued)

LIVER-GUT	**PKD2-S818XxS818X X33_HOM**	**PKD2-S818XxS818X X37_HOM**	**PKD2-S818XxS818X X42_HOM**	**PKD2-S818XxS818X X58_HOM**
Stomach lumen	abnormal - small	abnormal - small	abnormal - very constricted/small	abnormal - small
Pancreas	abnormal, R side, cystic; L lobe central and small	abnormal, R side, cystic; L lobe cystic, central and small	abnormal - large cysts on L lobe, R lobe central and cystic	abnormal - very cystic
Small intestine	abnormal	abnormal	abnormal	abnormal
KIDNEY-GONADS	**PKD2-S818XxS818X X33_HOM**	**PKD2-S818XxS818X X37_HOM**	**PKD2-S818XxS818X X42_HOM**	**PKD2-S818XxS818X X58_HOM**
Adrenals (R/L)	abnormal - vessel going through R adrenal	abnormal - vessel going through R adrenal - sup vena cava?	abnormal - vessel separating R adrenal from kidney - sup vena cava?	abnormal - vessel going through L adrenal - sup vena cava?
Kidney: upper pole (R/L)	abnormal - cystic	abnormal - cystic	abnormal - cystic	abnormal - cystic
Kidney: pelvic region (R/L)	abnormal - filled	abnormal - filled	abnormal - filled	abnormal - filled
Bladder	abnormal - constricted	normal	normal	abnormal - constricted
Spleen (L)	asplenic	normal	asplenic	abnormal - R side
Ovaries (R/L)	normal	-	-	-
Testes (post L "higher" vs R)	-	abnormal - cystic?	abnormal - cystic?	abnormal - cystic?
OTHER	**PKD2-S818XxS818X X33_HOM**	**PKD2-S818XxS818X X37_HOM**	**PKD2-S818XxS818X X42_HOM**	**PKD2-S818XxS818X X58_HOM**
Brown fat	abnormal shape, smaller	abnormal shape, smaller	abnormal shape, smaller	abnormal shape, smaller
Digits	normal	normal	normal	normal
Tail	normal	normal	normal	normal
Oedema	yes - severe	yes - severe	yes - severe	yes - severe
Spinal shape	normal	normal	normal	normal

Table A2.5 (continued)

BRAIN - CNS	**PKD2-S818XxS818X X62_HOM**	**PKD2-S818XxS818X X71_HOM**	**PKD2-S818XxS818X X72_HOM**
Midbrain (roof)	abnormal - thinner	abnormal - thinner	normal
Mesencephalic vesicle (4th)	abnormal - constricted	normal	normal
Midbrain	abnormal	normal	normal
3rd Ventricle	abnormal - distended; communicates with lateral V	abnormal - distended; communicates with lateral V	abnormal - distended
Lateral vesicles (R/L-emerging)	abnormal - distended; communicate with 3rd V	abnormal - distended; communicate with 3rd V	normal
Cerebellum	abnormal	normal	normal
Choroid Plexus (in lateral vesicles)	abnormal - missing?	normal	normal
CP (med. 4th V)	abnormal - smaller	abnormal - smaller	abnormal - smaller
Semicircular canal (R/L)	normal	normal	normal
4th V + median sulcus	abnormal - distended laterally	abnormal - distended laterally	abnormal - distended laterally
Trigeminal V G. (R/L)	abnormal shape	abnormal shape	abnormal shape
Olfactory lobe	abnormally spaced - hole between/underneath	abnormally spaced - hole between/underneath	abnormally spaced - hole between/underneath
Rathke's pouch	normal	normal	normal
Emerging cervical spinal cord	abnormal - distended subarachn. Space; hindbrain/pons abnormal	abnormal - distended subarachn. Space; hindbrain/pons abnormal	abnormal - distended subarachn. Space; hindbrain/pons abnormal
FACE (Ear, Nose, Eye)	**PKD2-S818XxS818X X62_HOM**	**PKD2-S818XxS818X X71_HOM**	**PKD2-S818XxS818X X72_HOM**
Cochlea (R/L)	normal	normal	normal
Pinna (R/L)	normal	normal	normal
Nasal septum (primordium)	normal	normal	normal
Nasal cavity	normal	abnormal - constricted	normal
Vibrissae	normal	normal	normal
Intra retinal space	normal	normal	normal
Hyaloid cavity	abnormal - constricted	normal	normal
Lens	abnormal - small cysts R lens	abnormal - small cysts	abnormal - small cysts
Eyelids	normal	normal	normal

Table A2.5 (continued)

FACE (Mouth)	**PKD2-S818XxS818X X62_HOM**	**PKD2-S818XxS818X X71_HOM**	**PKD2-S818XxS818X X72_HOM**
Eustachian tube	normal	normal	normal
Soft palate	abnormal - cleft palate	abnormal - cleft palate	abnormal - cleft palate
Epiglottis	normal	normal	normal
Tongue	abnormal shape?	abnormal shape?	abnormal shape?
Lower molar tooth (R/L)	normal	normal	normal
Upper molar tooth (R/L)	normal	normal	normal
Thyroid (R/L)	normal	normal	normal
Submandibular gland (R/L)	abnormal size/shape	abnormal size/shape	abnormal - smaller
C6 vertebra +DRG	abnormal - displaced DRG	abnormal - displaced DRG	abnormal - displaced DRG
Oeseophagus	normal	normal	normal
Trachea	normal	normal	normal
HEART-LUNGS	**PKD2-S818XxS818X X62_HOM**	**PKD2-S818XxS818X X71_HOM**	**PKD2-S818XxS818X X72_HOM**
Thymus (R/L)	abnormal - displaced/smaller	abnormal - displaced/smaller	abnormal - displaced/smaller
Vena cava (R/L)	2x inferior vena cava, L larger	normal	2x inferior vena cava, R-sided azygos
Sternum primordium	normal	normal	normal
First rib	normal	normal	normal
Ductus Arteriosus	absent	absent	reversed (R side)
DA wall	absent	absent	reversed (R side)
Lung: cranial lobe (R/L)	abnormal shape; 4:4 lungs	abnormal shape; 4:2 lungs	abnormal shape; 4:4 lungs
Main bronchus (R/L)	normal	normal	normal
Aorta	abnormal; IAA	abnormal; separate but fused Ao and PA, inverted descending, transposed	abnormal - reversed descending, fused but separate to PA

Table A2.5 (continued)

HEART-LUNGS	**PKD2-S818XxS818X X62_HOM**	**PKD2-S818XxS818X X71_HOM**	**PKD2-S818XxS818X X72_HOM**
Atrium (R/L)	abnormal - L atrium -> inf. V. cava	abnormal - missing L atrium	abnormal - no connection between L A and V
Ventricles (R/L)	communication between Vs	communication between Vs	communication between Vs
Lung: Middle lobes (R/L)	abnormal shape; 4:4 lungs	abnormal shape; 4:2 lungs	abnormal shape; 4:4 lungs
Tricuspid valve (R Ventricle)	hard to assess	normal	normal
Mitral valve (L Ventricle)	hard to assess	abnormal - missing L atrium	normal
Interventricular Septum	Abnormal - interrupted	Abnormal - interrupted	Abnormal - interrupted
Heart apex	Dextrocardia		Dextrocardia
Lung: Accesory R lung	abnormal shape; 4:4 lungs	abnormal shape; 4:2 lungs	abnormal shape; 4:4 lungs
Lung: Caudate lobe	abnormal shape; 4:4 lungs	abnormal shape; 4:2 lungs	abnormal shape; 4:4 lungs
LIVER-GUT	**PKD2-S818XxS818X X62_HOM**	**PKD2-S818XxS818X X71_HOM**	**PKD2-S818XxS818X X72_HOM**
Diaphragm (R/L domes)	normal	normal	normal
Peritoneal cavity	abnormal - constricted	abnormal - constricted	abnormal - constricted
Liver (R/L lobes)	normal	normal	abnormal - inverted
Interlobular space	abnormal	abnormal	abnormal
Caudate lobe	abnormal - missing?	abnormal - missing?	abnormal - L side
Stomach pyloric antrum	abnormal - R side	normal	abnormal - R side
Stomach fundus	normal	normal	normal
Stomach lumen	abnormal - very constricted/small	abnormal - small	abnormal - very constricted/small
Pancreas	abnormal - large cysts on R lobe, L lobe central	abnormal - cystic R and L lobes	abnormal - cystic R and L lobe, L lobe central
Small intestine	abnormal	normal	abnormal

Table A2.5 (continued)

KIDNEY-GONADS	**PKD2-S818XxS818X X62_HOM**	**PKD2-S818XxS818X X71_HOM**	**PKD2-S818XxS818X X72_HOM**
Adrenals (R/L)	normal	abnormal - vessel going through L adrenal - sup vena cava?	normal
Kidney: upper pole (R/L)	abnormal - cystic	abnormal - cystic	abnormal - cystic
Kidney: pelvic region (R/L)	normal	normal	abnormal - filled
Bladder	abnormal - constricted	normal	normal
Spleen (L)	abnormal - R side	normal	abnormal - R side
Ovaries (R/L)	-	normal	-
Testes (post L "higher" vs R)	abnormal - looks like small cysts but hard to asssess	-	abnormal - cystic mesonephros/testis?
OTHER	**PKD2-S818XxS818X X62_HOM**	**PKD2-S818XxS818X X71_HOM**	**PKD2-S818XxS818X X72_HOM**
Brown fat	abnormal shape	abnormal shape, smaller	abnormal shape, smaller
Digits	normal	normal	normal
Tail	normal	normal	normal
Oedema	yes - severe	yes	yes - severe
Spinal shape	abnormal	normal	normal

Table A2.6: µCT data from PKD-R870XxR870X embryos

BRAIN - CNS	**PKD2-R870XxR870X X1_R870X-HET**	**PKD2-R870XxR870X X3_HOM**	**PKD2-R870XxR870X X4_R870X-HET**
Midbrain (roof)	normal	normal	normal
Mesencephalic vesicle (4th)	normal	normal	normal
Midbrain	normal	normal	normal
3rd Ventricle	normal	abnormal	normal
Lateral vesicles (R/L-emerging)	normal	abnormal - distended	normal
Cerebellum	hard to assess	abnormal - distended	normal
Choroid Plexus (in lateral vesicles)	hard to assess	abnormal	normal
CP (med. 4th V)	normal	hard to assess	normal
Semicircular canal (R/L)	normal	normal	normal
4th V + median sulcus	normal	abnormal - distended laterally	normal
Trigeminal V G. (R/L)	normal	abnormal shape	normal
Olfactory lobe	normal	abnormally spaced	abnormally spaced
Rathke's pouch	normal	normal	normal
Emerging cervical spinal cord	normal	abnormal - slightly distended subarachn. Space	normal
FACE (Ear, Nose, Eye)	**PKD2-R870XxR870X X1_R870X-HET**	**PKD2-R870XxR870X X3_HOM**	**PKD2-R870XxR870X X4_R870X-HET**
Cochlea (R/L)	normal	normal	normal
Pinna (R/L)	normal	normal	normal
Nasal septum (primordium)	normal	normal	normal
Nasal cavity	normal	abnormal - constricted	abnormal - constricted
Vibrissae	normal	abnormal	normal
Intra retinal space	normal	normal	normal
Hyaloid cavity	normal	abnormal - structure inside	normal
Lens	normal	normal	abnormal - small cysts?
Eyelids	normal	normal	normal

Table A2.6 (continued)

FACE (Mouth)	**PKD2-R870XxR870X X1_R870X-HET**	**PKD2-R870XxR870X X3_HOM**	**PKD2-R870XxR870X X4_R870X-HET**
Eustachian tube	normal	normal	normal
Soft palate	normal	abnormal - cleft palate	normal
Epiglottis	normal	abnormal - smaller	normal
Tongue	normal	abnormal shape	normal
Lower molar tooth (R/L)	normal	normal	normal
Upper molar tooth (R/L)	normal	normal	normal
Thyroid (R/L)	normal	normal	normal
Submandibular gland (R/L)	normal	abnormal shape and smaller	normal
C6 vertebra +DRG	normal	abnormal - slightly displaced?	normal
Oeseophagus	normal	normal	normal
Trachea	normal	normal	normal
HEART-LUNGS	**PKD2-R870XxR870X X1_R870X-HET**	**PKD2-R870XxR870X X3_HOM**	**PKD2-R870XxR870X X4_R870X-HET**
Thymus (R/L)	normal	abnormal shape and displaced	normal
Vena cava (R/L)	normal	bilateral inf. Vena cava	normal
Sternum primordium	normal	normal	normal
First rib	normal	normal	normal
Ductus Arteriosus	normal	inverted	normal
DA wall	normal	normal	normal
Lung: cranial lobe (R/L)	normal	abnormal - 3:2	normal
Main bronchus (R/L)	normal	normal	normal
Aorta	normal	IAA	normal

Table A2.6 (continued)

HEART-LUNGS	**PKD2-R870XxR870X X1_R870X-HET**	**PKD2-R870XxR870X X3_HOM**	**PKD2-R870XxR870X X4_R870X-HET**
Atrium (R/L)	normal	abnormal - L atrium -> inf vena cava	normal
Ventricles (R/L)	normal	abnormal - interrupted septation	normal
Lung: Middle lobes (R/L)	normal	abnormal - 3:2	normal
Tricuspid valve (R Ventricle)	normal	hard to assess	normal
Mitral valve (L Ventricle)	normal	normal	normal
Interventricular Septum	normal	abnormal - looks interrupted	normal
Heart apex	normal	Dextrocardia	normal
Lung: Accesory R lung	normal	abnormal - 3:2	normal
Lung: Caudate lobe	normal	abnormal - 3:2	normal
LIVER-GUT	**PKD2-R870XxR870X X1_R870X-HET**	**PKD2-R870XxR870X X3_HOM**	**PKD2-R870XxR870X X4_R870X-HET**
Diaphragm (R/L domes)	normal	normal	normal
Peritoneal cavity	normal	abnormal - constricted	normal
Liver (R/L lobes)	normal	normal	normal
Interlobular space	normal	abnormal	normal
Caudate lobe	normal	abnormal - missing	normal
Stomach pyloric antrum	normal	abnormal - inverted	normal
Stomach fundus	normal	normal	normal
Stomach lumen	normal	abnormal - constricted	normal
Pancreas	normal	abnormal - cystic, inverted; L lobe?	normal
Small intestine	normal	abnormal - inverted	normal

Table A2.6 (continued)

KIDNEY-GONADS	**PKD2-R870XxR870X X1_R870X-HET**	**PKD2-R870XxR870X X3_HOM**	**PKD2-R870XxR870X X4_R870X-HET**
Adrenals (R/L)	normal	normal	normal
Kidney: upper pole (R/L)	normal	abnormal - cystic	normal
Kidney: pelvic region (R/L)	normal	abnormal - filled	normal
Bladder	normal	abnormal - missing	normal
Spleen (L)	normal	abnormal - inverted and abnormal position relative to st.	normal
Ovaries (R/L)	normal	-	normal
Testes (post L "higher" vs R)	-	abnormal - cystic	-
OTHER	**PKD2-R870XxR870X X1_R870X-HET**	**PKD2-R870XxR870X X3_HOM**	**PKD2-R870XxR870X X4_R870X-HET**
Brown fat	normal	abnormal shape	normal
Digits	normal	normal	normal
Tail	normal	normal	normal
Oedema	normal	Yes	normal
Spinal shape	normal	normal	normal

Table A2.6 (continued)

BRAIN - CNS	**PKD2-R870XxR870X X6_HOM**	**PKD2-R870XxR870X X8_HOM**	**PKD2-R870XxR870X X48_R870X-HET**
Midbrain (roof)	normal	normal	normal
Mesencephalic vesicle (4th)	normal	normal	normal
Midbrain	normal	normal	normal
3rd Ventricle	abnormal	normal	normal
Lateral vesicles (R/L-emerging)	abnormal - distended	normal	normal
Cerebellum	abnormal - distended	normal	normal
Choroid Plexus (in lateral vesicles)	abnormal	normal	normal
CP (med. 4th V)	abnormal - smaller	abnormal - smaller	normal
Semicircular canal (R/L)	normal	normal	normal
4th V + median sulcus	abnormal - distended laterally	abnormal - distended laterally	normal
Trigeminal V G. (R/L)	abnormal shape	abnormal shape	normal
Olfactory lobe	abnormally spaced	abnormally spaced	abnormally spaced
Rathke's pouch	normal	normal	normal
Emerging cervical spinal cord	abnormal - slightly distended subarachn. space	abnormal - slightly distended subarachn. space	normal
FACE (Ear, Nose, Eye)	**PKD2-R870XxR870X X6_HOM**	**PKD2-R870XxR870X X8_HOM**	**PKD2-R870XxR870X X48_R870X-HET**
Cochlea (R/L)	normal	normal	normal
Pinna (R/L)	normal	normal	normal
Nasal septum (primordium)	normal	normal	normal
Nasal cavity	normal	abnormal - constricted	normal
Vibrissae	abnormal	normal	normal
Intra retinal space	normal	normal	normal
Hyaloid cavity	abnormal - structure inside	normal	normal
Lens	normal	abnormal - small cysts	normal
Eyelids	normal	normal	normal

Table A2.6 (continued)

FACE (Mouth)	**PKD2-R870XxR870X X6_HOM**	**PKD2-R870XxR870X X8_HOM**	**PKD2-R870XxR870X X48_R870X-HET**
Eustachian tube	normal	normal	normal
Soft palate	abnormal - cleft palate	abnormal - cleft palate	normal
Epiglottis	abnormal - smaller	normal	normal
Tongue	abnormal shape	normal	normal
Lower molar tooth (R/L)	normal	normal	normal
Upper molar tooth (R/L)	normal	normal	normal
Thyroid (R/L)	normal	normal	normal
Submandibular gland (R/L)	abnormal shape and smaller	abnormal shape and smaller	normal
C6 vertebra +DRG	abnormal - displaced	abnormal - displaced	normal
Oeseophagus	normal	normal	normal
Trachea	normal	normal	normal
HEART-LUNGS	**PKD2-R870XxR870X X6_HOM**	**PKD2-R870XxR870X X8_HOM**	**PKD2-R870XxR870X X48_R870X-HET**
Thymus (R/L)	abnormal - displaced	abnormal - displaced	normal
Vena cava (R/L)	abnormal - L sided vena cava	2 x L sided inf. Vena cava (attached, one is smaller	normal
Sternum primordium	normal	normal	normal
First rib	normal	normal	normal
Ductus Arteriosus	abnormal - missing	normal	normal
DA wall	abnormal - missing	normal	normal
Lung: cranial lobe (R/L)	abnormal 3:4	abnormal 4:4	normal
Main bronchus (R/L)	normal	normal	normal
Aorta	abnormal, inverted - Ao out of R ventricle; PA connected to Ao arch but not L ventricle	abnormal - transposed (Ao out of R, PA out of L)	normal

Table A2.6 (continued)

HEART-LUNGS	**PKD2-R870XxR870X X6_HOM**	**PKD2-R870XxR870X X8_HOM**	**PKD2-R870XxR870X X48_R870X-HET**
Atrium (R/L)	abnormal - no communication between R V and A	abnormal - no cummunication between R V and A	normal
Ventricles (R/L)	abnormal - no outlet for R ventricle	abnormal - IVS defect	normal
Lung: Middle lobes (R/L)	abnormal 3:4	abnormal 4:4	normal
Tricuspid valve (R Ventricle)	abnormal - missing	abnormal - missing	normal
Mitral valve (L Ventricle)	normal	normal	normal
Interventricular Septum	normal	abnormal - interrupted	normal
Heart apex	Mesocardia	Mesocardia	normal
Lung: Accesory R lung	abnormal 3:4	abnormal 4:4	normal
Lung: Caudate lobe	abnormal 3:4	abnormal 4:4	normal
LIVER-GUT	**PKD2-R870XxR870X X6_HOM**	**PKD2-R870XxR870X X8_HOM**	**PKD2-R870XxR870X X48_R870X-HET**
Diaphragm (R/L domes)	normal	normal	normal
Peritoneal cavity	abnormal - constricted	abnormal - constricted	normal
Liver (R/L lobes)	abnormal - inverted	abnormal - symmetric?	normal
Interlobular space	abnormal	abnormal	normal
Caudate lobe	abnormal - missing	abnormal - inverted and small	normal
Stomach pyloric antrum	abnormal - inverted	abnormal - inverted	normal
Stomach fundus	normal	normal	normal
Stomach lumen	abnormal - constricted	abnormal - constricted	normal
Pancreas	abnormal - cystic, inverted; L lobe displaced on R	abnormal - cystic, inverted; L lobe displaced centrally	normal
Small intestine	abnormal - inverted	abnormal - inverted	normal

Table A2.6 (continued)

KIDNEY-GONADS	**PKD2-R870XxR870X X6_HOM**	**PKD2-R870XxR870X X8_HOM**	**PKD2-R870XxR870X X48_R870X-HET**
Adrenals (R/L)	abnormal - L adrenal displaced slightly by azygos?	normal	normal
Kidney: upper pole (R/L)	small cysts	Abnormal, cystic	normal
Kidney: pelvic region (R/L)	abnormal - filled	abnormal - filled	normal
Bladder	normal	normal	normal
Spleen (L)	abnormal - inverted and abnormal position relative to st.	abnormal - inverted and abnormal position relative to st.	normal
Ovaries (R/L)	normal	normal	normal
Testes (post L "higher" vs R)	-	-	-
OTHER	**PKD2-R870XxR870X X6_HOM**	**PKD2-R870XxR870X X8_HOM**	**PKD2-R870XxR870X X48_R870X-HET**
Brown fat	abnormal shape	abnormal shape	normal
Digits	normal	normal	normal
Tail	normal	normal	normal
Oedema	Yes - severe	Yes - severe	normal
Spinal shape	normal	normal	normal

Table A2.6 (continued)

BRAIN - CNS	**PKD2-R870XxR870X X49_HOM**	**PKD2-R870XxR870X X57_HOM**	**PKD2-R870XxR870X X81_HOM**
Midbrain (roof)	normal	normal	normal
Mesencephalic vesicle (4th)	normal	abnormal - smaller	abnormal - smaller
Midbrain	normal	normal	abnormal shape
3rd Ventricle	normal	normal	abnormal - distended and communicate with lateral vesicles
Lateral vesicles (R/L-emerging)	abnormal - slightly distended/oddly spaced	abnormal - slightly distended/oddly spaced	abnormal - distended and communicate with 3rd v
Cerebellum	normal	abnormal shape/distended	abnormal shape/distended
Choroid Plexus (in lateral vesicles)	normal	normal	abnormal - missing?
CP (med. 4th V)	abnormal - smaller	abnormal - smaller	abnormal shape
Semicircular canal (R/L)	normal	normal	normal
4th V + median sulcus	abnormal - laterally distended	abnormal - laterally distended	abnormal - distended laterally
Trigeminal V G. (R/L)	abnormal shape	abnormal shape	abnormal shape
Olfactory lobe	abnormally spaced	abnormally spaced	abnormal shape
Rathke's pouch	normal	normal	normal
Emerging cervical spinal cord	abnormal - slightly distended subarachn. Space	abnormal - slightly distended subarachn. Space	abnormal - slightly distended subarachn. Space, enlarged spinal canal
FACE (Ear, Nose, Eye)	**PKD2-R870XxR870X X49_HOM**	**PKD2-R870XxR870X X57_HOM**	**PKD2-R870XxR870X X81_HOM**
Cochlea (R/L)	normal	normal	normal
Pinna (R/L)	normal	normal	normal
Nasal septum (primordium)	normal	normal	normal
Nasal cavity	normal	abnormal - constricted	normal
Vibrissae	normal	normal	normal
Intra retinal space	normal	normal	normal
Hyaloid cavity	normal	normal	normal
Lens	normal	abnormal - cysts?	normal
Eyelids	normal	normal	normal

Table A2.6 (continued)

FACE (Mouth)	**PKD2-R870XxR870X X49_HOM**	**PKD2-R870XxR870X X57_HOM**	**PKD2-R870XxR870X X81_HOM**
Eustachian tube	normal	normal	normal
Soft palate	abnormal - cleft palate	abnormal - cleft palate	abnormal - cleft palate
Epiglottis	normal	normal	abnormal - smaller
Tongue	abnormal - smaller	abnormal - smaller	abnormal shape
Lower molar tooth (R/L)	normal	normal	normal
Upper molar tooth (R/L)	normal	normal	normal
Thyroid (R/L)	normal	normal	normal
Submandibular gland (R/L)	abnormal shape and smaller	abnormal shape and smaller	abnormal shape and smaller
C6 vertebra +DRG	abnormal - displaced	abnormal - displaced	abnormal - displaced
Oeseophagus	normal	normal	normal
Trachea	normal	normal	normal
HEART-LUNGS	**PKD2-R870XxR870X X49_HOM**	**PKD2-R870XxR870X X57_HOM**	**PKD2-R870XxR870X X81_HOM**
Thymus (R/L)	abnormal - displaced	abnormal - smaller	abnormal - displaced
Vena cava (R/L)	abnormal - R sided azygos	abnormal - bilateral azygos (R smaller), 2x R-sided inf. Vena cava	normal
Sternum primordium	normal	normal	normal
First rib	normal	normal	normal
Ductus Arteriosus	normal	normal	normal
DA wall	normal	normal	normal
Lung: cranial lobe (R/L)	abnormal 4+:4; lobation on R middle?	abnormal - 4:4	abnormal - 4:3
Main bronchus (R/L)	normal	normal	normal
Aorta	normal	transposed	normal

Table A2.6 (continued)

HEART-LUNGS	**PKD2-R870XxR870X X49_HOM**	**PKD2-R870XxR870X X57_HOM**	**PKD2-R870XxR870X X81_HOM**
Atrium (R/L)	normal	abnormal - no septation	abnormal - missing L atrium
Ventricles (R/L)	abnormal - IVS defect	abnormal - IVS defect	abnormal - constricted
Lung: Middle lobes (R/L)	abnormal 4+:4; lobation on R middle?	abnormal - 4:4	abnormal - 4:3
Tricuspid valve (R Ventricle)	normal	normal	normal
Mitral valve (L Ventricle)	normal	normal	abnormal - missing
Interventricular Septum	abnormal - interrupted	abnormal - interrupted	normal
Heart apex	normal	Mesocardia	Mesocardia
Lung: Accesory R lung	abnormal shape	abnormal - 4:4	abnormal - 4:3
Lung: Caudate lobe	abnormal 4+:4; lobation on R middle?	abnormal - 4:4	abnormal - 4:3
LIVER-GUT	**PKD2-R870XxR870X X49_HOM**	**PKD2-R870XxR870X X57_HOM**	**PKD2-R870XxR870X X81_HOM**
Diaphragm (R/L domes)	normal	normal	normal
Peritoneal cavity	abnormal - constricted	abnormal - constricted	abnormal - constricted
Liver (R/L lobes)	normal	abnormal	normal
Interlobular space	abnormal	abnormal	normal
Caudate lobe	abnormal - missing	abnormal - missing	normal
Stomach pyloric antrum	normal	normal	normal
Stomach fundus	normal	normal	normal
Stomach lumen	abnormal - constricted	abnormal - constricted	abnormal - constricted
Pancreas	abnormal - cystic	abnormal - cystic	abnormal - cystic
Small intestine	normal	normal	normal

Table A2.6 (continued)

KIDNEY-GONADS	**PKD2-R870XxR870X X49_HOM**	**PKD2-R870XxR870X X57_HOM**	**PKD2-R870XxR870X X81_HOM**
Adrenals (R/L)	abnormal - R adrenal displaced by azygos	normal	normal
Kidney: upper pole (R/L)	Abnormal, cystic	Abnormal, cystic	Abnormal, cystic?
Kidney: pelvic region (R/L)	abnormal - filled	abnormal - filled	abnormal - filled
Bladder	normal	normal	abnormal - distended
Spleen (L)	normal	abnormal shape	abnormal shape and position
Ovaries (R/L)	normal	normal	normal
Testes (post L "higher" vs R)	-	-	-
OTHER	**PKD2-R870XxR870X X49_HOM**	**PKD2-R870XxR870X X57_HOM**	**PKD2-R870XxR870X X81_HOM**
Brown fat	abnormal shape	abnormal shape	abnormal shape
Digits	normal	normal	normal
Tail	normal	normal	normal
Oedema	yes - severe	yes - severe	yes - severe
Spinal shape	normal	normal	abnormal